ENAMEL-DENTINE JUNCTION MORPHOLOGY OF EXTANT HOMINOID AND FOSSIL HOMININ LOWER MOLARS

by Matthew Skinner

B.A. in Archaeology 2002, Simon Fraser University

A Dissertation submitted to

The Faculty of
The Columbian College of Arts and Sciences of The George Washington University in
Partial Fulfillment of the Requirements for the degree of
Doctor of Philosophy

May 18, 2008

Dissertation Directed By

Bernard A. Wood
University Professor of Human Origins

The Columbian College of Arts and Sciences of The George Washington University certifies that Matthew Skinner has passed the Final Examination for the degree of Doctor of Philosophy as of March 7, 2008. This is the final and approved form of the dissertation.

ENAMEL-DENTINE JUNCTION MORPHOLOGY OF EXTANT HOMINOID AND FOSSIL HOMININ LOWER MOLARS

Matthew Skinner

Dissertation Research Committee:

Bernard A. Wood, University Professor of Human Origins, Dissertation Director

Peter W. Lucas, Professor of Anthropology, Committee Member

Brian G. Richmond, Associate Professor of Anthropology, Committee Member

Dedication

This work is dedicated to all the fieldworkers whose efforts provided me with museum and fossil specimens to include in this thesis, the many museum staff who curate this material, and the past and present scientists who have studied teeth and provided me with so much insight into these amazing biological structures.

"As the dentine, regarded from the morphological viewpoint, is the most integral constituent of the tooth, its surface relief cannot be considered as a purely accidental feature with no morphological significance" Franz Weidenreich, 1945

Acknowledgments

I would like to begin by acknowledging Bernard Wood, the supervisor of my doctoral studies in the Hominid Paleobiology Doctoral Program at The George Washington University. First I would like to thank Bernard for accepting me as his student and for encouraging me to get the most out of my time at GWU. Bernard was very supportive of me both professionally and personally and provided me with many valuable opportunities to participate in research projects, laboratory internships, and fieldwork, all of which had a great influence on my education. “I am not interested in what a person *thinks*, but what they can *demonstrate*” was a statement Bernard made to me once, and which I have tried to remember during my own research endeavors.

Jean-Jacques Hublin, of the Max Planck Institute for Evolutionary Anthropology, also supervised my thesis project. Without Jean-Jacques' support and guidance I could not have conducted the projects included in this thesis. I am very grateful for the opportunity that Jean-Jacques gave to me to conduct my thesis research within the scope of his much broader research program on virtual paleoanthropology. I would like to thank Jean-Jacques for sharing his enthusiasm for paleoanthropology with me and for the critical and insightful observations he has contributed to this thesis.

I would like to thank Brian Richmond for his enthusiasm and the positive approach that he brought to all aspects of the doctoral program at GWU. I benefitted greatly from taking classes from Brian, from being his teaching assistant, and from his guidance on a number of projects I conducted during my doctoral studies. Through his research, teaching, and other scholarly activity Brian set a wonderful example to me and the other students of the HOMPAL program.

I would like to thank Alison Brooks for instilling in me the importance of an interdisciplinary approach to human evolutionary studies and of keeping up with all the literature; which she seems to do so effortlessly. Also, for her support of my thesis project and her encouragement to conduct my thesis research in Leipzig.

I would like to thank two people in particular for their assistance during my doctoral studies. Tanya Smith first suggested to me the possibility to work in the Department of Human Evolution at the MPI-EVA and this collaboration with my department at GWU is responsible for the data upon which my thesis is based. Tanya also encouraged me throughout my doctoral research, facilitated access to collections and collaborators, and inspired me by her own scientific endeavors. Philipp Gunz provided considerable assistance with the geometric morphometric analyses I employed in this thesis. He kindly allowed me to use software routines that he developed, taught me how to use them, and patiently helped with periodic difficulties I had with the analysis. Philipp also provided valuable discussions regarding the interpretation of the results of many analyses and in the broader implications of my research.

During my doctoral studies I was a student to many faculty from three academic institutions. From GWU I would like to thank Peter Lucas, Patricia Hernandez, Robin Bernstein, and James Clark. From The MPI-EVA I would like to thank Zeresenay Alemseged, Katarina Harvati, Shannon McPherron, Tanya Smith, Philipp Gunz, Kornelius Kupczik, Anthony Olejniczak, Luke Premo, Michael Richards, and Heike Scherf. From the National Museum of Natural History I would like to thank Rick Potts and Kay Behrensmeyer.

I was fortunate to go through graduate school with students from two excellent anthropology departments. I thank you all for your support, both personal and professional, over the years and I look forward to being your colleague for many more. From the Hominid Paleobiology Doctoral Program GWU: Janine Chalk, Paul Constantino, Alexandra de Sousa, Tyler Faith, Felicia Gomez, David Green, Nicole Griffin, Catherine Haradon, Amanda Henry, Nicolas Lonergan, Holly Mortensen, Lisa Nevell, Robin Teague, Erin Marie Williams. From the Department of Human Evolution at the MPI-EVA: Kate Britton, Kyungcheol Choy, Robin Feeney, Sarah Freidline, Maria Hillier, Adeline Le Cabec, Olaf Nehlich, Anja Gumprich, Simon Neubauer, Philip Nigst, Morgan Roussel, Nandini Singh, Sahra Talamo, Nicolas Zwyns and Friederike Kachel.

For their assistance with the administration of my doctoral studies I would like to thank the administrative staff of the Department of Anthropology at GWU, including Jonathan Higman, Gopy Mann, and Phillip Williams and the administrative staff of the Department of Human Evolution at the MPI-EVA, including Diana Carstens, Silke Streiber, and Cornelia Schicke.

For fruitful discussions during the course of my doctoral studies I acknowledge Shara Bailey, Jukka Jernvall, Alistair Evans, Fred Grine, Mark F. Skinner, Paul Constantino, Anthony Olejniczak, Kornelius Kupczik, Robin Feeney, Christine Verna, Tanya Smith, Tim Weaver, Luke Premo, and Barth Wright.

I would like to acknowledge Heiko Temming, Andreas Winzer, Micha Gasch, Dennis Reinhardt, Gert Wollney, Rasesh Kapadia for their assistance with technical aspects of my thesis and for their participation in the computed tomography scanning projects from which some of the thesis sample were derived.

Access to dental specimens was kindly provided by the following individuals and institutions: Mike Raath, Andre Keyser and Colin Menter of the University of Witwatersrand, Johannesburg, South Africa; Francis Thackeray and Stephanie Potze of the Transvaal Museum, Northern Flagship Institution, Pretoria, South Africa; Antonio Rosas of the Museo Nacional de Ciencias Naturales, Madrid, Spain; Ottmar Kullmer of the Senckenberg Museum, Frankfurt, Germany; Christophe Boesch, Mandy Jay and Mike Richards of the Max Planck Institute for Evolutionary Anthropology, Leipzig, Germany; Rick Potts and David Hunt of the National Museum of Natural History, Washington, DC, USA; Robert Asher, Hendrik Turni and Irene Mann of the Museum für Naturkunde, Berlin, Germany; Emmanuel Gilissen and Wim Wendelen of the Royal Museum for Central Africa, Tervuren, Belgium.

Various aspects of my thesis research received funding support from the following: The George Washington University Selective Excellence Fellowship Program; the National Science Foundation's Integrative Graduate Education and Research Traineeship Program; the European Virtual Anthropology Network; the Marie Curie Research Training Network MRTN-CT-019564; the Spanish MEC Grant CGL-2006-02131; The Max Planck Society.

Finally I would like to thank my mother for her support throughout my life and for all of the sacrifices she made for her children. Also, for instilling in me a strong work ethic and the drive to do a job well. I would like to thank my father for taking me to the badlands of Alberta, Canada to look for dinosaur fossils as a small boy. I believe my fascination with fossil teeth and my love of the outdoors derives from those hot days in the prairies. I would also like to thank him for leading by his example as a scientist, for

teaching me during my undergraduate degree at Simon Fraser University and for encouraging me to apply to GWU where my doctoral studies began. I would like to thank Jean McKendry for all of her support throughout my life and for her devotion to our family. I would like to thank my brother Todd and his wife Andrea for all of their support over the years and for allowing me to live vicariously through their lives in the 'real world.' I would also like to thank my sister, Sarah Kate, for her support and for inspiring me with her strength of character and love of life.

Abstract of Dissertation

ENAMEL-DENTINE JUNCTION MORPHOLOGY OF EXTANT HOMINOID AND FOSSIL HOMININ LOWER MOLARS

This thesis is comprised of four individual projects (chapters two to five) which are based upon an examination of the enamel-dentine junction (EDJ) of lower molars in various extant hominoids and fossil hominins. Collectively, these manuscripts represent the first comprehensive analyses of EDJ morphology in a range of hominoid taxa and at the high degree of resolution made possible through the use of micro-computed tomography. They explore the taxonomic relevance of EDJ morphology, both quantitatively and qualitatively, and in doing so reveal how detailed aspects of the outer enamel surface morphology develop. They also provide insights into the developmental processes that determine the form of the functional interface between the dentition and the food, upon which natural selection acts.

The first chapter introduces the goals of the thesis and reviews relevant literature that is pertinent to the various topics within the thesis. It also provides a detailed discussion of the materials and methods used to image and analyze EDJ morphology. Chapter two demonstrates that when the morphology of the EDJ can be captured in sufficient detail, analysis of its morphology can discriminate between species and subspecies of extant chimpanzees. Chapter three extends these findings to an analysis of lower molars belonging to *Australopithecus africanus* and *Paranthropus robustus* from southern Africa and demonstrates that EDJ morphology is distinctive both between each taxon, as well as between first, second, and third molars of each taxon. Chapter four examines the expression of four dental traits on the lower molars of a range of extant and

extinct hominoids (including fossil hominins). It demonstrates that these traits originate at the EDJ, that the EDJ is primarily responsible for their degree of expression, and that when examined across a wide range of taxa the morphological variability in the expression of these traits can be considerable. The fifth chapter focuses specifically on one dental trait, the protostylid, and examines its EDJ manifestation in samples of *Australopithecus africanus* and *Paranthropus robustus*. The results of this analysis reveal taxon-specific patterns in protostylid expression that are difficult to detect at the enamel surface as well as evidence that current definitions of the trait itself should be re-examined.

Table of Contents

CHAPTER 1: INTRODUCTION, LITERATURE REVIEW, MATERIALS, AND METHODS

Introduction

Teeth dominate the vertebrate fossil record due to their high degree of mineralization and thus they are relied upon in the definition and diagnoses of fossil taxa. Furthermore, because teeth do not remodel during the lifetime of an individual the external morphology of the enamel and their internal microanatomy can be used to reconstruct their development. Quantitative and qualitative analyses have demonstrated that the external morphology of the enamel can readily distinguish genera, species and even sub-species of hominoids, track patterns of modern human migrations and help delineate regional grouping of modern humans (Johanson, 1974; Uchida, 1992, 1996, 1998a,b; Scott and Turner, 1997 and references therein; Pilbrow 2003, 2006a,b). The morphology of the external enamel surface is also used to sort the hominin fossil record into taxa and to reconstruct the evolutionary relationships among these taxa (e.g., Robinson, 1956; Sperber, 1974; Wood and Abbott, 1983; Wood et al., 1983; Suwa et al., 1994; Bailey, 2002, 2006; Grine, 2004; Hlusko, 2004; Irish and Guatelli-Steinberg, 2003; Guatelli-Steinberg and Irish, 2005; Bailey and Lynch, 2005; Bailey and Hublin, 2006). The goals of this thesis are to extend this research through an investigation of whether details of the shape of the interface between the enamel cap and the underlying dentine (i.e., the enamel-dentine junction) can A) improve the utility of the morphology of the crowns of lower molars of extant hominoids and fossil hominins for alpha taxonomy, and B) improve our understanding of the development of morphological features (so-called discrete dental traits) as seen on the external surface of lower molar crowns.

While teeth are relatively plentiful in the hominin fossil record and make up large percentages of the known hypodigms for many hominin taxa they are variably worn. Unerupted specimens can be pristine in their preservation of the original morphology of the tooth crown, others have lost most of the morphology of the enamel cap, and heavily worn specimens exhibit exposure of the underlying dentine. This variable preservation of the original enamel surface limits our ability to compare those detailed aspects of crown morphology that are necessary to discriminate between extant apes at the species and sub-species level. With different levels of attrition the homology of many of the smaller structures present on the crowns of fossil teeth is violated, and all that is left are relatively gross measures of crown shape (e.g., length and width of the crown). Such gross measurements are limited in their ability to discriminate fossil hominin taxa whose discrimination, based on other skeletal morphology, is well supported. Thus, it is often not possible to utilize the discriminatory potential of teeth in fossil samples. What is needed is a structure that A) is homologous among teeth, B) carries information about the detailed morphology of tooth shape, and C) retains that information even in teeth where attrition has removed much of the external morphology of the enamel.

It has long been acknowledged that the enamel-dentine junction (EDJ), which underlies the enamel cap of primate teeth, carries considerable information about the shape of the external surface of the intact tooth crown (Kraus, 1952; Korenhof, 1960, 1961, 1982; Nager, 1960; Kraus and Jordan, 1965; Sakai et al., 1965, 1967a,b, 1969; Sakai and Hanamura, 1971, 1973a,b; Corruccini, 1987a,b, 1998; Schwartz et al., 1998; Sasaki and Kanazawa, 1999; Skinner et al., 2008) including taxonomically relevant shape information (Corruccini, 1998; Olejniczak et al., 2004, 2006, 2007; Macchiarelli et al.,

2006; Suwa et al., 2007; Skinner et al, nd). Furthermore, the EDJ remains in a pristine state throughout the initial stages of tooth wear (and even longer in thicker enameled, relatively low-cusped hominin taxa). Study of the EDJ, however, has been limited by the difficulty in imaging this surface non-destructively. This has prevented assessment of the potential of this surface for determining the taxonomic affiliation of fossil specimens, for understanding the development of morphological traits on the enamel surface, and for characterizing variation in tooth crown shape in fossil hypodigms.

The two goals of this thesis are addressed through a series of questions related to the morphology of the EDJ:

- **Does the EDJ, like the unworn enamel surface, accurately discriminate between hominoid species and subspecies?** This question is explored in chapter two through a comparison of lower molar EDJ morphology in two species of *Pan* (*Pan paniscus* and *Pan troglodytes*) and two subspecies of *Pan troglodytes* (*verus* and *troglodytes*)
- **Can the EDJ, preserved in partially worn fossil hominin teeth, be used to assess the taxonomy of fossil specimens?** This question is the topic of chapter three which compares lower molar EDJ morphology between two species of hominin from southern Africa: *Australopithecus africanus* and *Paranthropus* (*Australopithecus*) *robustus*.
- **What is the contribution of the EDJ to the presence and morphological expression of discrete dental traits on lower molars?** This question is addressed in chapter four through an examination of the EDJ expression of four lower molar dental traits (cusp 6, cusp 7,

protostylid and trigonid crest pattern) in a range of extant and extinct hominoid taxa (including fossil hominins).

- **Are there morphological differences in protostylid expression at the EDJ between *Au. africanus* and *P. robustus*?** This question is addressed in chapter five through an analysis of protostylid expression at the enamel surface and EDJ of a large sample of molars.

The data used to address each of these questions are digital reconstructions of the surface of the enamel cap and the EDJ of molar teeth acquired non-destructively through microcomputed tomography (μCT). This technology allows the production of high resolution reconstructions of each surface that are necessary to examine the detailed morphological features present on molar teeth. These surface reconstructions are analyzed qualitatively, through visual inspection, and quantitatively, through traditional mensuration as well as within a geometric morphometric framework. The latter allow both a quantitative analysis of complex shapes and a means of visualizing the shape differences present between both taxa and tooth type (e.g., first, second, and third molars).

Chapters two to five are written in the form of individual manuscripts. This is because some manuscripts are already published (Chapter 4) and others are in various stages of submission at the time of the writing of this thesis. This first chapter presents a review of the literature relevant to the topics addressed in each chapter and a detailed discussion of the materials and methods incorporated into the thesis. The final chapter of the thesis summarizes the results of the previous chapters, and discusses the implications

of the results for our understanding of how tooth morphology develops and how variation in tooth morphology is incorporated into dental and paleoanthropological research.

Terminology

There are a number of terms used thoughout this thesis that require some explanation. The first set relates to the use of the taxonomic terms hominid, hominine and hominin and, in recognition of the genetic similarities between *Pan* and *Homo sapiens*, follows Wood and Richmond (2000). The term hominid refers to members of the family Hominidae including all the extant great apes (i.e., *Gorilla*, *Pan*, *Pongo*, and modern humans), all fossil apes more closely related to these extant taxa than to any other extant taxon, and fossil hominins – see below), the term hominine refers to members of the subfamily Homininae (including chimpanzees, bonobos, modern humans, fossil panins and fossil hominins – see below), the term panin refers to members of the tribe Panini (i.e., modern chimpanzees and bonobos and all fossil taxa more closely related to modern chimpanzees and bonobos than to any other extant taxon), and the term hominin refers to members of the tribe Hominini (i.e., modern humans and all fossil taxa more closely related to modern humans than to any other extant taxon).

The nomenclature used to identify the cusps on lower molars is that commonly used in vertebrate paleontology (Fig. 1.1). This includes the protoconid (mesiobuccal cusp), metaconid (mesiolingual cusp), entoconid (distolingual cusp), hypoconid (distobuccal cusp), and hypoconulid (distal cusp). Underlying each of these cusps is a dentine horn referred to by the same name (e.g., protoconid dentine horn). The terms Ma and Ka stand for millions of years ago and thousands of years ago, respectively.

History of EDJ imaging

Many attempts to image the EDJ have incorporated the chemical removal the enamel cap (e.g., Kraus, 1952; Nager, 1960; Sakai et al., 1965, 1967a,b, 1969; Sakai and Hanamura, 1971, 1973a,b; Corruccini, 1987b, 1998; Corruccini and Holt, 1989; Sasaki and Kanazawa, 1999; Kono et al., 2002). This method provided reasonable access to EDJ morphology, but it required prior preservation of the enamel surface (usually by casting) and suffered from potential damage to the EDJ during the removal of adhering enamel (e.g., see Corruccini and Holt, 1989). A fortunate opportunity to examine EDJ morphology in molar teeth occurred with the discovery by G. H. R. von Koenigswald of many hundreds of naturally preserved enamel caps from around Sangiran, Central Java, Indonesia. These modern human teeth derive from medieval burials and were collected over a five year period from 1935 to 1940 (Weidenreich, 1945, Korenhof, 1960). Plaster endocasts of these enamel caps formed the basis of a series of publications on the collection (Korenhof, 1960, 1961, 1978, 1982). This series of teeth and endocasts revealed considerable information about the degree of concordance between the EDJ and enamel surface (see below) but the methodology could not reliably document the presence or absence of fine details of the morphology of the EDJ. For example, Korenhof (1960) noted a lack of any definitive features underlying mesial marginal ridge tubercles on the upper molars, however, corresponding EDJ features have been noted subsequently by other authors (Kraus and Jordan, 1965).

Another major source of information about EDJ shape came from developing tooth germs removed from jaws. One of the most comprehensive studies of this kind was

an analysis of deciduous and permanent molars undertaken by Kraus and Jordan (1965), which included illustrations of the growth of the EDJ and the subsequent pattern of enamel deposition over its surface. Photographs of the tooth germs, chemically-stained to reveal the mineralized portions, demonstrated that morphological features visible at the enamel surface are present on the EDJ (more precisely the inner enamel epithelium of a developing tooth germ) prior to enamel deposition. Another important study using this method was that published by Kraus and Oka (1967) in which they demonstrated that "wrinkled" enamel on the surface of hominoid and modern human teeth derived from ridges and crests present on the EDJ prior to enamel deposition. In the most recent and comprehensive analysis of primate tooth germs, Swails (1993) examined monkeys, apes and modern humans to compare taxonomic and phylogenetic signals in the ontogenetic trajectory of molar tooth germs.

Computed tomography (CT) is an ideal methodology for studying internal structures because it is non-destructive to the tissues and provides 3D volumetric data. CT has been employed to image internal tooth structure, but many of these studies were concerned with imaging the EDJ in order to measure enamel thickness rather than to assess EDJ morphology itself (Conroy, 1991; Grine, 1991, Macho and Thackeray, 1992; Conroy et al., 1995; Schwartz et al., 1998). The study by Schwartz and colleagues (1998) examined the concordance between the EDJ and OES with regard to Carabelli's trait expression in hominin upper molars. Their systematic attempt to address the contribution of the EDJ to this dental trait provided equivocal support for the consistent presence of the trait at the EDJ. This was because of limited spatial resolution and the limitation that this feature could only be assessed within a single slice.

The spatial resolution of medical grade CT (e.g., 0.5 – 1.0 mm per pixel) is not sufficient to accurately assess detailed morphological features on the EDJ, or their correspondence with equivalent features on the outer enamel surface (OES). In the last decade so-called micro-computed tomographic (μCT) scanners have become available for anthropological research. These tomographic scanners have a superior spatial resolution reaching approximately 5-50 micrometers (μm) for most dental anthropological applications, allowing surface reconstructions of the EDJ and OES to be generated that are able to capture the complex morphology present on tooth crowns. The majority of studies utilizing μCT have focused primarily on enamel thickness with less discussion of EDJ shape variation (Kono et al., 2000; Kono, 2004; Suwa and Kono, 2005; Olejniczak, 2006; Olejniczak and Grine, 2006; Smith et al., 2006b) although more recent publications have used μCT to address the taxonomic distinctiveness of enamel thickness and EDJ shape in extant and fossil taxa (Olejniczak et al., 2004; Olejniczak and Grine, 2005; Olejniczak, 2006; Macchiarelli et al., 2006; Kunimatsu et al., 2007; Suwa et al., 2007; Olejniczak et al., 2008, nd).

Two-dimensional studies of EDJ shape

One method of studying EDJ shape is to examine it in cross-section. One reason for this is practical as the production of histological sections used for study of enamel thickness gives access to EDJ shape as well. As large histological collections of modern human teeth (and a small sample of primates and fossil hominins) have already been produced, it is a good opportunity to further utilize these specimens. Olejniczak and colleagues (2004) examined EDJ shape in the maxillary molars of anthropoid primates

and concluded that EDJ cross-sectional shape through the mesial cusps discriminates between taxa at the family, genus and species level. An analysis of modern human molars by Smith and colleagues (2006a) found some evidence for population differences and metameric variation along the molar row. Olejniczak and colleagues (2008) examined dentine horn height in 2D (based on single µCT slices) in *Gigantopithecus blacki* and noted similarities with extant *Pongo* in having relatively short dentine horns compared to African apes and humans. An analysis of dentine height, assessed from radiographs, showed no significant differences between modern humans and Neanderthals although linear measurements incorporating enamel height, dentine height and pulp accurately discriminated between the two taxa (Zilberman et al., 1992). Shimizu (2002) examined cross-sectional images of cercopithecoid monkeys and suggested that the shape of the EDJ and the distribution of enamel over the dentine horns contributed to the maintenance of functional efficiency as the molars worn down. This is one of the few studies that directly addresses the role that tooth crown conformation plays in the functional morphology of teeth. In summary, 2D studies of EDJ shape have shown promise for addressing taxonomic and functional questions but have been limited in their taxonomic scope and because they assess a single section through a complex 3D structure are potentially misleading with regard to the assessment of some morphological features.

Three-dimensional studies of EDJ shape

In Butler's (1956) comprehensive review of the current knowledge of how molars grow were the following observations relevant to the present study: a) minor features of the OES may or may not involve the EDJ, b) wrinkling on the OES of hominoids has an

EDJ component, c) enamel deposition can mask the presence of small cuspules originating at the EDJ, d) that the EDJ and OES will be more similar in shape in thin-enameled than in thick-enameled taxa, e) cusps can be defined as the locations where the formation of dentine and enamel begins, and f) ridges are less developmentally stable than cusps.

Kraus (1952) examined the correlation between bi-apical cusp diameters and angles in modern humans to determine the reliability with which cusp configurations could be reconstructed in worn fossil teeth. His results did not support a strong predictive relationship between EDJ and OES morphology for such variables. Kraus and Jordan's (1965) analysis of deciduous and permanent molar tooth germs identified the basic sequence by which each molar attains its overall shape during soft tissue growth and mineralization. They noted variability in the sequence of cusp coalescence during mineralization likely linked to variation in EDJ shape, and they noted many similarities between modern human molar EDJ morphology at various stages of development and the molar morphology of extant and extinct primates, mammals and reptiles. Their observations suggested to them that the processes by which teeth form different shapes have been conserved across many lineages and over deep evolutionary time and that the developmental stages through which modern human primary molars pass "recapitulate the adult forms of fossils which are postulated as representatives of stages in the evolution of the human molars (Kraus and Jordan, 1965:164)."

As mentioned above the series of papers by Korenhof (1960, 1961, 1978, 1982) represent one of the most comprehensive analyses of modern human molar EDJ morphology. Among his many observations were that the EDJ a) preserves more

phylogenetically conservative morphology than the OES, b) shows details that are not evident at the enamel surface, and c) is indicative of how features present on more generalized primate teeth have been incorporated into structures on modern human teeth. Korenhof also proposed theories about evolutionary trends in particular aspects of molar morphology that are present at the EDJ and can be compared to molar features of extant and fossil primates.

Sakai and colleagues published a series of papers on the EDJ and OES of all tooth types of modern humans (Sakai et al., 1965, 1967a,b, 1969; Sakai and Hanamura, 1971, 1973a,b). The close similarity in shape between the EDJ and OES of major crown features is evident in their publications indicating the origin of these features on the EDJ. With regard to the phylogenetic signal preserved in each surface they conclude that "the characters of the dentinoenamel junction show phylogenetically more primitive or conservative conditions in relation to the exterior surface of the enamel layer…" and that "a morphological study of the dentionoenamel junction should play an important role in morphologic interpretation of various dental traits and studies on phylogeny of the dentition (Sakai and Hanamura, 1973b)."

Corruccini and colleagues published a series of papers examining the EDJ of primates (Corruccini, 1982, 1987a,b, 1998, Corruccini and Holt, 1989). Corruccini (1982) confirmed the clarity with which morphological features, such as accessory cusps and crests, can be seen at the EDJ and noted similarities between modern human and chimpanzee molar EDJ morphology that are less evident at the enamel surface. In a taxonomically broad study of primate EDJ molar morphology Corruccini (1987a) noted a number of cases of features present at the EDJ that were not seen at the OES.

Interestingly, cases of EDJ hypocones with no OES equivalent, as well as, the opposite pattern were present in modern human molars. Based on EDJ morphology it was also suggested that the hypocone may not be developmentally homologous among living primates, having evolved from different portions of the crown in different taxa (Corruccini, 1987a, Corruccini and Holt, 1989). Corruccini (1998) found that the EDJ tended to be more similar in shape to the expected plesiomorphous condition and showed similarities between modern humans and African apes and between callitrichines and pitheciines that are not evident at the OES.

Surface reconstructions of the EDJ and OES, derived using μCT, have also been used to establish and compare developmental trajectories within and between modern human teeth (Smith et al., 1997; Avishai et al., 2004). They noted that the increase in intercusp distance at the OES was due to a difference in cusp angulation rather than an increase in enamel thickness and that EDJ morphology and enamel deposition can contribute in different ways to total cusp size and volume between cusps on the same molar crown.

Sasaki and Kanazawa (1999) examined morphological traits, including the protostylid and trigonid crest pattern, on the EDJ of lower deciduous molars of modern humans. Echoing the findings of earlier studies it was shown that the EDJ preserves a more accurate record of the presence of these features and that small features at the EDJ can be masked by thick enamel. Suwa and Kono (2005) noted the consistent reduction in dentine horn height between first and second lower molars in modern humans. Macchiarelli and colleagues (2006) commented on the apparent EDJ surface complexity of Neanderthal molars compared to modern humans, but due to the very small sample

size in their analysis and the simplistic quantification of surface complexity (i.e., measured as EDJ surface area) this apparent distinction requires further study.

Due to small sample sizes in the majority of these studies, emphasis was placed on the degree to which the EDJ preserved plesiomorphic morphology and how closely EDJ morphology tracked inferred phylogenetic relationships among taxa, rather than on the reliability of the EDJ to discriminate among closely related taxa (e.g., at the species or subspecies level). One of the goals of this thesis is to compare larger samples of relatively few taxa to assess variability in dental trait morphology and the degree to which the EDJ can reliably discriminate closely related taxa.

Odontogenesis

This section outlines current knowledge of how tooth crown morphology develops and highlights aspects of development that can lead to morphological variability of crown features. As this thesis focuses on identifying and interpreting molar crown variability in extant and fossil hominids, this review serves as the basis from which variation in EDJ morphology, preserved in fully formed molars, can be interpreted. It begins with a review of modern human tooth development as understood through the histological analysis of tooth germs following Ten Cate (2007). This is followed by a review of what is known about the developmental genetics of mouse tooth growth as this field is providing significant advances in our understanding of how teeth grow. Finally, I discuss the implications of this new developmental genetic paradigm for interpreting morphological variation of molar tooth crowns in primates and fossil hominins.

Embryology of odontogenesis based on histology. Modern human teeth are initiated from the maxillary, frontonasal and mandibular processes of the developing embryo and their formation is divided into five stages: primary epithelial band (dental lamina), bud, cap, bell, and crown stages. In the first stage horseshoe-shaped primary epithelial thickenings form in positions corresponding to the future dental arches in the upper and lower jaws. Continued epithelial cell proliferation, within the dental lamina, results in localized epithelial thickenings that mark the locations of future teeth. The bud stage begins when the oral epithelium invaginates into the underlying mesenchyme resulting in the formation of a bud-like structure.

The *early cap stage* is characterized by a condensation of mesenchymal cells beneath the epithelial ingrowth that is caused by the failure of these cells to produce extracellular matrix. The late cap stage is characterized by the formation of the dental organ (containing epithelial cells), which sits over the dental papilla (containing condensed mesenchymal cells) like a cap. The dental follicle, also comprised of condensed mesenchymal cells, surrounds the dental papilla and dental organ. Collectively these three structures form the tooth germ.

The *bell stage* of tooth development is characterized by the histodifferentiation and morphodifferentiation of epithelial cells within the dental organ. These cells differentiate into the outer enamel epithelium (at the outside surface of the dental organ), the inner enamel epithelium (over the dental papilla), the stellate reticulum (within the dental organ and surrounded by the outer and inner enamel epithelium), and the stratum intermedium (located between the inner enamel epithelium and the stellate reticulum). The stellate reticulum contains glycoaminoglycans which are hydrophilic and provide for

a high proportion of water within the dental organ to maintain its shape and separation between the inner and outer enamel epithelia.

The *crown stage* is characterized by continued mineralization of the dental hard tissues that commenced at the bell/crown stage boundary. Beginning at the site of future cusp tips and moving down the cusp walls, the cells of the inner enamel epithelium cease mitotic activity and elongate into column-shaped cells with the nucleus adjacent to the stratum intermedium. Subsequently, the cells of the dental papilla beneath the epithelium increase in size and differentiate into odontoblasts. After the odontoblasts deposit predentine and dentine begins to form, the columnar cells of the inner enamel epithelium differentiate further into fully formed ameloblasts, which begin to secrete enamel matrix on top of the dentinal surface. As new odontoblasts continue to differentiate, moving down the inner surfaces of the cusp walls, new ameloblasts also differentiate cervically, while more mature ameloblasts begin to deposit enamel in long prisms as they migrate towards the eventual crown surface. The cervix of the tooth is located at the cemento-enamel junction where ameloblast differentiation and enamel formation ceases. Odontoblasts continue to proliferate apically to form the tooth roots. Cementum, deposited by cementoblasts, covers the root surface and anchors the tooth into the surrounding alveolar bone by incorporating fibers of the periodontal ligament into its sequentially deposited hard tissue layers.

The dentition of modern humans consists of both deciduous and permanent sets of teeth. The morphogenesis of the incisors, canines and premolars of the permanent dentition progresses through the same stages of development as their deciduous precursors, beginning with the formation of a diverticulum on each developing deciduous

tooth germ that will eventually form the permanent tooth bud. The molars of the permanent dentition, which in modern humans have no deciduous predecessors, develop from posterior migrations of the dental laminae beneath the lining epithelium of the oral mucosa and into the underlying mesenchyme, as the mandible and maxilla increase in size.

Developmental genetics of murine odontogenesis. Recent experimentation using mice has identified many of the primary genes and signaling pathways responsible for the formation of the dental tissues and their temporospatial activity during tooth growth. This work has been the impetus for the generation and testing of new developmental models that attempt to explain the processes behind the dental phenotypes that are present in mice and other mammal groups.

The development of all mammalian teeth involves reciprocal signaling between the oral epithelium and the neural crest-derived mesenchyme and is thus limited to the first branchial arch as this is the only location in which these two tissues occur. While teeth can be initiated in neural crest-derived mesenchyme from the second branchial arch, no initiation occurs in the presence of non-oral epithelium (Lumsden, 1988; Mina and Kollar, 1987). The pervasiveness of cranial neural crest (CNC) cells in the development of the teeth and the mandible in mice has been demonstrated by Chai and colleagues (2000) who determined that CNCs contribute to the development of the condensed dental mesenchyme, dental papilla, odontoblasts, dentine matrix, pulp, cementum, periodontal ligaments, the mandible and the articulating disc of the temporomandibular joint.

Tissue recombination experiments, *in situ* hybridization, and gene knockout experiments have identified the numerous genes and transcription factors involved in the

various stages of tooth morphogenesis. Members of four families of signaling proteins are iteratively and reciprocally expressed between the oral epithelium and mesenchyme throughout murine tooth morphogenesis: bone morphogenetic proteins (BMPs), fibroblast growth factors (FGFs), Sonic hedgehog (*Shh*) and Wnt proteins (Ferguson et al., 2000a). Also, the same transcription factors are often present at each stage of tooth development (e.g., *p21*, *Msx2*, *Lef1*, *Barx1*, and *Dlx2*).

A pattern of nested expression of FGF8 and BMP2 and BMP4 is believed to control the spatial pattern of *Pax9* expression associated with tooth bud formation (Neubuser et al., 1997). *Shh* has also been linked to bud formation as it is expressed in the tip of the epithelium that invaginates into the mesenchyme (Dassule et al., 2000). Other signaling molecules linked to bud formation by knockout experiments include *Msx1* (all teeth arrested at the bud stage) (Satokata and Maas, 1994), *Lef1* (failure of dental papilla formation resulting in rudimentary bud formation) (van Genderen et al., 1994), *Gli2-/-Gli3+/-* (no maxillary incisor buds), *Gli2-/-Gli3-/-* (all teeth arrested at the bud stage), *Dlx1-/-Dlx2-/-* (no maxillary molar buds), and *Activin A-/-* (no incisor or mandibular molar buds) (Line, 2003). Redundancy is evident in many of these signaling molecules, as only in double knockout mutants is any phenotypic effect evident.

The shape of the tooth crown is determined during the cap and bell stages. Specifically, this involves the differential proliferation of epithelial and mesenchymal cells controlled in time and space by a structure called the *enamel knot*. This differential growth results in the folding of the epithelium that creates the basic shape of the crown, with the shape of the occlusal surface dictated by the subsequent growth of the cusp(s). The enamel knot is a non-proliferative signaling center similar to the apical ectodermal

ridge (AER) present in developing limbs, and its induction is a prerequisite for the tooth to develop into the cap stage (Jernvall and Thesleff, 2000). The non-proliferation of enamel knot cells is thought to be maintained by the high prevalence of FGF receptors in the enamel knot area and the expression of *p21*, a cyclin-dependent kinase inhibitor that is associated with cells ceasing to divide and with beginning terminal differentiation (*p21* is also expressed in the non-proliferating AER in limbs). Given that knockouts of *p21* do not result in altered adult dental phenotypes it is likely that *p21* is functionally redundant with other inhibitors around the enamel knot (Jernvall and Jung, 2000). By the late cap stage the enamel knot has disappeared through apoptosis in association with BMP4 expression (Jernvall et al., 1998).

Developmental data contradict arguments that complex, multicuspid teeth evolved through the amalgamation of numerous monocuspid teeth (Donoghue, 2002). In multicuspid teeth, the apoptotic disappearance of the primary enamel knot, is followed by the formation of secondary enamel knots at the sites of future cusp tips. Like primary enamel knots, secondary enamel knots are non-proliferative and are removed apoptotically in association with BMP4 expression (Jernvall and Thesleff, 2000). The spacing of secondary enamel knots (and their associated cusps) is important in determining crown shape. It is thought the nested expression of FGF4 (linked to epithelial cell proliferation and cusp formation) and BMP4 and/or *Shh* (inhibiting the Fgf4 signal) regulate the distance between cusps and overall cusp size (Jernvall and Thesleff, 2000). FGF4, *Shh*, *Lef1* and *p21* show similar correlations between pre-cusp expression patterns and eventual cusp morphology, suggesting that they are all involved in cusp patterning

(Jernvall et al., 2000). *Edar* has also been implicated in the determination of cusp number and tooth number in mice (Tucker et al., 2004).

In summary, odontogenesis occurs through sequential and reciprocal signaling within the oral epithelium, and between the oral epithelium and the underlying mesenchyme, and it involves the same signaling families (e.g., FGFs, BMPs, Wnts and *Shh*) and the iterative use of the same signaling pathways, which are controlled, in large part, by primary and secondary enamel knots (non-proliferative signaling centers similar to the AER of developing limbs). The complete dental arcade of modern humans then can been viewed as the collective development of individual teeth that have either single secondary enamel knots in the case of monocuspid teeth, or multiple secondary enamel knots in the case of multicuspid teeth. Based on this research, new models have been proposed account for both the different tooth types in heterodont dentitions and cusp patterning on the crowns of multicuspid teeth.

Determination of tooth type: the odontogenic homeobox code model. Butler (1956) proposed a gradient model of dental patterning in which concentration gradients of unspecified molecules determine separate fields in which incisors and molars develop. Osborn (1978) suggested a clone model in which different populations of mesenchymal cells populated the first branchial arch which eventually gave rise to incisor and molar specific mesenchymal cells. Based on recent developmental genetic research, the odontogenic homeobox code (OHC) model posits that teeth are serially homologous structures and tooth type is determined by nested and restricted homeobox gene expression in the maxillary and mandibular mesenchyme (Sharpe, 1995; Thomas et al., 1997). It is currently believed that it is the coexpression of homeobox genes in the

mesenchyme, induced by signals from the oral epithelium, which determines tooth type in mice. Molars grow where *Barx1* and *Dlx2* overlap, and incisors grow where *Msx1* and *Msx2* overlap (Ferguson et al., 2000a; Ferguson et al., 2000b).

This model was derived in part from gene knockout experiments that resulted in either the loss of different tooth classes (e.g. maxillary molars) or a change in tooth shape (e.g. molars forming in the incisor region). For example, using exogenous Noggin protein beads to inhibit BMP4, which normally restricts expression of *Barx1* to the presumptive molar region of the mandible, Tucker and colleagues (1998) were able to induce expression of *Barx1* in the presumptive incisor region of the mandible, and transform tooth identity from an incisor to a molar. It seems reasonable that the determination of tooth types present in primates that are not present in mice (i.e., premolars and canines) is similarly controlled by the nested expression of homeobox genes. Under the OHC model there is not one specific gene that is responsible for each tooth type, and because the code is overlapping it can specify a wide range of subtle differences in tooth shape (Cobourne and Sharpe, 2003).

Patterning cascade mode of cusp development. A patterning cascade mode of tooth development, inspired by the developmental genetic research discussed above, has recently been proposed to explain the variation in cusp size, cusp spacing and total cusp number observed in multicuspid tooth crowns (Weiss et al., 1998; Polly, 1998; Jernvall, 2000; Jernvall and Thesleff, 2000). The primary tenet of this model is that the mechanisms inducing cusp formation and mechanisms controlling growth of cusps are both active throughout crown development; this continuous interaction between inductive and morphogenetic mechanisms is referred to as being morphodynamic. Under a

morphodynamic model cusp initiation is sequential and the location and size of later forming cusps is influenced by the location and size of previously forming cusps (Salazar-Ciudad et al., 2003). In developmental terms, the positioning of later forming secondary enamel knots (and their associated cusps) is dependent on the positioning of previously forming secondary enamel knots. For example, when a broader inhibition field around the initial enamel knot(s) increases cusp spacing, cusp number will either be reduced or the later-forming cusps will be smaller in size. Conversely, when a narrower inhibition field decreases cusp spacing the number of cusps will be increased or the later-forming cusps will be larger.

This prediction has been experimentally demonstrated by a number of studies. Kangas and colleagues (2004) determined that altering of expression levels of a signal gene (Eda) had profound effects on the resulting dental phenotype with underexpression resulting in smaller molars with fewer cusps, and overexpression resulting in the formation of supernumerary molars and molars with more cusps. Kassai and colleagues (2005) identified ectodin, a bone morphogenetic protein inhibitor, as one contributing factor controlling the size and spacing of mouse enamel knots, as well as, the number of molars.

Jernvall (2000) stresses that while large phenotypic differences can result from minor developmental changes affecting cusp spacing and growth, it is not always necessary to have a change in developmental information for cusp patterning to evolve (in terms of either the gain or loss of cusps). For example, if other factors are held constant under the patterning cascade model, an increase in overall tooth crown size will tend to result in the appearance of more cusps and a decrease in crown size will tend to

diminish cusp number. Cai and colleagues (2007) in a recent analysis using heterospecific recombinations of tissues of molar tooth germs of mice and rats determined that dental epithelium was responsible for cusp size and dental mesenchyme responsible for tooth size. Thus, cusp number and patterning is regulated by overall tooth size and cusp size. This could be an important factor when weighing the phylogenetic significance of variation in cusp number between closely related taxa of differing body size. Jernvall and Jung (2000) note that teeth with complex, multicuspid crowns may have independent patterning cascades for different parts of the tooth (e.g., trigonid vs. talonid) or different groups of cusps (e.g., paracone-protocone-Carabelli cascade and a paracone-metacone cascade). If true, such a developmental scenario would have clear implications for interpreting patterns of variation and covariation of cusp morphology across the tooth crown.

Interpreting molar crown variation within a developmental framework. What are the implications of the development of molar teeth, as discussed above, for the interpretation of morphological variation in the EDJ. Under a simple model that is applicable to the study of fully formed teeth, two processes occur that are primarily responsible for the morphology of the tooth crown that erupts into the mouth. The first process is the growth and folding of the inner enamel epithelium (IEE) prior to mineralization. It is within the IEE that enamel knots form and their location marks the site of future dentine horns (pointed, conical structures similar in shape to, and underlying the cusps seen on the OES). Dentine horns appear sequentially on the developing IEE. The timing of initiation and spatial relationships between these dentine

horns dictate the overall appearance of the tooth crown in terms of its cusps. The final form of the IEE is preserved in the tooth crown as the EDJ.

The second process involves the mineralization of the tooth germ. Deposition of enamel matrix on the tooth germ begins at the tips of the dentine horns and proceeds down their slopes. These individual islands of mineralizing enamel eventually coalesce in the valleys between dentine horns and the mineralization front continues extending until it reaches the cervix, or neck, of the tooth. Because the IEE can continue to grow between mineralizing dentine horns until they coalesce, the early process of IEE growth and folding and the later process of enamel deposition are not completely distinct and the former is likely partially influenced by the latter. How the enamel deposition alters the shape of the outer enamel surface, from a default shape that is the EDJ, is dictated by the rate at which ameloblasts differentiate, their daily secretion rate and the duration over which they secrete enamel. It is important to remember that both the EDJ and enamel distribution can express variation in a population, upon which natural selection can act. Thus, changes in tooth crown morphology may involve early and/or late developmental processes.

"Only by knowing the developmental processes generating a character can we make reliable inferences on inheritance and character independence" (Jernvall and Jung, 2000:185). This statement reflects the increasing role that developmental genetics will play as researchers attempt to evaluate the phylogenetic signal present in different aspects of tooth crown morphology. Morphological characters used in phylogenetic systematics are assumed to be independent of each other and to satisfy the criteria of homology. Understanding their development and evolvability is an important step in validating these

assumptions. Developmental research is also offering new definitions of homology with which systematists must grapple: “homology is not just a static genetic code readable deep inside the genome, but rather, it is a readout of the information stored in the dynamic cusp-making program (Jernvall and Jung, 2000:187).”

In an attempt to evaluate dental characters from a developmental perspective Jernvall and Jung (2000) grouped dental characters into four categories: initiation, termination, cusp shape and configuration characters. Variation in the timing of initiation of cusps affects individual cusp size and cusp number. Small cusps are more likely to show size differences and there would be higher potential for homoplasy in the presence/absence of small cusps. Specific examples outlined by Jernvall and Jung (2000) are hypocone size, nanopithexfold size, paraconule size, talonid height and cristid obliqua size. Variation in the timing of the termination of growth affects the morphology of both individual cusps and the tooth crown as a whole. Early termination of crown growth results in shorter crowns and a decreased frequency of small cusps. Differential timing in the termination of growth between cusps influences cusp spacing, relative cusp size, and the presence of lophs between cusps.

Cusp shape characters are also influenced by variation in the relative growth of the epithelium and mesenchyme that affect the pointedness or bluntness of cusps, and the convexity of the cusp walls. Configuration characters are influenced by differences in the spatial organization of cusps prior to initiation, in association with secondary enamel knots, and beginning with the first forming cusps and propagating along the crown. Thus there should be correlation between mesial and distal cusp configurations (Jernvall and Jung, 2000). Examples of this are the positions of the hypocone and paraconid and the

orientation of the cristid obliqua. So if cusp pattern is the product of a dynamic developmental program and the same developmental processes may relate aspects of individual cusp shape and size, the independence of certain types of tooth crown characters becomes doubtful. However, such conclusions are based on murine studies that have some major limitations when extrapolated to other mammal groups. Mice do not have successional sets of teeth, they have one incisor in each half of each dental arcade that is continuously growing, and they have a diastema in place of premolars.

Researchers interested in the evolution of extant and extinct primate dentitions are beginning to incorporate developmental data into reinterpretations of the growth processes responsible for the variation present in primate dental patterning (Jernvall and Jung, 2000), as well as in reassessments of the validity of dental characters historically used in primate phylogenetics (McCollum and Sharpe, 2001). In this thesis I examine the presence and variation of EDJ dental traits, such as accessory cusps, within the context of this developmental paradigm.

Taxonomy of the common chimpanzee

Two species of chimpanzee are commonly recognized: *Pan paniscus* and *Pan troglodytes*. *Pan paniscus*, also referred to as the bonobo or pygmy chimpanzee, is found in the Democratic Republic of the Congo and its range is confined by the Congo River that serves as geographic barrier (Kortland, 1995). The species distinction between *Pan paniscus* and *Pan troglodytes* has been supported by both morphological studies (e.g., Johanson, 1974; Shea et al., 1993; Uchida, 1996, Pilbrow, 2006a and references therein) and by molecular studies (Ruvolo et al., 1994; Morin et al., 1994; Won and Hey, 2005;

Becquet et al., 2007). The commonly recognized subspecies of *Pan troglodytes* include: *Pan troglodytes verus* (western chimpanzees separated by the Dahomey gap), *Pan troglodytes vellorosus* (Nigerian chimpanzees separated by the Sanaga River), *Pan troglodytes troglodytes* (central chimpanzees separated by the Ubangi River), and *Pan troglodytes schweinfurthii* (eastern chimpanzees separated by the Ubangi River and Congo River).

While the subspecies distinction of each of these taxa is debated (Fischer et al., 2006) and is more strongly supported for some taxa (e.g., *P. t. verus*) than others (e.g., the distinction between *P. t. troglodytes* and *P. t. schweinfurthii*), evidence supporting their distinction is both morphological (Johanson, 1974; Shea et al., 1993; Uchida, 1996, Pilbrow, 2003, 2006a) and molecular (Morin et al., 1994; Stone et al., 2002; Won and Hey, 2005; Gonder et al., 2006; Becquet et al., 2007). Both morphological and genetic evidence suggest that *P. t. verus* is the most distinctive (either due to earlier genetic isolation or smaller effective population size) of the other three subspecies. Genetic diversity is relatively low for *P. t. verus* and *P. paniscus* compared to *P. t. troglodytes* which is shows the highest genetic diversity (Becquet et al., 2007). Due to methodological differences current molecular based estimates for the divergence time between *Pan* species and subspecies differ among studies. Based on two recent analyses a cautious estimate for the divergence of *P. paniscus* and *P. troglodytes* is 1.5 – 1.0 Ma, and between *P. t. verus* and the central and eastern subspecies is 0.9 -0.5 Ma (Won and Hey, 2005; Becquet et al., 2007).

Molar morphology of southern African fossil hominins

In this thesis I compare the molar morphology of two southern African fossil hominins: *Australopithecus africanus* and *Paranthropus robustus*. While the generic distinction between these taxa is not central to the topic of this thesis it is adopted following the arguments for a both a grade and clade distinction between these taxa (see Wood and Constantino, 2007 and references therein). *Australopithecus africanus* is well represented by craniodental (and some postcranial) fossils from the sites of Sterkfontein, Makapansgat, Taung and Gladysvale, South Africa. These fossils date to between 3.0 and 2.4 Ma. *Paranthropus robustus* fossils derive from the sites of Kromdraai, Swartkrans, Gondolin, Drimolen, and Cooper's Cave, South Africa, which are dated to 2.0 – 1.5 Ma. The following is a review of those aspects of molar crown morphology that distinguish the two taxa.

Robinson (1956) observed that mandibular molars are larger in *P. robustus* than in *Au. africanus* and exhibit a size gradient of $M_1<M_2<M_3$ in the former and $M_1<M_2>M_3$ in the latter. Wood and Abbott (1983) noted a molar size gradient of $M_1<M_2\approx M_3$ for both taxa and Suwa and colleagues (1994) found significant crown size difference in M_1 (*P. robustus* larger), but non-significant differences in the crown size of M_2 and M_3. Wood and Abbott (1983) found no significant difference in crown shape (*contra* Robinson [1956] who suggested that *P. robustus* molars are more oval in shape while *Au. africanus* molars are more rectangular). In an analysis of cusp areas Wood and colleagues (1983) noted that M_1s of *P. robustus* and *Au. africanus* differed significantly in the relative size of the protoconid, metaconid and hypoconulid, while M_2s and M_3s exhibited significant relative size difference only in the hypoconulid. They argued that robust taxa trend towards a reduction of the protoconid and metaconid and an increase in the entoconid and

hypoconulid in M_1 and M_2, and that fissure pattern is similar between taxa at each molar position. Suwa and colleagues (1994) found that *P. robustus* tended to exhibit a relatively smaller protoconid area (M_1, M_2 and M_3), a relatively larger hypoconulid (M_1), and relatively larger entoconid (M_2). Robinson (1963, cited in Wood et al., 1983) also suggested that *P. robustus* teeth are low cusped compared to *Au. africanus*. Grine (2004) documented considerable overlap in mesiodistal and buccolingual diameters of upper and lower molars between *Au. africanus* and *P. robustus/crassidens*.

With regard to discrete dental traits Robinson (1956) noted a tendency for well-developed protoconidal cingulum in *Au. africanus* that is not well-developed in *P. robustus*. Wood and Abbott (1983) noted a greater incidence of protostylid expression in *P. robustus*, but more marked expression when present in *Au. africanus*. Hlusko (2004) found significantly different frequency distributions (although Bonferonni correction eliminated its statistical significance) of protostylid expression between *Au. africanus* and *P. robustus*. She noted that *Au. africanus* tends toward a bimodal distribution, with either no expression or a high degree of expression, while *P. robustus* is the opposite with an approximately normal distribution of protostylid expression, and consequently, that it is frequency distribution that separates the two taxa and not a central tendency. Guatelli-Steinberg and Irish (2005) also found that *Au. africanus* exhibited greater expression protostylid (LM1). It is worth noting that Robinson (1956) considered that treatment of the protostylid as a unit character (Dahlberg, 1950; Hlusko, 2004) was not supported due to the presence of a cingulum farther back on the buccal surface as well as on the whole mesial face of the crown. Greater frequency (Robinson, 1956; Wood and Abbott, 1983, Guatelli-Steinberg and Irish, 2005) and relative size (Suwa et al., 1994) of C6 in molars

of *P. robustus* compared to those of *Au. africanus* has been noted as well as a higher incidence of C7 of *Au. africanus* (Wood and Abbott, 1983; Guatelli-Steinberg and Irish, 2005). Irish and Guatelli-Steinberg (2003) found a high frequency of a MTC on LM1 (but check frequency) in *Au. africanus*. Robinson (1956) noted that *Au. africanus* can exhibit a double anterior fovea while only a single fovea is present in *P. robustus* and a flatter slope on buccal face than lingual in *Au. africanus*.

Based on both quantitative and qualitative dental traits, the taxonomic distinction between *Au. africanus* and *P. robustus* is well supported. Although for any particular tooth, or for an unknown specimen, the reliability of linear dimensions, relative cusp areas, or discrete trait analysis to provide a clear taxonomic affiliation is limited. One of the goals of this thesis is to explore whether comparisons of the detailed shape of the EDJ would provide a more reliable means of determining the taxonomic affinities of fossil hominin teeth.

Materials

The complete list of molar teeth used in each analysis of this thesis are given in Appendix A. A number of teeth are used in multiple analyses, and they are identified in the Appendix. The sample includes *P. paniscus* (Pp) and two subspecies of *P. troglodytes* (Pt), *P. t. troglodytes* (Ptt) and *P. t. verus* (Ptv). The Ptt sample derives from the Museum für Naturkunde (denoted as ZMB) in Berlin, Germany and the subspecies designation is based on localities (located in Cameroon or Gabon) from which the specimens originate. The Ptv sample derives from a skeletal collection housed at the Max Planck Institute for Evolutionary Anthropology in Leipzig, Germany (MPI-EVA). The collection derives

from naturally deceased individuals collected within the research mandate of the Taï Chimpanzee Project based in the Taï National Park, Republic of Côte d'Ivoire, and only Ptv is present in this area. The Pp sample derives from the Royal Museum for Central Africa in Tervuren, Belgium (MRAC). Species designation is based on locality information and museum catalogue information associated with each specimen. Nine additional individuals from the Museum für Naturkunde and two from the Royal Museum for Central Africa are either captive specimens, or do not have locality information. All molars are from associated mandibles from which the tooth type is determined (e.g., first or second mandibular molar).

The *Gorilla g. beringei* specimens derive from mandibles curated at the National Museum of Natural History (NMNH), Smithsonian Institution, Washington, USA. They were collected in Rwanda and their taxonomic affiliation is based on museum records. The three *Pongo pygmaeus* molars are curated at ZMB and their taxonomic affiliation, when available, is based on museum records. Two modern human molars also come from the NMNH, but they are from a collection of isolated specimens and therefore their tooth type is not certain and they are considered either first or second molars. Two modern human molars derive from mandibles belonging to Bronze Age burials. One is curated by Headland Archaeology Ltd (HA), Edinburgh, Scotland and the other by the Hull and East Riding Museum (HE), Hull, UK.

The fossil hominin sample includes *Au. africanus* molars from the site of Sterkfontein Member 4 (Moggi-Cecchi et al., 2006) and *P. robustus* molars from the sites of Swartktrans, Gondolin and Drimolen (Robinson, 1956; Tobias et al., 1977; Grine 1989; Menter et al., 1999; Keyser et al., 2000; De Ruiter, pers. comm. 2006). These

specimens are curated at the Transvaal Museum (TM), Northern Flagship Institution, Pretoria and The University of Witwatersrand (UW), Johannesburg, South Africa. The taxonomic affiliation and tooth type for each specimen were determined from the above references. Four molars belonging to *H. neanderthalensis* derive from the site of El Sidron, Spain (Rosas et al., 2006) and are curated at the Museo Nacional de Ciencias Naturales (MNCN), Madrid, Spain. The single *Gigantopithecus blacki* specimen is curated at the Senckenberg Forschungsinstitut und Naturmuseum (SFN), Frankfurt, Germany and was collected by von Koenigswald from a Chinese drugstore in Hong Kong (Weidenreich, 1945; von Koenigswald, 1952). This tooth is listed as a third molar (Specimen 4) by von Koenigswald (1952), however, it is not clear what the criteria were for this designation. Given the divergent distal root I believe it is possible that this molar is a second molar from an immature individual.

Methods

Many of the methods employed were used in multiple analyses and are discussed in each chapter as appropriate. In this section I discuss a number of methodological issues in greater detail than in specific chapters as the chapters were written in manuscript form, which necessitates a limited discussion of methodological issues in some cases. The methods discussed below include 1) micro-computed tomography, 2) tissue segmentation and surface generation protocols, and 3) geometric morphometric analyses, and 4) visualization of EDJ shape differences.

Micro-computed tomography

Microcomputed tomography of dental specimens was completed using two tomographic scanners. The first system is a SKYSCAN 1172 Desktop Scanner and the following scan parameters were used: 100 Kv, 94 mA, 2.0mm aluminum and copper filter, 0.12 – 0.15 rotation step, 1024 x 1024 or 2048 x 2048 matrix, 360 degrees of rotation, 2 frame averaging. Raw projections were converted into TIFF image stacks using NRecon (parameters: ring artifact correction = 10; beam hardening = 30%). Pixel dimensions and slice thickness between reconstructed serial images were isometric with resolutions ranging between 14 and 28 microns (µm) (e.g., isometric voxels of 14 µm × 14 µm × 14 µm to 28 µm × 28 µm × 28 µm).

The second system is a SCANCO µCT40 and the following scan parameters were used: 70 Kv, 114 µA, 0.36 rotation step, 1024 x 1024 matrix, 180 degrees of rotation, no frame averaging. Pixel dimensions and slice spacing of the resultant images were 16µm. In some cases image stacks were downsampled from their original resolution in order to reduce the size of the data and facilitate processing of the tomographic scans. The effect of downsampling on the resulting analyses of EDJ shape is addressed below.

Tissue segmentation and surface generation protocols

To facilitate tissue segmentation, the complete image stack for each tooth was filtered using a three-dimensional median filter (kernel size of 1 or 3) followed by a mean of least variance filter (kernel size of 1 or 3), implemented as a computer-programmed macro. This filtering process results in more homogenous tissue classes (e.g., enamel vs. dentine) and allocates pixels with intermediate gray-scale values at tissue interfaces (i.e., air-enamel, enamel-dentine, air-dentine) to the appropriate tissue (Schulze and Pearce,

1994). The effect of filtering on the resulting analyses of EDJ shape is addressed below. The choice of kernel size was dictated by the degree of contrast between enamel and dentine tissue. When contrast is high (i.e., the range of gray-scale values representing each tissue are distinct and with little overlap) a kernel size of one is used. When contrast is low a kernel size of three is used in order to reduce the need for significant amounts of manual segmentation.

Filtered image stacks were imported into the Amira software package (v4.1, www.amiravis.com) and enamel and dentine tissues were segmented using the 3D voxel value histogram and its distribution of gray-scale values, which typically presents a trimodal distribution with one peak representing dentine, another peak representing enamel, and a third peak representing air and background noise in the image stack. In fossil teeth where the enamel and dentine differ substantially in their degree of mineralization (and therefore their densities, and thus also in the ability of X-rays to pass through them), the filtering process results in gray-scale pixel value distributions for each tissue that do not overlap. In other teeth, diagenetic alteration (e.g., dentine remineralization) may result in similar tissue densities and thus overlapping gray-scale pixel value ranges for enamel and dentine (Olejniczak and Grine, 2006). Even after filtering, there is often an incomplete separation between the two, and a decision must be made about the range of gray-scale values allocated to each tissue. Only teeth in which there was a clear separation of enamel and dentine, resulting in well-distinguished gray-scale values and accurate representations of the EDJ, were included. Operationally, this meant that if the tooth could not be segmented using a filter kernel size of 1 or 3 it was

removed from the study as larger kernel sizes prevent accurate representations of the EDJ and OES.

After segmentation, the enamel cap and EDJ are reconstructed as triangle-based surface models using Amira (surface generation module using unconstrained smoothing parameter). The OES and EDJ of a chimpanzee molar are illustrated in Fig. 1.1. Small portions of the enamel cap or EDJ are missing in some teeth, or are damaged due to cracks, and in these cases the defects were corrected digitally using the software Geomagic Studio 10 (www.geomagic.com). Teeth that show evidence of significant damage or missing areas were excluded from the study. In a few teeth that were minimally worn the tips of the dentine horns were repaired using the "Fill Holes" feature in Geomagic Studio 10. In specimens that preserved only the enamel cap, a surface model of the EDJ was created by digitally removing the occlusal surface of the reconstructed enamel cap surface model.

Geometric morphometric analysis protocols

The GM analysis of EDJ shape involves a number of steps that are outlined in detail below. These steps can be summarized as 1) the collection of anatomical landmarks, 2) the derivation of a homologous set of landmarks for each specimen; 3) Procrustes superimposition of the landmarks of each specimen, 4) statistical analyses of shape variation within and between groups, and 5) visualization of shape variation within and between groups.

Collection of anatomical landmarks. EDJ surface models (PLY format) were imported into Amira for the collection of the Cartesian coordinates of three sets of

anatomical landmarks (see Chapter 2, Fig. 2.1). The first set (referred to as "MAIN") included eight landmarks: one on the tip of the dentine horn of each primary cusp [i.e., protoconid (1), metaconid (2), entoconid (3), hypoconid (4) and hypoconulid (5)], one at the lowest point on the crests connecting, respectively, the protoconid and metaconid (6), the protoconid and hypoconid (7), and the hypoconid and hypoconulid (8). The second set (referred to as the "RIDGE" curve) includes landmarks (approximately 50-70) along the top of the ridges running between each of the five dentine horns. This set of landmarks forms a closed ellipse, beginning at the tip of the protoconid and proceeding anticlockwise in a lingual direction. In the case of teeth with accessory cusps (e.g., cusp 6 or cusp 7) these dentine horns were ignored and landmarks were collected on either side of the feature. The third set (referred to as the "CERVIX" curve) includes landmarks (approximately 40-50) along the cervix, or cemento-enamel junction, of the tooth crown. This set of landmarks also forms a closed ellipse, beginning on the cervix below the protoconid dentine horn and proceeding anticlockwise in a lingual direction. Where small fragments of enamel were missing at the cervix its location was estimated. Landmark datasets were exported as text files.

Derivation of homologous landmarks. For each specimen a single set of homologous landmarks and semilandmarks is derived from the three landmark files discussed above. For both the RIDGE and CERVIX curve landmark sets a smooth curve is interpolated using a cubic spline function (note: a cubic spline is used so that the curve is forced to pass through each measured coordinate). Interpolated curves are then resampled to achieve identical point counts between specimens – these resampled points were used as semilandmarks. In the case of the RIDGE curve the eight MAIN landmarks

are projected onto the curve dividing it into eight sections. For each section a large sample of very closely spaced points are computed along the curve and the distances between adjacent points are calculated and summed to approximate the length along the curve between the MAIN landmarks. Each length is divided by a given number and the coordinate location at each equally spaced distance is recorded. The number of divisions between the MAIN landmarks is: ten between #2 and #3 and #3 and #5, seven between #2 and #6 and #1 and #6, five between #1 and #7 and #7 and #4, four between #4 and #8 and #8 and #5. In the case of the cervix curve, its length is calculated in the same way and 70 equidistantly spaced points are derived.

These equidistantly spaced points are then used as starting positions for the semilandmark algorithm: semilandmarks were iteratively allowed to slide along their respective curves (i.e., RIDGE curve [N =60 including the eight MAIN landmarks] and CERVIX curve [N = 70]) to minimize the bending energy of the thin-plate spline interpolation function computed between each specimen and the sample Procrustes average. We used the algorithm of Bookstein (1997; Gunz et al., 2005) that allows points to slide along tangents to the curve. These tangents were approximated for each semilandmark by the vector between the two neighboring points. Only the tips of the dentine horns were used as fixed landmarks, all other points were treated as semilandmarks. After sliding these semilandmarks are considered homologous for the purpose of multivariate analyses.

Procrustes superimposition. The homologous set of landmarks and semilandmarks is converted to shape coordinates by Generalized Least Squares Procrustes superimposition (Gower, 1975; Rohlf and Slice, 1990). This removes information about

location and orientation from the raw coordinates and standardizes each specimen to unit centroid size; a size-measure computed as the square root of the sum of squared Euclidean distances from each landmark to the specimen's centroid (Dryden and Mardia, 1998). All data preprocessing was done in Mathematica v6.0 (www.wolfram.com) using a software routine written by Philipp Gunz.

Analysis of EDJ shape. Two statistical methods were used to assess EDJ shape variation between taxon and tooth type in chapters two and three. A principal components analysis (PCA) of shape coordinates (Bookstein, 1991; Rohlf, 1993) after Procrustes superimposition is an eigen-decomposition of the variance-covariance matrix of Procrustes coordinates. It creates a set of hypothetical variables (principal components or PC), that are linear combinations of the original variables. Beginning with the first PC, it produces orthogonal axes which represent major aspects of shape variation (Hammer and Harper, 2006).

A canonical variates analysis (CVA) was used to assess the degree of EDJ shape difference between taxa and tooth type and to identify those aspects of shape that best separate groups. In each case the CVA was computed as linear discriminants in the software package R (www.r-project.org) in the subspace of the first few principal components (i.e., using only a subset of all PCs) of the Procrustes shape coordinates. Projecting into a lower dimensional subspace was necessary because the number of variables (i.e., landmarks) greatly exceeded the sample size (i.e., molar teeth); using too many variables to compute the discriminant axes can result in an unrealistic and unstable degree of discrimination. The decision as to the number of PCs to incorporate into the CVA was guided by a protocol in which the specimen labels were randomized and the

resulting CVA was assessed with different numbers of PCs included. The number of PCs included (usually 5-10) did not exceed the point at which randomized labels began to exhibit clustering patterns in the resulting CVA. In other words, it was confirmed that there was no separation between randomly relabeled groups. This phenomenon of clustering in a randomized dataset is illustrated in Fig. 1.2. A CVA of original second molar data using 6 PCs exhibits marked separation among the groups. With randomized data, clustering appears with the inclusion of an increasing number of PCs.

The accuracy with which EDJ shape correctly classifies molars, according to species and tooth type, was tested by cross validating the canonical variates analysis. In this process each specimen in turn was considered unclassified and then classified by all the others using posterior probabilities. Classification was implemented in R with groups assigned equal prior probabilities.

Visualization of EDJ shape change

An advantage of the geometric morphometric methodology employed to compare EDJ morphology is that differences in EDJ shape can be visualized in 3D using the quantitative results of the statistical analyses. To do so, an EDJ surface model can be deformed with respect to changes in shape among specimens in the study sample (Gunz and Harvati, 2007). This method is employed in two ways in this thesis. First, it is used to visualize the mean shape of groups (e.g., the mean shape of the first molar of *Au. africanus* compared to the mean shape of the first molar of *P. robustus*). Second, it is used to visualize shape differences along canonical variate axes that separate species and/or molar type (chapter three). The first step involves the creation of a generic EDJ

surface model. This was accomplished by collecting several thousand landmarks in Amira on the EDJ of one molar of the study sample (either a *Pan* molar or a hominin molar). These points were converted to a triangulated surface model (PLY file format) using Geomagic Studio 10 (*wrap* module). The thin-plate spline interpolation function between the landmarks of this specimen and the appropriate mean configuration Procrustes shape space was used to bring this surface model into Procrustes shape space. Finally, a thin-plate spline interpolation was computed to morph this generic surface model (now in Procrustes shape space) into a target form. For the visualization of the mean shape of a particular group the target form was the group average of Procrustes shape coordinates. For the visualization of a CVA axis the generic surface model (now in Procrustes shape space) was morphed by regressing all Procrustes shape coordinates on the respective CVA scores and adding a scaling factor.

The effect of downsampling image resolution on EDJ surface morphology

In most cases in the study sample, teeth were downsampled from an original resolution of ~14 µm voxel resolution to ~30 µm voxel resolution in order to reduce the amount of data to a more manageable level and to speed up the manual segmentation of some specimens. I tested the effect of downsampling on both qualitative and quantitative analyses in order to ensure that this source of variation was unlikely to influence the results of my analyses. To do so one chimpanzee tooth was downsampled to three different resolutions in Amira using the *resample* function (Triangle filter). This resulted in four image stacks with resolutions of 14 µm, 28 µm, 50 µm and 100 µm. Each image stack was filtered using a 3D median filter (kernel size = 1) and a mean of least variance

filter (kernel size = 1) to facilitate tissue segmentation. From each segmented stack a surface model of the EDJ was reconstructed (Fig. 1.3).

To test the influence of downsampling on the geometric morphometric analysis of EDJ shape a landmark data set (as discussed above) was collected on each EDJ surface. These four data sets were included in an analysis of EDJ shape as individual specimens, along with other chimpanzee teeth. Figure 1.4 presents the resulting PCA plot of the first and second principal components. As can be seen from this figure downsampling can influence the results of such analysis, particularly when the degree of downsampling exceeds a factor of two (e.g., represented by the 50 µm and 100 µm models). This is likely due to the differences in the height of the dentine horns and the location of the cervix which are altered with increasingly downsampled data.

For the qualitative test the EDJ surfaces generated from each resolution were compared with respect to pertinent aspects of shape (e.g., dentine horn shape and size of the main cusps, crest morphology, accessory cusp dentine horn morphology, and cervix position). There are only minor alterations in the morphology of the EDJ between the 14 µm and 28 µm surface models. The dentine horns of the primary cusps are similar in their degree of pointedness, those of the accessory cusps (in this case a double C6) are still identifiable, and the crests on the slopes of the dentine horns are similar in their degree of expression. The 50 µm surface model exhibits blunter dentine horns on both primary and accessory cusps and crests which are less pronounced. The 100 µm surface model is markedly different in its qualitatively assessed shape from the original EDJ surface. Dentine horn morphology is substantially altered, the crest morphology is absent within the occlusal basin and the mesial dentine horn of the double C6 is absent. The results of

this assessment suggest that accurate evaluation of qualitative morphology of the EDJ of hominoid teeth requires a voxel resolution no less ~50 µm and preferably less than 30 µm.

The effect of filtering microCT images on EDJ surface morphology

Filtering of microCT images is a widely accepted method to increase the signal to noise ratio within the image stacks and to facilitate tissue segmentation. Filtering does, however, alter the original data and therefore it was necessary to assess the affect of filtering on the data collected in this thesis. To do so a single chimpanzee tooth (voxel size of 14 µm) was assessed with no filtering, with a 3D median filter and mean of least variance filter each having a kernel size of one, and with a 3D median filter and mean of least variance filter each having a kernel size of three. For each filtered data set the dentine tissue was segmented and the EDJ surface reconstructed.

To test the influence of filtering on the geometric morphometric analysis of EDJ shape a landmark data set was collected on each EDJ surface. These three data sets were included in an analysis of EDJ shape as individual specimens, along with other chimpanzee teeth. Figure 1.4 presents the resulting PCA plot of the first and second principal components. As can be seen from this figure filtering with kernel sizes of one or three has little influence the results position of the specimen in Procrustes shape space and thus little influence on EDJ shape as captured by landmarks.

To test the influence of filtering on qualitatively assessed aspects of EDJ shape (e.g., dentine horn shape and size of the main cusps, crest morphology, accessory cusp dentine horn morphology, and cervix position) surface models resulting from each filter

combination were compared with a model derived with no filtering to the original data. As can be seen from Fig. 1.5 variation in the filter settings from no filtering, to kernel sizes of one and three has little affect on the morphology that is of interest for this thesis. The morphology of dentine horns and crest features is not altered significantly even when a filter size of 3 is used. Thus scoring of discrete traits involving accessory cusps and crests will not be significantly altered by the use of image filtering.

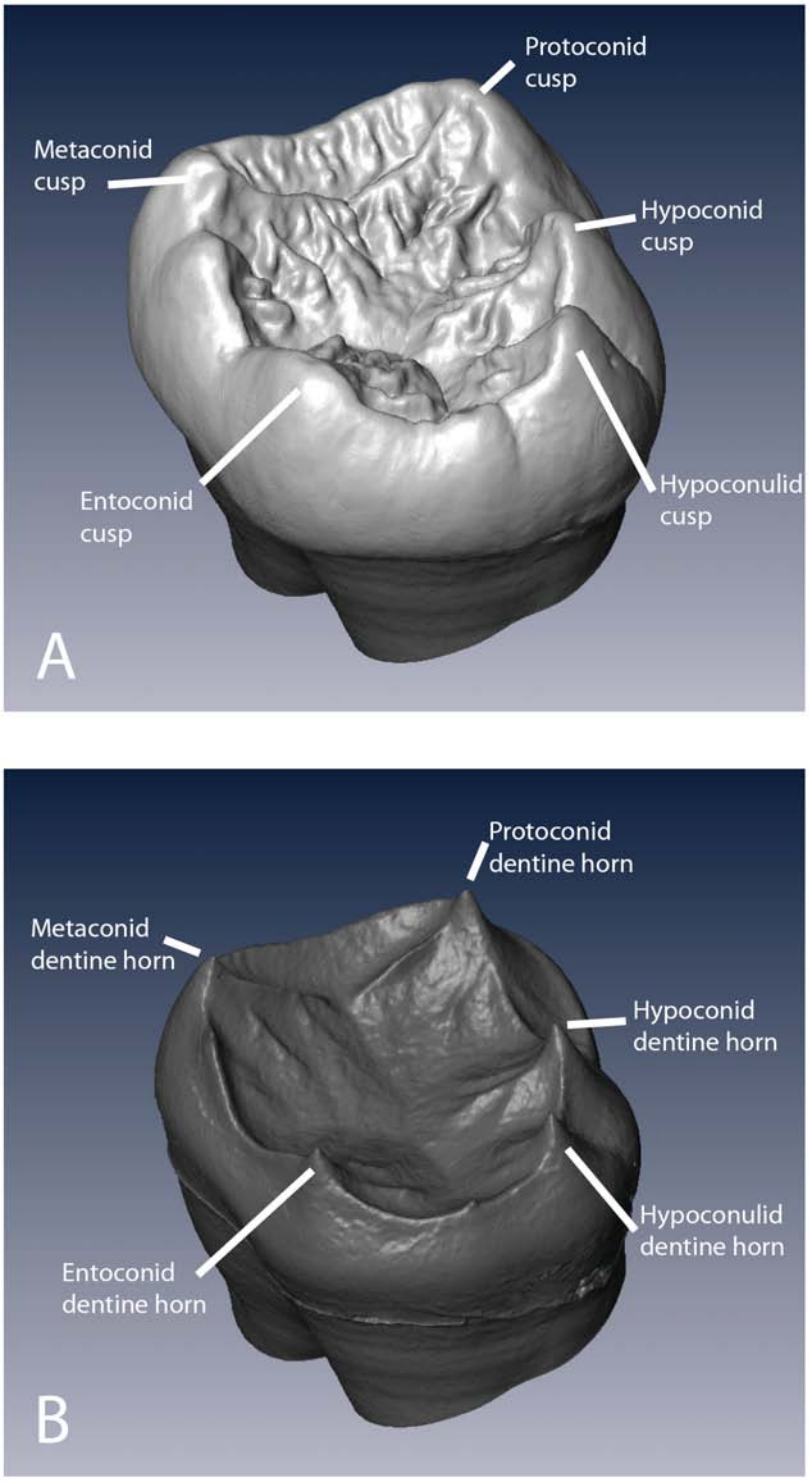

Figure 1.1. Surface reconstructions of the **A**) outer enamel surface and **B**) enamel-dentine junction. The major cusps on the OES and dentine horns on the EDJ are labeled.

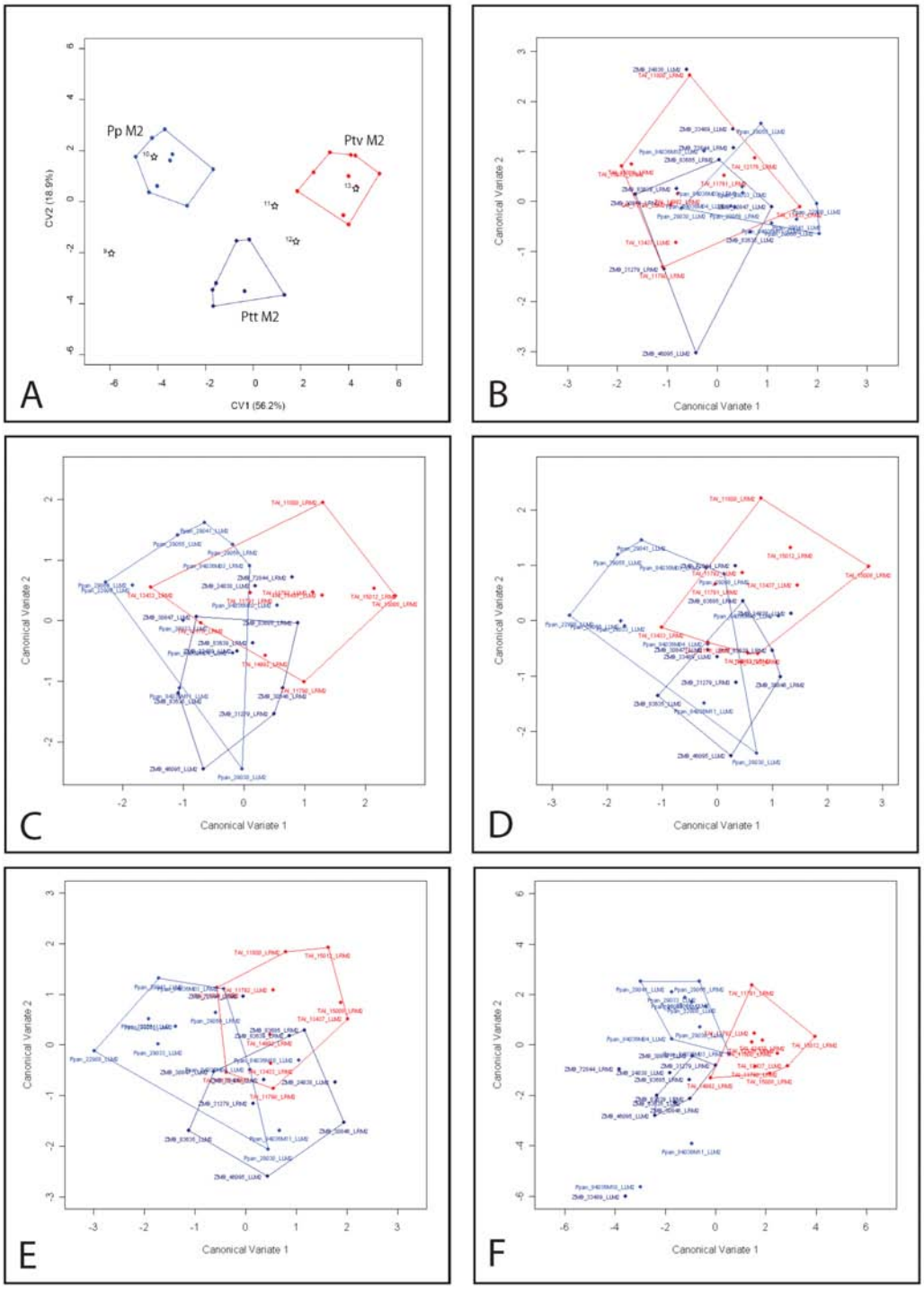

Figure 1.2. These CVA plots illustrate the potential problem of including a large number of PCs in a CVA analysis. A) CVA of original second molar data using 6 PCs showing strong separation between groups. With randomized data, which should exhibit no clustering, clustering is achieved with the inclusion of an increasing number of PCs. **B**) – **F**) CVAs based on 4, 6, 8, 10, 20 PCs respectively. The degree of overlap in (C) supports the use of 6 PCs in the original analysis.

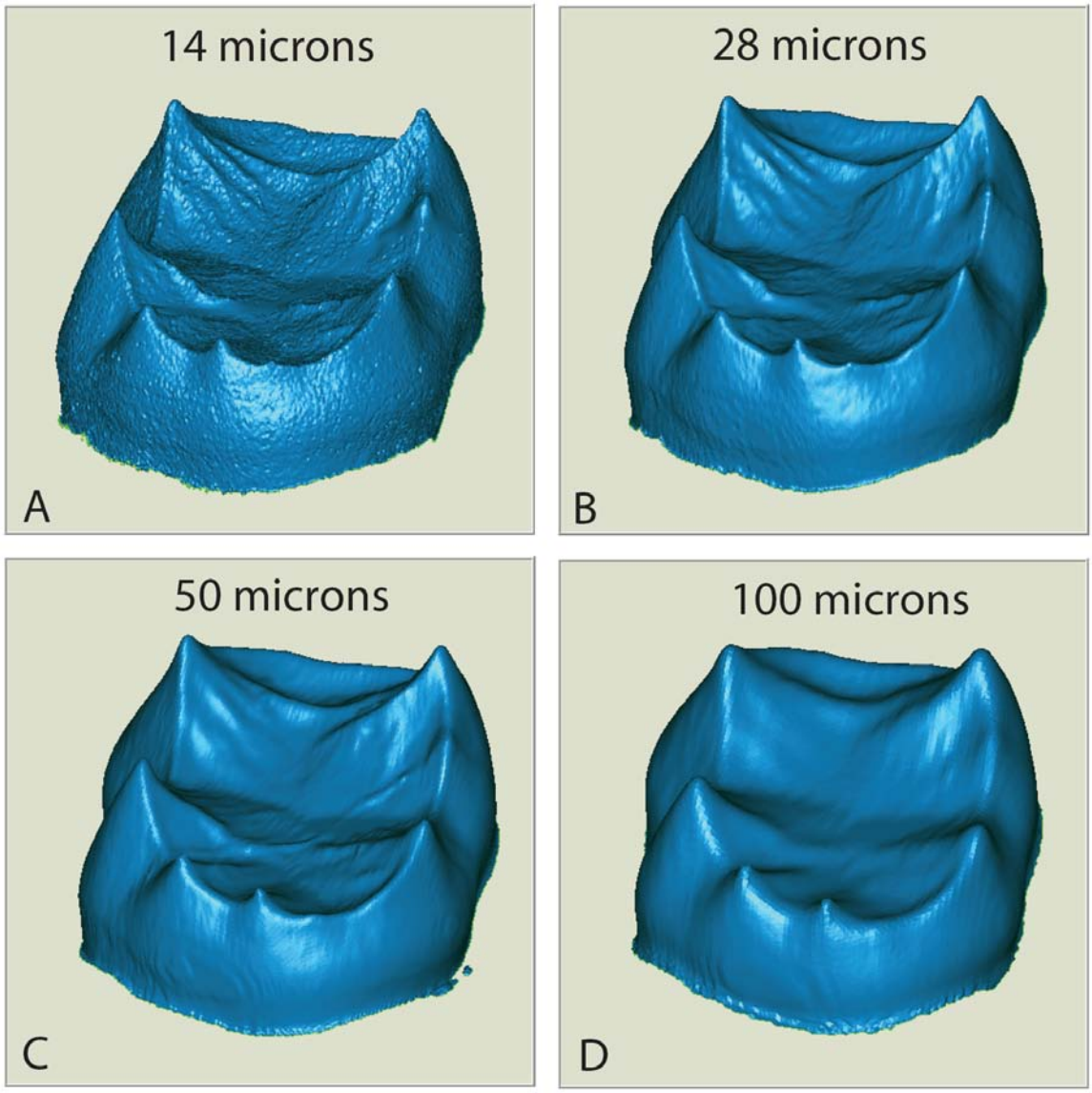

Figure 1.3. Illustration of the affect of downsampling the resolution of microCT image stacks on the resulting surface reconstruction of the EDJ. **A**) original 14 µm voxel size; **B**) 28 µm; **C**) 50 µm; **D**) 100 µm.

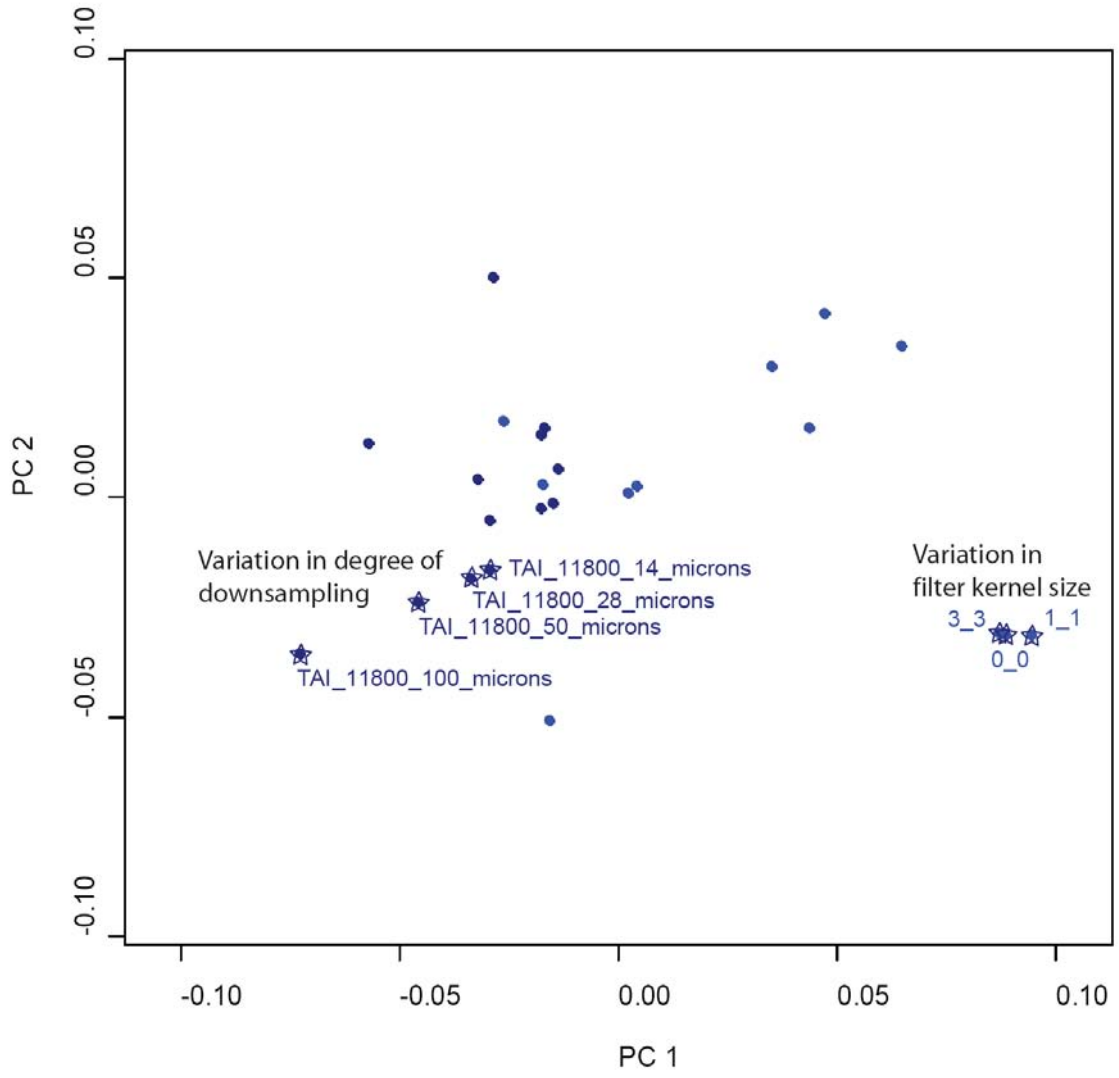

Figure 1.4. Principal component analysis assessing the influence of downsampling and filtering on the analysis of EDJ shape. Downsampling does not have a significant influence on Procrustes distances until resolutions reach 50 microns and greater. There is little influence on Procrustes distance either not using a filter or when the filter kernel size is 1_1 or 3_3.

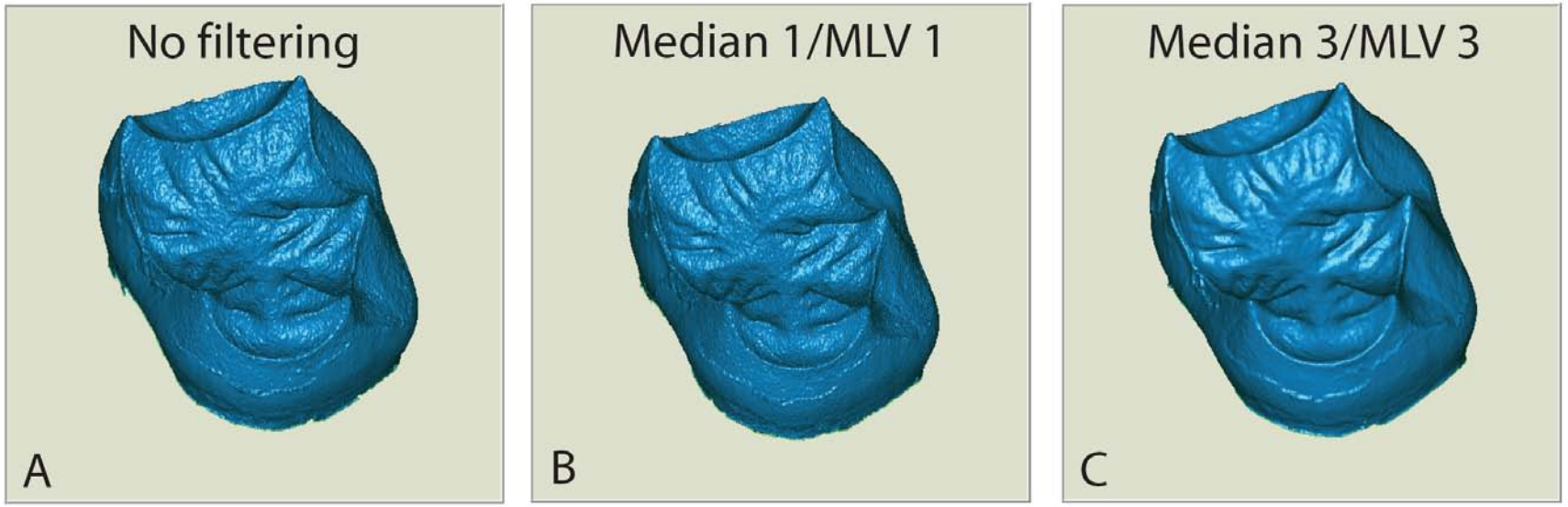

Figure 1.5. Illustration of the affect of filtering on the resulting surface reconstruction of the EDJ. **A**) No filtering; **B**) median and mean of least variance (MLV) with a kernel size of 1; **C**) median and mean of least variance with a kernel size of 3.

CHAPTER 2: DISCRIMINATION OF SPECIES AND SUBSPECIES OF *PAN* USING THE EDJ MORPHOLOGY OF LOWER MOLARS

Abstract

Previous research has demonstrated that species and subspecies of *Pan* can be distinguished on the basis of the shape of their molar crowns. Thus, there is potential for fossil hominin taxa to be distinguished at similar taxonomic levels, but because of occlusal attrition the surface morphology of tooth crowns is often absent in fossil teeth. The enamel-dentine junction (EDJ) of molar teeth possesses considerable information regarding the original shape of the tooth and is preserved longer than the outer enamel surface (OES). In this study we investigate whether the shape of the EDJ of lower first and second molars can distinguish species and subspecies of *Pan*. Micro-computed tomography is employed to non-destructively image the EDJ and geometric morphometric analytical methods are used to compare EDJ shape among samples of *Pan paniscus* (N = 17), *Pan t. troglodytes* (N = 14), and *Pan t. verus* (N = 18). The classification of specimens of unknown taxonomic affiliation (N = 13) is also assessed. Results indicate that EDJ morphology successfully distinguishes among both species and subspecies of *Pan* and can support the designation of unknown specimens to both taxon and molar type. Morphological differences in EDJ shape among taxa are subtle and relate to the relative height and spacing of the dentine horns, the height of the dentine crown, and the shape of the crown base.

Introduction

Molar crown morphology has been used to address taxonomic questions in extant apes (Johanson, 1974; Hartman, 1988; Uchida, 1992, 1996, 1998a,b; Pilbrow, 2003, 2006a,b) and fossil hominins (e.g., Robinson 1956; Sperber, 1974; Wood and Abbott, 1983; Wood et al., 1983, Wood, 1991; Suwa et al., 1994). The taxonomic distinctiveness of molar crown shape has most recently been demonstrated by Pilbrow (2003, 2006a) who, based on a large number of linear crown measurements, was able to distinguish between species, subspecies and even populations of African apes (particularly chimpanzees).

The description and analysis of newly discovered hominin fossil teeth has traditionally been limited to gross linear dimensions (e.g., buccolingual and mesiodistal diameter of the crown). This is understandable because in a partially worn fossil tooth not many aspects of shape can be measured and defended as being homologous. More recently measurements such as cusp surface areas and crown base shape have improved the discrimination of taxa, but considerable overlap often remains, limiting the taxonomic level at which closely related taxa can be distinguished. Unfortunately, the availability of these linear and areal measurements on worn fossil teeth is limited by attrition, and this limitation restricts our ability to apply analytical methods which incorporate the complexity of the shape of the OES.

It has long been acknowledged that the enamel-dentine junction (EDJ), which underlies the enamel cap of primate teeth, carries information about the original shape of the tooth crown (Kraus, 1952; Korenhof, 1960, 1961, 1982; Nager, 1960; Kraus and Jordan, 1965; Sakai et al., 1965, 1967a,b, 1969; Sakai and Hanamura, 1971, 1973a,b;

Corruccini, 1987a,b, 1998; Schwartz et al., 1998; Sasaki and Kanazawa, 1999; Skinner et al., 2008) and that it can be used as a source of taxonomically-relevant data (Corruccini, 1998; Olejniczak et al., 2004, 2007; Macchiarelli et al., 2006; Suwa et al., 2007; Skinner et al, nd). Furthermore, it is homologous among teeth and taxa, provides considerable scope for capturing detailed information about tooth shape, and is preserved throughout the initial stages of tooth wear (and longer in thicker-enameled, relatively bunodont lower-cusped hominin taxa).

The goal of this project is to assess the taxonomic distinctiveness of the EDJ morphology of lower molars in species and subspecies of *Pan*. If it can be demonstrated that the *Pan* EDJ can distinguish these taxonomic levels, then it is likely that the same method will have utility for discriminating the species and subspecies of the other genera within the *Pan*/*Homo* clade.

Chimpanzee taxonomy

Two species of chimpanzee are commonly recognized: *Pan paniscus* and *Pan troglodytes*. *Pan paniscus*, also referred to as the bonobo or pygmy chimpanzee, is found in the Democratic Republic of the Congo and its range is confined by the Congo River. The species distinction between *P. paniscus* and *P. troglodytes* has been supported by both morphological (e.g., Coolidge, 1933; Johanson, 1974; Shea et al., 1993; Uchida, 1996, Pilbrow, 2006a and references therein) and molecular studies (Ruvolo et al., 1994; Morin et al., 1994; Won and Hey, 2005; Becquet et al., 2007).

There are a number of commonly recognized subspecies of *Pan troglodytes* whose ranges are separated by geographic barriers: *Pan troglodytes verus* (western

chimpanzees separated by the Dahomey gap), *Pan troglodytes vellorosus* (Nigerian chimpanzees separated by the Sanaga River), *Pan troglodytes troglodytes* (central chimpanzees separated by the Ubangi River), and *Pan troglodytes schweinfurthii* (eastern chimpanzees separated by the Ubangi River and Congo River). While the subspecies distinction of each of these taxa is debated (Fischer et al., 2006) and is more strongly supported for some taxa (e.g., *P. t. verus*) than others (e.g., the distinction between *P. t. troglodytes* and *P. t. schweinfurthii*) evidence supporting their distinction is both morphological (Johanson, 1974; Shea et al., 1993; Uchida, 1996, Pilbrow, 2003, 2006a) and molecular (Morin et al., 1994; Stone et al., 2002; Won and Hey, 2005; Gonder et al., 2006; Becquet et al., 2007). Both morphological and genetic evidence suggest that *P. t. verus* is the most distinctive (either due to earlier genetic isolation or smaller effective population size) from the other three subspecies.

Hypotheses

Based on the results of previous studies (reviewed above) that have demonstrated the distinctiveness of molar crown shape among species and subspecies of *Pan*, and the evidence that the EDJ contributes significantly to crown shape (Korenhof, 1960; Kraus and Jordan, 1965; Corruccini, 1987a, 1998) we test two hypotheses. First, whether EDJ morphology of molar tooth crowns successfully distinguishes between species and subspecies of chimpanzee. Second, whether the subspecies of *P. troglodytes* are more similar in shape to each other than either is to *P. paniscus* and support phylogenetic relationships based on morphological and genetic data. Support for these hypotheses would suggest that the factors which have lead to divergence in tooth shape between taxa

act on the processes of early tooth development when the shape of the EDJ is being established. Lack of support for these hypotheses would suggest that EDJ morphology carries a more conservative taxonomic and phylogenetic signal and that differences in enamel growth are responsible for the findings of previous studies of the shape of the enamel surface.

In order to test these hypotheses we performed a geometric morphometrics analysis of anatomical landmarks collected on the surface of the EDJ. The EDJ surface of each molar was non-destructively imaged using micro-computed tomography. Anatomical landmarks on the EDJ were chosen to capture the overall crown shape of the dentine crown, including crown height, dentine horn height, dentine horn spacing and the shape of the cervix. This methodology not only allows the quantitative assessment of shape differences among taxa, but it also allows useful visual depictions of the shape differences that distinguish taxa. The first hypothesis was tested by assessing the accuracy with which molars were correctly classified to their known taxonomic affiliation and the second was tested by comparing the phenetic similarity between taxa against phylogenetic expectations based on molecular data. As for the teeth whose taxonomy is not so well established, for some of them there is strong circumstantial evidence (where and by whom they were recovered) and this information can be compared with the taxonomic affinities suggested by the EDJ morphology.

Materials and Methods

Study sample

The first and second mandibular molars used in the study sample are listed in Tables 2.1 and 2.2, respectively. The sample includes *P. paniscus* (Pp) and two subspecies of *P. troglodytes* (Pt), *P. t. troglodytes* (Ptt) and *P. t. verus* (Ptv). The Ptt sample derives from the Museum für Naturkunde (denoted as ZMB) in Berlin, Germany and the subspecies designation is based on localities (located in Cameroon or Gabon) from which the specimens originate. The Ptv sample derives from a skeletal collection housed at the Max Planck Institute for Evolutionary Anthropology in Leipzig, Germany (MPI). The collection derives from naturally deceased individuals collected within the research mandate of the Taï Chimpanzee Project based in the Taï National Park, Republic of Côte d'Ivoire. The subspecies designation is based on the fact that only Ptv is present in this area. The Pp sample derives from the Royal Museum for Central Africa in Tervuren, Belgium (MRAC). Species designation is based on locality information and museum catalogue information associated with each specimen.

Nine additional individuals from the Museum für Naturkunde and two from the Royal Museum for Central Africa are either captive specimens or do not have locality information (Table 2.3). These specimens are treated as having an unknown taxonomic affiliation in order to compare their morphology to specimens of the other taxa. All molars are from associated mandibles from which tooth type is determined (e.g., first or second mandibular molar).

Microcomputed tomography

Each tooth was microCT scanned using a SKYSCAN 1172 Desktop Scanner (100Kv, 94mA, 2.0mm aluminum and copper filter, 0.12 rotation step, 360 degrees of

rotation, 2 frame averaging). Raw projections were converted into TIFF image stacks using NRecon (parameters: ring artifact correction = 10; beam hardening = 30%). Pixel dimensions and slice spacing of the resultant images ranged between 10 – 20 micrometers, or microns (µm). To reduce the size of the resulting files, teeth were downsampled to a resolution of 30 µm using Amira (Triangle filter).

EDJ surface reconstruction

To facilitate tissue segmentation, the complete image stack for each tooth was filtered using a three-dimensional median filter (kernel size of 3) followed by a mean of least variance filter (kernel size of 3), implemented as a computer-programmed macro. This filtering process results in more homogenous tissue classes (e.g., enamel vs. dentine) and allocates pixels with intermediate gray-scale values at tissue interfaces (i.e., air-enamel, enamel-dentine, air-dentine) to the appropriate tissue (Schulze and Pearce, 1994).

Filtered image stacks were imported into the Amira software package (v4.1, www.amiravis.com) and enamel and dentine tissues were segmented using the 3D voxel value histogram and its distribution of gray-scale values, which typically presents a trimodal distribution with one peak representing dentine, another peak representing enamel, and a third peak representing air and background noise in the images. Only teeth in which there was a clear separation of enamel and dentine, resulting in well-distinguished gray-scale values and accurate representations of the EDJ, were used in the study.

After segmentation, the EDJ is reconstructed as triangle-based surface model using Amira (surface generation module using unconstrained smoothing parameter).

Small portions of the EDJ are missing in some teeth, and in these cases the defects were corrected digitally using the software Geomagic Studio v.10 (www.geomagic.com). Teeth which showed evidence of significant damage or missing areas were excluded from the study. In a few minimally worn teeth the tips of the dentine horns were repaired. In specimens that preserved only the enamel cap, a surface model of the EDJ was created by digitally removing the occlusal surface of the reconstructed enamel cap surface model.

Collection of landmarks

EDJ surface models (PLY format) were imported into Amira for the collection of three sets of 3D anatomical landmarks (Fig. 2.1). The first set (referred to as "MAIN") included eight landmarks: one on the tip of the dentine horn of each primary cusp [i.e., protoconid (1), metaconid (2), entoconid (3), hypoconid (4) and hypoconulid (5)], one at the lowest point on the crests connecting, respectively, the protoconid and metaconid (6), the protoconid and hypoconid (7), and the hypoconid and hypoconulid (8). The second set (referred to as the RIDGE curve) includes 3D coordinates (approximately 50-70) along the top of the ridges running between each of the five dentine horns. This set of landmarks forms a closed ellipse, beginning at the tip of the protoconid and moving anticlockwise in a lingual direction. In the case of teeth with accessory cusps (e.g., cusp 6 or cusp 7) these dentine horns were ignored and points were collected on either side of the dentine horn. The third set (referred to as the CERVIX curve) includes 3D coordinates (approximately 40-50) along the cervix, or cemento-enamel junction, of the tooth crown. This set of landmarks also forms a closed ellipse, beginning below the protoconid dentine horn and moving anticlockwise in a lingual direction. Where small

fragments of enamel were missing at the cervix its location was estimated. Landmark datasets were exported as text files. We tested the influence of downsampling (from 15-30 microns) and filtering (no filtering, kernel sizes of 1 and kernel sizes of 3) on landmark configurations of a single specimen. The distance in Procrustes shape space between the original specimens and those that had been downsampled or filtered with different settings was minimal and considerably less than distances from the original specimen to any other individuals of the same species or tooth type.

Derivation of homologous landmarks

For each specimen a single set of homologous landmarks and semilandmarks is derived from the three landmark files discussed above. For both the RIDGE and CERVIX curve landmark sets a smooth curve is interpolated using a cubic spline function (note: a cubic spline is used so that the curve is forced to pass through each measured coordinate). Interpolated curves are then resampled to achieve identical point counts between specimens – these resampled points were used as semilandmarks. In the case of the RIDGE curve the eight MAIN landmarks are projected onto the curve dividing the curve into eight sections. For each section a large sample of very closely spaced points are computed along the curve and the distances between adjacent points are calculated and summed together to approximate the length along the curve between the MAIN landmarks. Each length is divided by a given number and the coordinate location at each equally spaced distance is recorded. The number of divisions between the MAIN landmarks is: ten between #2 and #3 and #3 and #5, seven between #2 and #6 and #1 and #6, five between #1 and #7 and #7 and #4, four between #4 and #8 and #8 and #5. In the

case of the cervix curve, its length is calculated in the same way and 70 equally spaced points are derived.

These equidistantly spaced points are then used as starting positions for the semilandmark algorithm: semilandmarks were iteratively allowed to slide along their respective curves (i.e., RIDGE curve [N =60 including the eight MAIN landmarks] and CERVIX curve [N = 70]) to minimize the bending energy of the thin-plate spline interpolation function computed between each specimen and the sample Procrustes average. We used the algorithm of Bookstein (1997; Gunz et al., 2005) that allows points to slide along tangents to the curve. These tangents were approximated for each semilandmark by the vector between the two neighboring points. Only the tips of the dentine horns were used as fixed landmarks, all other points were treated as semilandmarks. After sliding these semilandmarks are considered homologous for the purpose of multivariate analyses.

Procrustes superimposition

The homologous set of landmarks and semilandmarks is converted to shape coordinates by Generalized Least Squares Procrustes superimposition (Gower, 1975; Rohlf and Slice, 1990). This removes information about location and orientation from the raw coordinates and standardizes each specimen to unit centroid size; a size-measure computed as the square root of the sum of squared Euclidean distances from each landmark to the specimen's centroid (Dryden and Mardia, 1998). All data preprocessing was done in Mathematica v6.0 (www.wolfram.com) suing a software routine written by PG.

Analysis of EDJ shape

Two statistical methods were used to assess EDJ shape variation in the study sample: principal components analysis (PCA) and canonical variates analysis (CVA). A PCA of shape coordinates (Bookstein, 1991; Rohlf, 1993) after Procrustes superimposition is an eigen-decomposition of the variance-covariance matrix of Procrustes coordinates. A CVA was computed as linear discriminants in the software package R (www.r-project.org) in the subspace of the first few principal components (i.e., using only a subset of all PCs) of the Procrustes shape coordinates. Projecting into a lower dimensional subspace was necessary because the number of variables greatly exceeded our sample size; using too many variables to compute the discriminant axes results in an unrealistic and unstable degree of discrimination. Our decision as to the number of PCs to incorporate into the CVA was guided by a protocol in which the specimen labels were randomized and the resulting CVA was assessed with variable numbers of PCs included. The number of PCs included (in these analyses 5-10) did not exceed the point at which randomized labels began to exhibit clustering patterns in the resulting CVA. In other words, we confirmed that we would find no separation with randomly rearranged group labels.

The accuracy with which EDJ shape correctly classifies molars, according to species and tooth type, was tested by cross validating the canonical variates analysis. In this process each specimen in turn was considered unclassified and then classified by all the others using posterior probabilities. Classification was implemented in R; groups were assigned equal prior probabilities.

Visualization of EDJ shape variation

To visualize the shape variation of the EDJ between taxa and between molar types we employed a method which allows a template EDJ surface reconstruction to be deformed to match the mean shape of a particular group (Gunz and Harvati, 2007). Several thousand points were collected on the EDJ surface of one specimen and converted to a triangulated surface model using Geomagic Studio. We then used the thin-plate spline interpolation function between the landmark configuration of this specimen and the appropriate mean configuration in Procrustes space, to warp the vertices of this surface into Procrustes space. Processed in this way the mean shape of each group was visualized and compared.

Results

First molars

The PCA of Procrustes shape coordinates of the first molar sample is illustrated in Fig. 2.2a (PC1 = 31.8% and PC2 = 16% of total variation). A CVA, based on the first five PCs (explaining 72.3% of the total variation) of first molar dataset is presented in Fig. 2.2b. Collectively, CV1 (65%) and CV2 (13%) separate the three taxa. The combination of overlap in the PCA and marked separation along the first two CVs suggests that there are consistent, but small scale, differences in shape between the taxa. Using a cross-validation analysis of the CVA the accuracy of classification to species and subspecies is presented in Table 2.1. Three molars are misclassified at the species level and one molar is misclassified at the subspecies level. These results support our first

hypothesis regarding the taxonomic distinctiveness of EDJ shape for first molars. To test the second hypothesis we calculate the Procrustes distance (based on the first five PCs) between the mean first molar shape of each taxon (Table 2.4). Based on the first molars the null hypothesis is rejected as the distance in Procrustes shape space is greater between Ptt and Ptv than the distance between either subspecies and Pp.

The mean shape of the first molar of each taxon is illustrated in Fig. 2.3. The mean shape of Pp M1s compared to the mean shape of the combined Pt M1 sample is visualized in Fig. 2.4a. This represents the shape differences at the species level and includes a relatively narrower trigonid and wider talonid (particularly in the more distal placement of the entoconid and hypoconulid) in Pt compared to Pp and a reduction in the relative height of the talonid dentine horns in Pt compared to Pp. The mean shape differences in the two subspecies, Ptt and Ptv, are illustrated in Fig. 2.4b. Ptt M1s exhibit a relatively taller dentine crown, taller dentine horns, and a narrower talonid whereas Ptv M1s exhibit a shorter dentine crown, shorter dentine horns, and a wider talonid.

Second molars

The principal component analysis of the second molar sample is illustrated in Fig. 2.5a (PC1 = 26.9% and PC2 = 20.6%). A CVA, based on the first six PCs (explaining 75.1% of the total variation) of the second molar dataset is presented in Fig. 2.5b. As with the analysis of first molars, the combination of CV1 (56.2%) and CV2 (18.9%) separates the three taxa. The cross-validation analysis of the CVA is presented in Table 2.2. All second molars are correctly classified at the species level and only one Pt molar is misclassified at the subspecies level. These results support our first hypothesis regarding

the taxonomic distinctiveness of EDJ shape for second molars. Contrary to the analysis of first molars, the second hypothesis is supported as the distance in Procrustes shape space is less between Ptt and Ptv than the distance between either subspecies and Pp (Table 2.4).

The mean shape of the second molar of each taxon is illustrated in Fig. 2.6. The mean shape of Pp M2s compared to the mean shape of the combined Pt M2 sample is visualized in Fig. 2.7a. The shape differences at the species level include relatively centrally-placed dentine horns in Pt M2s compared to more laterally-placed dentine horns in Pp M2s resulting in a relatively larger occlusal basin in the latter. The hypoconulid dentine horn of Pt M2s is also relatively smaller compared to that of Pp M2s. The mean shape differences in M2s of the two subspecies, Ptt and Ptv, are illustrated in Fig. 2.7b. Ptt second molars exhibit a buccolingually-narrower crown base, relatively taller dentine horns and a taller dentine crown, while Ptv molars exhibit a wider, more rectangular, crown base, a wider occlusal basin, shorter dentine horns, and a shorter dentine crown.

Classification of specimens with unknown taxonomic affiliation

The specimens whose provenience, and thus taxonomy, is not certain (Table 2.3) were included in a CVA analysis and classified in relation to the study sample. In some cases we can make an informed guess regarding the taxonomy of these specimens based on other information. We can also examine how stable the classification is for each specimen within each of four analyses (Table 2.3). The basis for the classification of the "unknown" first molars can be visualized in Fig. 2.2b and that of the "unknown" second molars in Fig. 2.5b. These must be interpreted with caution as they only represent two

CV axes and thus they are susceptible to projection errors. A CVA, using the first 10 PCs (83% of total variation) of a PCA based on the combined sample of first and second molars, is illustrated in Fig. 2.8.

The three molars (from two individuals; #1, #9, #10) from the Royal Museum for Central Africa were collected by the same individual and in the same year as other specimens of Pp, and this is consistent with their classification as *Pan paniscus* in all of the analyses. Specimen #8 and #13 are the first and second molars, respectively, from the same individual; a captive specimen from a zoo in Berlin, Germany. The molars are consistent in their classification of this individual as Ptv. Specimen #4 which, based on the CVA analyses, is consistently classified as a first molar of *P. paniscus*. In the museum catalogue this specimen is listed as being "taken on board in Matadi." Matadi is a city in Democratic Republic of the Congo located on the Congo River which divides the ranges of Ptt and Pp. It is possible that this specimen belonged to a Pp individual, but is incorrectly listed in the museum catalogue as belonging to Pt (it is also worth noting that the specimen could have been catalogued prior to the recognition of Pp as a species). Specimen #5, which was originally listed as a first molar is classified in this analysis as a Ptt second molar. This specimen is listed as deriving from Katsema, Cameroon, which would suggest that the taxonomic affiliation is correct. As this is the only specimen misclassified to tooth type a return trip to the museum is planned to confirm that the tooth type designation is sound. A number of specimens are consistent in their species and subspecies designation (e.g., #1, #2, #4, #5, #8-13) while three are consistent in their species designation but inconsistent in their subspecies classification (e.g., #3, #6, and #7).

Discussion

The goal of this project is to assess the taxonomic distinctiveness of the EDJ morphology of lower molars in species and subspecies of *Pan*. If it can be demonstrated that the *Pan* EDJ carries information useful for distinguishing groups at these taxonomic levels, then it is likely the same methods will have utility for discriminating among the species and subspecies of other genera within the *Pan*/*Homo* clade. It is important to establish reliable taxonomic hypotheses for fossil hominins, and to re-assess them as new discoveries are made. Taxonomic decisions that partition the fossil record into the hypodigms are essential for any further exploration of the evolutionary history and paleobiology of the hominin clade.

There have been three previous studies of the taxonomic differences in tooth morphology of *Pan* that are particularly relevant to the results of this study. The first was by Johanson (1974) who examined metric and non-metric dental variation in Pp and in the three subspecies of Pt and noted significant differences in both metric (MD and BL dimensions) and non-metric variables between Pp and Pt and significant differences in non-metric variables among the three subspecies of Pt. He also noted the distinctiveness of Ptv compared to the other subspecies of Pt. Uchida (1992, 1996) examined craniodental variation among hominoids. Her analyses of the dentition included linear dimensions, cusp areas, and frequency of non-metric traits. Her findings echoed Johanson's regarding metrical differences in lower molar morphology between Pp and Pt, but differed in that significant metrical differences were found between Ptv and Ptt including: relative size of the protoconid on M1 and M2 (Ptv larger), relative size of the

hypoconid on M1 and M2 (Ptt larger), M2 crown shape (Ptv relatively wider buccolingually). Cusp area measurements also distinguished Ptv from the other Pt subspecies. The distinctiveness in EDJ morphology at the species and subspecies level revealed in our analysis is consistent with these results.

Pilbrow (2003, 2006a) examined morphometric variation in African ape teeth, including chimpanzee molars, based on a comprehensive set of linear measurements and angles on the tooth crown. Pilbrow demonstrated significant morphometric variation between species, subspecies and individual populations of *Pan*. Mahalanobis distances between populations of chimpanzee resulted in four groups consistent with Pp, Ptv, Ptt, and Pts. Based on shape variables, the classification accuracies in Pilbrow's analysis were: Pp – M_1~70% and M_2~88%; Pt – M_1~90% and M_2 ~93%; Ptt - M_1 ~52% and M_2 ~62%; Ptv - M_1~80% and M_2~70%. Due to the small sample sizes of our analysis we do not place strong confidence in the classification accuracies based on EDJ shape, however, we believe it reasonable to conclude that at a minimum they are as good as, if not slightly better than those based on the OES (particularly for the Ptt sample). We suggest that this may be due to the fact that unlike methods that use 2D occlusal photographs our protocol captures variation in crown height and dentine horn height.

The results we have presented indicate that EDJ morphology is distinctive at both the species and subspecies level in *Pan*. Thus, the principles of parsimony would suggest that the null hypothesis is that the EDJ morphology of the teeth of fossil hominins, who share a most recent common ancestor with extant chimpanzees, is also likely to preserve taxonomically relevant shape information at the same taxonomic levels. Indeed, EDJ morphology, based on high-resolution CT images, is beginning to be used for the

diagnosis of new hominid taxa (Suwa et al., 2007). An analysis of EDJ shape in two southern African hominin taxa, *Australopithecus africanus* and *Paranthropus robustus*, indicates that EDJ morphology distinguishes both taxon and tooth type in lower molars (Skinner et al., nd).

Genetic diversity is relatively low for Ptv and Pp compared to Ptt (Becquet et al., 2007). While our results are consistent with this pattern with the Ptt samples covering a larger proportion of shape space (and hence morphological variability) than Pp or Ptv, this may also be due to sampling bias; particularly with the Ptv sample which derives from a temporally and geographically restricted sample. Due to methodological differences current molecular based estimates for the divergence time between *Pan* species and subspecies differ among studies. Based on two recent analyses a cautious estimate for the divergence of Pp and Pt is 1.0 – 1.5 Ma and between Ptv and the central and eastern subspecies is 0.5 -0.9 Ma (Won and Hey, 2005; Becquet et al., 2007). Based on the genetic data the predictions would be that the phenetic distance between Ptt and Ptv would be less than the distance between either of the former taxa and Pp. The results for the test of our second hypothesis, addressing whether EDJ morphology matches this prediction are equivocal. The null hypothesis is rejected for first molars and accepted for second molars. The small sample sizes for each group prevent a rigorous test of this hypothesis and future research should increase sample sizes which would flesh out intra-taxonomic patterns of variability.

Previous authors have suggested that the EDJ carries a more conservative taxonomic signal than the OES (e.g., Korenhof, 1960; Sakai and Hanamura, 1973a,b; Corruccini, 1987b; Sasaki and Hanazawa, 1999). While our results indicate that the EDJ

carries a strong taxonomic signal it is difficult to assess how this relates to the taxonomic signal of the OES. This is for two reasons. First, unworn teeth are very difficult to find, even in large museum collections, and second our methodology is difficult to apply to the OES as the placement of landmarks on the more rounded surface of the OES is more subjective than along the sharp ridge that runs between the dentine horns. Future research into the taxonomic and phylogenetic utility of tooth structure (including EDJ and enamel cap morphology) should increase sample sizes of high-resolution EDJ data to assess expected levels of intraspecific variation. Furthermore, it may be that a combination of EDJ morphology and the morphology of the enamel cap will be most effective for distinguishing closely related taxa, as selection for OES crown morphology (or even the functional morphology of a partially worn tooth, see below) can occur during the formation of the EDJ and/or be related to the distribution of enamel deposited over the EDJ.

As noted by Uchida (1996) it is difficult to point out any obvious functional significance of the shape differences between subspecies and species. EDJ shape differences are subtle and include slight variations in the shape of the crown base, the size and height of the dentine horns and the placement of the dentine horns across the crown. Such differences can result in increase in occlusal basin size and volume or the size of shearing crests. However, the EDJ surface analyzed and visualized in this study does not independently interact with food being masticated. In the unworn tooth that surface is the culmination of EDJ shape and differential enamel distribution, and in partially worn teeth can include the worn enamel cap and areas of exposed dentine which can create functional crests in themselves (King et al., 2005). Enamel cap morphology and the

correlation between the EDJ and OES will need to be assessed in each taxon to determine the extent to which EDJ shape is translated to the OES, and thus work out whether the shape of the former can be used for interpreting the function of the latter.

Conclusion

This study tested the hypotheses that A) the EDJ morphology of molar tooth crowns could distinguish between species and subspecies of extant chimpanzees, and B) that the two subspecies of *Pan troglodytes* are more similar in shape to each other than either is to *Pan paniscus*. The first hypothesis is supported based on the high accuracy with which individual teeth are classified to the appropriate species and subspecies. The second hypothesis was rejected for first molars and accepted for second molars and requires further investigation. Morphological differences between extant *Pan* taxa are subtle, but they can be visualized by the geometric morphometric approach employed in this study. Our results suggest that EDJ morphology carries taxonomically relevant information that can be incorporated into analyses of fossil hominids.

Table 2.1. First molars with their pre-established taxonomic affiliation and their classification[1] in each analysis.

Specimen	Taxon	M1_sp	M1/M2_sp	M1_ssp	M1/M2_ssp
MRAC_27009_M1	*Pan paniscus*	Pp	Pp	Pp	Pp
MRAC_29010_M1	*Pan paniscus*	Pp	Pp	Pp	Pp
MRAC_29016_M1	*Pan paniscus*	Pp	Pp	Pp	Pp
MRAC_29024_M1	*Pan paniscus*	Pp	Pp	Pp	Pp
MRAC_29026_M1	*Pan paniscus*	Pp	Pp	Pp	Pp
MRAC_29030_M1	*Pan paniscus*	Pp	Pp	Pp	Pp
MRAC_29048_M1	*Pan paniscus*	Pp	Pp	Pp	Pp
MRAC_5374_M1	*Pan paniscus*	Pt	Pp	Ptv	Ptt
MPI_11791_M1	*Pan t. verus*	Pt	Pt	Ptv	Ptv
MPI_11792_M1	*Pan t. verus*	Pt	Pt	Ptv	Ptv
MPI_11798_M1	*Pan t. verus*	Pt	Pt	Ptv	Ptv
MPI_11800_M1	*Pan t. verus*	Pt	Pt	Ptv	Ptv
MPI_13433_M1	*Pan t. verus*	Pt	Pt	Ptv	Ptv
MPI_14992_M1	*Pan t. verus*	Pt	Pt	Ptt	Ptt
MPI_14995_M1	*Pan t. verus*	Pt	Pt	Ptv	Ptv
MPI_15011_M1	*Pan t. verus*	Pt	Pt	Ptv	Ptv
ZMB_0A16207_M1	*Pan t. troglodytes*	Pt	Pt	Ptt	Ptt
ZMB_15849_M1	*Pan t. troglodytes*	Pt	Pt	Ptt	Ptt
ZMB_30847_M1	*Pan t. troglodytes*	Pp	Pt	Pp	Ptt
ZMB_35526_M1	*Pan t. troglodytes*	Pt	Pt	Ptt	Ptt
ZMB_83604_M1	*Pan t. troglodytes*	Pt	Pt	Ptt	Ptt
ZMB_83623_M1	*Pan t. troglodytes*	Pp	Pp_M2	Pp	Pp_M2
ZMB_83673_M1	*Pan t. troglodytes*	Pt	Pt	Ptt	Ptt
	Total	20/23 (87%)	22/23 (96%)	19/23 (83%)	20/23 (87%)

1. Misclassifications at the species level are shaded in dark grey and at the subspecies level in light grey. When tooth type is also misclassified the tooth type classification is listed.

Table 2.2. Second molars with their pre-established taxonomic affiliation and their classification[1] in each analysis.

Specimen	Taxon	M2_sp	M1/M2_sp	M2_ssp	M1/M2_ssp
MRAC_22908_M2	*Pan paniscus*	Pp	Pp	Pp	Pp
MRAC_29030_M2	*Pan paniscus*	Pp	Pp	Pp	Pp
MRAC_29033_M2	*Pan paniscus*	Pp	Pp	Pp	Pp
MRAC_29041_M2	*Pan paniscus*	Pp	Pp	Pp	Pp
MRAC_29055_M2	*Pan paniscus*	Pp	Pp	Pp	Pp
MRAC_29056_M2	*Pan paniscus*	Pp	Pp	Pp	Pp
MRAC_29066_M2	*Pan paniscus*	Pp	Pp	Pp	Pp
MRAC_84036M03_M2	*Pan paniscus*	Pp	Pp	Pp	Pp
MRAC_84036M04_M2	*Pan paniscus*	Pp	Pp	Pp	Pp
MPI_11790_M2	*Pan t. verus*	Pt	Pt	Ptv	Ptv
MPI_11791_M2	*Pan t. verus*	Pt	Pt	Ptv	Ptv
MPI_11792_M2	*Pan t. verus*	Pt	Pt	Ptv	Ptv
MPI_11800_M2	*Pan t. verus*	Pt	Pt	Ptv	Ptv
MPI_12176_M2	*Pan t. verus*	Pt	Pt	Ptt	Ptt
MPI_13433_M2	*Pan t. verus*	Pt	Pt	Ptv	Ptv
MPI_13437_M2	*Pan t. verus*	Pt	Pt	Ptv	Ptv
MPI_14992_M2	*Pan t. verus*	Pt	Pt	Ptv	Ptv
MPI_15008_M2	*Pan t. verus*	Pt	Pt	Ptv	Ptv
MPI_15012_M2	*Pan t. verus*	Pt	Pt	Ptv	Ptv
ZMB_30846_M2	*Pan t. troglodytes*	Pt	Pt	Ptt	Ptt
ZMB_30847_M2	*Pan t. troglodytes*	Pt	Pt	Ptt	Ptt
ZMB_31279_M2	*Pan t. troglodytes*	Pt	Pt	Ptt	Ptt
ZMB_46095_M2	*Pan t. troglodytes*	Pt	Pt	Ptt	Ptt
ZMB_83635_M2	*Pan t. troglodytes*	Pt	Pt	Ptt	Ptt
ZMB_83639_M2	*Pan t. troglodytes*	Pt	Pt	Ptt	Ptt
ZMB_83685_M2	*Pan t. troglodytes*	Pt	Pt	Ptt	Ptt
	Total	26/26 (100%)	26/26 (100%)	25/26 (96%)	25/26 (96%)

1. Misclassifications at the species level are shaded in dark grey and at the subspecies level in light grey. When tooth type is also misclassified the tooth type classification is listed.

Table 2.3. List of specimens with unknown taxonomic affiliation and their classification in each analysis.

#[1]	Specimen	Provenience information[2]	M1_sp	M1/M2_sp	M1_ssp	M1/M2_ssp
1	MRAC_84036M11_M1	Collected by the same individual as other Pp specimens (Pp?)	Pp	Pp	Pp	Pp
2	ZMB_0A809_M1	None (?)	Pt	Pt	Ptv	Ptv
3	ZMB_20811_M1	None (?)	Pt	Pt	Ptv	Ptt
4	ZMB_32052_M1	"Taken on board in Matadi" (?)	Pp	Pp	Pp	Pp
5	ZMB_32356_M1	Katsema, Cameroon (Ptt?	Pt	Pt	Ptt	Ptt_M2
6	ZMB_47506_M1	Zoo specimen from Berlin (?)	Pt	Pt	Ptt	Ptv
7	ZMB_6983_M1	Listed in museum catalogue as coming from west Africa (Ptv?)	Pt	Pt	Ptv	Ptt
8	ZMB_72844_M1	Zoo specimen from Berlin (?)	Pt	Pt	Ptv	Ptv
	Specimen	**Provenience information**	**M2_sp**	**M1/M2_sp**	**M2_ssp**	**M1/M2_ssp**
9	MRAC_84036M10_M2	Collected by the same individual as other Pp specimens (Pp?)	Pp	Pp	Pp	Pp
10	MRAC_84036M11_M2	Collected by the same individual as other Pp specimens (Pp?)	Pp	Pp	Pp	Pp
11	ZMB_24838_M2	Bugoie Wald, Rwanda? (Pts)	Pt	Pt	Ptt	Ptt
12	ZMB_33489_M2	Egypt (?)	Pt	Pt	Ptv	Ptv
13	ZMB_72844_M2	Zoo specimen from Berlin (?)	Pt	Pt	Ptv	Ptv

1. Numbers at left indicate the location of specimens in the various PCA and CVA plots.

Table 2.4. Procrustes distance between each taxon for each analysis.

M_1s (5PCs)	PpM_1	$PttM_1$	$PtvM_1$	Consistent with phylogenetic expectations?[1]
PpM_1	0.000			
$PttM_1$	0.060	0.000		NO
$PtvM_1$	0.067	0.079	0.000	
M_2s (6PCs)	PpM_2	$PttM_2$	$PtvM_2$	
PpM_2	0.000			
$PttM_2$	0.076	0.000		YES
$PtvM_2$	0.075	0.070	0.000	
M_1/M_2s (10PCs)	PpM_1/M_2	$PttM_1/M_2$	$PtvM_1/M_2$	
PpM_1/M_2	0.000			
$PttM_1/M_2$	0.040	0.000		NO
$PtvM_1/M_2$	0.042	0.046	0.000	

1. To meet phylogenetic expectations the distance between Ptt and Ptv should be less than the distance of either subspecies to Pp.

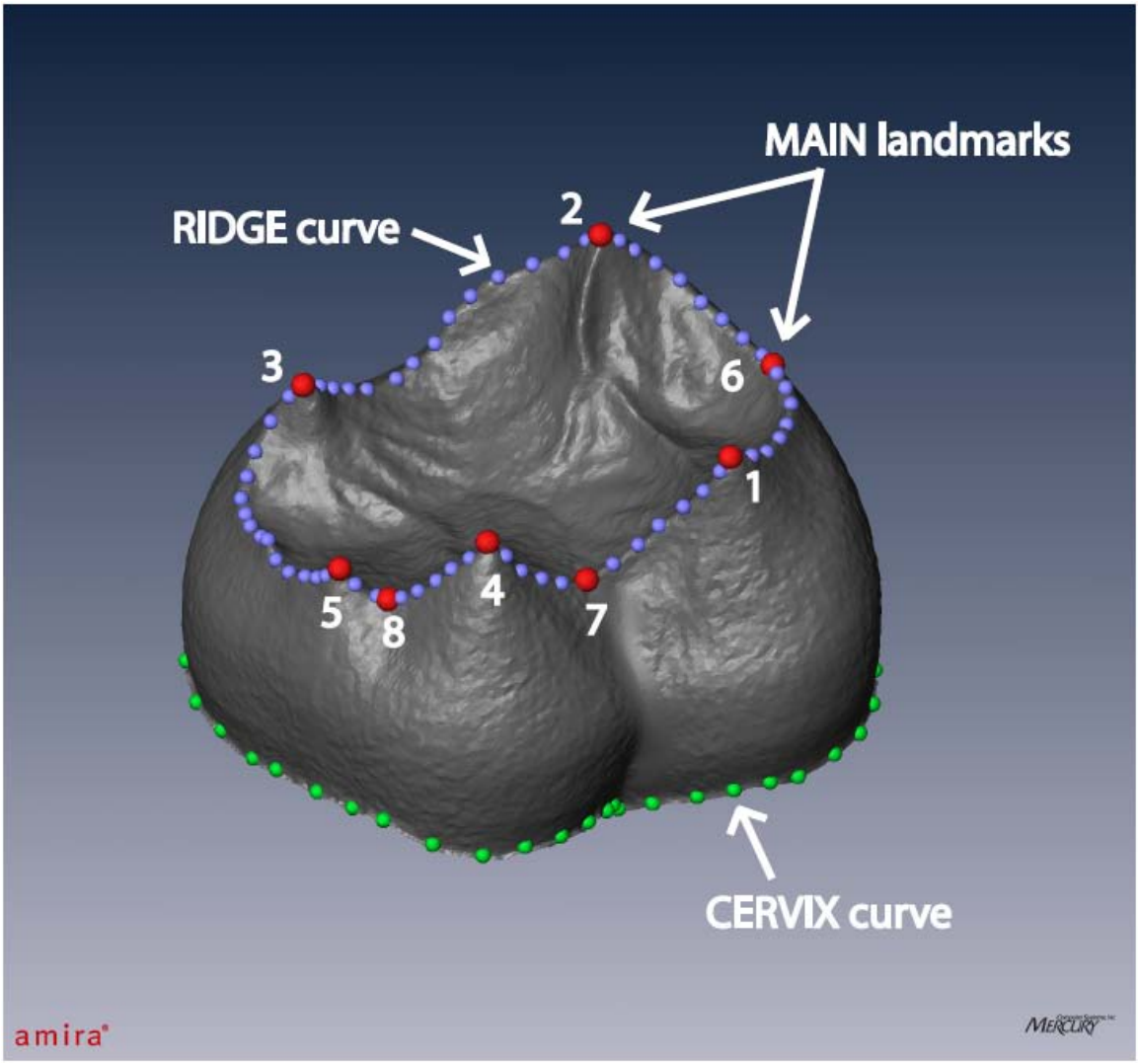

Figure 2.1. EDJ surface model of a lower molar illustrating the anatomical landmarks used to capture EDJ shape. Landmarks are collected on the tips of the dentine horns and in the troughs between the mesial and buccal dentine horns (red spheres), along the RIDGE curve that runs between the dentine horns (purple spheres), and around the CERVIX curve (green spheres). Numbers refer to MAIN landmark set (see text for details).

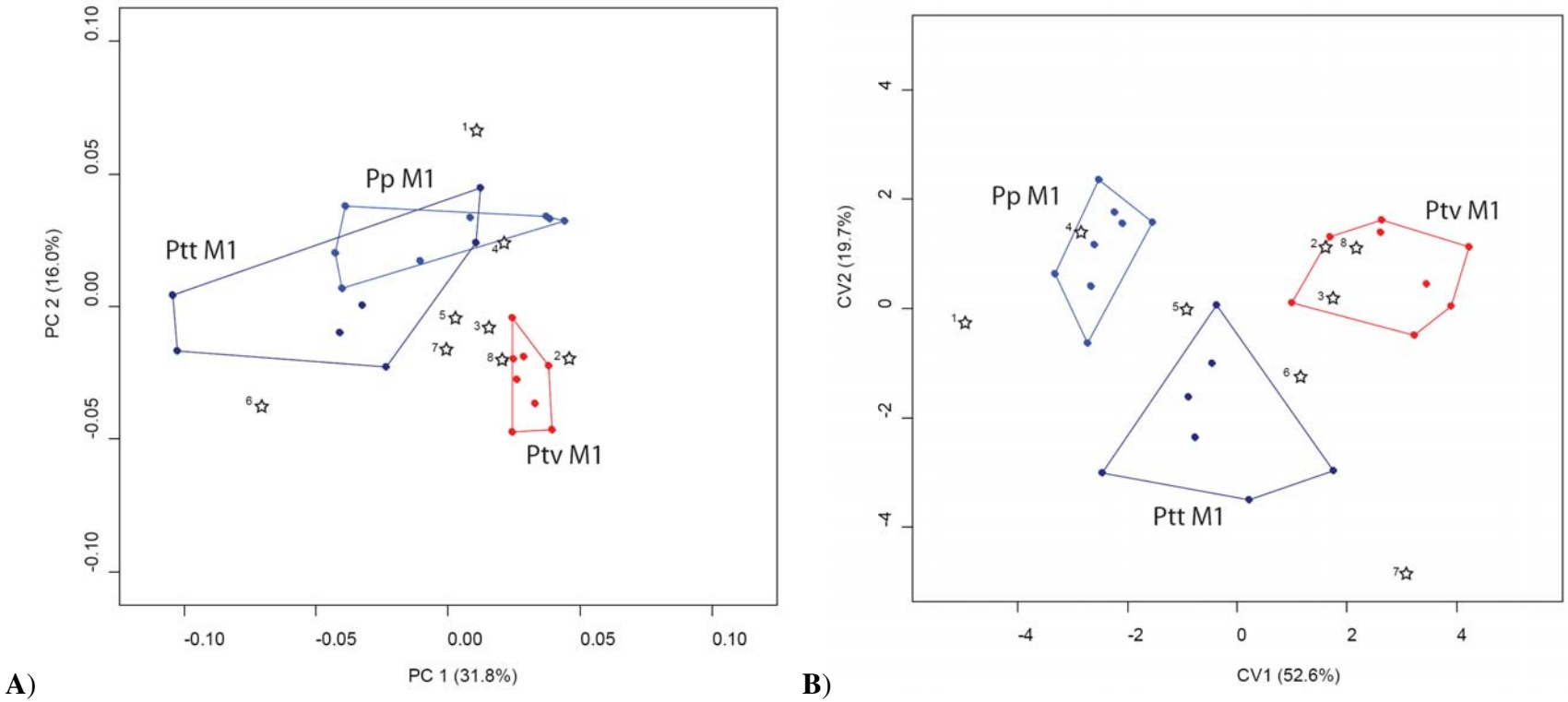

Figure 2.2. **A**) PCA of the M_1 sample. **B**) CVA of the M_1 sample based on the first five PCs (explaining 72.3% of total variation). For both PCA and CVA grouping is by subspecies. Open stars with numbers indicate the position of specimens of unknown taxonomic affiliation (see Table 2.3). Abbreviations are as in text.

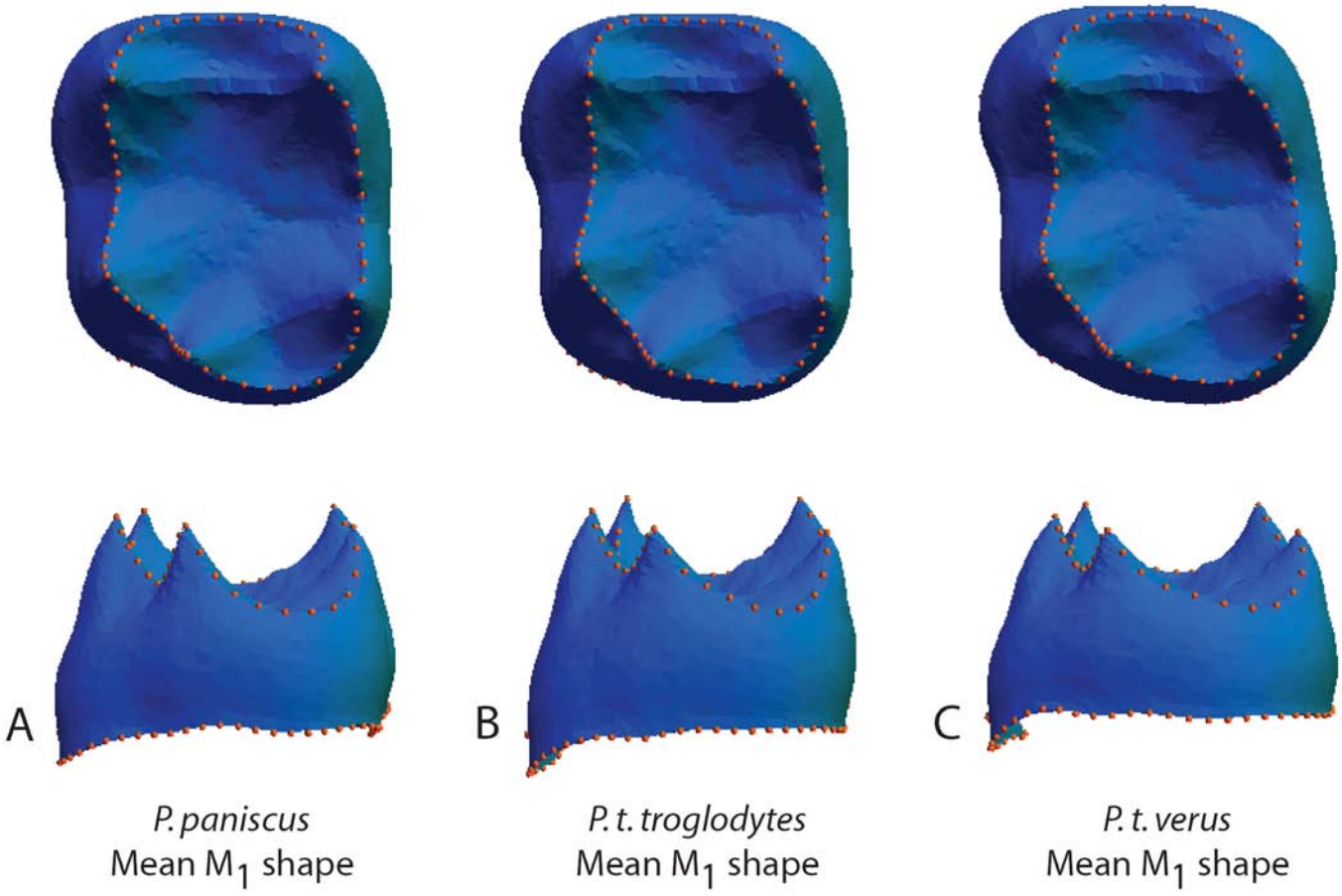

Figure 2.3. EDJ surface models of mean M_1 shape in occlusal (top) and distal (bottom) view. **A**) *P. paniscus*; **B**) *P. t. troglodytes*; **C**) *P. t. verus*. Orange spheres denote anatomical landmarks used in shape analysis.

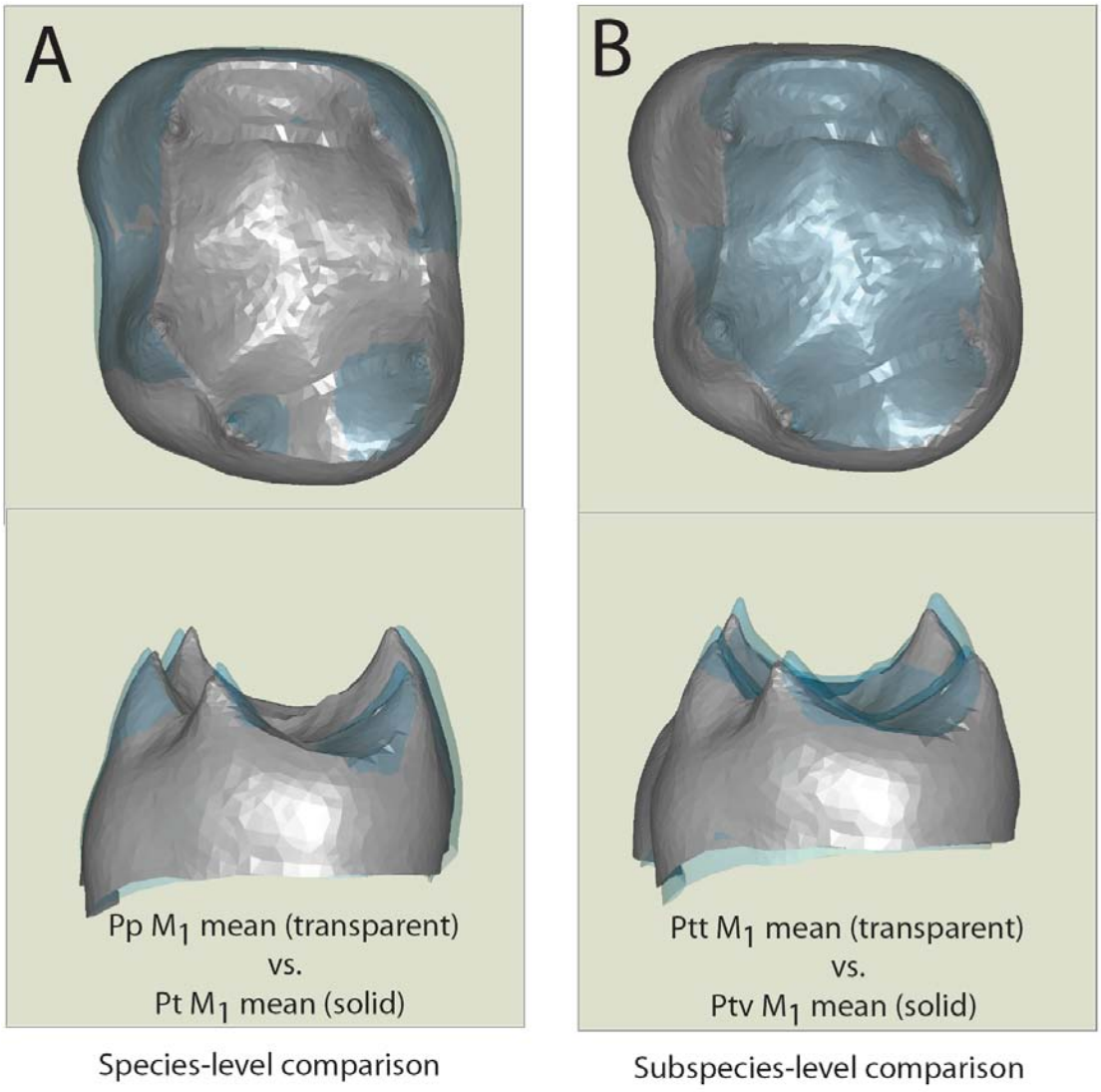

Figure 2.4. Comparison of mean EDJ shape of M_1. **A**) Species-level comparison between the mean *P. paniscus* M_1 (transparent) shape and the mean shape of the combined *P. troglodytes* M_1 (solid) sample. **B**) Subspecies-level comparison between the mean *P. t. troglodytes* M_1 (transparent) shape and the mean *P. t. verus* M_1 (solid) shape.

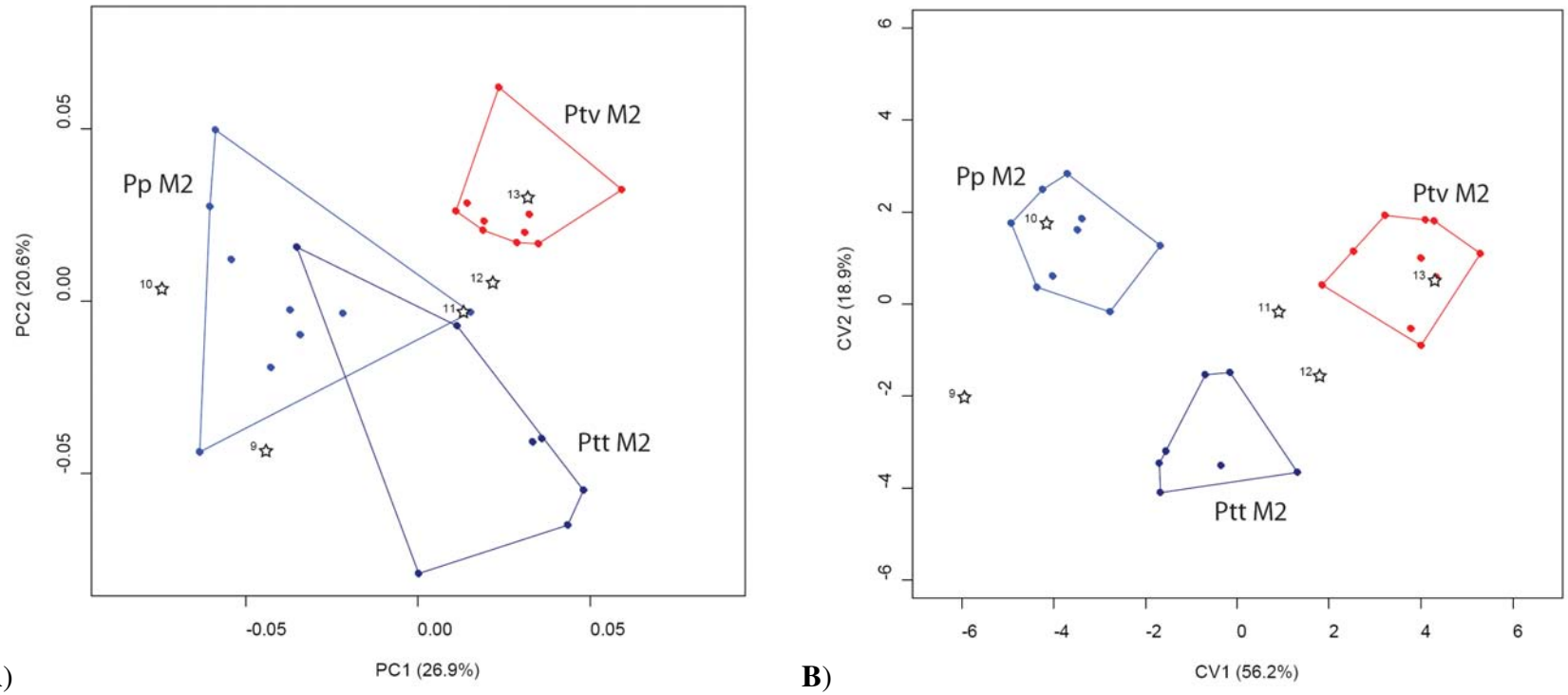

A) **B**)

Figure 2.5. **A**) PCA of the M_2 sample. **B**) CVA of the M_2 sample based on the first six PCs (explaining 75.1% of total variation). For both PCA and CVA grouping is by subspecies. Open stars with numbers indicate the position of specimens of unknown taxonomic affiliation (see Table 2.3). Abbreviations are as in text.

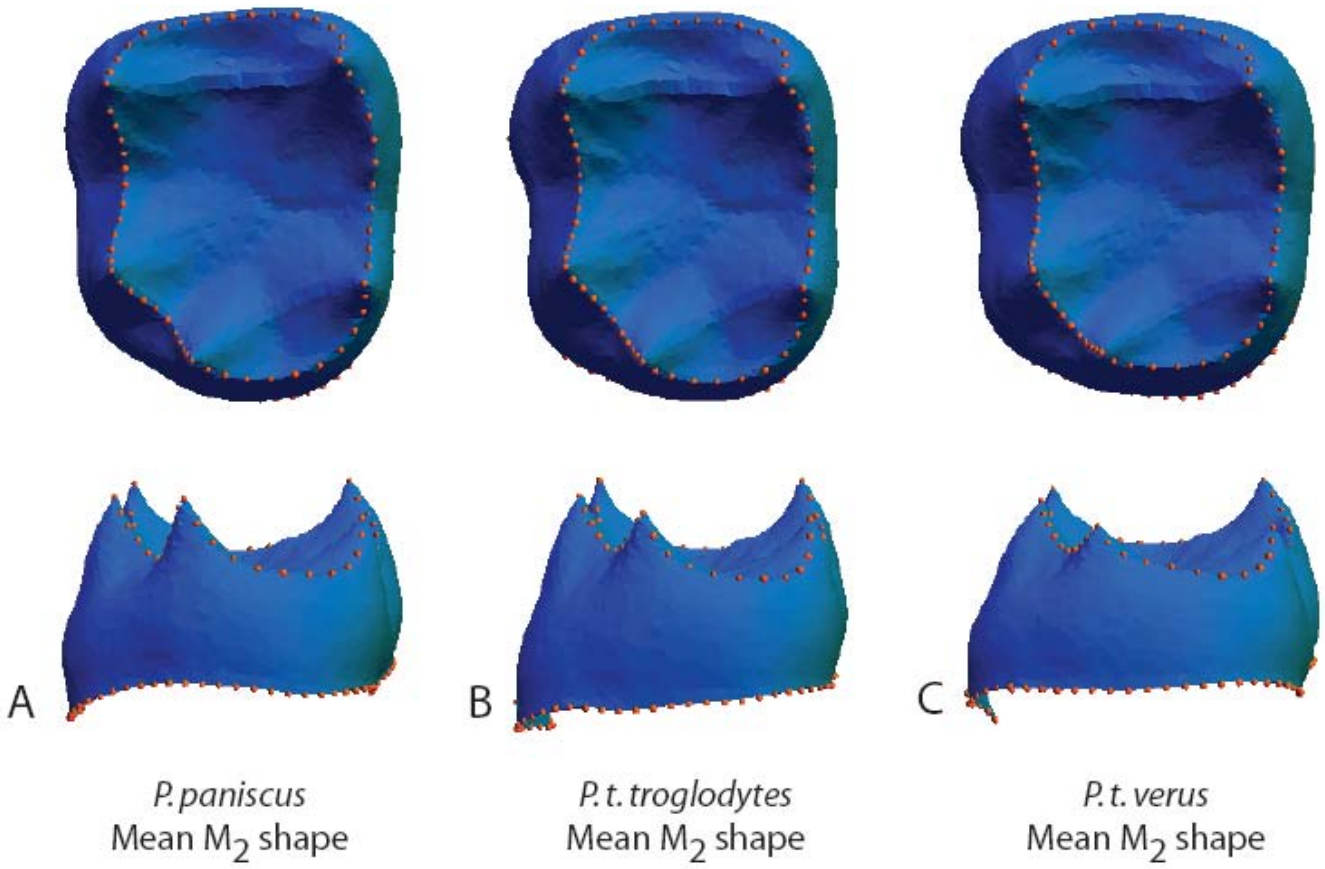

Figure 2.6. EDJ surface models of mean M_2 shape in occlusal (top) and distal (bottom) view. **A**) *P. paniscus*; **B**) *P. t. troglodytes*; **C**) *P. t. verus*. Orange spheres denote anatomical landmarks used in shape analysis.

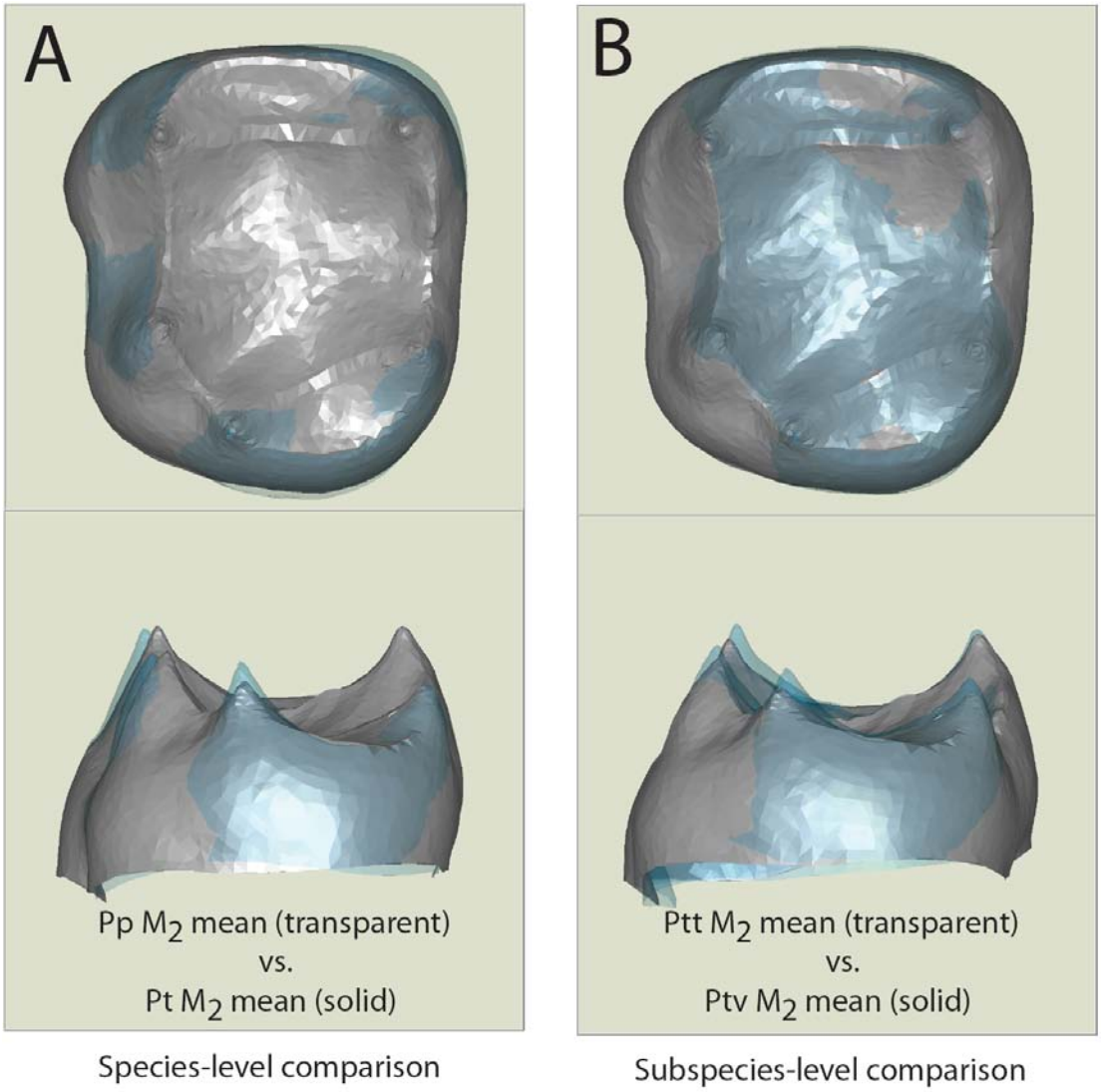

Figure 2.7. Comparison of mean EDJ shape of M_2. **A**) Species-level comparison between the mean *P. paniscus* M_2 (transparent) shape and the mean shape of the combined *P. troglodytes* M_2 (solid) sample. **B**) Subspecies-level comparison between the mean *P. t. troglodytes* M_2 (transparent) shape and the mean *P. t. verus* M_2 (solid) shape.

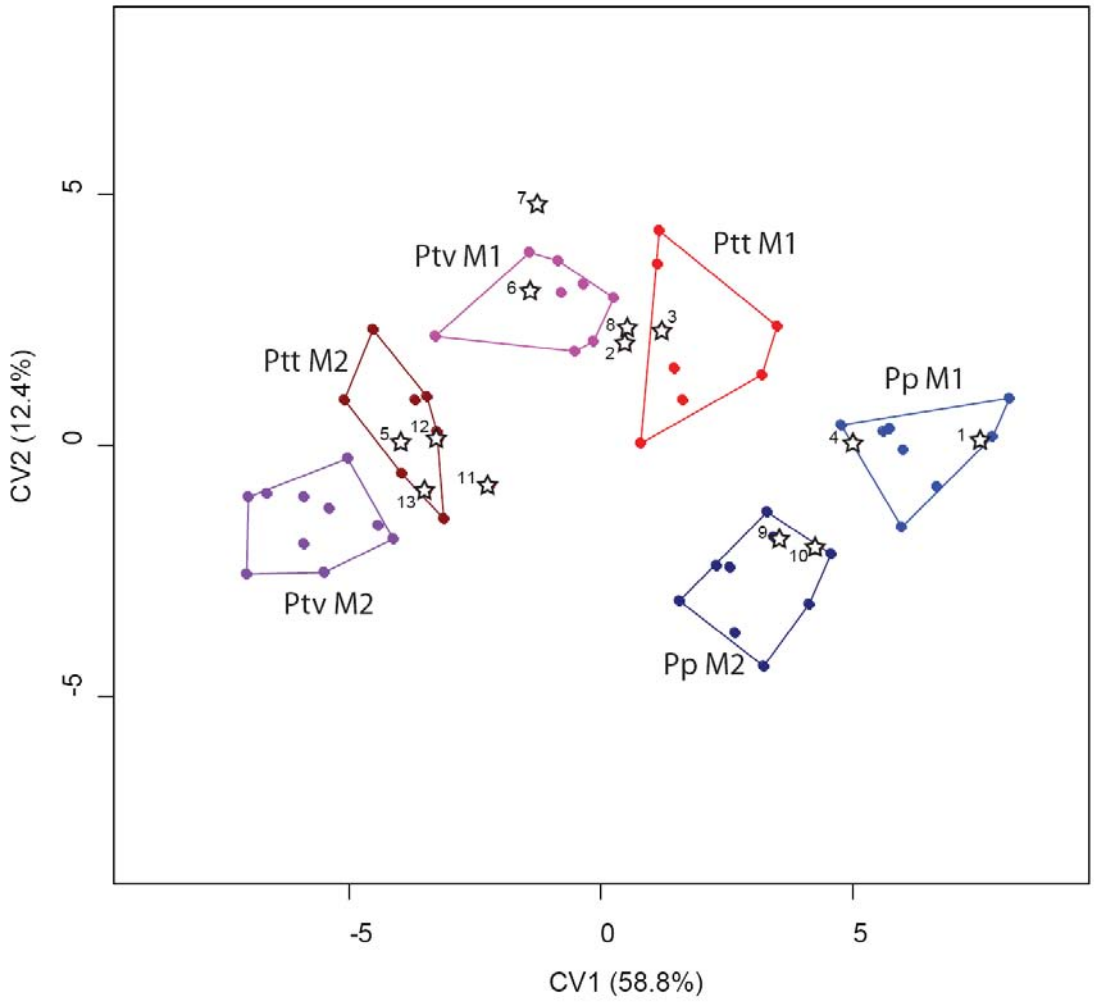

Figure 2.8. CVA of the combined M_1/M_2 sample based on the first 10 PCs (explaining 83.0% of total variation). For CVA grouping is by subspecies and tooth type. Open stars with numbers indicate the position of specimens of unknown taxonomic affiliation (see Table 2.3). Abbreviations are as in text.

CHAPTER THREE: ENAMEL-DENTINE JUNCTION (EDJ) MORPHOLOGY DISTINGUISHES THE LOWER MOLARS OF *AUSTRALOPITHECUS AFRICANUS* AND *PARANTHROPUS ROBUSTUS*

Abstract

Tooth crown morphology plays a central role in hominin systematics, but the removal of the outer enamel surface by dental attrition reduces, sometimes drastically, the sizes of the samples available for study. This effectively eliminates from consideration the type of detailed crown morphology that has been shown to discriminate among hominin taxa. The enamel-dentine junction (EDJ) is the developmental precursor of the outer enamel surface, yet its morphology is only affected after considerable attrition. In this paper we explore whether the form of the EDJ can be used to distinguish between the mandibular molars of two southern African fossil hominins: *Paranthropus* (or *Australopithecus*) *robustus* (*P. robustus*) and *Australopithecus africanus* (*A. africanus*.) We made high resolution images of the EDJ and used geometric morphometrics to compare EDJ molar shape differences between species, in addition to documenting metameric variation along the molar row within each species. Landmarks were collected along the marginal ridge which runs between adjacent dentine horns and around the circumference of the cervix. Our results suggest that the morphology of the EDJ can distinguish lower molars of these southern African hominins, but it can also discriminate first, second, and third molars within each taxon. These results confirm previous findings that the EDJ is a useful taxonomic tool as it preserves taxonomically valuable shape information in worn teeth.

Introduction

Given the prevalence of teeth in the hominin fossil record it is not surprising that dental morphology plays a central role in hominin species diagnoses and that dental evidence features prominently in attempts to generate phylogenetic hypotheses. Molar crown morphology has been shown to be distinctive among extant higher primate species and subspecies (Johanson, 1974; Uchida, 1992, 1996; Pilbrow, 2003, 2006), and between many fossil hominin taxa (e.g., Weidenreich, 1937; Robinson, 1956; Sperber, 1974; Wood and Abbott, 1983; Wood et al., 1983; Wood, 1991; Suwa et al., 1994; Suwa, 1996; Bailey, 2002, 2006; Grine, 2004; Hlusko, 2004; Irish and Guatelli-Steinberg, 2003; Guatelli-Steinberg and Irish, 2005). Unfortunately, dental attrition degrades the information content of enamel morphology by removing measurable aspects of homologous morphology. Using less comprehensive measures of tooth shape can result in considerable overlap between taxa which can be well-differentiated based on other skeletal anatomy.

It is known that the shape of the enamel-dentine junction (EDJ) quite closely mirrors the shape of the outer enamel surface (OES) (Butler, 1956; Korenhof, 1960, 1961) and that unlike the OES the EDJ is preserved intact in partially worn teeth. Previous analyses have demonstrated that primate EDJ morphology carries useful taxonomic and phylogenetic information (e.g., Corruccini, 1987, 1998; Olejniczak et al., 2004, 2007; Skinner et al., 2008) and can successfully discriminate between species and subspecies of chimpanzee (Skinner, 2008). If the EDJ is at least as taxonomically valuable as the OES then sample sizes of hominin teeth available for analysis could be increased by adding teeth that have lost the OES either by antemortem attrition or by postmortem abrasion, but which still retain the EDJ in its pristine state.

The morphology of lower molar tooth crowns, such as overall crown size, relative cusp areas and molar size gradients, has been noted to distinguish *P. robustus* and *A. africanus* (Robinson, 1956; Sperber, 1974; Wood and Abbott, 1983; Wood et al., 1983; Suwa et al., 1994; Suwa, 1996; Grine, 2004). However, for many tooth crown variables there is considerable overlap between these taxa. This study extends this research by comparing both within- and between-species variation in EDJ morphology in *A. africanus* and *P. robustus*. We do this by employing high resolution microCT to image the EDJ surface, geometric morphometrics to capture the details of its shape, and multivariate analytical methods to compare EDJ shape among taxa and molar position.

Materials and Methods

The study sample comprised isolated mandibular molars from collections housed at the Transvaal Museum, Pretoria, South Africa and the University of Witwatersrand, Johannesburg, South Africa (Table 3.1). Teeth from Swartktrans, Gondolin and Drimolen (Robinson, 1956; Tobias et al., 1977; Grine 1989; Menter et al., 1999; Keyser et al., 2000; De Ruiter, pers. comm. 2006) constitute the *P. robustus* sample, and teeth from Sterkfontein Member 4 (Tobias et al., 1977; Moggi-Cecchi et al., 2006) make up the *A. africanus* sample. These references were used to establish the taxonomy of each specimen and in the case of isolated teeth, their position in the molar row. In some cases molars are of known position because they derive from mandibular specimens (e.g., SK6) or because they are part of an associated dentition (e.g., STW537). A sample of isolated molars, whose position along the molar row is uncertain, is listed in Table 3.2 along with previous classifications based on the above references (see also Suwa, 1996). These

molars are treated as unknown in our analysis and an attempt is made to assess their likely position along the molar row using aspects of EDJ shape.

All molars preserved intact occlusal EDJ surfaces with the exception of three specimens discussed below in the section describing EDJ surface reconstruction. Some scanned teeth could not be included in this project because the effects of diagenesis were such that it was not possible to tell the dentine from the enamel. In the case of teeth with antimeres, the side that was better preserved tooth was included for analysis. Due to the limitations of the object size that could fit into the portable microCT scanner used in this study, few molars from mandibular specimens could be included.

Microcomputed tomography

Each tooth was microCT-scanned using a SKYSCAN 1172 Desktop Scanner (100Kv, 94mA, 2.0mm aluminum and copper filter, 0.12 rotation step, 360 degrees of rotation, 2 frame averaging). Raw projections were converted into TIFF image stacks using NRecon (parameters: ring artifact correction = 10; beam hardening = 30%). Pixel dimensions and slice spacing of the resultant images ranged between 10 – 20 micrometers, or microns (µm). To reduce the size of the resulting files, teeth were down-sampled to 30 µm using Amira (Triangle filter).

EDJ surface reconstruction

To facilitate tissue segmentation, the complete image stack for each tooth was filtered using a three-dimensional median filter (kernel size of 3) followed by a mean-of-least-variance filter (kernel size of 3), implemented as a computer-programmed macro. This filtering process results in more homogenous tissue classes (e.g., enamel vs. dentine)

and allocates pixels with intermediate gray-scale values at tissue interfaces (i.e., air-enamel, enamel-dentine, air-dentine) to the appropriate tissue (Schulze and Pearce, 1994).

Filtered image stacks were imported into the Amira software package (v4.1, www.amiravis.com) and enamel and dentine tissues were segmented using the 3D voxel value histogram and its distribution of gray-scale values, which typically presents a trimodal distribution with one peak representing dentine, another peak representing enamel, and a third peak representing air and background noise in the images. In fossil teeth where the enamel and dentine differ substantially in their degree of mineralization (and thus in the ability of X-rays to pass through them), the filtering process results in gray-scale pixel value distributions for each tissue that do not overlap. In other teeth, diagenetic alteration (e.g., dentine remineralization) may result in similar tissue densities and thus overlapping gray-scale pixel value ranges for enamel and dentine (Olejniczak and Grine, 2006). Even after filtering, there is often an incomplete separation between the two, and a decision must be made about the range of gray-scale values allocated to each tissue. Only teeth in which there was a clear separation of enamel and dentine, resulting in well-distinguished gray-scale values and accurate representations of the EDJ, were used in the study.

After segmentation, the EDJ was reconstructed as triangle-based surface model using Amira (surface generation module using unconstrained smoothing parameter). Small portions of the EDJ are missing in some teeth, and in these cases the defects were corrected digitally using the software Geomagic Studio 10. Teeth that showed evidence of significant damage or missing areas were excluded from the study. SKX5002 and GDA2 possess one (protoconid) and two (protoconid and hypoconid) exposed dentine horn tips, respectively. In each case this exposure is minor and the tips were

reconstructed digitally (Fill holes option in Geomagic Studio 10). A crack was digitally repaired in STW3 using surface editing functions in Geomagic Studio 10. In specimens that preserved only the enamel cap, a surface model of the EDJ was created by digitally removing the occlusal surface of the reconstructed enamel cap surface model.

Collection of landmarks

The EDJ surface models (PLY format) were imported into Amira 4.0 for the collection of three sets of 3D anatomical landmarks (Fig. 3.1). The first set (referred to as "MAIN") included eight landmarks: one on the tip of the dentine horn of each primary cusp [i.e., protoconid (1), metaconid (2), entoconid (3), hypoconid (4) and hypoconulid (5)], one at the mid-point on the marginal crest connecting the protoconid and metaconid (6), and one on the lowest point on the marginal ridge between the protoconid and hypoconid (7) and the hypoconid and hypoconulid (8), respectively. Landmarks were not collected in the trough between the metaconid and entoconid or between the entoconid and hypoconulid because of the variable presence of accessory cusps in these areas which violates the homology of these locations between molars.

The second set (referred to as the "RIDGE" curve) includes landmarks (approximately 50-70) along the top of the ridges running between each of the five dentine horns. This set of landmarks forms a closed ellipse, beginning at the tip of the protoconid and moving in a lingual direction. In the case of teeth with accessory cusps (e.g., cusp 6 or cusp 7) these dentine horns were ignored and points were collected on either side.

The third set (referred to as the "CERVIX" curve) includes landmarks (approximately 40-50) along the cervix, or cemento-enamel junction, of the tooth crown.

This set of landmarks also forms a closed ellipse, beginning below the protoconid dentine horn and moving in a lingual direction. Where small fragments of enamel were missing at the cervix its location was estimated.

Landmark datasets were exported as text files. Due to post-mortem damage the CERVIX curve is not present in all specimens and thus sample sizes differ between analyses. Specimens preserving both RIDGE and CERVIX curves (n = 23) and RIDGE curves only (n = 28) are listed in Tables 3.1 and 3.2. We tested the influence of downsampling (from 15-30 microns) and filtering (no filtering, kernel sizes of 1 and kernel sizes of 3) on landmark configurations of a single specimen. The distance in Procrustes shape-space between the original specimens and those that had been downsampled or filtered with different settings were minimal and considerably less than distances from the original specimen to any other individuals of the same species or tooth type (Skinner, 2008).

Derivation of homologous landmarks

For each specimen a single set of homologous landmarks and semilandmarks was derived from the three landmark files discussed above as follows. For both the RIDGE and CERVIX curve landmark sets a smooth curve was interpolated using a cubic spline function (a cubic spline is used so that the curve is forced to pass through each measured coordinate). In the case of the CERVIX curve an arbitrary first point is chosen at the base of the protoconid dentine horn and a cubic spline is fitted beginning at the first point and moving lingually around the circumference of the cervix to the last point.

Interpolated curves were then resampled to achieve identical point counts between specimens – these resampled points were used as semilandmarks. In the case of the

RIDGE curve, the eight MAIN landmarks were projected onto the curve dividing the curve into eight sections. For each section a large sample of very closely spaced points were computed along the curve and the distances between adjacent points were calculated and summed together to approximate the length along the curve between MAIN landmarks. Each length was divided by a given number and the coordinate location at each equally spaced distance was recorded (the number of landmarks between MAIN landmarks are illustrated in brackets in Fig. 3.1). In the case of the cervix curve, its length was calculated in the same way and 70 equally spaced points were derived.

These equidistantly spaced points are then used as starting positions for the semilandmark algorithm: semilandmarks were iteratively allowed to slide along their respective curves (i.e., RIDGE curve [n =55] and CERVIX curve [n = 70]) to minimize the bending energy of the thin-plate spline interpolation function computed between each specimen and the Procrustes average for the sample. We used the algorithm of Bookstein (1997; Gunz et al., 2005) that allows points to slide along tangents to the curve. These tangents were approximated for each semilandmark by the vector between the two neighboring points. Only the tips of the dentine horns were used as fixed landmarks, all other points were treated as semilandmarks. After the application of the sliding algorithm these semilandmarks were considered homologous for the purpose of multivariate analyses.

Procrustes superimposition

The homologous landmarks and semilandmarks (after sliding) were converted to shape coordinates by Generalized Least Squares Procrustes superimposition (Gower, 1975; Rohlf and Slice, 1990). This removed information about location and orientation

from the raw coordinates and standardized each specimen to unit centroid size, a size-measure computed as the square root of the sum of squared Euclidean distances from each landmark to the specimen's centroid (Dryden and Mardia, 1998). All data preprocessing was done in Mathematica v6.0 (www.wolfram.com) using a software routine written by PG.

Analysis of EDJ shape

EDJ shape was compared in a number of different analyses within both shape space (i.e., with all specimens size-standardized) and in form space (i.e., including the log of centroid size as a variable along with the shape coordinates). By using both methods it is possible to determine whether size and/or shape differentiates particular specimens. Analyses were conducted using both CERVIX and RIDGE landmarks, CERVIX only, and RIDGE only; for each of the foregoing combinations *A. africanus* and *P. robustus* were analyzed as a single, combined, sample.

Two statistical methods were used to assess EDJ shape variation in the study sample: principal components analysis (PCA) and canonical variates analysis (CVA). A PCA of shape coordinates (Bookstein, 1991; Rohlf, 1993) after Procrustes superimposition is an eigen-decomposition of the variance-covariance matrix of Procrustes coordinates. A CVA was computed as linear discriminants in the software package R (www.r-project.org) in the subspace of the first few principal components (i.e., using only a subset of all PCs) of the Procrustes shape coordinates. It was necessary to use a lower dimensional subspace because the number of variables greatly exceeded our sample size. If too many variables are used to compute the discriminant axes it results in unrealistic and unstable levels of discrimination. Our decision as to the number of PCs

to incorporate into the CVA was guided by a protocol in which the specimen labels were randomized and the resulting CVA was assessed with variable numbers of PCs included. The number of PCs included (in these analyses 5-8) did not exceed the point at which the specimens with randomized labels began to exhibit clustering patterns in the resulting CVA. In this way, we ensured that we only used a subset of PCs that did not generate separation among the samples with randomly assigned group labels.

The accuracy with which EDJ shape correctly classifies molars, according to species and molar position, was tested by cross validating the CVA. In this process each specimen in turn was considered unclassified and then classified by all the other molars of known position using posterior probabilities. Classification was implemented in R and groups were assigned equal prior probabilities.

Visualization of EDJ shape variation

To visualize the shape variation between taxa and between molar position we employed a method which allows a 3D triangulated surface reconstruction of the EDJ to be deformed to match the mean configuration of particular molar positions for each taxon (Gunz and Harvati, 2007). First, several thousand points were measured on the dentine surface of one specimen (STW412B) and converted to a triangulated surface (PLY file format) using Geomagic Studio 10. Because no shape data were collected within the occlusal basin of the EDJ this area of the surface was purposely defeatured. We then used the thin-plate spline interpolation function between the landmarks configuration of this specimen and a template configuration in Procrustes space to warp the vertices of this surface into Procrustes space. Finally we computed a thin-plate spline between this template and a target form (e.g., the mean configuration of the *P. robustus* M1 sample) to

morph the vertices of the surface. In order to visualize the differences between the surfaces representing the mean shapes of the molar representing each taxon, they were superimposed in Amira with one surface rendered transparent for better visual comparison.

Results

Figures 3.2a and 3.3a illustrate the results of the principal component analyses of the complete landmark dataset (i.e., RIDGE curve and CERVIX curve) in shape space and form space, respectively. While there is some separation between molar positions in each plot the considerable degree of overlap on the first two PCs indicates broad size and shape similarity among the molars in this sample. The canonical variate analysis of shape space (using 7 PCs) and form space (using 8 PCs) of the complete landmark dataset are illustrated in Figures 3.2b and 3.3b, respectively. Collectively, the first and second canonical variates in each analysis separate taxa and molar position (the percentage of total variance explained by each CV is listed). The combination of considerable overlap along the first two principal component axes and separation in the CVA indicates that it is small scale shape differences that separate taxa and molar position and the low percentage of total variance explained by the first and second CVs in each analysis indicates that these small scale shape differences account for relatively little of the overall shape variation. Specimens of unknown molar position are plotted with stars in both the PCA and CVA analyses. The reader is reminded that two dimensional plots of multidimensional analyses can suffer from projection errors and therefore the spatial association of unknown specimens with different groups should be not be over interpreted. The PCA and CVA analyses of the RIDGE only and CERVIX only datasets

reveal similar results, albeit with somewhat less distinction in the CVA analyses (not shown).

Classification using EDJ shape

Table 3.1 lists the classification to taxon and molar position of molars of known position within each type of analysis (i.e., CERVIX and RIDGE, RIDGE only and CERVIX only). Misclassifications to *molar position* are indicated with light shading and to *taxon* with dark shading. The most reliable classification results from the inclusion of shape information on both the RIDGE and CERVIX curves (78% and 91% in shape space and form space respectively). The inclusion of centroid size as a variable (i.e., the 'form' columns in Table 3.1) also appears to increase the classification accuracy when incorporating all landmarks, and for the RIDGE only analysis (79% and 93% in shape space and form space, respectively). The CERVIX only analysis performs particularly poorly with many misclassifications to both taxon and molar position (65% and 70% in shape space and form space, respectively). The small sample sizes of all groups (but particularly for *A. africanus* molars) render the results of the CVAs somewhat unstable. Altering the number of PCs included in the CVA can result in different classifications (usually to molar position) for one or two specimens, however, the relative degree of separation between taxon and molar position and the overall classification accuracy does not change substantially. The reasons for this instability are primarily the small sample sizes for particular molar positions, but it may also be due to the similarity in shape between certain molar types (see below).

The classification of unassigned molars is listed in Table 3.2. In addition to classifications based on each curve, analyses were also conducted in shape space for each

taxon separately. As discussed above, the classification of these specimens is also relatively unstable when differing numbers of PCs are included in the CVA, so we do not consider these results reliable. One possible exception is SK104 which, in all analyses is classified as a *P. robustus* first molar and this agrees with previous studies (Tobias et al., 1977; Suwa, 1996).

Metameric molar shape variation

Figure 3.4 illustrates the mean shape of the first, second and third molars of *A. africanus* and *P. robustus*. More direct comparisons of M1 vs. M2 and M2 vs. M3 shape are illustrated in Figure 3.5 (*A. africanus*) and 6 (*P. robustus*). Some trends in shape change between M1 and M3 are shared between these taxa. There is a reduction in crown height between M1 and M2 (a pattern that is more marked in *A. africanus*, Fig. 3.5a) and a marked reduction in the height of dentine horns between M1 and M2 (Figs. 3.5a/b, 3.6a/b). This pattern is not shared between M2 and M3, for the latter molar exhibits relatively tall mesial dentine horns and a minor decrease in the relative height of the distal dentine horns.

There is an increase in the mesiodistal length of the cervix along the molar row, being shortest in M1 and longest in M3 (this difference is particularly marked in *P. robustus*). There is a buccolingual expansion of the cervix in *A. africanus* M2 compared to its M1, and a reduction in buccolingual breadth between M2 and M3 (particularly in the distal half of the crown). A similar change in cervix shape is present in *P. robustus*, with the reduction in the buccolingual breadth of the distal crown between M2 and M3 being even more marked, with the M3 having a more triangular crown base (Fig. 3.4f and 3.6d). In *P. robustus*, the marked inter-radicular extensions of the enamel cap that

characterize the M1 are less pronounced in the M2 (see also lingual view of M2 in Fig. 3.7c).

There are also changes in the relative position of the dentine horns that can be assessed by comparing the position of their tips in the transparent and solid surface models. Some noteworthy differences include the relatively more centrally placed dentine horns on the talonid of the *P. robustus* M3 compared to the M2 (Fig. 3.6c/d). In contrast, *A. africanus* has more centrally placed dentine horns on the M2 compared to the M3 (Fig. 3.5c/d).

Taxonomic differences in mean molar shape

Figure 7 illustrates comparisons between *A. africanus* and *P. robustus* at each molar position. Dentine horn height is slightly higher in *A. africanus* compared to *P. robustus* in all molar positions. Crown height is greater in the M1 of *A. africanus* (ignoring somewhat the cervical extensions in the *P. robustus* M1). The dentine horns of the *A. africanus* M2 appear more centrally placed (Fig. 3.7d) than in *P. robustus* (the position of the dentine horns of the other molars does not substantially differ). The lingual margin of the cervix of the *A. africanus* M2 is not centrally compressed as in *P. robustus* and, not surprisingly, the distal half of the *P. robustus* M3 exhibits a buccolingually narrow and distally extended cervix compared to that of *A. africanus*.

Discussion

Both *A. africanus* and *P. robustus* exhibit similar EDJ shape differences between first, second and third molars, with some differences being more marked in one taxon than in the other (e.g., distal expansion of the crown base in *P. robustus* M3s). It is a

reasonable, but untested assumption, that EDJ morphology, in conjunction with differential enamel distribution, has an impact on tooth function and the metameric differences in EDJ shape identified here imply different biomechanical responses of the molars in each position under functional loading. Furthermore, these results suggest that the exposure of dentine and the creation of secondary shearing crests (Shimizu, 2002; King et al., 2005) would differ substantially between first molars and more distal molars in both taxa. The taxonomic differences in EDJ shape, while consistently separating *A. africanus* from *P. robustus* in discriminant analysis, are more subtle at each molar position and this may result in equally subtle differences in functional morphology at each position (i.e., *A. africanus* tending towards slightly taller dentine horns and crowns which could be associated with greater shearing potential or resistance to effects of abrasion). Thus, attempts to relate these morphological differences to differences in molar function and inferred dietary adaptations between *A. africanus* and *P. robustus* should take into account differences in the thickness and distribution of enamel over the EDJ in these taxa.

The small-scale, but consistent shape differences in EDJ morphology present between *A. africanus* and *P. robustus*, as well as between molar position within each of these species, can be compared to previous analyses of crown morphology of the outer enamel surface (e.g., Robinson, 1956; Wood and Abbott, 1983; Wood et al., 1983; Suwa et al., 1994). The differences in relative dentine horn height seen in the mean EDJ shapes are consistent with Robinson's suggestion (1963; cited in Wood et al., 1983) that *P. robustus* teeth are low cusped compared to *A. africanus*. But any differences are quite small at the EDJ and the relative contributions of EDJ shape and enamel distribution across the enamel cap to this pattern should be explored. Robinson (1956) claimed there

were differences in crown shape between *A. africanus* and *P. robustus* (e.g., oval in *Paranthropus* and more rectangular in *Australopithecus*), but Wood and Abbott (1983) could not find statistically significant differences in a measured index of crown shape. In any event such differences are difficult to evaluate with our analysis of EDJ shape because our assessment of crown shape comes primarily from the cervix while previous analyses have examined dimensions of the enamel cap, which are influenced by differential enamel deposition. However, examination of mean molar shapes does suggest differences in the shape of the cervix between these taxa (particularly in the shape of *P. robustus* M3s) even though such differences were less reliable in relation to classification.

Wood and colleagues (1983) noted significant reduction the relative cusp areas of the protoconid and metaconid (M1) and an increase in the areas of the hypoconulid (M1, M2 and M3) in *P. robustus* compared to *A. africanus*. Similarly, Suwa and colleagues (1994) found that *P. robustus* exhibits relatively smaller protoconid areas (M1, M2 and M3), and relatively larger hypoconulid (M1) and entoconid (M2) areas. A number of factors make it difficult to assess mean EDJ shape with respect to relative cusp size. The locations of fissures, used to delineate cusps at the OES, are difficult to determine from the EDJ as their pattern is dictated by a combination of EDJ shape, enamel extension rates and the interaction of mineralizing fronts of ameloblasts at coalescence points. Furthermore, the relative placement of dentine horns and the expansion or contraction of the location of the cervix, as well as differential enamel distribution, all influence relative cusp size as it is traditionally measured. Certainly the distal expansion of the cervix in *P. robustus* agrees with the demonstrated increase in the relative size of the hypoconulid. Comparisons of relative dentine horn volume could facilitate assessments of the relative

contribution of EDJ shape and enamel deposition to taxonomically distinctive patterns of relative cusp size (Avishai et al., 2004).

Our results have demonstrated differences in lower molar shape between *P. robustus* and *A. africanus* that have the potential to be incorporated into taxonomic and tooth type assessments of isolated teeth. These findings are also consistent with Suwa (1996) who used a combination of cusp area, crown shape and fissure pattern to achieve accurate classifications of first and second molars within samples of *A. africanus* and *P. robustus*, although classification accuracy was reduced when taxonomic affiliation was treated as unknown. The higher accuracy of Suwa's results compared to our own suggests that patterns of enamel distribution between the two taxa may generate taxon specific morphology that is not present at the EDJ (although the substantially larger samples used by Suwa are also likely to be a contributing factor). Assessing reliability of hominin EDJ shape for these purposes will require larger samples and in particular, molars from jaws whose position is certain and whose taxonomic affiliation can be based on other aspects of craniodental morphology. Currently, we have no similar data for East African fossil hominins such as *P. boisei* and *P. aethiopicus*, which would allow an assessment of the implications for the shape differences identified here to the ongoing debates regarding the monophyletic nature of *Paranthropus* (see Wood and Constantino, 2007). The debate about *Paranthropus* monophyly would also benefit from equivalent analyses of EDJ shape variation in upper molars and upper and lower premolars.

Conclusion

The results of this study show that there are small-scale, but consistent differences in EDJ shape between the lower molars of *A. africanus* and *P. robustus* and that these

taxa share consistent patterns of EDJ shape that serve to distinguish first, second, and third molars. The EDJ preserves much of the shape information that is preserved on the outer enamel surface of unworn and partially worn teeth and can be used to incorporate worn teeth into taxonomic and phylogenetic analyses. This will result in larger samples for nearly all early hominin taxa. Furthermore, EDJ shape may be useful in assessing the taxonomic affiliation and tooth type (if it is ambiguous) of unknown specimens, as well as allowing researchers to reassess previous assignments. The reliability of EDJ shape to classify molars would benefit from the inclusion of specimens from mandibles whose molar position is certain and whose taxonomic affiliation can be based on other aspects of morphology.

Table 3.1. Study sample and classification accuracy of molars whose position is considered known.

Specimen	Molar position	RIDGE and CERVIX – Shape (7PCs)	RIDGE and CERVIX – Form (8PCs)	CERVIX ONLY - Shape (8PCs)	CERVIX ONLY – Form (8PCs)	RIDGE ONLY – Shape (8PCs)	RIDGE ONLY – Form (8PCs)
DNH60B	*P. robustus* M1	*P. rob* M2	*P. rob* M1	*P. rob* M1	*P. rob* M1	*P. rob* M1	*P. rob* M1
SK828	*P. robustus* M1	*P. rob* M1	*P. rob* M1	*P. rob* M1	*P. rob* M1	*P. rob* M1	*P. rob* M1
SK843	*P. robustus* M1	*P. rob* M1	*P. rob* M1	*P. rob* M1	*P. rob* M1	*P. rob* M1	*P. rob* M1
STW309A	*A. africanus* M1	*A. afr* M1	*A. afr* M1	*A. afr* M2	*A. afr* M2	*A. afr* M1	*A. afr* M1
STW421A	*A. africanus* M1	*A. afr* M1	*A. afr* M1	*A. afr* M2	*P. rob* M2	*P. rob* M1	*P. rob* M1
DNH60C	*P. robustus* M2	*P. rob* M2	*P. rob* M2	*P. rob* M2	*A. afr* M3	*P. rob* M2	*P. rob* M2
SK6	*P. robustus* M2	*P. rob* M2	*P. rob* M2	*P. rob* M2	*P. rob* M2	*P. rob* M2	*P. rob* M2
SK843	*P. robustus* M2	*P. rob* M2	*P. rob* M2	*P. rob* M2	*A. afr* M2	*P. rob* M2	*P. rob* M2
SK1587B	*P. robustus* M2	*P. rob* M2	*P. rob* M2	*P. rob* M2	*P. rob* M2	*P. rob* M2	*P. rob* M2
STW213	*A. africanus* M2	*A. afr* M2	*A. afr* M2	*A. afr* M2	*P. rob* M2	*A. afr* M2	*A. afr* M2
STW308	*A. africanus* M2	----	----	----	----	*A. afr* M2	*A. afr* M2
STW412B	*A. africanus* M2	*A. afr* M2	*A. afr* M2	*A. afr* M3	*A. afr* M2	*A. afr* M2	*A. afr* M2
STW424	*A. africanus* M2	----	----	----	----	*A. afr* M2	*A. afr* M2
STW537	*A. africanus* M2	*A. afr* M3	*A. afr* M2	*A. afr* M2	*A. afr* M2	*A. afr* M2	*A. afr* M2
STW560E	*A. africanus* M2	*A. afr* M2	*A. afr* M2	*A. afr* M3	*A. afr* M3	*A. afr* M2	*A. afr* M2
SK6	*P. robustus* M3	*P. rob* M3	*P. rob* M3	*A. afr* M3	*A. afr* M3	*P. rob* M3	*P. rob* M3
SK22	*P. robustus* M3	*P. rob* M3	*P. rob* M3	*P. rob* M3	*P. rob* M3	*P. rob* M3	*P. rob* M3
SK75	*P. robustus* M3	*P. rob* M3	*P. rob* M3	*P. rob* M3	*P. rob* M3	*A. afr* M3	*P. rob* M3
SK841B	*P. robustus* M3	*P. rob* M3	*P. rob* M3	*P. rob* M3	*P. rob* M3	*A. afr* M3	*A. afr* M3
SK851	*P. robustus* M3	----	----	----	----	*P. rob* M3	*P. rob* M3
SKX5002	*P. robustus* M3	*P. rob* M3	*P. rob* M3	*P. rob* M2	*P. rob* M3	*P. rob* M3	*P. rob* M3
SKX5014	*P. robustus* M3	*A. afr* M3	*A. afr* M3	*P. rob* M3	*P. rob* M3	*A. afr* M3	*P. rob* M3
SKX10642	*P. robustus* M3	*P. rob* M2	*P. rob* M3	*P. rob* M3	*P. rob* M3	*P. rob* M3	*P. rob* M3
STW280	*A. africanus* M3	----	----	----	----	*A. afr* M3	*A. afr* M3
STW491	*A. africanus* M3	*P. rob* M3	*A. afr* M3	*P. rob* M3	*P. rob* M3	*A. afr* M3	*A. afr* M3
STW529	*A. africanus* M3	*A. afr* M3	*A. afr* M3	*A. afr* M2	*A. afr* M2	*P. rob* M3	*A. afr* M3
STW537	*A. africanus* M3	*A. afr* M2	*A. afr* M2	*A. afr* M2	*A. afr* M2	*A. afr* M2	*A. afr* M3
STW560B	*A. africanus* M3	----	----	----	----	*A. afr* M3	*A. afr* M3

Table 3.2. Classification of unassigned molars within each analysis.

Specimen	Previous molar position assignments[1]	RIDGE and CERVIX – Shape (7PCs)	RIDGE and CERVIX – Form (8PCs)	CERVIX ONLY – Shape (8PCs)	CERVIX ONLY – Form (8PCs)	RIDGE ONLY – Shape (8PCs)	RIDGE ONLY – Form (8PCs)	*P. robustus* RIDGE and CERVIX – Shape (7PCs)	*A. africanus* RIDGE and CERVIX – Shape (5PCs)
P. robustus									
DNH67	M1 (4)	----	----	----	----	*P. rob* M1	*P. rob* M1	----	----
GDA2	M2 (3)	*P. rob* M2	*P. rob* M3	*P. rob* M2	*A. afr* M2	*P. rob* M3	*P. rob* M3	*P. rob* M2	----
SK1	M2 (1)	*P. rob* M1	*P. rob* M2	*P. rob* M1	*P. rob* M2	*P. rob* M2	*P. rob* M2	*P. rob* M1	----
SK104	M1 (1); M1 (2)	*P. rob* M1	*P. rob* M1	*P. rob* M1	*P. rob* M1	*P. rob* M1	*P. rob* M1	*P. rob* M1	----
SK3974	M1 (1)	*P. rob* M1	*P. rob* M1	*P. rob* M2	*P. rob* M1	*P. rob* M2	*P. rob* M2	*P. rob* M2	----
A. africanus									
STS9	M1 (1); M1/2 (2)	*P. rob* M2	*P. rob* M2	*A. afr* M2	*A. afr* M2	*A. afr* M3	*P. rob* M2	----	*A. afr* M3
STW3	M2 (5)	*A. afr* M2	*A. afr* M3	*A. afr* M2	*A. afr* M2	*A. afr* M3	*A. afr* M3	----	*A. afr* M2
STW145	M1 (5)	*A. afr* M2	*A. afr* M2	*A. afr* M1	*A. afr* M1	*A. afr* M2	*A. afr* M2	----	*A. afr* M2
STW520	M3 (5)	----	----	----	----	*A. afr* M2	*A. afr* M2	----	----

1. Molar position assignments based on the following references: 1) Tobias et al., 1977; 2) Suwa, 1996; 3) Menter et al., 1999; 4) Keyser et al., 2000; 5) Moggi-Cecchi et al., 2006

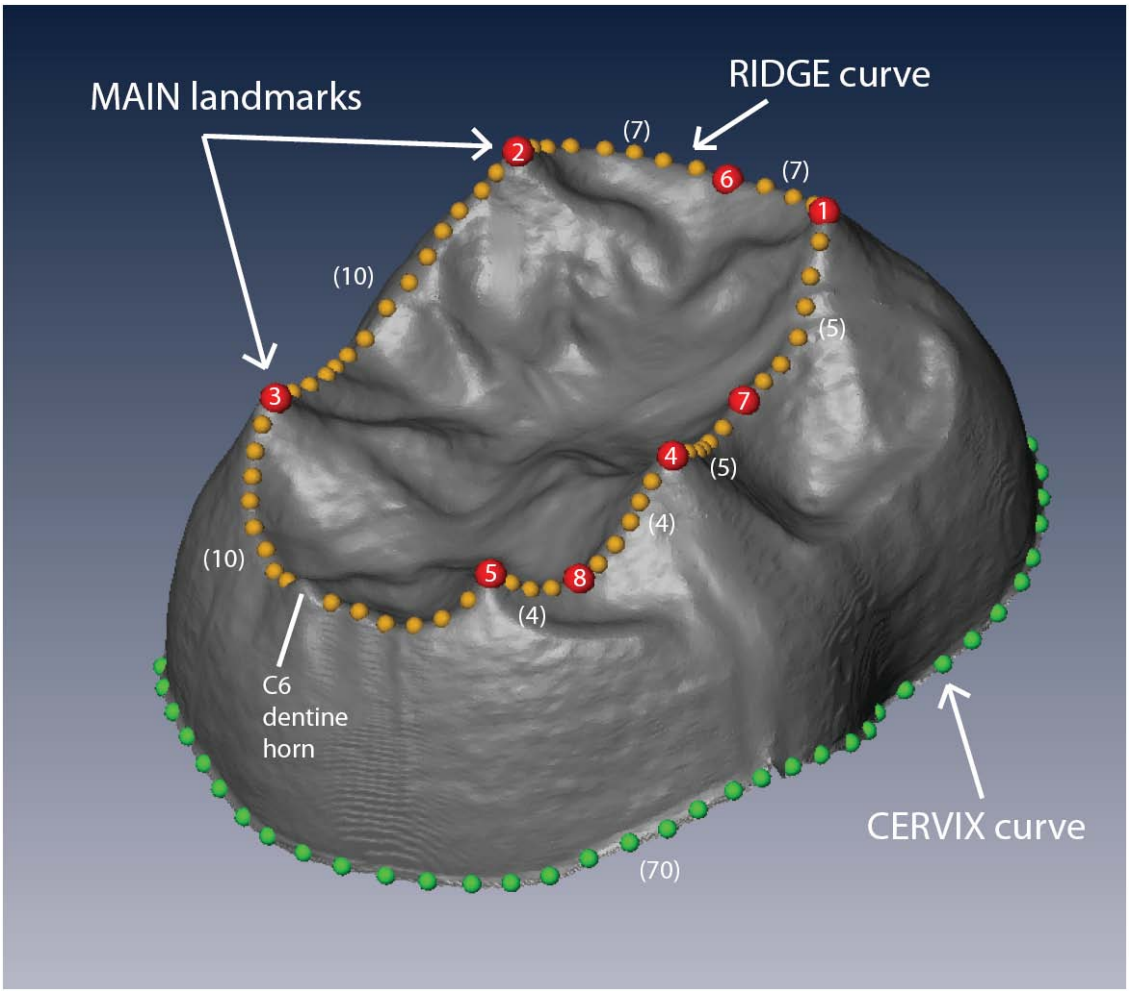

Figure 3.1. EDJ surface model of a lower molar (SK1587B) illustrating the anatomical landmarks used to capture EDJ shape. MAIN landmarks are collected on the tips of the dentine horns and in the troughs between the mesial and buccal dentine horns (red spheres), along the RIDGE curve that runs between the dentine horns (yellow spheres), and around the CERVIX curve (green spheres). Numbers in brackets refer to the number of equally spaced semilandmarks derived between MAIN landmarks for the RIDGE curve and on the CERVIX curve (see text for details). Landmarks shown here are those collected on the original specimens and are not the same as those generated from the sliding semi-landmark routine used to create a homologous set of landmarks between all specimens. Note that landmarks are collected on either side of the C6 dentine horn and are not included in the RIDGE curve.

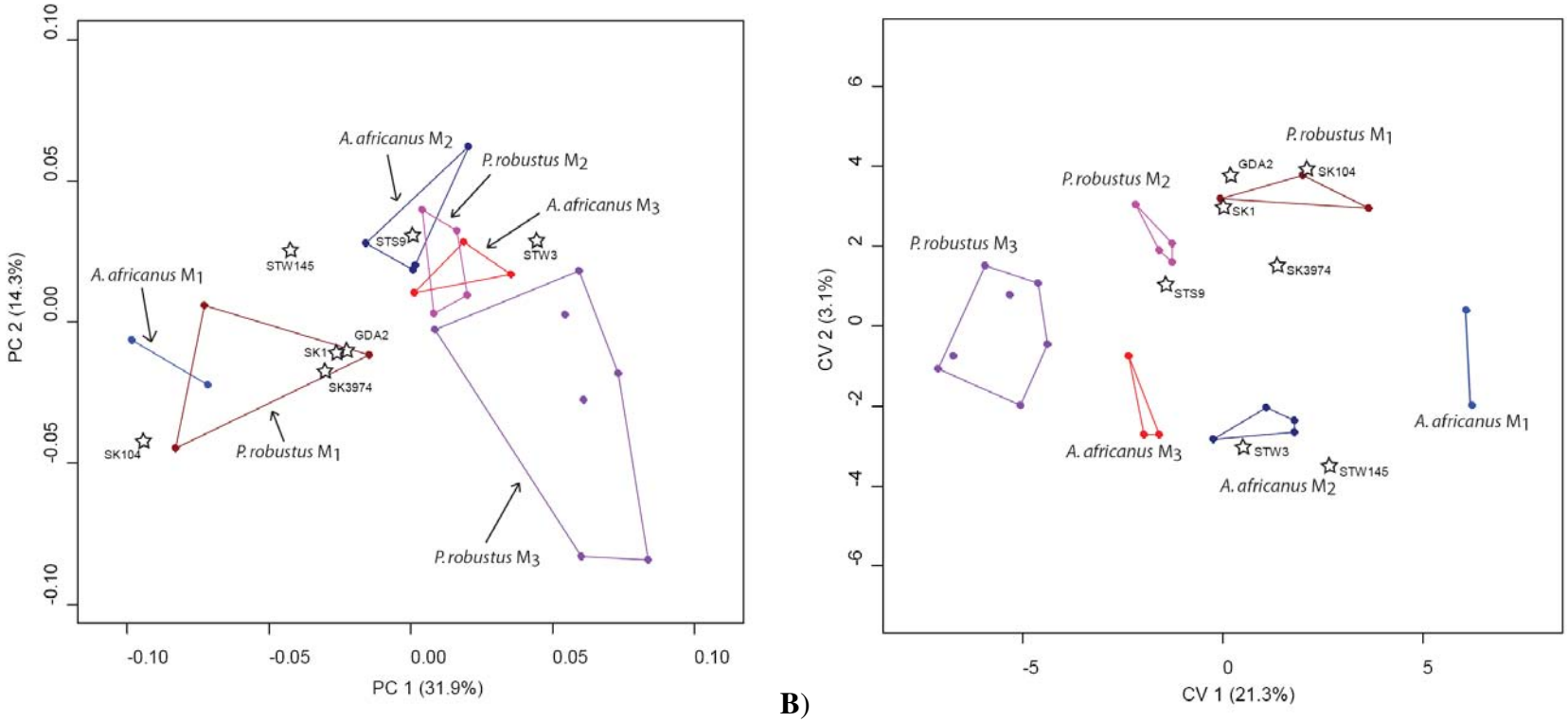

A) **B**)

Figure 3.2. PCA (**A**) and CVA (**B**) of EDJ morphology in shape space. CVA calculated using the first seven principal components separates both taxon and molar type. Groups are identified using polygons, while the two *A. africanus* M1s are joined by a line. Specimens whose molar type is uncertain are denoted by stars. Spatial association between specimens should be interpreted with caution as only two dimensions of a multidimensional shape space are represented.

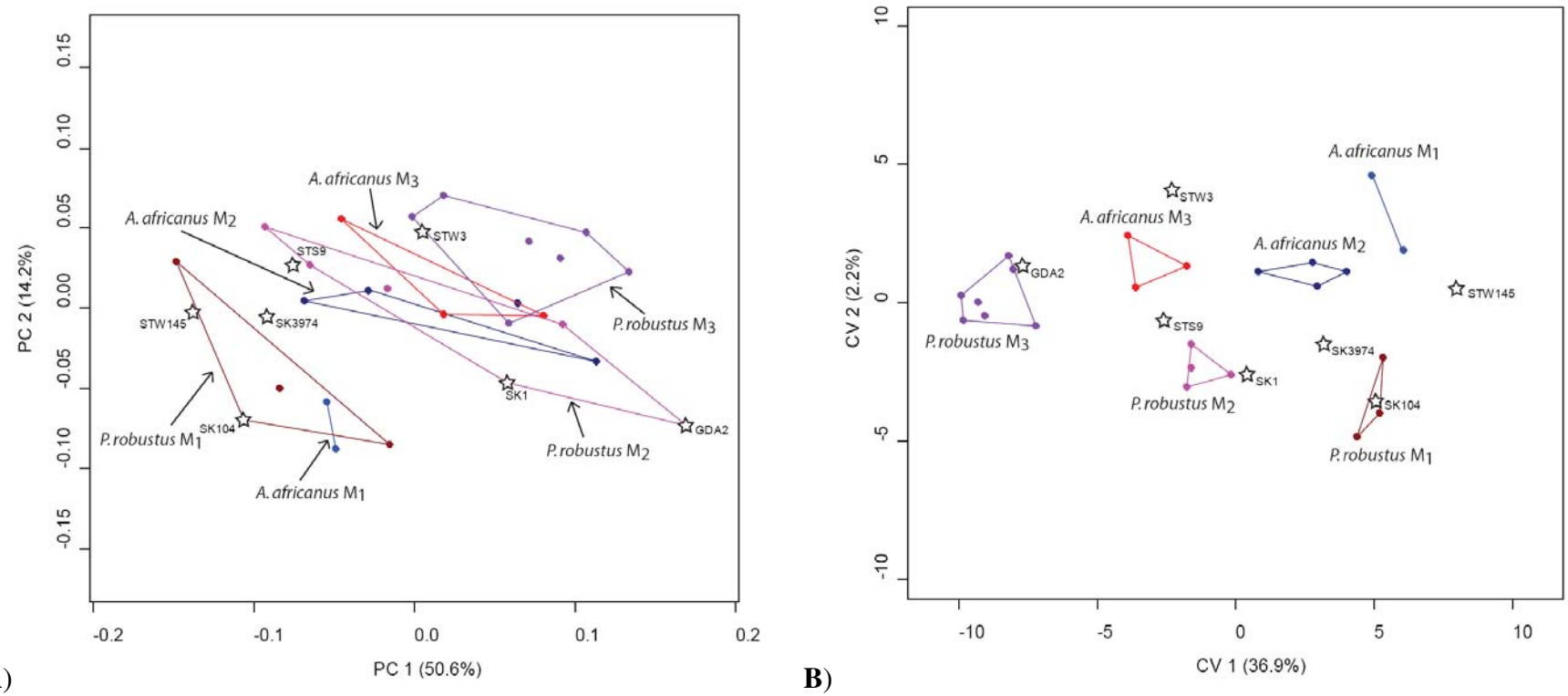

A) **B**)

Figure 3.3. PCA (**A**) and CVA (**B**) of EDJ morphology in form space. CVA calculated using the first eight principal components separates both taxon and molar type. Groups are identified using polygons, while the two *A. africanus* M1s are joined by a line. Specimens whose molar position is uncertain are denoted by stars. Spatial association between specimens should be interpreted with caution as only two dimensions of a multidimensional shape space are represented.

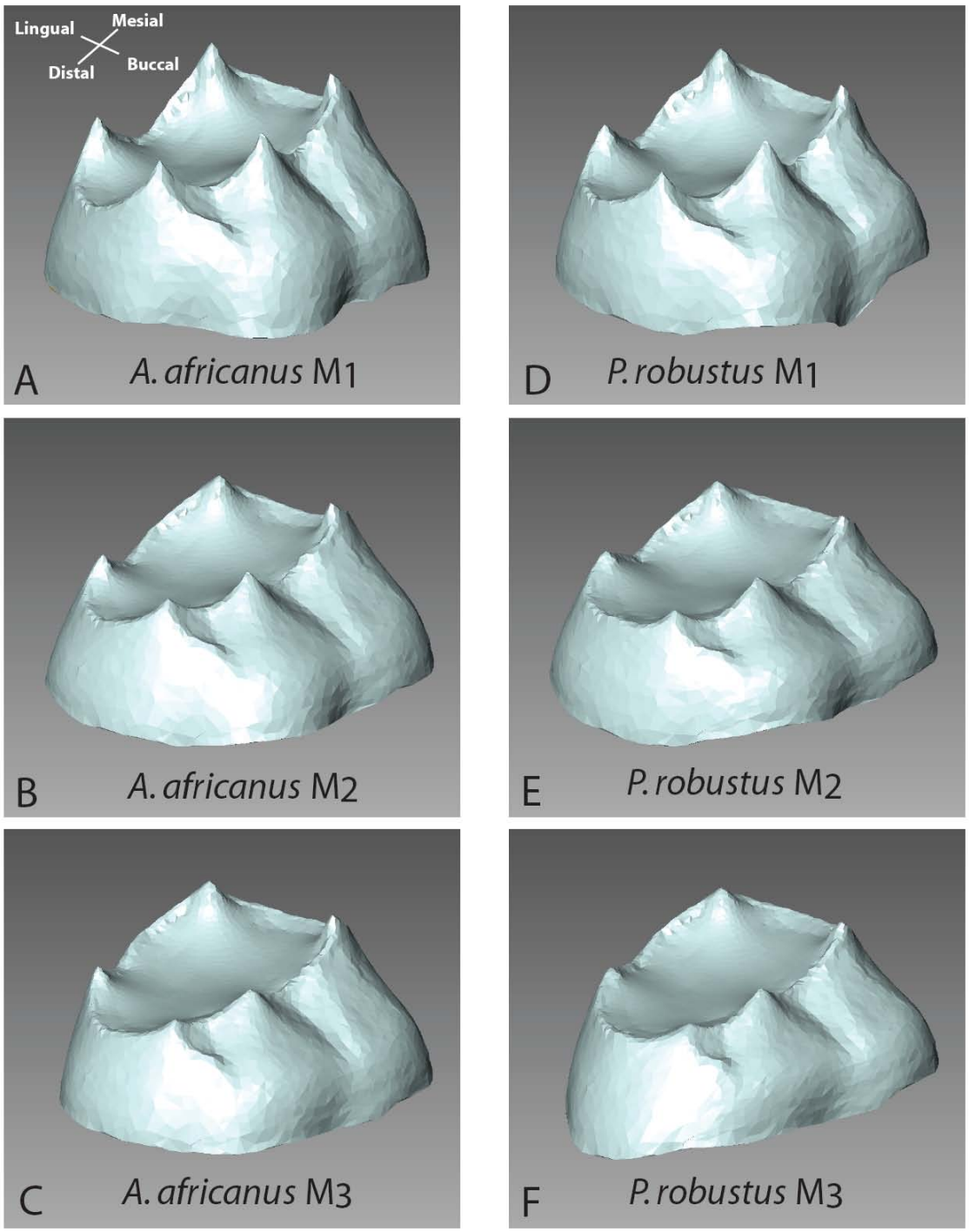

Figure 3.4. Illustrations of the mean shape of each molar type for *A. africanus* and *P. robustus*. These surface models are generated by warping a generic EDJ surface to match the mean configuration of RIDGE and CERVIX landmarks for each group. Note the differences in relative dentine horn height and cervix shape.

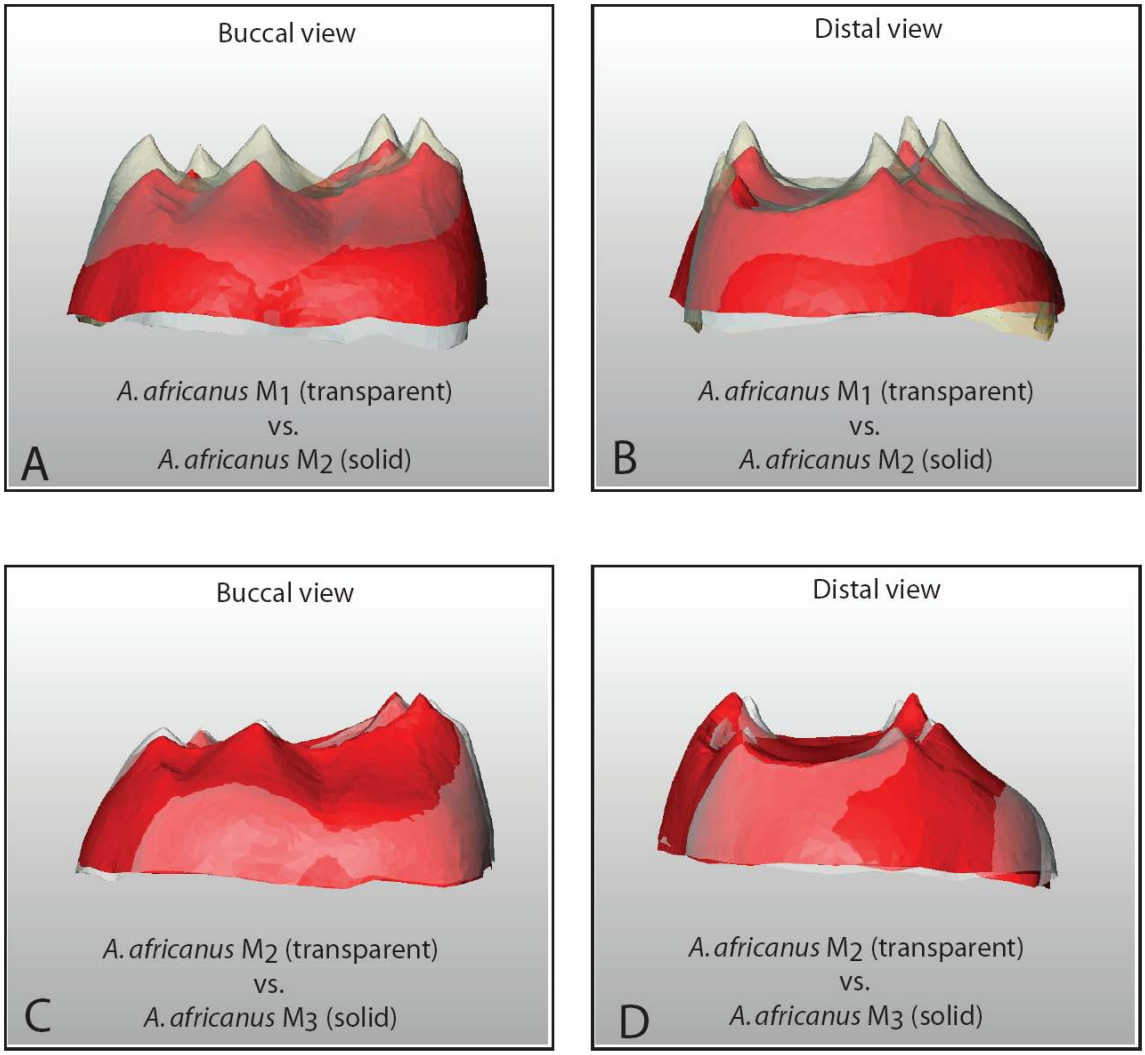

Figure 3.5. Comparison of metameric variation along the molar row in *A. africanus*. In each case one surface is made transparent to facilitate comparison. M1 compared to M2 in buccal (**A**) and distal (**B**) view. M2 compared to M3 in buccal (**C**) and distal (**D**) view.

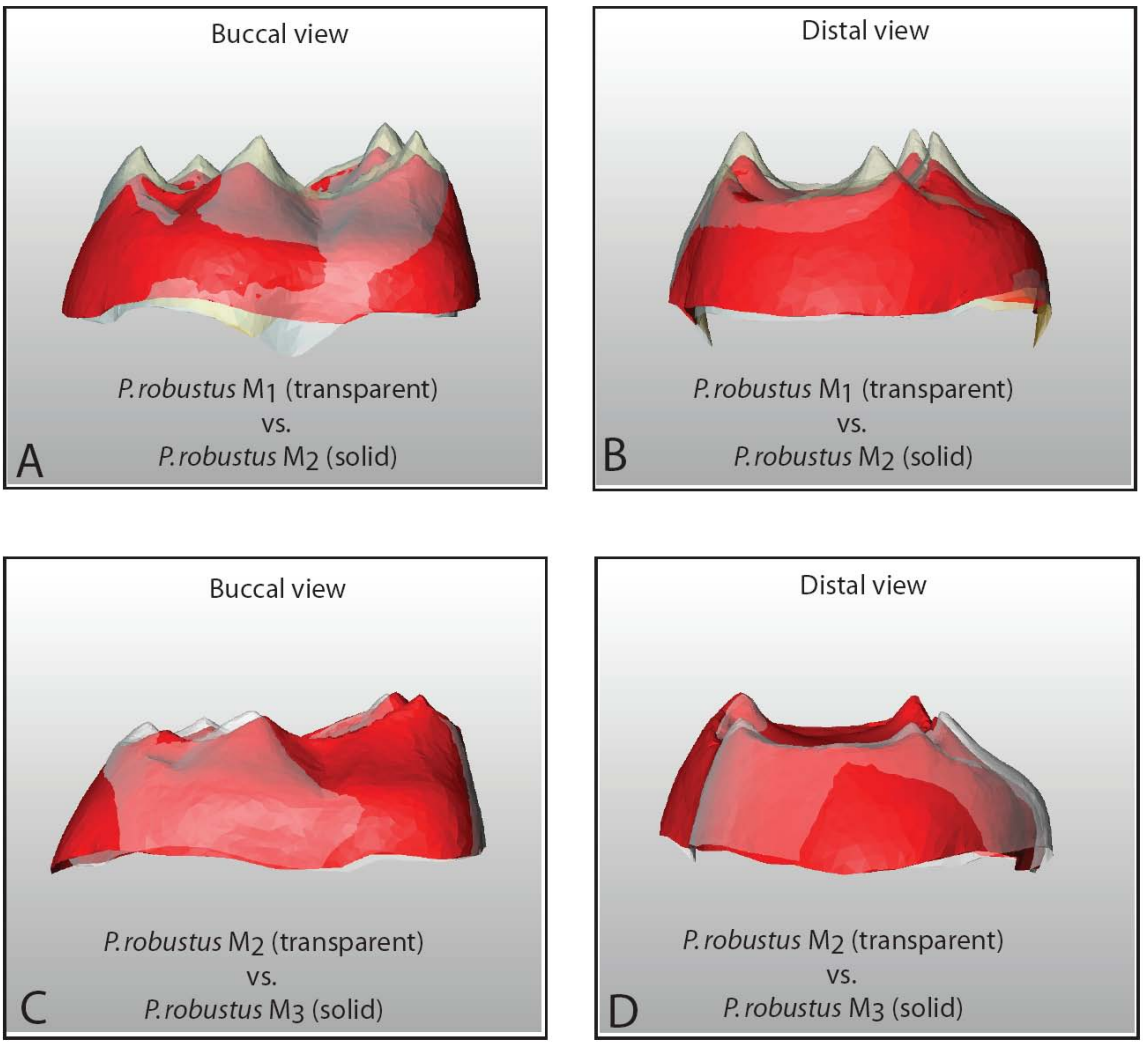

Figure 3.6. Comparison of metameric variation along the molar row in *P. robustus*. In each case one surface is made transparent to facilitate comparison. M1 compared to M2 in buccal (**A**) and distal (**B**) view. M2 compared to M3 in buccal (**C**) and distal (**D**) view.

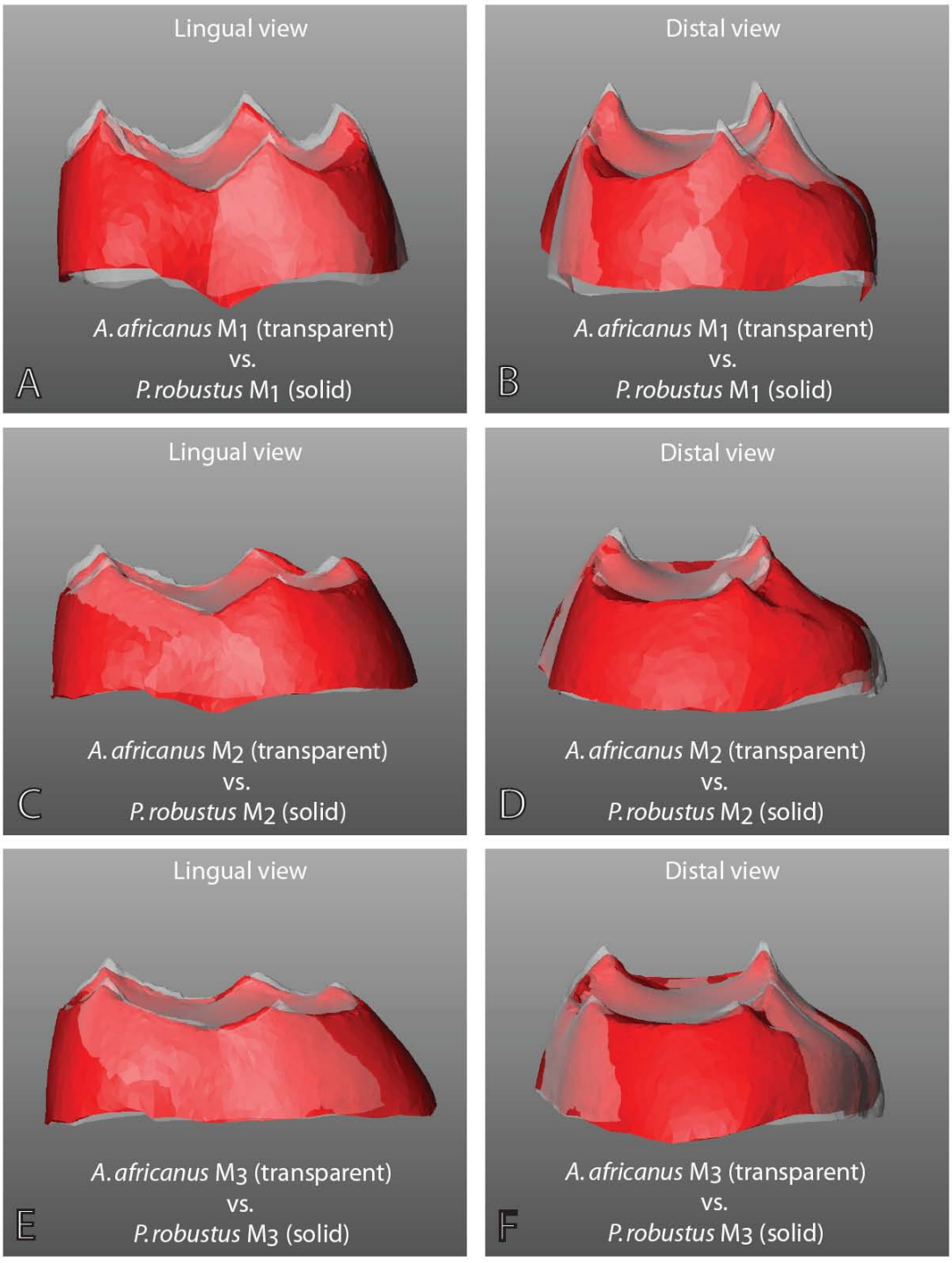

Figure 3.7. Taxonomic differences in EDJ shape at each molar position. In each case one surface is made transparent to facilitate comparison. First molar comparison in lingual (**A**) and distal (**B**) view. Second molar comparison in lingual (**C**) and distal (**D**) view. Third molar comparison in lingual (**E**) and distal (**F**) view.

CHAPTER 4: DENTAL TRAIT EXPRESSION AT THE ENAMEL-DENTINE JUNCTION OF LOWER MOLARS IN EXTANT AND FOSSIL HOMINOIDS

Abstract

Discrete dental traits are used as proxies for biological relatedness among modern human populations and for alpha taxonomy and phylogeny reconstruction within the hominin clade. We present a comparison of the expression of lower molar dental traits (cusp 6, cusp 7, trigonid crest pattern, and protostylid) at the enamel-dentine junction (EDJ) in a variety of extant and fossil hominoid taxa, in order to assess the contribution of the EDJ to the morphology of these traits at the outer enamel surface (OES). Molars (n = 44) were imaged nondestructively using high-resolution microCT, and three-dimensional surface models of the EDJ and OES were created to compare trait expression at each surface. Our results indicate that these dental traits originate at the EDJ, and that the EDJ is primarily responsible for their degree of expression at the OES. Importantly, variable trait morphology at the EDJ (often not easily recognizable at the OES) indicates that different developmental processes can produce traits that appear similar at the enamel surface, suggesting caution in intra- and intertaxonomic comparisons. The results also highlight the importance of the EDJ for understanding the morphological development of discrete traits, and for establishing graded scales of variation to compare trait frequency among groups for the purpose of taxonomic and/or phylogenetic analysis. Finally, this study demonstrates that imaging the EDJ of both worn and unworn fossil hominin teeth provides a novel source of information about tooth development and variation in crown morphology.

Introduction

Tooth crown morphology plays a critical role in hominin systematics in that it is relevant to hypotheses of alpha taxonomy, the assignment of fossil specimens to hominin taxa, and the reconstruction of the evolutionary history of the hominin clade. The presence and degree of expression of discrete traits at the outer enamel surface (OES) of teeth is an important component of these morphological analyses. Over the last three decades, a concerted effort has been made to standardize the classification of dental traits and to investigate how their expression varies within and among modern human populations (e.g., Turner et al., 1991). Discrete dental traits have come to play a central role in inferring biological relationships among modern humans (Scott and Turner, 1997, and references therein), living nonhuman primates (Johanson, 1974; Uchida, 1996; Pilbrow, 2003, 2006a), fossil hominoids (Pilbrow, 2006b), and fossil hominins (e.g., Weidenreich, 1937; Robinson, 1956; Wood and Abbott, 1983; Suwa et al., 1996; Bailey, 2002; Hlusko, 2004; Bailey and Lynch, 2005; Guatelli-Steinberg and Irish, 2005; Bailey and Wood, 2007; Martinón-Torres et al., 2007).

Traditional analyses of discrete traits make two assumptions. First, trait morphology that appears similar at the OES in different teeth is the result of developmental processes that are similar enough to allow valid comparisons within and between groups. Second, the OES is adequate for the formulation of standardized classifications of trait variation (often taking the form of grades from minor to marked trait expression). However, given how teeth grow, it is possible that different developmental processes can result in similar morphology at the OES, confounding the definition, classification, and comparison of discrete-trait morphology. During molar tooth development, major aspects of crown morphology such as cusps form on a

basement membrane (membrana praeformativa) that serves as the template upon which a layer of enamel is deposited (Butler, 1956, 1999). In mature teeth, the shape of this membrane is preserved as the enamel-dentine junction (EDJ), and trait expression at the OES is the culmination of EDJ shape and differential enamel distribution. This study tests these assumptions about trait morphology at the OES by examining the shape of the enamel-dentine junction (EDJ) as a proxy of trait development that is preserved in fully formed teeth.

To understand how different developmental processes can result in similar trait morphology at the OES, consider the following analogy. An artist is producing two sculptures (equivalent to the fully formed tooth crown) using a wireframe template (equivalent to the EDJ) and clay (equivalent to enamel). The artist can produce two sculptures that are identical at their outer surfaces in two ways. First he can begin with identically shaped wireframes and place an identical distribution of clay over each. Conversely, he can begin with wireframes that differ in shape but apply different distributions of clay over each to produce an identical shape at the surface. Furthermore, two sculptures that differ in the shape of their surfaces can each contain identical wireframes. Few studies of discrete dental traits have included information about the shape of the wireframe, or EDJ, template (but see Schwartz et al., 1998).

The utility of the EDJ for understanding the developmental basis of crown morphology has been demonstrated by a number of previous studies (Korenhof, 1960, 1961, 1982; Nager, 1960; Kraus, 1952; Kraus and Jordan, 1965; Sakai et al., 1965, 1967a,b, 1969; Sakai and Hanumura, 1971, 1973a,b; Corruccini 1987a,b, 1998, Schwartz et al., 1998; Sasaki and Kanazawa, 1999; Olejniczak et al., 2004; Macchiarelli et al., 2006). Most of these studies showed that the *gross* morphology of the OES is primarily

determined by the shape of the EDJ, with the shape of the enamel cap having only a minor influence on the morphology of the OES. Butler (1956: 32–33) noted: "Allowing for such modifications due to the deposition of enamel it remains true that the main features of the crown pattern, and many of its minor details, are already present in the membrane praeformativa before the hard tissues have developed." However, the relative contribution of the EDJ and the enamel cap to the expression of the smaller morphological features of the tooth crown, which constitute discrete traits of fossil and living hominins and hominoids, remains a topic of debate. Depending on the feature in question, both concordance and a lack of concordance between the EDJ surface and OES have been reported (e.g., Korenhof, 1960; Kraus, 1952; Corruccini and Holt, 1989; Schwartz et al., 1998; Olejniczak et al., 2004).

Nager (1960) decalcified 96 human teeth to compare the shapes of the OES and the EDJ of the same tooth. Based on his observations he defined three types of structures. (Nager [1960] used the term *crown relief* to refer to morphological structures, but for the purpose of this discussion, we will use the term *trait*.) A "primary-definitive" trait consists of structures that are present on both the EDJ and on the unworn OES. This category includes structures whose morphology is altered slightly when enamel is deposited over the surface of the growing tooth (e.g., the discrepancy between a pointed dentine horn and its overlying, more blunt enamel cusp does not preclude the "cusp" from being a primary-definitive trait). A "primary-temporary" trait consists of structures that are present on the EDJ, but cannot be observed on the unworn OES. An example of the latter is the hypocone-protocone ridge present at the EDJ of human upper molars, which is not visible at the enamel surface (Korenhof, 1960: Plate XIII, specimen MMSD 381). A "secondary" trait consists of structures not seen on the EDJ, but which are

evident on the OES (e.g., primary occlusal fissures present at the OES that have no corresponding fissurelike morphology at the dentine surface).

This study examines four dental traits of the lower molars—cusp 6, cusp 7, trigonid crest pattern, and the protostylid—with the aim of determining the relative contributions of the EDJ and the enamel cap to their expression at the OES in a variety of extant and extinct hominoids (Fig. 4.1). These traits are found in all hominin and extant great ape species, and they are thought to provide information about taxonomy and/or phylogeny (e.g., Johanson, 1974; Wood and Abbott, 1983; Suwa et al., 1996; Uchida, 1996; Pilbrow, 2003, 2006b; Bailey, 2002, 2006; Bailey and Hublin, 2006; Bailey and Wood, 2007; Martinón-Torres et al., 2007). A cusp 6 (also called a tuberculum sextum or entoconulid, and referred to hereafter as C6) is a cusp or cuspule on a lower molar within the distal fovea, lingual to the hypoconulid, or cusp 5 (Turner et al., 1991). A cusp 7 (also called a tuberculum intermedium, interconulid, or metaconulid, and referred to hereafter as C7) is a cusp or cuspule occurring in the lingual groove between the metaconid and entoconid (Turner et al., 1991; Hlusko, 2002). Trigonid crest pattern refers to the midtrigonid crest (defined as a transverse ridge or loph that connects the middle part of the two mesial cusps) and the distal trigonid crest (defined as a transverse ridge or loph that connects the distal aspect of the two mesial cusps) (Korenhof, 1982; Wu and Turner, 1993). A protostylid was described by Dahlberg (1950: 16) as "an elevation or ridge of enamel on the anterior part of the buccal surface of the lower molars, which ascends from the gingival end of the buccal groove and extends mesio-occlusally."

We ask three questions about each trait. Does it originate at the EDJ? What is the relative contribution of the EDJ to trait expression at the OES? Is the process of trait development, as inferred from the shape of the EDJ and overlying enamel cap, consistent

among the study taxa? If a trait can be considered primary-definitive under Nager's classification, then the EDJ expression of a trait can be incorporated into its formal definition and may inform the establishment of taxon-specific trait-scoring standards; the importance of the latter has been noted by a number of authors (e.g., Reid and Van Reenen, 1995; Van Reenen and Reid, 1995; Irish and Guatelli-Steinberg, 2003; Hlusko, 2004; Bailey and Wood, 2007). Furthermore, if it is shown that the EDJ is either a proxy for OES morphology or is more informative than the OES, then worn fossil teeth may be used in the analysis of discrete traits.

Materials and Methods

Study sample

Table 4.1 lists the molars included in this study. A range of living and extinct hominid and hominin taxa (following the taxonomy of Wood and Richmond, 2000) were included to capture variation for each trait within taxa, as well as variation in trait morphology among taxa. While sex is known for some specimens, it is not incorporated as a variable in our analysis due to the limited sample sizes for all taxa. First, second, and third molars were included, and in a few cases, metameric teeth from the same individual were examined. Modern human specimens include North American aboriginals and Early Bronze Age specimens from Great Britain. Extant hominoids include *Pan troglodytes verus*, *Gorilla gorilla beringei*, and *Pongo pygmaeus* ssp. The fossil taxa include *Gigantopithecus blacki*, *Australopithecus africanus*, *Paranthropus robustus*, and *Homo neanderthalensis*.

Micro-computed tomography and surface reconstruction

In order to produce three-dimensional reconstructions of the EDJ and the OES, each tooth was scanned using either the SKYSCAN 1172 Desktop MicroCT (scan parameters: 100Kv, 94μA, 2.0mm aluminum and copper filter, 2048 x 2048 matrix, 0.12 rotation step, 360 degrees of rotation, 2 frame averaging) or SCANCO μCT40 (scan parameters: 70Kv, 114μA, 1024 x 1024 matrix, 0.36 rotation step, 180 degrees of rotation) computed tomographic scanner. Pixel dimensions and slice thickness between reconstructed serial images were isometric with resolutions ranging between 13 and 50 microns (μm) (e.g., isometric voxels of 13 μm × 13 μm × 13 μm to 50 μm × 50 μm × 50 μm).

To facilitate tissue segmentation, the complete image stack for each tooth was filtered using a three-dimensional median filter (kernel size of 3), followed by a mean of least variance filter (kernel size of 3), implemented as a computer-programmed macro. This filtering process results in more homogeneous tissue classes (e.g., enamel vs. dentine) and allocates pixels with intermediate gray-scale values at tissue interfaces (i.e., air-enamel, enamel-dentine, air-dentine) to the appropriate tissue (Schulze and Pearce, 1994). The effect of the filtering process on the morphology of the reconstructed surfaces was assessed by overlaying surfaces derived from unfiltered images over surfaces derived from filtered images and examining differences in shape. The effect of filtering on surface morphology is minimal compared to the size of the structures (e.g., cusps and crests) that constitute the discrete traits being analyzed. An exception is that the size and shape of very small tubercles (e.g., <0.5 mm in length) cannot be discerned using this methodology (discussed below).

Filtered image stacks were imported into the Amira software package (v4.1, www.amiravis.com), and enamel and dentine tissues were segmented by evaluating the

3D-voxel-value histogram and its distribution of gray-scale values, which typically presents a trimodal distribution with one peak representing dentine, another peak representing enamel, and a third peak representing air and background noise in the images. For unfossilized teeth of extant taxa, in which enamel and dentine tissues differ substantially in their degree of mineralization (and therefore their densities and the ability of X-rays to pass through them), the filtering process results in gray-scale pixel-value distributions for each tissue that do not overlap. In fossil teeth, diagenetic alteration (e.g., dentine remineralization) sometimes results in similar tissue densities for enamel and dentine, and thus overlapping gray-scale pixel-value ranges for each tissue (Olejniczak and Grine, 2006). Even after filtering, there is often an incomplete separation between the two, and a decision must be made about the range of gray-scale values allocated to each tissue. All of the teeth in this study evinced a clear separation of enamel and dentine, resulting in well-distinguished gray-scale values and accurate representations of the EDJ. Specimens that could not be segmented to produce accurate surface reconstructions were excluded from the study.

After segmentation, the OES and the EDJ were reconstructed as triangle-based surface models in Amira 4.0 (surface generation module using unconstrained smoothing parameter), which can be rotated and enlarged interactively to view and compare trait expression. In specimens that preserved only the enamel cap, a surface model of the EDJ was created by digitally removing the occlusal surface of the model of the reconstructed enamel cap surface.

Results

The manifestation of each trait at the EDJ and the influence of enamel deposition on trait manifestation at the OES are described below. Trait distribution within and among taxa is addressed, although sample sizes are too small to warrant strong inferences to be drawn regarding intertaxonomic differences in trait presence/expression.

Cusp 6

Variation in C6 manifestation at the EDJ of molars in the study sample is summarized schematically in Figure 4.2 and can be separated into two types. The first type, referred to here as the "hypoconulid-type" C6, is characterized by a dentine horn (DH) on the lingual slope of the hypoconulid DH (Figs. 4.2b, 4.3a). The shape of this feature resembles a smaller version of the adjacent hypoconulid DH. In a number of specimens, this DH was duplicated, with both horns occurring in proximity to the hypoconulid DH and resembling serially developed structures. These specimens are characterized as having a double hypoconulid-type C6 (Figs. 4.2c, 4.3b). These types of C6 are most common in the *P. t. verus* sample but were also present in the *H. sapiens* sample (Table 4.2). The close association of this type of C6 with the hypoconulid is not always apparent from the OES, particularly in partially worn teeth. Furthermore, in some chimpanzee teeth, a double hypoconulid-type C6 can only be identified at the EDJ (Fig. 4.3b) due to tooth wear on the distal margin of the tooth crown.

The second type of C6, referred to here as the "fovea-type" C6, takes the form of a DH on the marginal ridge of the distal fovea between the hypoconulid and entoconid (Figs. 4.2d, 4.3c). This type can be differentiated from the hypoconulid-type because its DH is separate from the hypoconulid DH and entoconid DH. In high-cusped teeth, such

as those of *G. g. beringei*, this type of C6 can be a tubercle on a cingulumlike shelf on the distal marginal ridge of the EDJ (seen on the OES of Fig. 4.1). Taxa exhibiting the fovea-type C6 include *G. blacki*, *A. africanus*, *P. robustus*, *H. neanderthalensis*, *P. pygmaeus* ssp., and *G. g. beringei*. Similar to the hypoconulid-type discussed above, the fovea-type C6 can also appear in a duplex form, with two DH-like features on the margin of the distal fovea (schematically represented in Fig. 4.2e). One specimen of *H. sapiens* had both types of C6 at the EDJ (schematically represented in Fig. 4.2f).

In both *A. africanus* and *P. robustus*, which have the fovea-type C6 when present, enamel distribution has a marked influence on the shape of the C6 at the OES. The small DH(s) at the EDJ corresponds with a relatively large cusp at the OES. This contrasts with all of the other taxa, in which the relative size of the C6 DH(s) is similar to the relative size of the C6 cusps at the OES. Thus, in these thickly enameled taxa (Grine and Martin, 1988), enamel distribution has a greater influence on C6 shape at the OES than in thinly enameled taxa.

Another variant (possibly similar developmentally to a C6) was observed in one *P. t. verus* molar and in one *G. g. beringei* molar (Fig. 4.3d). In these specimens, a small cusp is present on the OES on a crest that joins the entoconid to the hypoconulid (the presence of this crest is variable within and among most of the study taxa). In both teeth, this cusp corresponds to a DH at the EDJ located on a crest between the entoconid DH and hypoconulid DH.

Cusp 7

Variation in C7 manifestation at the EDJ of molars in the study sample is summarized schematically in Figure 4.4. Like the C6 trait, there are two main types of

C7. The first type of C7, referred to as the "metaconulid-type," is manifested at the EDJ as a protuberance or DH-like feature on the end of a shoulder on the distal ridge of the metaconid DH (Fig. 4.4c and 4.5a). This shoulder can be faint or pronounced, and it can occur at varying distances from the metaconid DH (Figs. 4.4d, 4.5b). This type seems consistent with grade 1A of the ASUDAS classification of cusp 7 (Turner et al., 1991).

The second type of C7, referred to as the "interconulid-type," is manifest at the EDJ by a DH of variable size on the low point of the marginal ridge between the DHs of the metaconid and entoconid (Figs. 4.4f, 4.5c,d). In some cases, this type of C7 appears more spatially associated with the metaconid, as evidenced by a less-developed trough between the C7 DH and the metaconid compared to the trough between it and the entoconid DH (Fig. 4.4e). This type corresponds with grades 1–4 of the ASUDAS classification of cusp 7. The metaconulid-type C7 is present in *P. t. verus, G. g. beringei* and *A. africanus*, while the interconulid-type is present in *H. sapiens*, *H. neanderthalensis*, *P. robustus*, *A. africanus*, and *G. blacki*; no C7 was observed in *P. pygmaeus*.

Differential enamel distribution does not greatly influence the manifestation of C7 at the OES, but distinguishing between a cuspule at the OES over a pronounced shoulder of the metaconid, and a cuspule at the OES over a small DH on the shoulder of the metaconid, is difficult based on OES morphology alone. Dental attrition does not obscure C7 morphology at the OES in this sample. In one *A. africanus* (STW 560A) specimen, the OES exhibits both of the types of C7 discussed here (the EDJ presenting a DH under the interconulid-type and only a slight ridge elevation below the metaconulid-type C7).

Trigonid crest pattern (TCP)

Variation in trigonid crest patterning at the EDJ is summarized schematically in Figure 4.6. The first type consists of either weakly pronounced or well-pronounced crests on the slopes of the protoconid and metaconid DHs, which extend from the tips of the DHs towards the occlusal basin (Figs. 4.6a,b and 4.7a). The second type consists of pronounced but separate crests that extend across the occlusal basin (Figs. 4.6c, and 4.7c). The third type is a single crest between the tips of the metaconid and protoconid DHs, with or without accompanying minor crests (Figs. 4.6e, 4.7b). In the fourth type, mesial and middle crests (either both complete or one interrupted) link the protoconid and metaconid DHs (Figs. 4.6f,g, 4.7d). Other minor variations in the study sample are not discussed here (e.g., Fig. 4.6d,h).

Homo neanderthalensis exhibits the most prominent trigonid crest expression at the EDJ, characterized in some specimens by a single sharp crest between the metaconid and protoconid DHs with no other associated crest features. *Pan t. verus* is most variable in TCP, while *P. robustus*, *A. africanus*, and *G. blacki* present little in the way of trigonid crest morphology. The relationship between the informal types of TCP above and two other discrete dental traits, mesial and distal trigonid crests (Korenhof, 1982, Sasaki and Kanazawa, 1999), is addressed below.

In unworn teeth, the TCP can, in most cases, be inferred accurately from the OES; however, moderate wear can make the interpretation of TCP difficult. In worn molars, the EDJ preserves trigonid crest features that form during the development of the tooth. Generally, our analysis supports the conclusion that trigonid crest pattern is primary-definitive in nature, with crest features present at the OES associated with matching crest features at the EDJ. Even small accessory crests observable at the OES have dentine analogues.

Protostylid

Variation in protostylid expression at the EDJ is summarized schematically in Figure 4.8. In this schematic representation, we have included morphological features on the mesial border of the protoconid DH and on the distal border of the hypoconulid DH. In minor forms of protostylid expression (Figs. 4.8b,c, 4.9a), small wrinkles/depressions are present at the EDJ. Such features may be located mesially on the slope of the protoconid DH, centrally between the protoconid and hypoconid DHs, and/or distally between the hypoconid and hypoconulid DHs. When the protostylid is strongly expressed, the cingular shelf is large, and it is the shape of the buccal slopes of the protoconid and hypoconid DHs that dictate the morphology of the buccal crown surface (Figs. 4.8d–f, 4.9b–d). We see no reason to exclude mesial and distal cingular features from the "protostylid" complex, and thus our analysis differs from some previous studies of this trait (e.g., Hlusko, 2004). Examination of the EDJ of molars in this sample suggests that these morphological features are the result of the same developmental processes. Taxa with marked protostylid expression include *A. africanus*, *P. robustus*, and *G. g. beringei*. All of the other taxa present minor expression of the protostylid (with the exception of the single *G. blacki* molar, which presents no protostylid morphology).

All of the OES structures included as a protostylid originate at the EDJ, with only a minor influence due to the differential deposition of enamel. In almost all cases, there is a consistent relationship between protostylid manifestations at the EDJ and at the OES, and therefore the protostylid is a primary-definitive trait. Even when the OES expression of the protostylid is complex, it is matched by an equivalent morphology at the EDJ (Fig. 4.9d). In a small number of cases, minor surface features on the buccal side of the buccal

DHs could not be detected at the OES, but the influence of dental attrition on the manifestation of this trait at the OES could not be ruled out in these cases.

Discussion

The aim of this study was to address three questions related to the development of discrete dental traits: Do the four dental traits originate at the EDJ? What is the contribution of the EDJ to trait expression at the OES? Is the process of trait development, as inferred from the shape of the EDJ and overlying enamel cap, consistent among the study taxa? With respect to the first two questions, our results are consistent: the presence and degree of morphological expression of C6, C7, trigonid crest pattern, and protostylid are dictated primarily by the EDJ. Enamel deposition rarely masks trait presence at the EDJ, nor are there any OES traits in the absence of EDJ expression. These results mean that the EDJ of moderately worn teeth may be used to assess the presence or absence of traits (e.g., the second C6 in Fig. 4.3b), and in unworn teeth, information about the EDJ may clarify the developmental basis of traits present at the OES. Our results demonstrate a strong correlation between the EDJ and OES morphology for the traits studied here, and they suggest a consistent predictive relationship between EDJ and OES morphology for the majority of dental traits incorporated into anthropological analyses (contra Kraus, 1952; Schwartz et al., 1998; Olejniczak et al., 2004).

The traits C6 and C7 are discussed together because they are both accessory cusps, albeit present in different parts of the tooth crown. In all molars, a feature scored as a C6 at the OES was located directly above a DH-like feature at the EDJ. In some cases, this DH was similar in shape to the DHs of the adjacent primary cusps (i.e., hypoconulid and entoconid) in its degree of pointedness and slope shape, while in other

cases, the DH was more like a tubercle with a low, blunt tip. The resolution of the microCT scan may influence the morphology of small EDJ features, and this must be considered in assessments of the original shape of diminutive DHs at the EDJ. Nonetheless, all C6s in the study sample can be classified as primary-definitive traits (sensu Nager, 1960), with clear evidence that the trait originates at the EDJ. As with most cusps, enamel deposition alters the shape of the DH through the creation of more convex cusp slopes and a blunter, rounded cusp tip.

In all teeth in which the C7 is large in relation to adjacent cusps, there is an equivalent DH-like feature at the EDJ. Even in teeth in which a small cuspule is located in the valley between the metaconid and entoconid, there is a corresponding elevation at the EDJ. Some manifestations of C7 at the OES (those corresponding to a type 1A under the ASUDAS) are more ambiguous at the EDJ. For example, while a cuspule-like morphology could be argued for the OES, the corresponding EDJ is marked by a protuberance rather than a distinct, isolated elevation of tissue that would be expected to underlie an enamel cuspule. Nonetheless, although concordance between the OES and EDJ in the metaconulid-type C7 is not as pronounced as the interconulid-type, it is still a primary-definitive trait under Nager's classification.

The nature of the developmental processes underlying accessory-cusp formation relates directly to our third question regarding developmental similarity of traits both within and between different taxa. Should a hypoconulid-type C6 in a *P. t. verus* specimen and a fovea-type C6 in a *G. g. beringei* specimen be coded as the same discrete trait for the purpose of phylogenetic analysis? From our observations, these two types appear to be the result of subtly different developmental processes (as an aside, we suggest that the term "entoconulid" as a synonym for C6 is inappropriate unless one is

specifically highlighting the spatial association of this accessory cusp with the entoconid). Similarly, the two types of C7, observed between the metaconid and entoconid, appear to represent different underlying developmental processes. This conclusion is supported by one *A. africanus* specimen (STW 560A) that exhibits both a metaconulid-type and interconulid-type C7 (complicating attempts to classify these two features under one trait).

Can developmental genetic research throw any light on these results? Recent research into cusp patterning on murine teeth (Jernvall and Jung, 2000; Jernvall and Thesleff, 2000) suggests that an accessory cusp at the OES, associated with a DH at the EDJ, corresponds to a secondary enamel knot, the presence and location of which is determined by the genetic pathways that control the expression domains of the gene products (Kassai et al., 2005). It has been suggested that the pattern of primary and secondary cusps on a mammalian tooth crown is the outcome of an iterative cusp-patterning program (Polly, 1998; Jernvall and Jung, 2000; Jernvall and Thesleff, 2000; Salazar-Ciudad et al., 2003), which is influenced both by the genes that control the spacing and size of DHs and/or the overall size of the crown. Cai et al. (2007) showed that, in mice and rats, epithelial tissue dictates cusp size and the underlying mesenchymal tissue dictates crown size. Under this paradigm, it is unlikely that a tooth would exhibit morphology resulting from a gene for a C6 or double-C6; rather, the pattern of spacing of secondary enamel knots probably results in the formation of (1) an accessory cusp adjacent to the hypoconulid and (2) another accessory cusp adjacent to that (Fig. 4.3b). Similarly, the difference between a metaconulid-type and an interconulid-type C7 may reflect patterns of growth (or differentiation) rates within the developing tooth germ rather than a one-to-one relationship between a gene and a feature. Our observations

indicate that DH-like features can appear in many locations on the EDJ (e.g., on a trigonid crest, between the hypoconid and hypoconulid DHs, or on a crest between the hypoconulid and entoconid DHs). Within a developmental paradigm that incorporates a patterning-cascade mode of cusp development (sensu Jernvall and Jung, 2000), it may be difficult to devise a simple coding scheme for accessory cusps that is consistent with their developmental origin. Examination of EDJ expression of accessory cusps reveals morphological variation that is less obvious at the OES, and that will need to be addressed as discrete-trait analysis extends beyond modern humans to other primate taxa.

While the majority of accessory cusps have corresponding DHs underlying them at the EDJ, in some specimens, there is only a faint corresponding elevation at the EDJ. In a number of specimens, C6s at the OES (in the range of 0.5–1.0 mm in diameter) presented morphology that, in terms of cuspule shape, must be attributed to the growth of the enamel rather than the EDJ template. Histological analyses of hominoid enamel formation have determined that the ameloblasts deposit more enamel per day over cusp tips (on average) compared to lateral or cervical regions of the tooth crown (Beynon et al., 1991). Assuming that DHs of C6s form in a similar manner to the DHs of the primary cusps (i.e., with the initiation of a secondary enamel knot), then ameloblasts in these locations may be depositing proportionately thicker enamel than adjacent regions. This could result in cusplike morphology at the OES and explain the apparent discrepancies between EDJ shape and the OES expression of accessory cusps seen in some teeth. Histological analysis of accessory cusps may throw light on the ontogeny of these features.

Examination of the EDJ proved especially valuable for the assessment and interpretation of trigonid crest expression in the study sample. Like accessory cusps,

trigonid crest patterns present at the OES derive from the EDJ. The high prevalence of a middle crest on the EDJ of the *H. neanderthalensis* sample supports conclusions by Bailey (2002) that the midtrigonid crest is a characteristic feature of this taxon compared to modern humans. However, more comparative studies are needed before it will be possible to say whether the manifestation of this trait in *H. neanderthalensis* is derived or primitive. Investigation of the EDJ has shown that trigonid crest patterning can be highly variable, and that sorting this variation into midtrigonid (Wu and Turner, 1993; Bailey, 2002) and a distal trigonid crest traits (Korenhof, 1982; Sasaki and Kanazawa, 1999) may be unwarranted for some taxa (e.g., *P. troglodytes* ssp.). Crest features between DHs, including mesial, middle, and distal trigonid crests, as well as the crest that periodically forms between the entoconid and hypoconulid DHs (Fig. 4.3d), may be related to structural properties (e.g., elasticity or turgidity) of the tissues involved in tooth growth and to their interactions during development. Butler (1956: 60–61) noted that ridges/crests "are probably produced by tensions set up in the epithelium by the relative movement of cusps, owing to unequal growth or to changes in the shape of the follicle." Crests may reflect the timing and rate of DH growth and their placement with respect to other DHs on the developing tooth germ.

Our analysis of the EDJ suggests that protostylid expression is influenced by three primary factors. First is the relative location of the DHs of the main buccal cusps (i.e., the DHs of the protoconid, hypoconid, and hypoconulid) with respect to the buccal margin of the tooth crown (e.g., centrally placed versus located near the lingual margin of the crown base). The relative placement of the buccal DHs can also be influenced by buccal expansion of the tooth crown base during growth. The second factor is the shape of the buccal aspect of the protoconid and hypoconid DHs (e.g., the presence of crests running

towards the cervical margin of the tooth; Figs. 4.8e,f, 4.9d), and the third factor (though of a lesser influence) is the thickness and distribution of enamel on the buccal side of the dentine crown. Thus, protostylid morphology, including crests, depressions, cusps, cuspules, wrinkles, and fissures, derives from the EDJ with only minor modification caused by the differential deposition of enamel. A possible exception to the minor influence of enamel deposition on OES expression of the protostylid is *P. robustus*, is an ongoing analysis of a larger sample of molars from this taxon (Skinner et al., unpub. data), which indicates that the relatively thick enamel of this taxon can mask EDJ expression in some cases. In answer to our third question, protostylid development appears similar among the study taxa.

If cingular remnants and furrowlike features on the mesial and distal portions of the buccal side of the crown are developmentally related, then they should not be considered as separate traits for the purpose of dental trait analysis (contra Hlusko, 2004). Robinson (1956: 199–120) considered the protostylid a complex character in South African fossil hominins due to "remnants of a cingulum farther back on the buccal surface as well as on the whole of the mesial face of the crown." The complexity of this trait within the hominoid clade has also been noted by Bailey and Wood (2007). If further evidence supports developmental nonindependence among mesial, central, and distal components of protostylid morphology, this trait could prove to be difficult to objectively and meaningfully subdivide into an ordinal scale. Examination of crown size and DH size/spacing, which are thought to be under separate genetic control (Harris and Dinh, 2006; Cai et al., 2007), may lead to a better understanding of protostylid variation within and among taxa.

Further research will explore the interaction between DH height and placement, the overall size of the molar crown, and the collective influence of all of these factors on the expression of C6s, C7s, trigonid crest pattern, and protostylids. We agree with Bailey and Wood (2007) that new scoring criteria need to be developed for several of the traits relevant to the study of early hominins, and we suggest that simultaneous examination of the EDJ in addition to the OES may help in the identification of independent discrete traits with a demonstrably similar pattern of development.

Conclusion

The results of this analysis indicate that the presence and degree of morphological expression of four dental traits (C6, C7, trigonid crest pattern, and protostylid) is largely determined by the factors controlling the shape of the EDJ, and that differential enamel deposition does not significantly alter the morphology of these traits or create traits at the outer enamel surface that are not present at the EDJ. For some traits, such as the protostylid and trigonid crest pattern, EDJ expression reveals considerable variation within nonhuman primate taxa that will require new trait descriptions and standardized classifications for comparison within and between taxa. In some cases, EDJ morphology suggests that traits that appear similar at the enamel surface in different taxa may not be the result of similar patterns of development, thus limiting their utility for phylogenetic analysis. Furthermore, because of the significant morphological contribution of the EDJ to trait expression at the OES, the EDJ of worn teeth may be used as a proxy for the OES expression of these traits, and this may well result in increases in the size of study samples of early hominin taxa.

Table 4.1. Composition of the lower molar sample.

Taxon	n	M_1	M_2	M_3	Source
P. t. verus	19	6	13		MPI-EVA
G. g. beringei	2		1	1	NMNH
P. pygmaeus ssp.	3	3			ZMB
G. blacki	1		1		SFN
H. sapiens	7	3	4		NMNH, MPI-EVA
H. neanderthalensis	4	4			MNCN
P. robustus	4	3	1		TM, UW
A. africanus	4	1	2	1	TM, UW

Source codes: MPI-EVA, Max Planck Institute for Evolutionary Anthropology, Leipzig, Germany; NMNH, National Museum of Natural History, Washington, DC, USA; ZMB, Museum für Naturkunde, Humboldt Universität, Berlin, Germany; SFN, Senckenberg Forschungsinstitut und Naturmuseum, Frankfurt, Germany; MNCN, Museo Nacional de Ciencias Naturales, Madrid, Spain, TM, Transvaal Museum, Pretoria, South Africa; UW, University of Witwatersrand, Johannesburg, South Africa.

Table 4.2. C6 frequency (as a ratio) by taxon and tooth type[1].

C6	Absent	Fovea	Hypoconulid	Double-F[2]	Double-H[2]
P. t. verus	4/19		12/19		3/19
G. g. beringei	1/2			1/2	
P. pygmaeus ssp.	2/3	1/3			
G. blacki		1/1			
H. sapiens[3]	4/7		1/7		1/7
H. neanderthalensis	3/4	1/4			
P. robustus	1/4	1/4		2/4	
A. africanus		3/4		1/4	

[1] Pooled analysis of all molar types ($M_{1–3}$).
[2] Double-F: double fovea-type; Double-H: double hypoconulid-type.
[3] One *H. sapiens* molar presented both a fovea-type and a hypoconulid-type C6

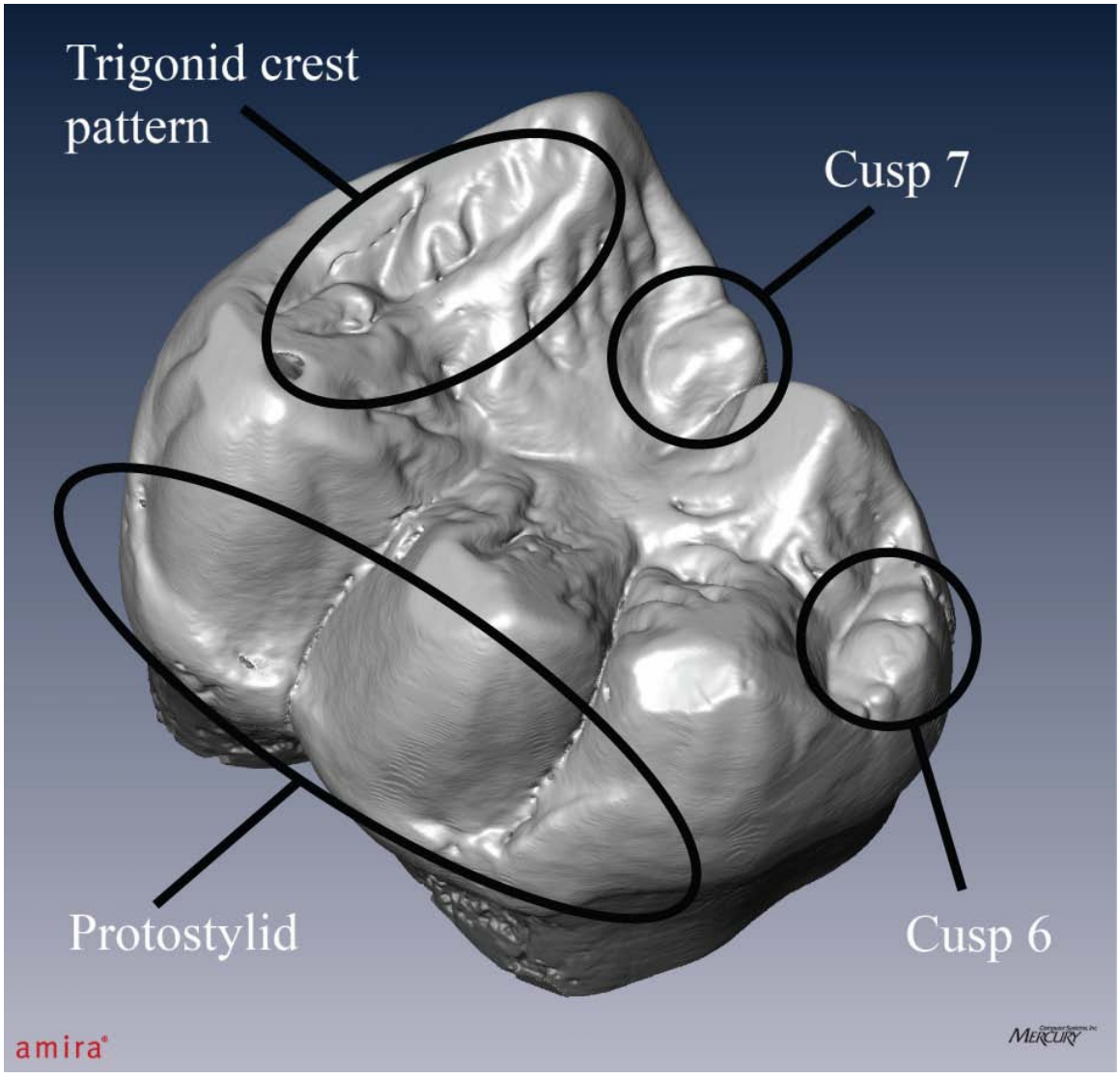

Figure 4.1. Virtual reconstruction of a *Gorilla gorilla beringei* lower left second molar highlighting the four discrete traits examined in this study: cusp 6, cusp 7, protostylid, and trigonid crest pattern (identified by black circles). The cusp 6 in this molar could be considered a double cusp 6 (discussed in text).

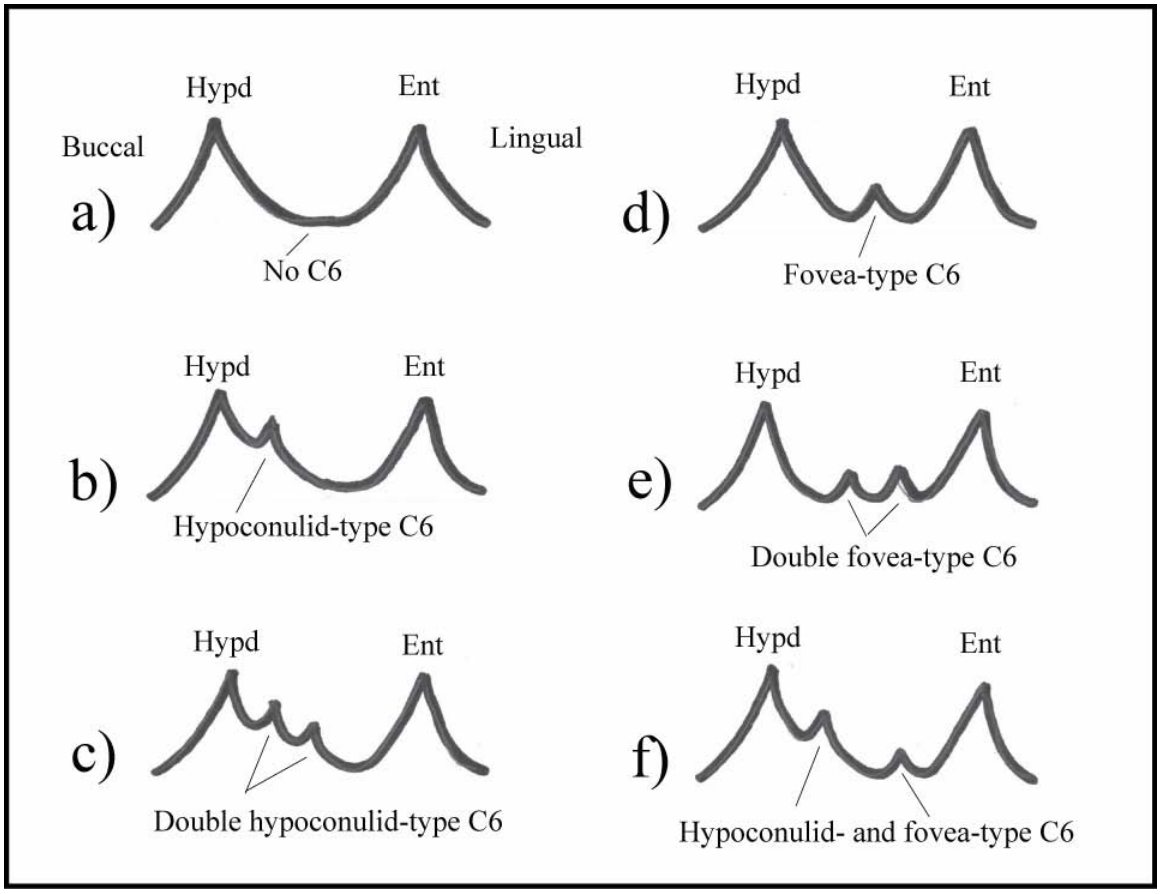

Figure 4.2. Schematic representation of C6 morphology present at the EDJ in the study sample. View is towards the distal face of the EDJ surface between the DHs of the hypoconulid (Hypd) and entoconid (Ent). (**a**) No C6 manifestation at the EDJ; (**b**) single hypoconulid-type C6 manifested as a DH-like feature on the lingual ridge of the hypoconulid; (**c**) double hypoconulid-type C6 manifested as two DH-like features on the lingual ridge of the hypoconulid DH; (**d**) single fovea-type C6 manifested as a DH-like feature between the hypoconulid DH and entoconid DH with no tendency for spatial association to either; (**e**) double fovea-type C6 manifested as two DH-like features between the hypoconulid DH and entoconid DH; (**f**) C6 complex exhibiting a single hypoconulid-type and single fovea-type DH between the hypoconulid DH and the entoconid DH.

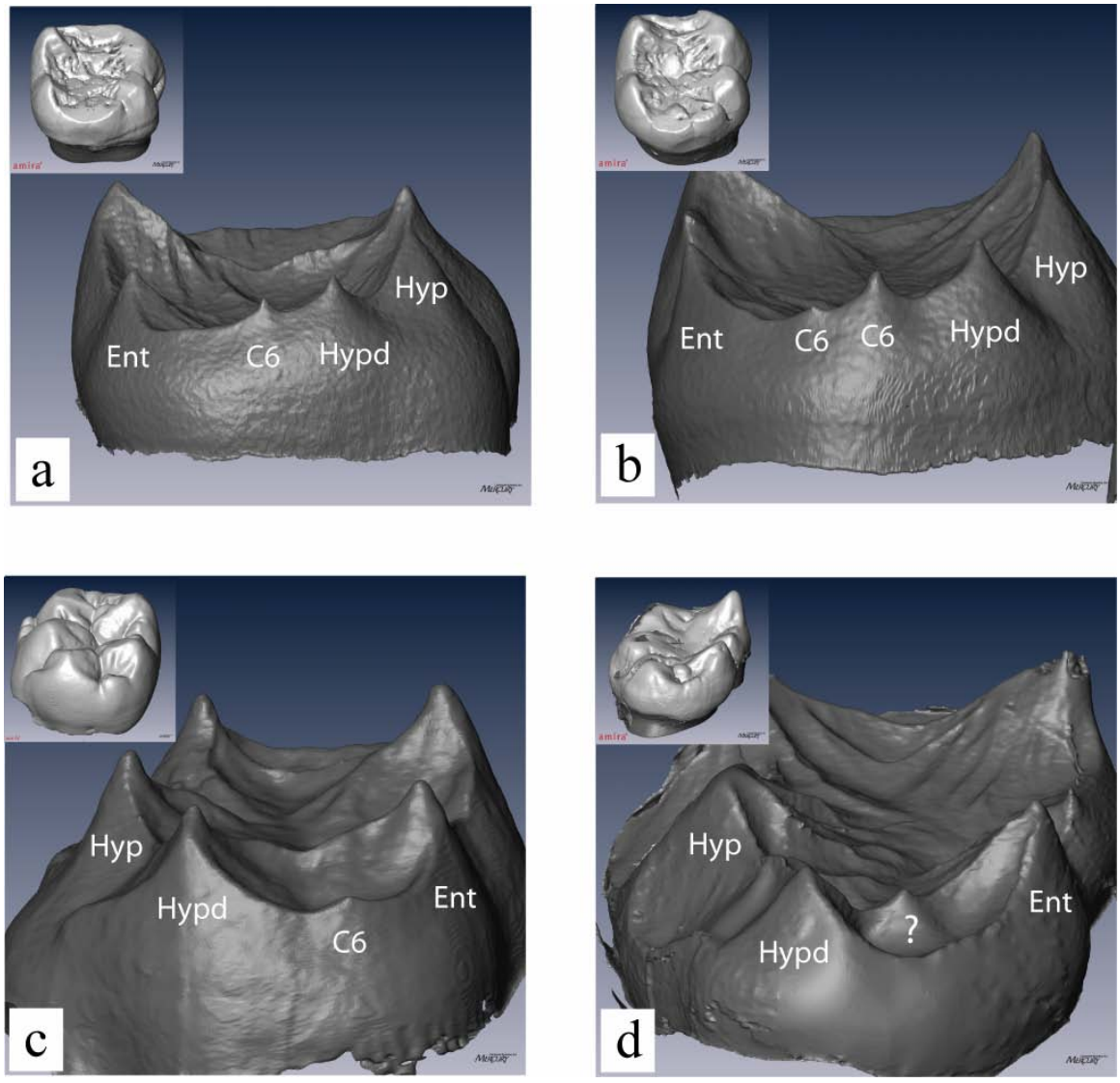

Figure 4.3. Selected examples of C6 expression at the EDJ in the study sample (OES of each specimen is inset in top left corner). Abbreviations are: Ent = entoconid, Hyp = hypoconid, Hypd = hypoconulid. (**a**) Single hypoconulid-type C6 on a lower second molar of *P. t. verus* (TAI 15012); (**b**) double hypoconulid-type C6 on a lower second molar of *P. t. verus* (TAI 11800); (**c**) single fovea-type C6 on a lower first molar of *A. africanus* (STW 421B); (**d**) DH-like feature located on a crest joining the entoconid and hypoconulid DHs of a lower second molar of *G. g. beringei* (NMNH 543034). The status of this feature as a manifestation of C6 is unclear. Images are not to scale.

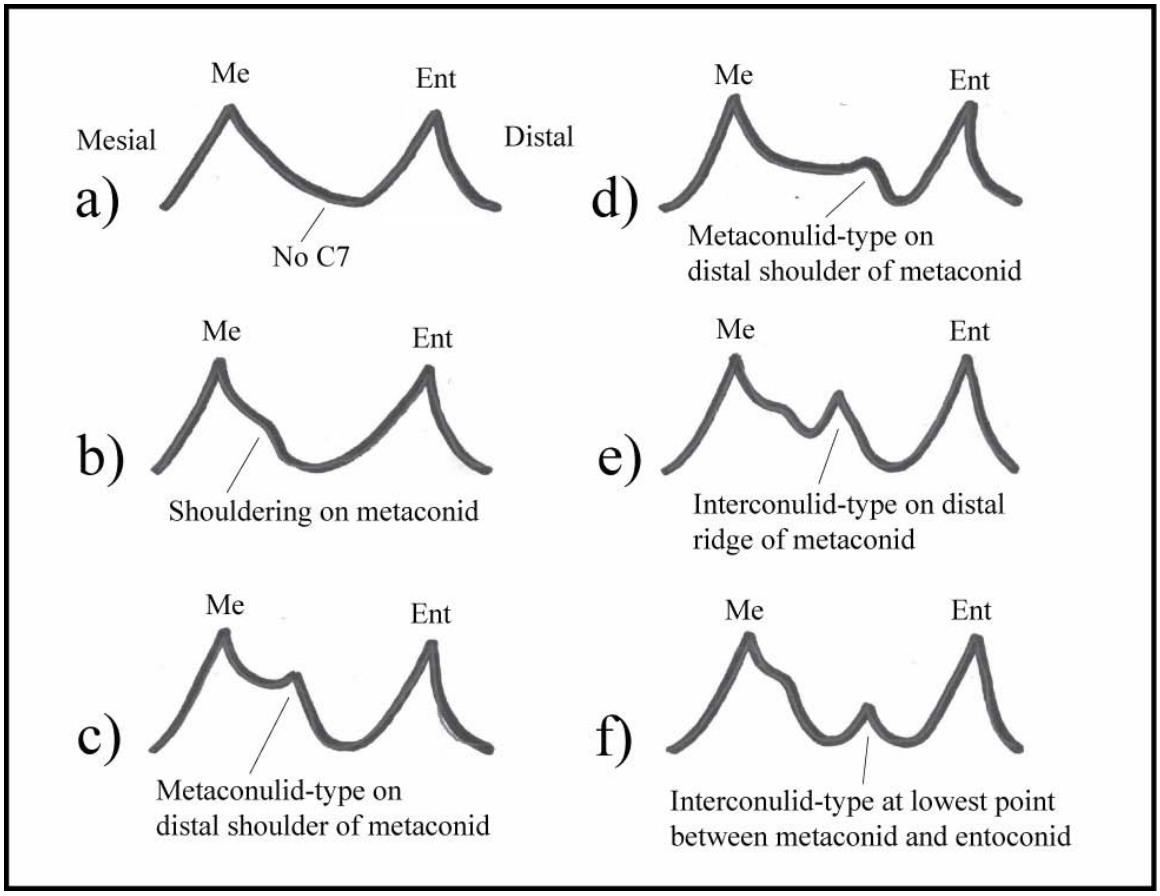

Figure 4.4. Schematic representation of C7 morphology present at the EDJ in the study sample. View is towards the lingual face of the EDJ surface between the DHs of the metaconid (Me) and entoconid (Ent). (**a**) No C7 manifestation at the EDJ; (**b**) moderately pronounced shoulder on the distal ridge of the metaconid DH; (**c**) metaconulid-type C7 on the distal shoulder of the metaconid DH, which in some cases can resemble a small DH-like feature; (**d**) a second example of a metaconulid-type C7 in which a DH-like feature is not closely associated with the metaconid DH; (**e**) interconulid-type C7 with a DH-like feature on the distal ridge (but separated from the shoulder by a trough) of the metaconid DH; (**f**) interconulid-type C7 with a DH-like feature at the low point on the ridge between the metaconid DH and entoconid DH.

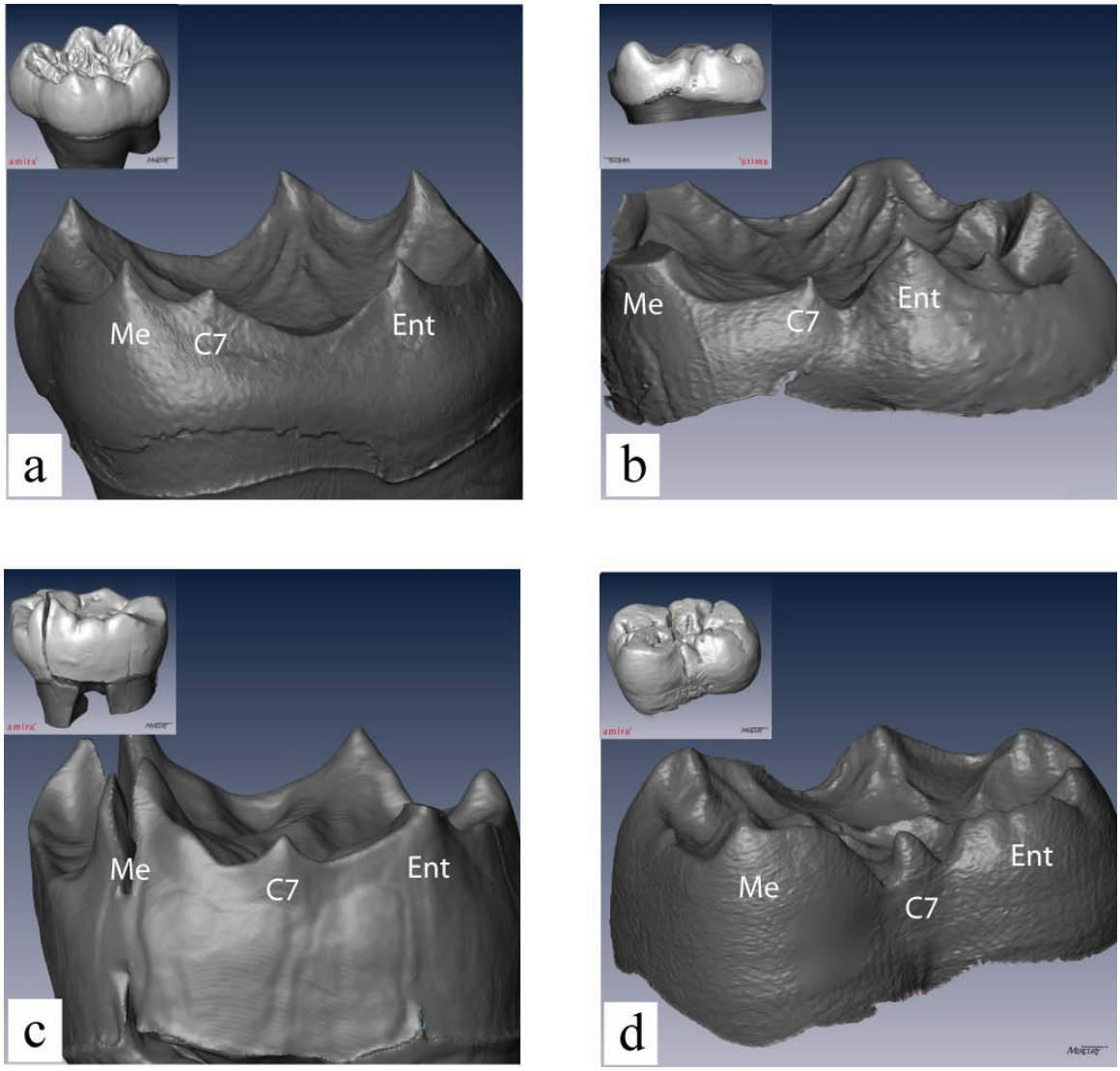

Figure 4.5. Selected examples of C7 expression at the EDJ in the study sample (OES of each specimen is inset in top left corner). Abbreviations are: Me = metaconid and Ent = entoconid. (**a**) Metaconulid-type C7 on the distal shoulder of the metaconid DH of a lower third molar of *P. t. verus* (TAI 11790); (**b**) metaconulid-type C7 farther removed from the metaconid DH of a lower second molar of *G. g. beringei* (NMNH 543034); (**c**) interconulid-type C7 on a lower second molar of *H. neanderthalensis* (SD 756); (**d**) interconulid-type C7 on a lower second molar of *G. blacki* (CA 736). Images are not to scale.

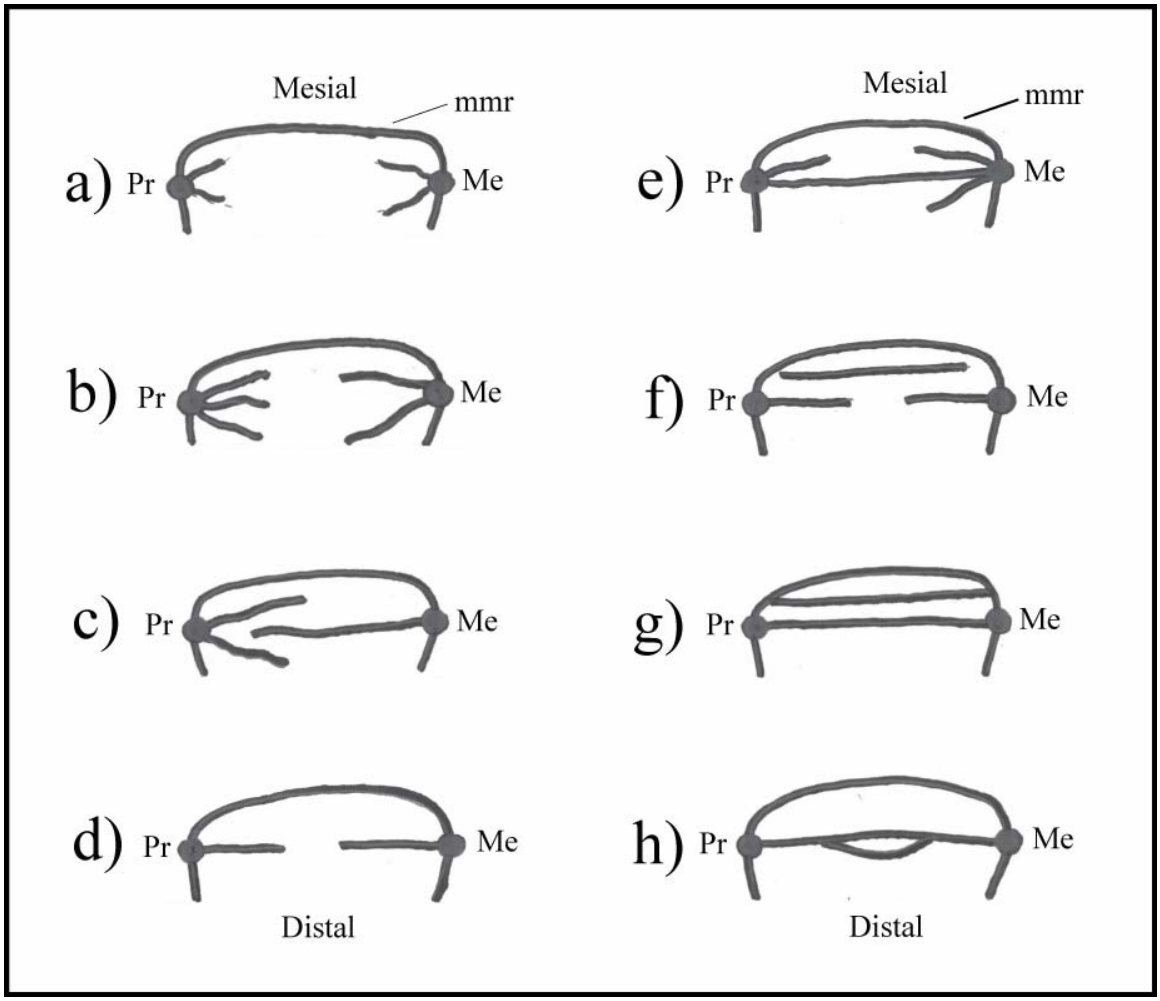

Figure 4.6. Schematic representation of TCP present at the EDJ in the study sample. View is towards the occlusal surface of the EDJ including the mesial marginal ridge (mmr) and the tips of the DHs (represented as solid black circles) of the protoconid (Pr) and metaconid (Me). (**a**) Small, minor crests associated with the Pr and Me DHs; (**b**) multiple large crests running towards the occlusal basin; (**c**) pronounced but separate crests that extend across the occlusal basin; (**d**) single pronounced crests running medially towards each other but not joined in the occlusal basin; (**e**) a single pronounced crest between the Pr and Me DHs with additional less pronounced crests also present; (**f**) a mesial crest and a middle crest, one of which is not complete; (**g**) a mesial (originating at or mesial to the DHs) and middle crest that are complete; (**h**) a middle crest with a small secondary crest in the occlusal basin. This schematic does not exhaust the manifestations of trigonid crest pattern seen in the study sample.

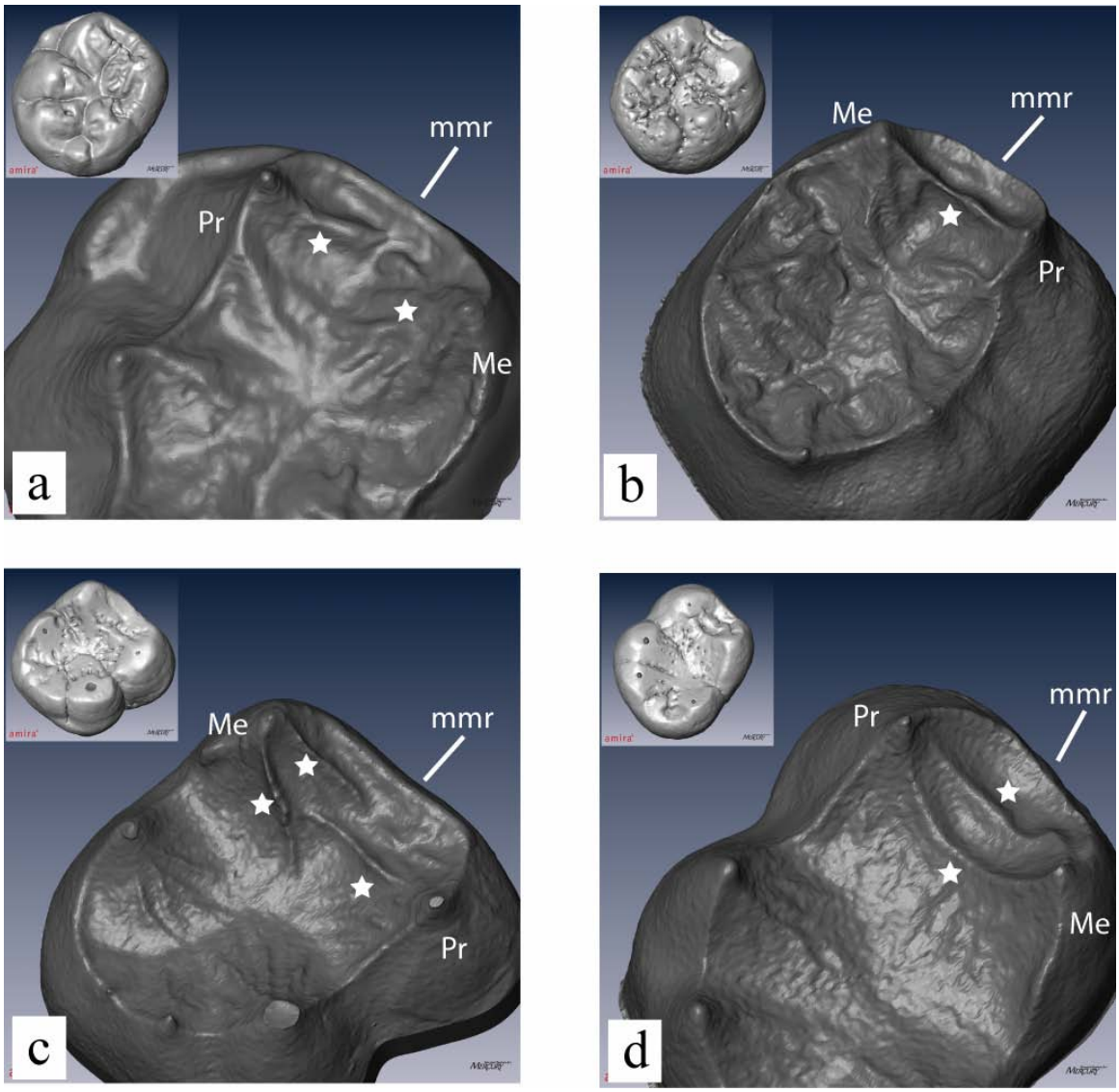

Figure 4.7. Selected examples of TCP expression at the EDJ in the study sample (OES of each specimen is inset in top left corner). Abbreviations: Pr = protoconid, Me = metaconid, mmr = mesial marginal ridge. Crest features are adjacent to white stars. (**a**) A large crest from the protoconid DH with multiple small crests on the metaconid DH (lower second molar of *A. africanus*, STW 424); (**b**) single, pronounced middle crest (lower first molar of *H. neanderthalensis*, SD 540); (**c**) two crests from the metaconid DH and one crest from the protoconid DH that do not join (lower second molar of *P. t. verus*, TAI 11779); (**d**) mesial and middle crests (lower first molar of *P. t. verus*, TAI 13433). Images are not to scale.

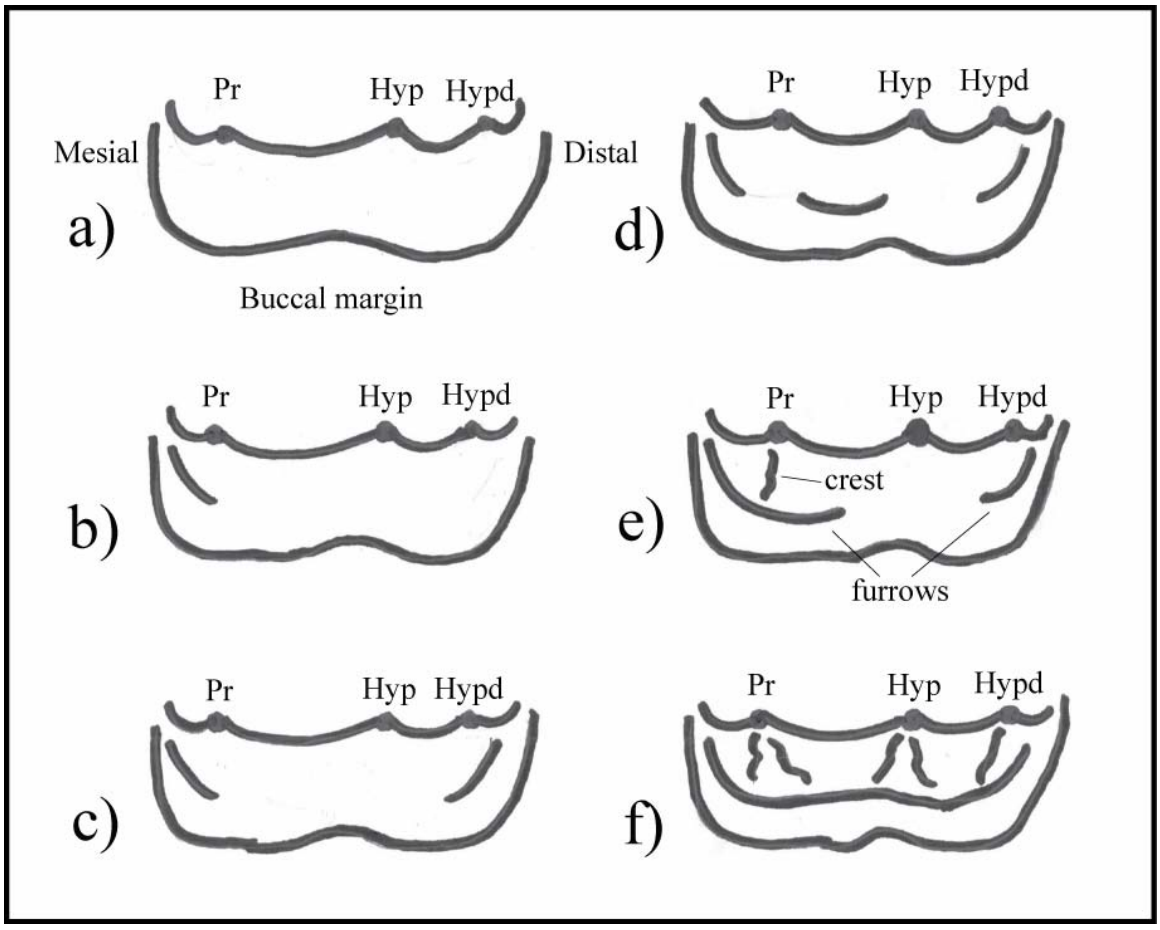

Figure 4.8. Schematic representation of protostylid variation present at the EDJ in the study sample. View is towards the buccal face of the EDJ including the buccal margin, the tips of the DHs (represented as solid black circles) of the protoconid (Pr), hypoconid (Hyp), and hypoconulid (Hypd), and the marginal ridge that runs between them. (**a**) No protostylid morphology along the buccal margin of the EDJ crown surface; (**b**) minor furrow on the mesial surface of the protoconid DH; (**c**) similar to (b) and a second furrow on the distal surface of the hypoconulid DH; (**d**) similar to (c) with a cingulumlike furrow between the protoconid DH and hypoconid DH; (**e**) pronounced furrow running from the mesial border of the protoconid DH to the mesial surface of the hypoconid DH with a furrow on the distal surface of the hypoconulid DH (small crests are variably manifest on the surface of the protoconid DH); (**f**) a continuous, cingulumlike furrow across the whole buccal margin of the EDJ in association with crests on the surfaces of the buccal DHs. This schematic is not exhaustive of the manifestations of protostylid morphology present in the study sample.

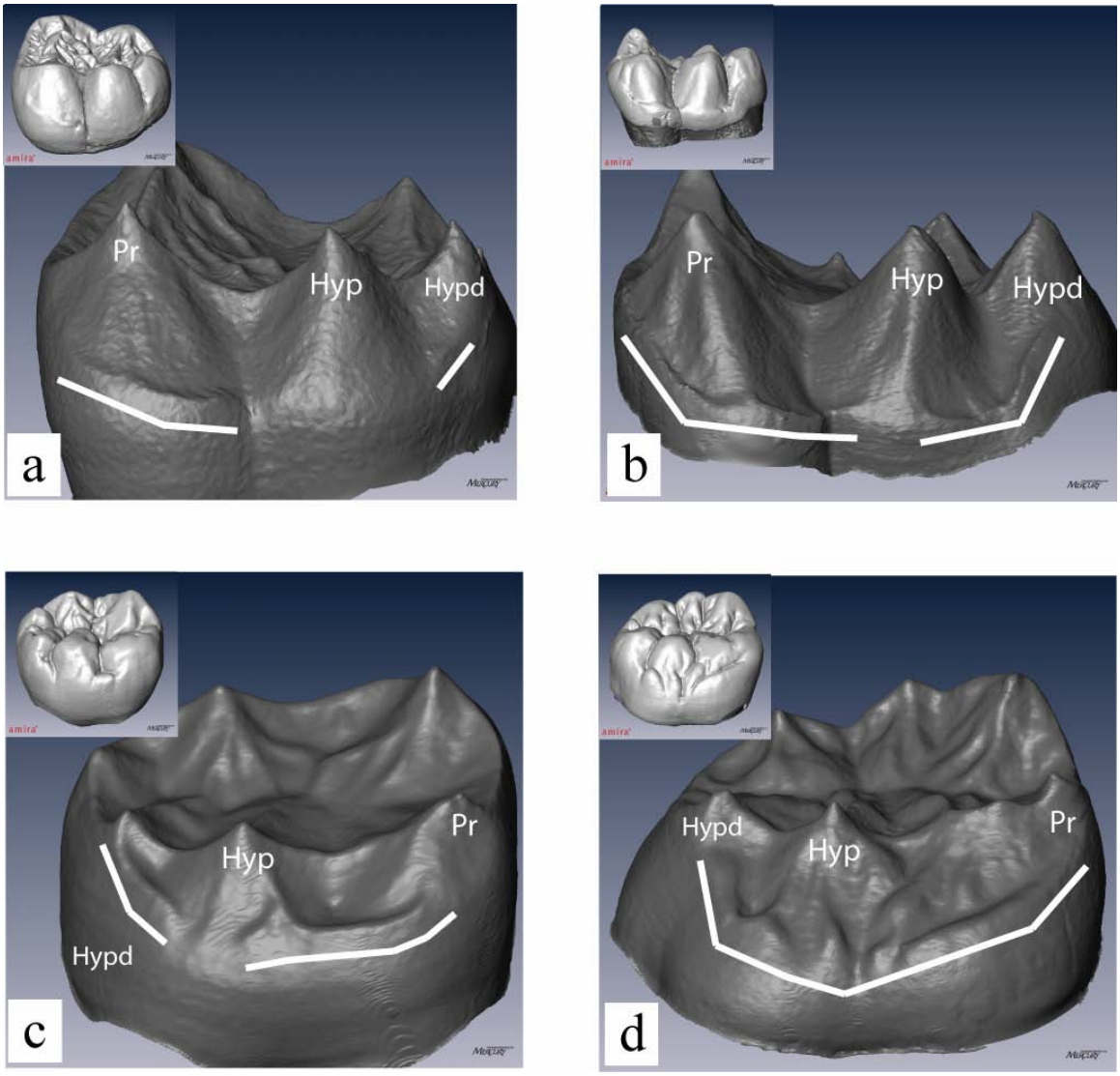

Figure 4.9. Selected examples of protostylid expression at the EDJ in the study sample (OES of each specimen is inset in top left corner). Abbreviations are: Pr = protoconid, Hyp = hypoconid, Hypd = hypoconulid. Features associated with the protostylid are highlighted by white solid lines. (**a**) Minor furrows extending across the buccal face of the protoconid DH and below the hypoconulid DH (lower second molar of *P. t. verus* (TAI 13437); (**b**) cingulumlike furrows extending across most of the buccal face (lower second molar of *G. g. beringei*, NMNH 543037); (**c**) prominent furrows below the hypoconulid DH and between the hypoconid and protoconid DHs (lower second molar of *P. robustus*, SK 3974); (**d**) prominent furrows along the mesiobuccal face of the EDJ with small tubercle features below the hypoconid DH that are also expressed on the enamel surface (lower second molar of *A. africanus*, STW 560E). Images are not to scale.

CHAPTER 5: PROTOSTYLID EXPRESSION AT THE OUTER ENAMEL SURFACE AND ENAMEL-DENTINE JUNCTION OF LOWER MOLARS OF *PARANTHROPUS ROBUSTUS* AND *AUSTRALOPITHECUS AFRICANUS*

Abstract

Distinctive expressions and incidences of discrete dental traits at the outer enamel surface (OES) form part of the diagnosis of many early hominin taxa. It has been argued that one of these discrete dental traits, the protostylid, can be used to discriminate among southern African Pliocene fossil hominin taxa. However, there is ongoing debate about A) the extent to which the shape of the enamel-dentine junction (EDJ) determines protostylid morphology, or whether differential enamel distribution makes a significant contribution to the morphology of the OES, and B) whether cingulum-like features on the mesial and distal aspects of the buccal face of mandibular molar tooth crowns are developmentally independent (and thus should be excluded from comparisons of protostylid morphology). This study addresses these issues by examining protostylid expression at the EDJ and at the OES of *Paranthropus robustus* (N = 22) and *Australopithecus africanus* (N = 28) mandibular molars. The results include evidence A) of statistically significant taxon-specific patterns of protostylid morphology at the EDJ that are not evident at the OES; B) of non-independence of isolated protostylid features across the buccal face of the EDJ; C) that differential enamel distribution can reduce morphological correspondence in protostylid expression between the EDJ and the OES, and D) that the protostylid retains its taxonomic relevance even in worn teeth.

Introduction

Tooth crown morphology has played a central role in the taxonomy and inferred phylogenetic relationships of Pliocene African hominins. The protostylid, a dental trait present on mandibular molars, has received particular attention because of its pronounced expression in a number of teeth attributed to *Paranthropus robustus* and *Australopithecus africanus* (Robinson, 1956; Wood and Abbott, 1983; Suwa et al., 1994; Hlusko, 2004; Irish and Guatelli-Steinberg, 2003; Guatelli-Steinberg and Irish, 2005). In a recent and comprehensive analysis of protostylid expression in these taxa Hlusko (2004) concluded that *P. robustus* can be distinguished from *Au. africanus* because the former taxon has a relatively high frequency of moderate protostylid expression, whereas the latter taxon has a relatively high number of specimens with either weak or strong expression.

Previous research has demonstrated that EDJ morphology of extant and fossil hominoid teeth shows both intra- and intertaxonomic differences in dental trait morphology that are not always evident at the outer enamel surface (Korenhof, 1960, 1961, 1982; Nager, 1960; Kraus and Jordan, 1965; Corruccini and Holt, 1989; Corruccini, 1998; Schwartz et al., 1998; Sasaki and Kanazawa, 1999; Skinner et al., 2008). The difficulty of assessing trait morphology is, of course, even more marked when wear has removed details of the morphology at the OES. However, the extent to which the shape of the EDJ determines protostylid expression, and the role played by differential enamel distribution on the expression of the protostylid at the outer enamel surface (OES) remain unclear. It is also unclear whether cingulum-like features across the mesial, central, and distal aspects of the buccal face of mandibular molar tooth crowns are developmentally independent, and should be incorporated into definitions and scoring of protostylid expression (Hlusko, 2004; Skinner et al., 2008).

In this study we assess protostylid expression in *P. robustus* and *Au. africanus* at the EDJ and the OES to address the following questions. Is there an EDJ equivalent of an OES protostylid? Are current definitions and scoring systems of the protostylid trait consistent with morphological features expressed at the EDJ? Are there species-specific differences in any EDJ protostylid morphology between *P. robustus* and *Au. africanus* that are not evident at the OES? Finally, in worn teeth can protostylid morphology at the EDJ be used for the purposes of taxonomy and phylogenetic reconstruction in place of its OES expression?

Materials and Methods

Study sample

The study uses fossils from collections housed at the Flagship Museum (formerly the Transvaal Museum) in Pretoria and at The University of Witwatersrand in Johannesburg, South Africa. First, second, and third mandibular molars (M_1, M_2 and M_3) were examined (Table 5.1). Molars attributed to *P. robustus* come from the sites of Swartktrans, Gondolin and Drimolen (Robinson, 1956; Tobias et al., 1977; Grine 1989; Menter et al., 1999; Keyser et al., 2000; De Ruiter, pers. comm. 2006) and those attributed to *Au. africanus* come from the site of Sterkfontein (Moggi-Cecchi et al., 2006). Taxonomic affiliations and information about tooth type were taken from these publications.

The specimens included in this study represent a subset of mandibular molars of *P. robustus* and *Au. africanus*. This is for two reasons. First, only isolated teeth (or teeth from small mandibular fragments) could be scanned with the portable micro-computed tomography scanner used for this study. Second, in some of the isolated teeth differential

mineralization during fossilization has resulted in the enamel and dentine having similar levels of radiopacity. In these cases the inability to segment the two tissues prevents visualization of the EDJ.

EDJ and OES surface reconstruction

Each tooth was imaged by a micro-computed tomography scanner (SKYSCAN 1172, Kontich, Belgium) at an isometric voxel resolution of 14 µm (100Kv, 94mA, 2.0mm aluminum and copper filter, 0.12 rotation step, 360 degrees of rotation, 2 frame averaging). Raw projections were converted into TIFF image stacks using NRecon (parameters: ring artifact correction = 10; beam hardening = 30%). To reduce the size of the resulting files, teeth were downsampled to 30 microns using Amira (*triangle* filter, v4.1, www.amiravis.com). To facilitate tissue segmentation, the complete image stack for each tooth was filtered using a three-dimensional median filter (kernel size of 3) followed by a mean of least variance filter (kernel size of 3), implemented as a computer-programmed macro. This filtering process results in more homogenous tissue classes (e.g., enamel vs. dentine) and allocates pixels with intermediate gray-scale values at tissue interfaces (i.e., air-enamel, enamel-dentine, air-dentine) to the appropriate tissue (Schulze and Pearce, 1994).

Filtered image stacks were imported into the Amira software package and enamel and dentine tissues were segmented using the 3D voxel value histogram and its distribution of gray-scale values, which typically presents a trimodal distribution with one peak representing dentine, another peak representing enamel, and a third peak representing air and background noise in the images. In fossil teeth where the enamel and dentine differ substantially in their degree of mineralization (and therefore their densities,

and thus also in the ability of X-rays to pass through them), the filtering process results in gray-scale pixel value distributions for each tissue that do not overlap. In other teeth, diagenetic alteration (e.g., dentine remineralization) may result in similar tissue densities and thus overlapping gray-scale pixel value ranges for enamel and dentine (Olejniczak and Grine, 2006). Only teeth in which there was a clear separation of enamel and dentine, resulting in well-distinguished gray-scale values and accurate representations of the EDJ, were used in the study. After segmentation, the EDJ is reconstructed as triangle-based surface model using Amira (*surface generation* module using unconstrained smoothing parameter). In specimens that preserved only the enamel cap, a surface model of the EDJ was created by digitally removing the occlusal surface of the reconstructed enamel cap surface model.

Defining the protostylid based on EDJ morphology

A protostylid was described by Dahlberg (1950:16) as "an elevation or ridge of enamel on the anterior part of the buccal surface of the lower molars, which ascends from the gingival end of the buccal groove and extends mesio-occlusally." The Arizona State University Dental Anthropology System (ASUDAS) defines the protostylid as a paramolar cusp found on the buccal surface of the protoconid that is normally associated with the buccal groove (Turner et al., 1991). Expression states under the ASUDAS system focus on a secondary groove that extends mesially from the buccal groove and culminating, in marked expression, as a cusp with a free apex. In the most recent and comprehensive analysis of protostylid expression in fossil hominins (Hlusko, 2004) a variable groove, or protoconid shelf, on the mesial aspect of the protoconid (e.g., visible in Type 1 in Hlusko's Fig. 1, 2004: 583) was excluded from the definition of the

protostylid. This was because there was not strong evidence indicating morphological covariation between this feature and morphology of the buccal groove. In order to clarify what morphological features at the EDJ of southern African fossil hominins should be included in the definition of the protostylid we examined the expression of all cingulum-like features on the mesial, central and distal aspects of the buccal face of the EDJ and OES.

Quantification of protostylid morphology at the OES and EDJ

In order to address any correspondence in protostylid expression between the OES and EDJ, as well as to test for species differences, the buccal face of each surface was divided into three regions (Fig. 5.1). The first region (referred to as *anterior*) begins at the mesial border of the crown and extends to a plane orthogonal to the long axis of the tooth and to the occlusal surface that passes through the tips of the two mesial cusps (at the OES or through the dentine horns). The second region (referred to as *middle*) extends from the end of the anterior region to a parallel plane that passes through either the tip of the OES hypoconid, or its dentine horn. The third region (referred to as *posterior*) begins at this latter plane and extends to the distal margin of the crown. Cingulum-like features (e.g., crests/ridges) on the surface of each specimen within each region were recorded and measured separately. Measurements were taken using the 3D measurement tool in Amira. In the case of curved ridges, linear segments were summed along the feature to capture its length. In order to account for overall size differences both between specimens, as well as between the OES and EDJ surfaces of each tooth, all measurements were scaled by the geometric mean (Mosimann, 1970; Jungers et al., 1995) of maximum mesiodistal length,

the maximum buccolingual breadth of the mesial portion of the crown, and the maximum buccolingual breadth of the distal portion of the crown.

Correspondence in protostylid morphology between the EDJ and the OES

The relationship between protostylid expression at the OES and EDJ can be of two types. On the one hand, protostylid morphology at the EDJ is not substantially altered by the deposition of enamel. Alternatively, differential enamel deposition can modify protostylid-like morphology at the EDJ, or create a protostylid at the OES that is not present at the EDJ. Clearly, the formal definition of the protostylid and the ability to score the feature at the OES would be affected if the relative contribution of the EDJ and enamel cap to trait expression at the OES differs within, or between, taxa. Correspondence within regions and across the whole buccal face was assessed quantitatively by deriving the ratio of crest(s) length at the EDJ divided by crest(s) length at the OES (multiplied by 100).

Species-specific differences in protostylid morphology

Previous analyses of protostylid expression at the OES between *P. robustus* and *Au. africanus* noted differences in the degree of expression, rather than in the kind of protostylid (Robinson, 1956; Hlusko, 2004). Skinner and colleagues (2008) noted evidence for species-specific differences in the EDJ morphology of other dental traits (e.g., for cusp 6 and trigonid crest pattern) that were difficult to detect at the OES. In this examination of protostylid-like EDJ morphology in *P. robustus* and *Au. africanus*, we assess whether there are differences in the degree of trait expression, and/or whether the

taxa display different patterns of protostylid expression at the EDJ that would suggest differences in the development of the trait.

Taxonomic comparison included both visual inspection of OES and EDJ expression of protostylid morphology, as well as, a statistical comparison of the overall length (and length within each of the three regions of the buccal face defined above) of protostylid features at each surface. After conducting a Kruskal-Wallis ANOVA to determine there were no significant differences between molar types for each variable, molars were grouped for the purpose of comparing species differences. Due to unequal variances between species for a number of measured variables a non-parametric Mann-Whitney U test was used to compare group medians. Differences are considered statistically significant at p-values at or below 0.05. In the case of antimeres the better preserved side was used.

Results

Defining the protostylid based on EDJ morphology

Morphology at the EDJ does not fit well into current definitions of the protostylid that were devised by studying its expression at the OES. There are two major areas of mismatch. First, many teeth present single or multiple crest-like features in the anterior, central, and posterior regions of the buccal face of the EDJ that appear to be linked morphologically. In Figures 5.2 and 5.3 we present a range of cingular features on the buccal face of the EDJ of *P. robustus* and *Au. africanus*, respectively. In the anterior region on molars from both taxa, crests are often present that are continuous with crests in the middle region (e.g., Fig. 5.2e,f, 5.3c,d,e). Crests in the posterior region that run from the tip of the hypoconulid dentine horn inferomedially are common in both taxa

(Figs. 5.2a-f, 5.3a-f). In many cases, such crests appear to represent the distal portion of a more, or less, continuous cingulum (e.g., Fig. 5.2a. 5.3e) suggesting that these features are developmentally linked. These findings contradict current definitions of the protostylid in which only centrally-located features can be incorporated into OES-based definitions of the protostylid.

The second discrepancy between the OES-based definitions and what is observed at the EDJ is that the buccal groove seen at the OES is not associated with any distinct structure at the EDJ, yet the form of the buccal groove at the OES (e.g., a mesially running secondary groove, or a V-shaped groove) is central to most classificatory schemes of protostylid expression. The buccal groove at the OES marks where the mineralizing fronts derived from the tips of the protoconid and hypoconid dentine horns meet, and its form is likely influenced by the depth and morphology of the concave EDJ surface between the two, whereas the protostylid morphology on the EDJ in this region tends to be a cingulum-like crest between the two dentine horns (Fig. 5.2b, 5.3d).

Correspondence in protostylid morphology between the EDJ and OES

Across the whole buccal face correspondence between the EDJ and OES in *Au. africanus* tends to be greater than in *P. robustus* although this taxonomic difference is not statistically significant (Table 5.2). When the anterior and middle regions are combined (crests tend to be continuous between these regions) there is significantly less correspondence between the OES and the EDJ in *P. robustus* than in *Au. africanus* ($p = 0.02$). This difference is because marked crest-like features between the protoconid and hypoconid dentine horns present at the EDJ of *P. robustus* are rarely matched in size or shape at the OES, and because of the strong correspondence between the OES and EDJ in

mesially-located crest features in *Au. africanus*. In the posterior region both taxa exhibit a similar lack of correspondence with crest-like features at the EDJ being much less prominent at the OES.

Species-specific differences in protostylid morphology

While the EDJ expression of protostylid morphology between *P. robustus* and *Au. africanus* does not differ significantly when taken along the whole length of the buccal face of the EDJ, the regional distribution of these crest features does differ significantly (Table 5.2, Fig. 5.4) between the taxa. For example, *P. robustus* exhibits significantly greater ($p = 0.04$) protostylid expression in the middle region (i.e., between the protoconid and hypoconid dentine horns), while *Au. africanus* exhibits significantly greater ($p = <0.001$) expression in the anterior region (i.e., mesial to the protoconid dentine horn). Both taxa exhibit crest-like features in the posterior region.

These differences form a qualitative difference in the pattern expression between the taxa that is apparent at the EDJ. That is *Au. africanus* molars (an exception is STW412A) tend to exhibit a crest-like feature at the EDJ that extends to the mesial side of the protoconid dentine horn, whereas *P. robustus* molars (an exception is SK104) exhibit crest-like features that extend no further than immediately below, or slightly distal to the protoconid dentine horn. The specimens from Drimolen and Swartkrans are consistent in their expression of the *P. robustus* pattern. There is also a difference in where the cingular ridge terminates in the central region of the buccal face of the EDJ. In *Au. africanus* it terminates between the protoconid and hypoconid dentine horns with the crest often dropping inferiorly towards the cervix (Fig. 5.3d,e, 5.5a,b). This contrasts with the most common pattern in *P. robustus*, which is for the crest to extend distally and

superiorly towards the tip of the hypoconid dentine horn to form a crescent pattern (Fig. 5.2b,c,e).

Protostylid expression at the OES reveals a slightly different pattern of species differences than at the EDJ. Similar to the pattern noted above for the EDJ, the OES of *Au. africanus* exhibits significantly longer crest features in the anterior region ($p = <0.001$). These anterior crest features, along with the lack of crest expression at the OES in the central region, contribute to a significant difference in crest length along the whole buccal face of the OES ($p = 0.04$).

Protostylid expression in worn fossil teeth

In Figure 5.5 we illustrate the OES and EDJ of four partially worn molars. While it is very difficult to detect any protostylid morphology at the OES in three of the molars (Fig. 5.5a,c,d), there is clear evidence of a protostylid equivalent at the EDJ. Furthermore, the species differences outlined above are evident at the EDJ, with the *Au. africanus* specimens showing a mesially-extended crest (Fig. 5.5a,b,d), whereas the *P. robustus* specimens have a marked crest between the protoconid and hypoconid dentine horns (Fig. 5.5c). It is notable that in STW520 (Fig. 5.5b), which has EDJ evidence of a protostylid, the *Au. africanus* pattern is not detectable at the OES even though wear does not appear to have significantly altered this region of the crown surface.

Discussion

We set out to relate current definitions and scoring systems of the protostylid dental trait, which have been based on the study of the OES, with what can be observed at the EDJ in the same location. In these Pliocene hominin taxa the protostylid at the EDJ

is in the form of a crest, or crests, along the buccal face of the crown below the dentine horns of the buccal cusps. As noted in a previous publication (Skinner et al., 2008) the presence, size and shape of the protostylid in hominoids is influenced by the size, shape and spacing of the dentine horns, the overall size of the molar crown, and the distribution of enamel. The taxonomic differences between the frequent expression at the EDJ in *Au. africanus* of a mesially-extended crest, versus marked crest expression between the protoconid and hypoconid dentine horns in *P. robustus*, are likely the result of differences in the interaction of the developmental processes that control the spacing of the buccal dentine horns and the relative width of the crown (Polly, 1998; Jernvall and Jung, 2000; Jernvall and Thesleff, 2000; Kassai et al., 2005). Note for example in Figure 5.3d and 5.3e, the relatively central position of the buccal dentine horns and the pronounced crest features along the buccal margin of the EDJ. The morphology that appears to characterize the *P. robustus* and *Au. africanus* patterns should not, in our opinion, be considered as different manifestations of a single feature along a morphological continuum of minor to marked expression. Although they are both manifestations of a cingulum feature resembling a crest, the crest-like feature is in different parts of the crown. It is also apparent that enamel thickness, which from a whole crown perspective is greater in *P. robustus* (Olejniczak et al., nd), appears to have more influence on the OES manifestation of protostylid morphology in *P. robustus* than it does in *Au. africanus*.

The protostylid can be present on the buccal face, in the distal, central, and mesial regions and its definition should not be limited to the region of the buccal groove (Robinson, 1956; but *contra* Dahlberg, 1950; Hlusko, 2004). Crest features along the whole buccal face of the EDJ appear to be the result of the same developmental processes. Furthermore we suggest that it may be incorrect to include a cusp feature in

the definition of the protostylid; particularly for the taxa included in this study. In none of the teeth in our sample did we find a dentine horn-like feature underlying a protostylid feature at the OES. While true cusps may form in the region adjacent to the protoconid, we suggest that these are the result of the formation of a secondary enamel knot, and not an especially pronounced expression of the protostylid, which as we have suggested above is a cingulum-derived crest feature. Thus, a cusp should not be considered as the end point on the continuum of protostylid expression. The association of the protostylid trait primarily with the buccal groove at the OES and the division of expression into "v-shaped" furrows, a "secondary groove," or a "paramolar cusp" are not warranted for these taxa (nor for many other hominoid taxa; see images in Skinner et al., 2008). The fidelity, homology, and consistency of expression of these variants need to be investigated more thoroughly before they can be included in definitions of this trait.

Any scoring system of protostylid expression equivalent to the ASUDAS for variations within and among modern human populations for the early hominin taxa we have investigated has to recognize the considerable variability in the presence and morphology of crest features along the buccal face of the dentine crown. Converting this variability into a graded continuum of expression, for the purpose of comparison among a range of taxa, may prove difficult. Scoring systems may need to be devised for different taxonomic comparisons and we encourage further examination of EDJ expression of protostylid morphology and other dental traits in order to establish appropriate definitions and scoring criteria for hominin taxa (Hlusko, 2004; Bailey and Wood, 2007; Martinón-Torres et al., 2007).

We found that the OES morphology does not faithfully replicate the EDJ morphology, and this suggests that differential enamel deposition contributes to the

differences in how the protostylid is expressed at the OES in *Au. africanus* and *P. robustus*. In unworn teeth with strongly expressed protostylid morphology, the OES may give a reasonable representation of what is present at the EDJ, however, as the degree of expression decreases and/or enamel thickness increases the reliability of the OES for accurately comparing protostylid morphology between these taxa is reduced. Visualizing the EDJ manifestation of this trait presents a new opportunity to improve our understanding of its development, our methods for comparing its presence, and the inferences that are drawn based on its variable manifestation in the fossil record. Trait definitions and scoring systems may require reference to both the OES and EDJ to insure their homology and maximize their potential for taxonomic and phylogenetic applications.

The concerns we have expressed regarding the definition and scoring of the OES protostylid feature do not negate the many previous studies that have noted differences in trait presence between the study taxa. Robinson (1956) noted a tendency for a better-developed protoconidal cingulum in *Au. africanus* than in *P. robustus*. Wood and Abbott (1983) noted a greater frequency of protostylid expression in *P. robustus*, but suggested that when a protostylid was present in *Au. africanus*, its expression was more marked. Hlusko (2004) noted that with respect to the protostylid at the OES, *Au. africanus* tends toward a bimodal distribution, with either no expression or a high degree of expression, while *P. robustus* has a more normally distributed expression of the protostylid. Consequently, Hlusko (2004) argues that it is frequency distribution that separates *Au. africanus* and *P. robustus* and not the central tendency, but Hlusko's definition of the protostylid excluded isolated more mesial crests which may influence this apparent taxonomic distinction. For example, STW 309A and STW 246 that are given as examples

of no protostylid expression (Type 1) and minor protostylid expression (Type 2) respectively (Hlusko, 2004:583), both possess marked mesial crests that we would argue, based on the results of this study, should be included in any assessment of protostylid expression. Guatelli-Steinberg and Irish (2005) also found that protostylids in *Au. africanus* mandibular first molars were more strongly expressed than in *P. robustus*. Our results are consistent with these previous studies in suggesting taxonomic differences in both degree and kind of protostylid expression with significant differences present in both the length and location of crests. A forthcoming study will address the relationship between protostylid expression at the OES and the EDJ in *P. boisei* from East Africa, and what that implies for ongoing investigations into the phylogenetic relationship among *Au. africanus*, *P. robustus*, and *P. boisei*.

Conclusion

Analysis of images of the EDJ obtained from teeth belonging to *Au. africanus* and *P. robustus* suggests that the protostylid features at the OES correspond to crest-like features along the buccal margin of the EDJ. We also suggest that these crest-like features, be they mesial, centrally-located, and/or distal, appear to be developmentally linked, and that researchers should be cautious about selectively excluding any of these features some for the purpose of scoring protostylid expression, as the location of crests may differentiate taxa. Differential enamel deposition can alter the EDJ morphology, particularly in the thicker-enameled molars of *P. robustus*. This means that protostylid expression at the OES cannot always be used as a proxy for the equivalent EDJ morphology and that the pattern that characterizes a taxonomically relevant expression of the trait at the OES might include contributions from both dentine and enamel.

A significant difference in the EDJ morphology of the protostylid is present between *Au. africanus* and *P. robustus.* In *Au. africanus* the crest-like structures at the EDJ extend mesially of the protoconid dentine horn, whereas in *P. robustus* the crest-like structures are more pronounced between the dentine horns of the protoconid and hypoconid. These differences enable teeth from these two taxa to be differentiated even when wear has removed the OES evidence of the protostylid.

Table 5.1. ***Au. africanus*** **and** ***P. robustus*** **mandibular molars included in this study.**

Au. africanus	Tooth	Site	*P. robustus*	Tooth	Site
STS 9	LRM1	Sterkfontein	DNH 60B	LRM1	Drimolen
STW 145	LRM1	Sterkfontein	DNH 67	LRM1	Drimolen
STW 291	LRM1	Sterkfontein	SK 104	LRM1	Swartkrans
STW 309A	LRM1	Sterkfontein	SK 828	LLM1	Swartkrans
STW 364	LRM1	Sterkfontein	SK 843	LLM1	Swartkrans
STW 421A	LRM1	Sterkfontein	SK 846A	LRM1	Swartkrans
STW 421B	LLM1	Sterkfontein	SK 3974	LRM1	Swartkrans
STW 3	LLM2	Sterkfontein	DNH 60C	LRM2	Drimolen
STW 213	LLM2	Sterkfontein	SK 1	LLM2	Swartkrans
STW 213	LRM2	Sterkfontein	SK 6	LRM2	Swartkrans
STW 308	LRM2	Sterkfontein	SK 843	LLM2	Swartkrans
STW 412A	LRM2	Sterkfontein	SK 1587B	LRM2	Swartkrans
STW 412B	LLM2	Sterkfontein	DNH 75	LRM3	Drimolen
STW 424	LLM2	Sterkfontein	SK 6	LRM3	Swartkrans
STW 537	LLM2	Sterkfontein	SK 22	LRM3	Swartkrans
STW 537	LRM2	Sterkfontein	SK 75	LRM3	Swartkrans
STW 560D	LLM2	Sterkfontein	SK 841B	LLM3	Swartkrans
STW 560E	LRM2	Sterkfontein	SK 851	LRM3	Swartkrans
STS 55B	LLM3	Sterkfontein	SKX 5002	LLM3	Swartkrans
STW 280	LRM3	Sterkfontein	SKX 5014	LRM3	Swartkrans
STW 491	LLM3	Sterkfontein	SKX 10642	LLM3	Swartkrans
STW 520	LRM3	Sterkfontein	SKX 10643	LRM3	Swartkrans
STW 529	LLM3	Sterkfontein			
STW 537	LRM3	Sterkfontein			
STW 537	LLM3	Sterkfontein			
STW 560A	LRM3	Sterkfontein			
STW 560B	LLM3	Sterkfontein			
TM 1520	LLM3	Sterkfontein			

Table 5.2. Comparison of correspondence[1] between the EDJ and OES and mean[2] protostylid crest length at the EDJ and OES.

Variable	*P. robustus*	n	*Au. africanus*	n	Mann-Whitney U3
Correspond. – anterior + middle	230.8 ± 169.3	15	117.3 ± 31.1	13	p = 0.02
Correspond. – posterior	203.1 ± 81.3	7	239.5 ± 142.4	9	Ns
Correspondence – whole buccal face	268.6 ± 207.1	15	172.9 ± 110.6	14	Ns
EDJ – anterior	2.4 ± 6.0	19	18.8 ± 9.4	20	p = <0.001
EDJ – middle	32.0 ± 10.5	19	23.1 ± 15.0	20	p = 0.04
EDJ – posterior	18.4 ± 11.7	19	19.3 ± 7.3	20	Ns
EDJ – whole buccal face	52.8 ± 19.6	19	61.3 ± 22.0	20	Ns
OES – anterior	1.6 ± 5.6	15	16.1 ± 12.1	16	p = <0.001
OES – middle	18.7 ± 7.7	15	18.2 ± 14.7	16	Ns
OES – posterior	5.5 ± 6.6	15	6.6 ± 8.3	16	Ns
OES – whole buccal face	25.9 ± 13.7	15	40.9 ± 23.6	16	p = 0.04

1. Each species value represents the mean of the ratio of crest length between the EDJ and OES for each specimen for a given portion of the tooth crown.
2. Each species value represents the mean of crest length scaled by a geometric mean of crown size for the EDJ and OES respectively.
3. While means for each variable are reported the Mann Whitney U test specifically tests whether the two groups were likely to come from populations with the same median values (ns = not statistically significant at or below p = 0.05)

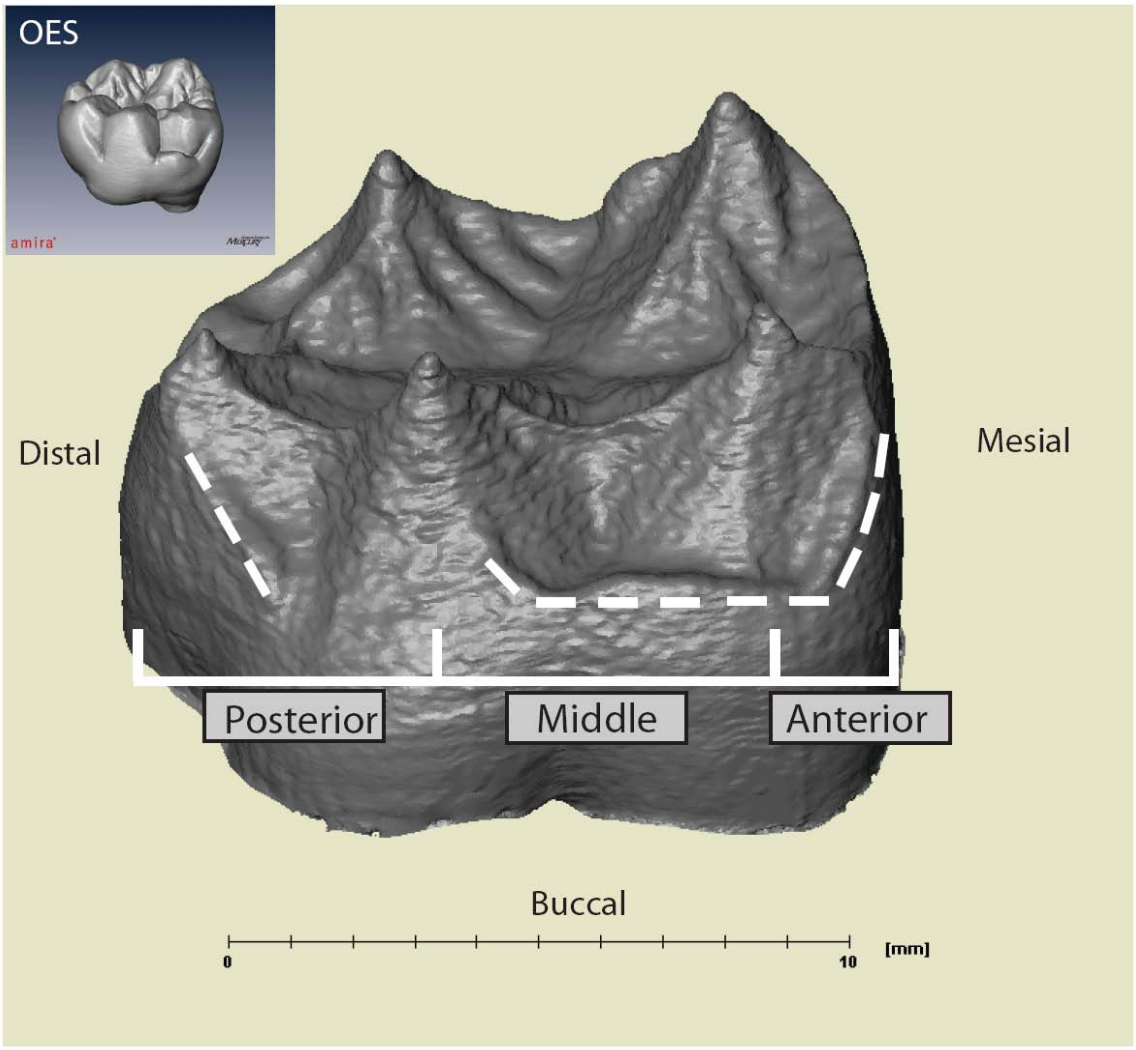

Figure 5.1. Surface model of the EDJ of a mandibular molar illustrating the division of the buccal crown face into three regions: anterior, middle, and posterior (OES surface is inset in top left corner). The dashed line marks which crest features are measured. The OES of each tooth is similarly partitioned and measured.

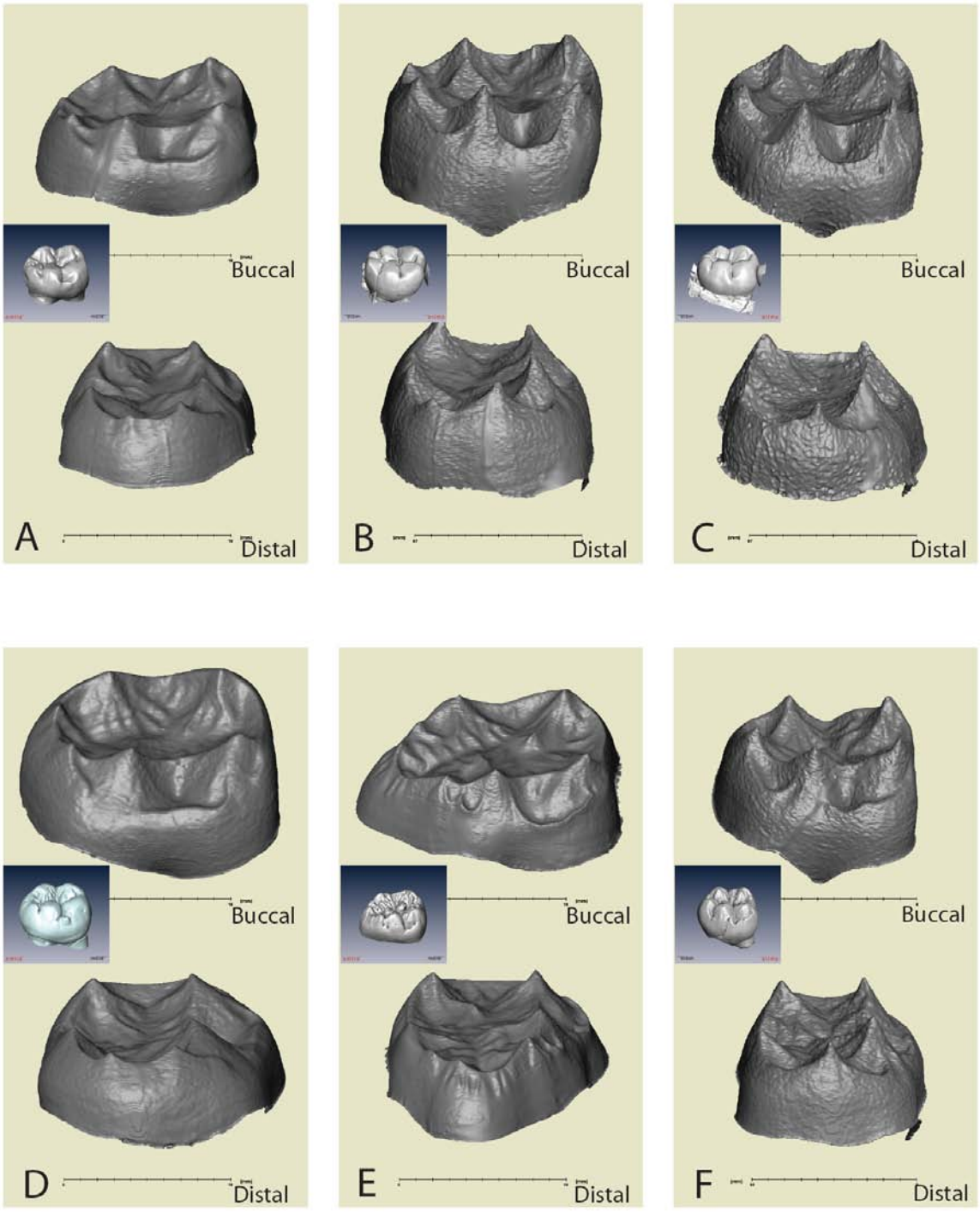

Figure 5.2. EDJ expression of protostylid morphology in six mandibular molars of *P. robustus* in both buccal (top) and distal (bottom) view (a buccal view of the OES surface of each tooth is inset at middle left). Note the prominent crests in the middle of the buccal face and the lack of cresting on the mesial side of the protoconid dentine horn. (**A**) SK1587B_RM_2; (**B**) SK828_LM_1 [mirrored]; (**C**) SK843_LM_1 [mirrored]; (**D**) SK6_RM_2; (**E**) SKX10643_RM_3; (**F**) SK104_LM_1 [mirrored].

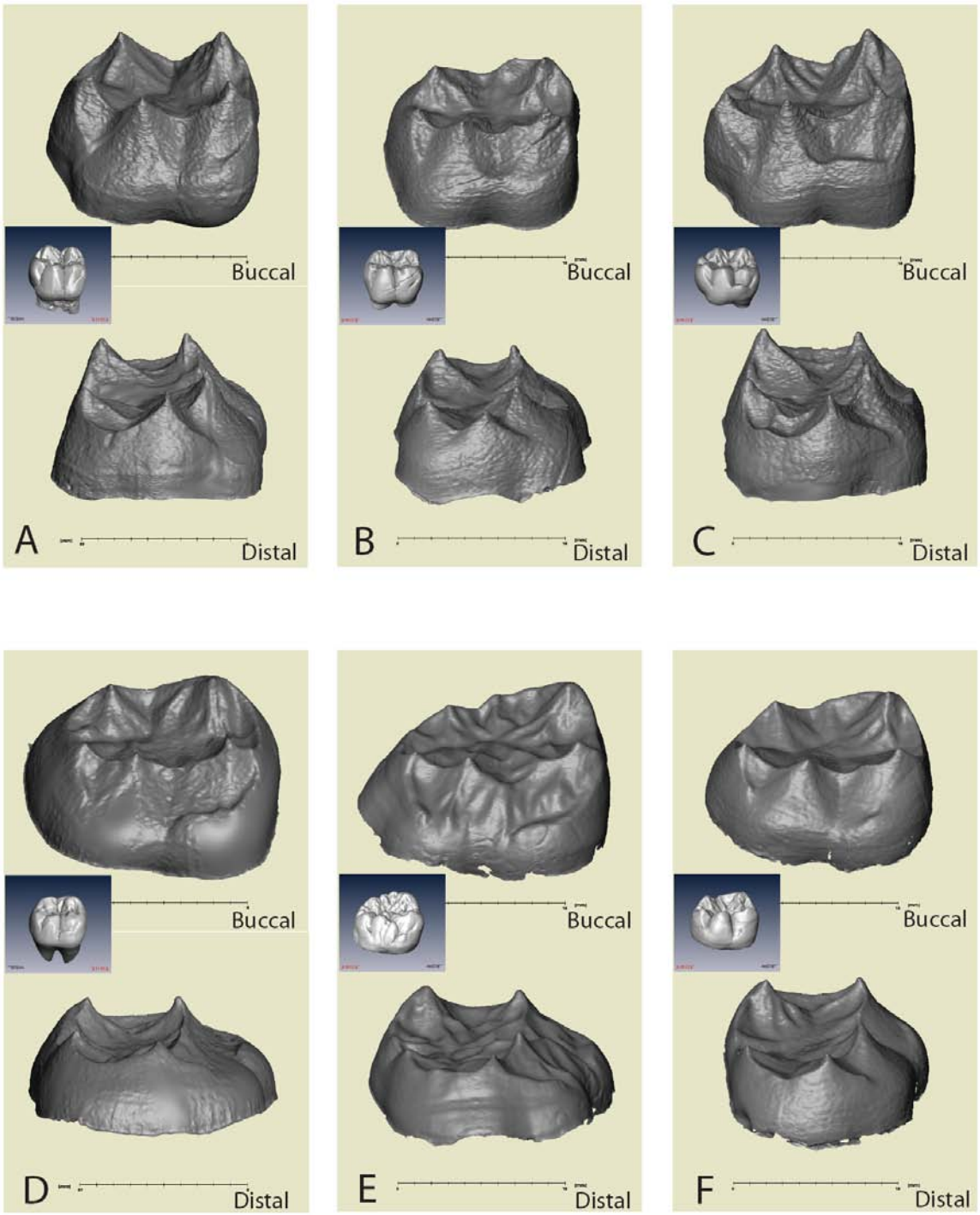

Figure 5.3. EDJ expression of protostylid morphology in six mandibular molars of *Au. africanus* in both buccal (top) and distal (bottom) view (a buccal view of the OES surface of each tooth is inset at middle left). Note the prominent crests in the anterior region of the buccal face extending around the base of the protoconid dentine horn. (**A**) STW309A_LRM1; (**B**) STW145_LRM1; (**C**) STW421A_LRM1; (**D**) STW537_LLM2 [mirrored]; (**E**) STW560A_LRM3; (**F**) STW412A_LRM2.

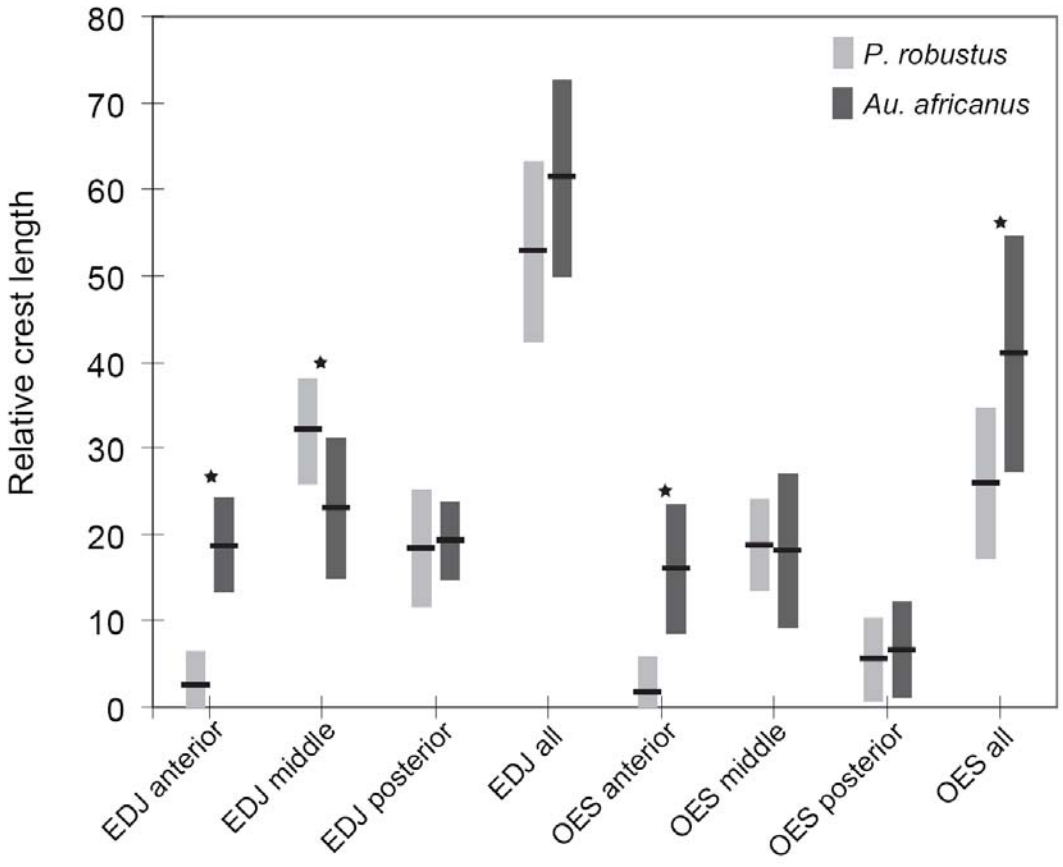

Figure 5.4. Relative protostylid crest length at the EDJ and OES in each region of the buccal face of the molar crown. Black bar denotes the mean and shaded bar represents the 95% confidence interval of each variable. Black stars highlight significant differences below p = 0.05.

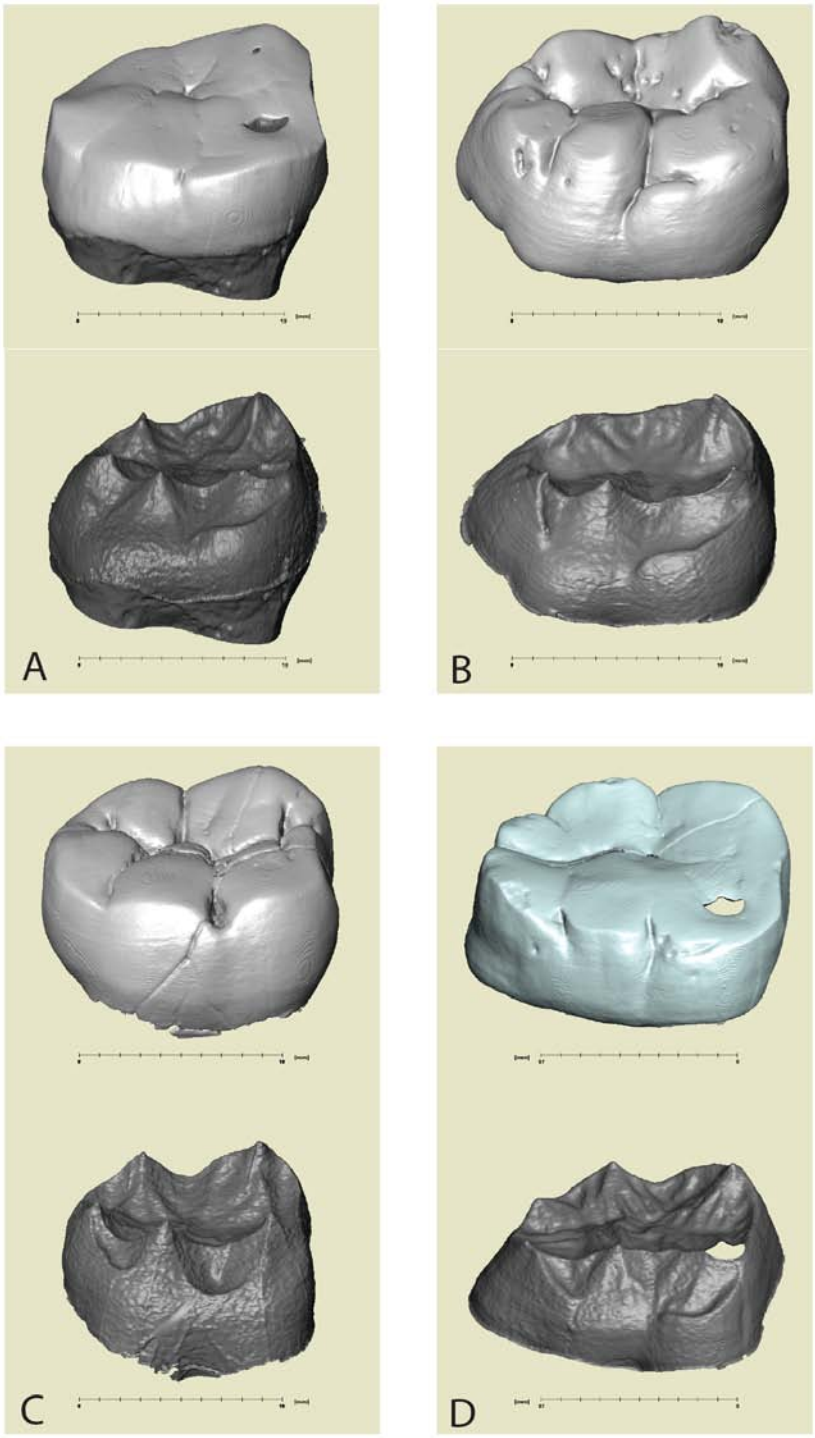

Figure 5.5. OES (top) and EDJ (bottom) expression of protostylid morphology in four mandibular molars exhibiting minor to marked wear. Note that assessing protostylid morphology at the worn enamel surface of these teeth is difficult to impossible. However, the EDJ surface reveals underlying taxon-specific protostylid morphology. (**A**) STW291_LRM1 [*Au. africanus*]; (**B**) STW520_LRM3 [*Au. africanus*]; (**C**) SK846A_LRM1 [*P. robustus*]; (**D**) TM1520_LLM3 [*Au. africanus* - mirrored].

CHAPTER 6: SUMMARY AND CONCLUSIONS

Thesis summary

This thesis focused on an examination of the enamel dentine junction (EDJ) of lower molars in various extant hominoids and fossil hominins. Collectively, these manuscripts represent the first comprehensive analyses of EDJ morphology in a range of hominoid taxa and at the high degree of resolution made possible through the use of micro-computed tomography. They explore the taxonomic relevance of EDJ morphology, both quantitatively and qualitatively, and in doing so reveal how detailed aspects of the outer enamel surface (OES) morphology develop. They also provide insights into the developmental processes that determine the form of the functional interface between the dentition and the food, upon which natural selection acts.

The first chapter introduced the aims of the thesis and reviews the relevant literature. It also provided a detailed discussion of the materials and methods used to image and analyze EDJ morphology. Chapter two demonstrated that when the morphology of the EDJ can be captured in sufficient detail, analysis of its morphology can discriminate between species and subspecies of extant chimpanzees. Chapter three extended these findings to an analysis of lower molars belonging to *Australopithecus africanus* and *Paranthropus robustus* from southern Africa and demonstrated that EDJ morphology is distinctive both between each taxon, as well as between first, second, and third molars of each taxon. Chapter four examined the expression of four dental traits on the lower molars of a range of extant and extinct hominoids (including fossil hominins). It demonstrated that these OES traits originate at the EDJ, that the EDJ is primarily responsible for their degree of expression, and that when examined across a wide range

of taxa the morphological variability in the expression of these traits can be considerable. The fifth chapter focused specifically on one dental trait, the protostylid, and examined its EDJ manifestation in samples of *Australopithecus africanus* and *Paranthropus robustus*. The results of this analysis revealed taxon-specific patterns in protostylid expression that are difficult to detect at the OES as well as evidence that current definitions of the trait itself should be re-examined. The EDJ can be used to address a number of important questions relating to dental anthropology and paleoanthropology, and because details of its morphology are preserved even in heavily worn teeth, the EDJ can play a unique role in generating hypotheses about the taxonomy and systematics of fossil hominin taxa.

Discussion and Conclusions

Interpretations of EDJ shape differences

The methodology employed in this thesis allows the visualization and analysis of detailed aspects of both OES and EDJ morphology. In some cases shape differences between taxa are marked and in some cases they are very subtle. Some may be related to the function of the tooth (e.g., differences in the relative height of the dentine horns) while some may reflect random genetic drift (e.g., slight shape differences between *Pan* subspecies). Now that high-resolution surface models of the dentine (including the roots and the dentine component of the crown) and enamel cap can be generated, efforts should be made to generate and test hypotheses of the functional significance of OES features (e.g., cingula, accessory cusps, dentine horn shape, crest patterning, dentine crown height, crown shape, and enamel distribution) using finite element modeling. The

consistent shape differences between first, second, and third molars revealed in these analyses should also be explored with regard to their functional significance. Using large pedigreed populations, quantitative genetic analysis could reveal the heritability of EDJ features (e.g., Hlusko and Mahaney, 2003), or based on expectations of population genetics one could explore whether subtle variation could arise by genetic drift rather than selection (Weaver et al., 2007).

Selection acting on EDJ and enamel cap morphology

Natural selection can act both on variation of the EDJ, during the growth and folding of the inner enamel epithelium early in the development of the tooth, and/or on differences in the way enamel is distributed over the EDJ. This selection will alter the shape of the features that are interacting with food both when the tooth first erupts into the mouth and as it wears down. Furthermore, it will alter the way in which the tooth reacts under different loading conditions and how it resists abrasion. The correspondence between tooth morphology and diet should be explored, not just with respect to the enamel surface, but also with regard to EDJ morphology.

Taxonomy and phylogeny

This thesis has confirmed that EDJ morphology can discriminate among major groups of primates and it has demonstrated the EDJ's ability to discriminate between closely related taxa. It may be that the combination of information about the EDJ and the OES may provide the most effective discrimination between closely related taxa. The pattern of phylogenetic relationships among the higher primates generated from

molecular evidence could also be used to investigate the taxonomic signal of EDJ and enamel cap morphology. And within the hominin clade the same morphological evidence could be used to test hypotheses of relationships, such as the proposed monophyletic relationship among megadont archaic hominins (*Paranthropus boisei* and *Paranthropus robustus*) from East and southern Africa, respectively. Under a model in which similarities in postcanine crown morphology are the result of convergence, it could be predicted that EDJ and enamel cap morphology are more similar between *P. robustus* and *Au. africanus* than between the former and *P. aethiopicus*/*P. boisei*, while under a model of shared ancestry the same morphology would be more similar among the megadont archaic taxa.

What are the implications for dental trait analysis?

Enamel dentine junction morphology may provide information that is independent of the OES, particularly in those taxa in which the enamel is thick enough to influence trait expression, and OES trait definitions may need to be refined and scoring systems amended. There are a number of outstanding issues regarding specific traits that can be resolved with high resolution images of the OES and EDJ. For example, it could be determined what lies beneath a so-called "split-hypocone" (Bermúdez de Castro and Martínez, 1986). The contribution of the EDJ to Carabelli's trait remains unclear (Schwartz et al., 1998). Preliminary observations suggest that, like most traits, Carabelli's originates at the EDJ, but in minor forms of expression enamel deposition can have a strong influence on manifestation at the OES. A better understanding of the development

of these traits would improve our overall understanding of how teeth grow and our interpretations of morphological variation.

Understanding EDJ development and testing of developmental models

The growing understanding of the genetics of tooth development has led to the development of models through which variability in tooth crown morphology can be interpreted. The applicability of these models, such as those that pertain to cusp patterning, tooth type determination, or to the relative size of molars (Kavanagh et al., 2007), to primates should be explored. As most of our understanding of the genetics of tooth development relates to the early stages of germ development (rather than on the behavior of enamel-depositing ameloblasts) the EDJ is the ideal structure upon which to assess the relevance of these models for generating a deeper understanding of the differences in primate tooth morphology.

The developmental basis of traits also needs to be evaluated. Does an accessory cusp always need to have an underlying dentine horn? What is the significance of variation in EDJ/OES crest morphology, and are the variable manifestations discrete, or are they the consequence of more general properties of the developing tooth germ? The developmental homology of some traits may not hold up under scrutiny of the EDJ. As our ability to visualize crown features in detail improves so too does our understanding of their development as well as their potential relatedness to other crown features.

Importance of making images of EDJ morphology widely available

While there have been a number of researchers who have recognized the importance of EDJ morphology for understanding tooth growth and tooth shape, there are only two sources, to my knowledge, of numerous images of the EDJ surface of modern humans (and none in non-human primates). These are Korenhof's 1960 publication on upper modern human molars and the book by Kraus and Jordan (1965) on fetal tooth germs. The answers to many of my own questions regarding tooth crown morphology were resolved by seeing the images available in these sources. These images, which are not widely available, are also pertinent to many current debates regarding tooth crown features. High-resolution computed tomography is becoming increasingly available to anthropologists and it is a reasonable endeavor, over the next decade, to image the EDJ in large samples of many extant and fossil primate taxa. Making these images available is facilitated by the internet and the ability to embed 3D surfaces into digital documents that can be manipulated by the reader. I believe that great strides could be made in our current understanding of tooth development, tooth variation and the evolution of dental phenotypes simply by making these images easily accessible to a wide audience. In many respects, and for many taxa, the morphology of the EDJ is a *tabula rasa*. Hopefully, this will change in the not too distant future.

References

Avishai, G., Müller, R., Gabet, Y., Bab, I., Zilberman, U., Smith, P., 2004. New approach to quantifying developmental variation in the dentition using serial microtomographic imaging. Microsc. Res. Tech., 65, 263-299.

Bailey, S.E., 2002. A closer look at Neanderthal postcanine dental morphology: the mandibular dentition. Anat. Rec. (New Anat.) 269, 148-156.

Bailey, S.E., 2006. Beyond shovel-shaped incisors: Neandertal dental morphology in a comparative context. Periodicum Biologorum 108, 253-267.

Bailey, S.E., Lynch, J.M., 2005. Diagnostic differences in mandibular P4 shape between Neandertals and anatomically modern humans. Am. J. Phys. Anthropol. 126, 268-277.

Bailey, S.E., Hublin, J-J., 2006. Dental remains from the Grotte du Renne at Arcy-sur-Cure (Yonne). J. Hum. Evol. 50, 485-508.

Bailey, S.E., Wood, B.A., 2007. Trends in postcanine occlusal morphology within the hominin clade: the case of *Paranthropus*. In: Bailey, S.E., Hublin, J.-J. (Eds.), Dental Perspectives on Human Evolution. Springer, Dordrecht, The Netherlands, pp. 33-52.

Becquet, C., Patterson, N., Stone, A. C., Przeworski, M., Reich, D., 2007. Genetic structure of chimpanzee populations. PLos Genet. 3(4), e66. doi:10.1371/journal.pgen.0030066.

Bermúdez de Castro, J.M., Martínez, I., 1986. Hypocone and metaconule: identification and variability on human molars. Int. J. Anthropol. 1, 165-168.

Beynon, A.D., Dean, M.C., Reid, D.J., 1991. On thick and thin enamel in hominoids. Am. J. Phys. Anthropol. 86, 295-309.

Bookstein, F.L., 1991. Morphometric Tools for Landmark Data: Geometry and Biology. Cambridge Univeristy Press, Cambridge.

Bookstein, F.L., 1997. Landmark methods for forms without landmarks: morphometrics of group differences in outline shape. Med. Image Anal. 1, 225-243.

Butler, P.M., 1956. The ontogeny of molar pattern. Biological Reviews 31, 30-70.

Butler, P.M., 1999. The relation of cusp development and calcification to growth. In: Mayhall, J.T., Heikkinen, T. (Eds.), Proceedings of the 11th International Symposium on Dental Morphology, Oulu, Finland, 1998. Oulu University Press, Oulu, Finland, pp. 26-32.

Cai, J., Cho, S.-W., Kim, J.-Y., Lee, M.-J., Cha, Y.-G., Jung, H.-S., 2007. Patterning the size and number of tooth and its cusps. Dev. Biol. 304, 499-507.

Chai, Y., Jiang, X., Ito, Y., Bringas Jr., P., Han, J., Rowitch, D.H., Soriano, P., McMahon, A.P. and Sucov, H.M., 2000. Fate of mammalian neural crest during tooth and mandibular morphogenesis. Development 127, 1671-1679.

Cobourne, M.T., Sharpe, P.T., 2003. Tooth and jaw: molecular mechanisms of patterning in the first branchial arch. Arch. Oral Biol. 48, 1-14.

Conroy, G.C., 1991. Enamel thickness in South African australopithecines: noninvasive evaluation by computed tomography. Palaeont. Afr. 28, 53-58.

Conroy, G.C., Lichtman, J.W., Martin, L.B., 1995. Brief communication: some obervations on enamel thickness and enamel prism packing in the Miocene hominoid *Otavipithecus namibiensis*. Am. J. Phys. Anthropol. 98, 595-600.

Coolidge, H.J., 1933. Pan paniscus. Pygmy chimpanzee from south of the Congo River. Am. J. Phys. Anthropol. 18, 1-57.

Corruccini, R.S., 1987a. The dentinoenamel junction in primates. Int. J. Primatol. 8, 99-114.

Corruccini, R.S., 1987b. Relative growth from the dentino-enamel junction in primate maxillary molars. J. Hum. Evol. 2, 263-269.

Corruccini, R.S., 1998. The dentino-enamel junction in primate mandibular molars. In: Lukacs, J.R. (Ed.), Human Dental Development, Morphology, and Pathology: A Tribute to Albert A. Dahlberg. University of Oregon Anthropological Papers, Portland, pp. 1-16.

Corruccini, R.S., Holt, B.M., 1989. The dentinoenamel junction and the hypocone in primates. Hum. Evol. 4, 253-262.

Dahlberg, A.A., 1950. The evolutionary significance of the protostylid. Am. J. Phys. Anthropol. 8, 15-25.

Dassule, H.R., Lewis, P., Bei, M., Maas, R., McMahon, A.P., 2000. Sonic hedgehog regulates growth and morphogenesis of the tooth. Development 127, 4775-4785.

Donoghue, P.C.J., 2002. Evolution of development of the vertebrate dermal and oral skeletons: unraveling concepts, regulatory theories, and homologies. Paleobiology 28, 474-504.

Dryden, I., Mardia, K.V., 1998. Statistical Shape Analysis. John Wiley & Sons, New York.

Ferguson, C., Hardcastle, Z., Sharpe, P., 2000a. Development and patterning of the dentition. In: Development, Growth and Evolution, O'Higgins, P., Cohn, M. (Eds.) Academic Press, London, pp. 188-205.

Ferguson, C.A., Tucker, A.S., Sharpe, P.T., 2000b. Temporospatial cell interactions regulating mandibular and maxillary arch patterning. Development 127, 403-412.

Fischer, A., Pollack, J., Thalmann, O., Nickel, B., Pääbo, S., 2006. Demographic history and genetic differentiation in apes. Curr. Biol. 16, 1133-1138.

Grine, F.E., 1989. New hominid fossils from the Swartkrans formation (1979-1986 excavations): craniodental specimens. Amer. J. Phys. Anthropol. 79, 409-449.

Grine, F.E., 1991. Computed tomography and the measurement of enamel thickness in extant hominoids: implications for its palaeontological application. Palaeont. Afr. 28, 61-69.

Grine, F.E., 2004. Description and preliminary analysis of new hominid craniodental remains from the Swartkrans Formation. In: Brain, C.K. (Ed.), A Cave's Chronicle of Early Man. Transvaal Museum, Pretoria, pp. 75-116.

Grine, F.E., Martin, L.B., 1988. Enamel thickness and development in *Australopithecus* and *Paranthropus*. In: Grine, F.E. (Ed.), Evolutionary History of the "Robust" Australopithecines. Aldine de Gruyter, New York, pp. 3-42.

Gonder, M.K., Disotell, T.R., Oates, J.F., 2006. New genetic evidence on the evolution of chimpanzee populations and implications for taxonomy. Int. J. Prim. 27, 1103-1127.

Gower, J.C., 1975. Generalized Procrustes analysis. Psychometrika 40, 33-51.

Guatelli-Steinberg, D., Irish, J.D., 2005. Early hominin variability in first molar dental trait frequencies. Am. J. Phys. Anthropol. 128, 477-484.

Gunz, P., Harvati, K., 2007. The Neanderthal "chignon": variation, integration, and homology. J. Hum. Evol. 52, 262-274.

Gunz, P., Mitteroecker, P., Bookstein, F.L., 2005. Semilandmarks in three dimensions. In: Slice, D.E. (Ed.), Modern Morphometrics in Physical Anthropology. Kluwer Academic/Plenum Publishers, New York, pp. 73-98.

Hammer, O., Harper, D., 2006. Paleontological Data Analysis. Blackwell Publishing, Oxford.

Harris, E.F., Dinh, D.P., 2006. Intercusp relationships of the permanent maxillary first and second molars in American whites. Am. J. Phys. Anthropol. 130, 514-528.

Hartman, S.E., 1988. A cladistic analysis of hominoid molars. J. Hum. Evol. 17, 489-502.

Hlusko, L.J., 2002. Expression types for two cercopithecoid dental traits (interconulus and interconulid) and their variation in a modern baboon population. Int. J. Primatol. 23, 1309-1318.

Hlusko, L.J., 2004. Protostylid variation in *Australopithecus*. J. Hum. Evol. 46, 579-594.

Hlusko, L.J., Mahaney, M.C., 2003. Genetic contributions to expression of the baboon cingular remnant. Arch. Oral Biol. 48, 663-672.

Irish, J., Gautelli-Steinberg, D., 2003. Ancient teeth and modern human origins: an expanded comparison of African Plio-Pleistocene and recent world dental samples. J. Hum. Evol. 45, 113-144.

Jernvall, J., Åberg, T., Kettunen, P., Keränen, S., Thesleff, I., 1998. The life history of an embryonic signaling center: BMP-4 induces p21 and is associated with apoptosis in the mouse tooth enamel knot. Development 125, 161-169.

Jernvall, J., 2000. Linking development with generation of novelty in mammalian teeth. Proc. Nat. Acad. Sci. U.S.A. 97, 2641-2645.

Jernvall, J., Jung, H.-S., 2000. Genotype, phenotype, and developmental biology of molar tooth characters. Year. Phys. Anthropol. 43, 171-190.

Jernvall, J., Keranen, S., Thesleff, I., 2000. Evolutionary modification of development in mammalian teeth: quantifying gene expression patterns and topography. Proc. Nat. Acad. Sci. U.S.A. 97, 14444-14448.

Jernvall, J.,Thesleff, I., 2000. Reiterative signalling and patterning during mammalian tooth morphogenesis. Mech. Dev. 92, 19-29.

Johanson, D.C., 1974. An odontological study of the chimpanzee with some implications for hominoid evolution. Ph.D. Dissertation, University of Chicago.

Jungers, W.L., Falsetti, A.B., Wall, C.E., 1995. Shape, relative size and size-adjustment in morphometrics. Yearb. Phys. Anthropol. 38, 137-161.

Kangas, A.T., Evans, A.R., Thesleff, I., Jernvall, J., 2004. Nonindependence of mammalian dental characters. Nature 432, 211-214.

Kassai, Y., Munne, P., Hotta, Y., Penttilä, E., Kavanagh, K., Ohbayashi, N., Takada, S., Thesleff, I., Jernvall, J., Itoh, N., 2005. Regulation of mammalian tooth cusp patterning by ectodin. Science 309, 2067-2070.

Kavanagh, K., Evans, A., Jernvall, J., 2007. Predicting evolutionary patterns of mammalian teeth from development. Nature 499, 427-432.

Keyser, A.W., Menter, C.G., Moggi-Cecchi, J., Pickering, T.R., Berger, L.R., 2000. Drimolen: a new hominid-bearing site in Gauteng, South Africa. S. Afr. J. Sci. 96, 193-197.

King, S.J., Arrigo-Nelson, S.J., Pochron, S.T., Semprebon, G.M., Godfrey, L.R., Wright, P.C., Jernvall, J., 2005. Dental senescence in a long-lived primate links infant survival to rainfall. Proc. Nat. Acad. Sci., U.S.A. 102, 16579-16583.

Kono, R.T., 2004. Molar enamel thickness and distribution patterns in extant great apes and humans: new insights based on a 3-dimensional whole crown perspective. Anthropol. Sci. 112, 121-146.

Kono, R.T., Suwa, G., Tanijiri, T., 2000. Three-dimensional reconstruction and analysis of serially scanned CT image data using CT-Rugle software. Gazolabo 11, 48-52 (in Japanese).

Kono R.T., Suwa, G., Tanijiri, T., 2002. A three-dimensional analysis of enamel distribution patterns in human permanent first molars. Arch. Oral Biol. 47, 867-875.

Korenhof, C.A.W., 1960. Morphogenetical Aspects of the Human Upper Molar. Uitgeversmaatschappij Neerlandia, Utrecht.

Korenhof, C.A.W., 1961. The enamel-dentine border: a new morphological factor in the study of the (human) molar pattern. Proc. Koninkl., Nederl. Acad. Wetensch. 64B, 639-664.

Korenhof, C.A.W., 1978. De evolutie van het ondermolaarpatroon en overblijfselen van het trigonid bij de mens (I). Ned. Tijdschr. Tandheelkd. 85, 456-495.

Korenhof, C.A.W., 1982. Evolutionary trends of the inner enamel anatomy of deciduous molars from Sangiran (Java, Indonesia). In: Kurtén, B. (Ed.), Teeth: Form, Function and Evolution. Columbia University Press, New York, pp. 350-365.

Kortlandt A., 1995. A survey of the geographical range, habitats and conservation of the pygmy chimpanzee (*Pan paniscus*): an ecological perspective. Prim. Cons. 16: 21-36.

Kraus, B.S., 1952. Morphologic relationships between enamel and dentin surfaces of lower first molar teeth. J. Dent. Res. 31, 248-256.

Kraus, B.S., Jordan, R., 1965. The Human Dentition Before Birth. Lea and Febiger, Philadelphia.

Kraus, B.S., Oka, S.W., 1967. Wrinkling of molar crowns: new evidence. Science 157, 328-329.

Kunimatsu, Y., Nakatsukasa, M., Sawada, Y., Sakai, T., Hyodo, M., Hyodo, H., Itaya, T., Nakaya, H., Saegusa, H., Mazurier, A., Saneyoshi, M., Tsujikawa, H., Yamamoto, A., Mbua, E., 2007. A new Late Miocene great ape from Kenya and its implications for the origins of African great apes and humans. Proc. Nat. Acad. Sci. U.S.A. 104, 19220-19225.

Line, S.R.P., 2003. Variation of tooth number in mammalian dentition: connecting genetics, development and evolution. Evol. Dev. 5, 295-304.

Lumsden, A.G., 1988. Spatial organization of the epithelium and the role of neural crest cells in the initiation of the mammalian tooth germ. Development 103, 155-169.

Macchiarelli, R., Bondioli, L., Debénath, A., Mazurier, A., Tournepiche, J.-F., Birch,W., Dean, C., 2006. How Neanderthal molar teeth grew. Nature 444, 748-751.

Macho, G.A., Thackeray, J.F., 1992. Computed tomography and enamel thickness of maxillary molars of Plio-Pleistocene hominids from Sterkfontein, Swartkrans, and Kromdraai, (South Africa): and exploratory study. Am. J. Phys. Anthropol. 89, 133-143.

Martinón-Torres, M., Bermúdez de Castro, J.M., Gómez-Robles, A., Arsuaga, J.L., Carbonell, E., Lordkipanidze, D., Manzi, G., Margvelashvili, A., 2007. Dental evidence on the hominin dispersals during the Pleistocene. Proc. Natl. Acad. Sci. U.S.A. 104, 13279-13282.

McCollum, M.A., Sharpe, P., 2001. Developmental genetics and early hominid craniodental evolution. BioEssays 23, 481-493.

Menter, C.G., Kuykendall, K.L., Keyser, A.W., Conroy, G.C., 1999. First record of hominid teeth from the Plio-Pleistocene site of Gondolin, South Africa. J. Hum. Evol. 37, 299-307.

Mina, M., Kollar, E.J., 1987. The induction of odontogenesis in non-dental mesenchyme combined with early murine mandibular arch epithelium. Arch. Oral Biol. 32, 123-127.

Moggi-Cecchi, J., Grine, F.E., Tobias, P.T., 2006. Early hominid dental remains from Members 4 and 5 of the Sterkfontein Formation (1966-1996 excavations): catalogue, individual associations, morphological descriptions and initial metric analysis. J. Hum. Evol. 50, 239-328.

Morin, P.A., Moore, J.J., Chakraborty, R., Jin, L., Goodall, J., Woodruff, D.S., 1994. Kin selection, social structure, gene flow, and the evolution of chimpanzees. Science 265: 1193-1201.

Mosimann, J.E., 1970. Size allometry: size, and shape variables with characteristics of the log normal and generalized gamma distributions. J. Am. Stat. Assoc. 655, 930-945.

Nager, G., 1960. Der vergleich zwischen dem räumlichen verhalten des dentin-kronenreliefs und dem schmelzrelief der zahnkrone. Acta Anat. 42, 226-250.

Neubuser, A., Peters, H., Balling, R., Martin, G.R., 1997. Antagonistic interactions between FGF and BMP signaling pathways: a mechanism for positioning the sites of tooth formation. Cell 90, 247-255.

Olejniczak, A.J., 2006. Micro-computed tomography of primate molars. Ph.D. Dissertation, Stony Brook University.

Olejniczak, A.J., Gilbert, C.C., Martin, L.B., Smith, T.M., Ulhaas, L., Grine, F.E., 2007. Morphology of the enamel-dentine junction in sections of anthropoid primate maxillary molars. J. Hum. Evol. 53, 292-301.

Olejniczak, A.J., Grine, F.E., 2005. High-resolution measurement of Neandertal tooth enamel thickness by micro-focal computed tomography. S. Afr. J. Sci. 101, 219-220.

Olejniczak, A.J., Grine, F.E., 2006. Assessment of the accuracy of dental enamel thickness measurements using micro-focal X-ray computed tomography. Anatomical Record A 288, 263-275.

Olejniczak, A.J., Martin, L.B., Ulhaas, L., 2004. Quantification of dentine shape in anthropoid primates. Ann. Anat. 186, 479-485.

Olejniczak, A.J., Smith, T.M., Wang, W., Potts, R., Ciochon, R., Kullmer, O., Schrenk, F., Hublin, J-J., 2008. Molar enamel thickness and dentine horn height in *Gigantopithecus blacki*. Am. J. Phys. Anthropol. 135, 85-91.

Olejniczak A.J., Smith T.M., Skinner M.M., Grine F.E., Feeney R.N.M., Thackeray J.F., Hublin, J.-J., n.d. Three-dimensional molar enamel distribution and thickness in *Australopithecus* and *Paranthropus*. Biology Letters.

Osborn, J.W., 1978. Morphogenetic gradients: fields versus clones. In: Development, Function and Evolution of Teeth, Butler, P.M., Joysey, K.A. (Eds.). Academic Press London, pp. 171-201.

Pilbrow, V., 2003. Dental variation in African apes with implications for understanding patterns of variation in species of fossil apes. Ph.D. Dissertation, New York University.

Pilbrow, V., 2006a. Population systematics of chimpanzees using molar morphometrics. J. Hum. Evol. 51, 646-662.

Pilbrow, V., 2006b. Lingual incisor traits in modern hominoids and an assessment of their utility for fossil hominoid taxonomy. Am. J. Phys. Anthropol. 129, 323-338.

Polly, P.D., 1998. Variability, selection, and constraints: development and evolution in viverravid (Carnivora, Mammalia) molar morphology. Paleobiology 24, 409-429.

Reid, C., Van Reenen, J., 1995. The Carabelli trait in early South African hominids: a morphometric study. In: Moggi-Cecchi, J. (Ed.), Aspects of Dental Biology: Paleontology, Anthropology and Evolution. International Institute for the Study of Man, Florence, pp. 299-304.

Robinson, J.T., 1956. The Dentition of the Australopithecinae. Transvaal Museum, Pretoria.

Robinson, J.T., 1963. Adaptive radiation in the australopithecines and the origin of man. In: Clark Howell, F., Bourliere, F. (Eds.), African Ecology and Human Evolution. Aldine: Chicago, pp. 385-416.

Rohlf, F.J., 1993. Relative warp analysis and an example of its application to mosquito wings. In: Marcus, L.F., Bello, E., Garcia-Valdecasas, A. (Eds.), Contributions to Morphometrics. Msueo Nacional de Ciencias Naturales, Madrid, pp. 131-159.

Rohlf, F.J., Slice, D., 1990. Extensions of the Procrustes method for the optimal superimposition of landmarks. Syst. Zool. 39, 40-59.

Rosas, A., Martínez-Maza, C., Bastir, M., García-Tabernero, A., Lalueza-Fox, C., Huguet, R., Ortiz, J.E., Julià, R., Soler, V., de Torres, T., Martínez, E., Cañaveras, J.C., Sánchez-Moral, S, Cuezva, S., Lario, J., Santamaría, D., de la Rasilla, M., Fortea, J., 2006. Paleobiology and comparative morphology of a late Neandertal sample from El Sidron, Asturias, Spain. Proc. Nat. Acad. Sci. U. S. A. 103, 19266-19271.

Ruvolo, M., Pan, D., Zehr, S., Goldberg, T., Disotell, T.R., von Dornum, M., 1994. Gene trees and hominoid phylogeny. Proc. Nat. Acad. Sci., U.S.A. 91, 8900-8904.

Sakai, T., Hanamura, H., 1971. A morphology study of enamel-dentin border on the Japanese dentition. Part V. Maxillary molar. J. Anthropol. Soc. Nippon 79, 297-322.

Sakai, T., Hanamura, H., 1973a. A morphology study of enamel-dentin border on the Japanese dentition. Part VI. Mandibular molar. J. Anthropol. Soc. Nippon 81, 25-45.

Sakai, T., Hanamura, H., 1973b. A morphology study of enamel-dentin border on the Japanese dentition. Part VII. General conclusion. J. Anthropol. Soc. Nippon 81, 87-102.

Sakai, T., Sasaki, I., Hanamura, H., 1965. A morphology study of enamel-dentin border on the Japanese dentition. Part I. Maxillary median incisor. J. Anthropol. Soc. Nippon 73, 91-109.

Sakai, T., Sasaki, I., Hanamura, H., 1967a. A morphology study of enamel-dentin border on the Japanese dentition. Part II. Maxillary canine. J. Anthropol. Soc. Nippon 75, 155-172.

Sakai, T., Sasaki, I., Hanamura, H., 1967b. A morphology study of enamel-dentin border on the Japanese dentition. Part III. Maxillary premolar. J. Anthropol. Soc. Nippon 75, 207-223.

Sakai, T., Sasaki, I., Hanamura, H., 1969. A morphology study of enamel-dentin border on the Japanese dentition. Part IV. Mandibular premolar. J. Anthropol. Soc. Nippon 77, 71-98.

Salazar-Ciudad, I., Jernvall, J., Newman, S., 2003. Mechanisms of pattern formation in development and evolution. Development 130, 2027-2037.

Sasaki, K., Kanazawa, E., 1999. Morphological traits on the dentino-ename junction of lower deciduous molar series. In: Mayhall, J.T., Heikkinen, T. (Eds.), Proceedings of the 11th International Symposium on Dental Morphology, Oulu, Finland, 1998. Oulu University Press, Oulu, Finland, pp. 167-178.

Satokata, I., Maas, R., 1994. Msx1 deficient mice exhibit cleft palate and abnormalities of craniofacial and tooth development. Nat. Genet. 6, 348-356.

Schulze, M.A., Pearce, J.A., 1994. A morphology-based filter structure for edge-enhancing smoothing. In Proceedings of the 1994 IEEE International Conference on Image Processing, pp. 530-534.

Scott, G.R., Turner II, C.G., 1997. The Anthropology of Modern Human Teeth. Cambridge University Press, Cambridge.

Schwartz, G.T., Thackeray, J.F., Reid, C., van Reenan, J.F., 1998. Enamel thickness and the topography of the enamel-dentine junction in South African Plio-Pleistocene hominids with special reference to the Carabelli trait. J. Hum. Evol. 35, 523-542.

Sharpe, P.T., 1995. Homeobox genes and orofacial development. Con. Tiss. Res. 32, 17-25.

Shea, B.T., Leigh, S.R., Groves, C.P., 1993. Mulivariate craniometric variation in chimpanzees: implications for species identification in paleoanthropology. In: Kimbel, W.H., Martin, L.B. (Eds.), Species, Species Concepts and Primate Evolution. Plenum Press, New York, pp. 265-296.

Shimizu, D., 2002. Functional implications of enamel thickness in the lower molars of red colobus (Procolobus badius) and Japanese macaque (Macaca fuscata). J. Hum. Evol. 43, 605-620.

Scott, G.R., Turner II, C.G., 1997. The Anthropology of Modern Human Teeth. Cambridge University Press, Cambridge.

Skinner, M.M. Gunz, P., Wood, B.A., Hublin, J-J., n.d. Enamel-dentine junction morphology distinguishes the lower molars of Australopithecus africanus and Paranthropus robustus. J. Hum. Evol.

Skinner, M.M, Wood, B.A., Boesch, C., Olejniczak, A.J., Rosas, A., Smith, T.M., Hublin, J-J., 2008. Dental trait expression at the enamel-dentine junction of lower molars in extant and fossil hominoids. J. Hum. Evol. doi:10.1016/j.jhevol.2007.09.012.

Smith, P., Gomorri, J.M., Spitz, S., Becker, J., 1997. Model for the examination of evolutionary trends in tooth development. Am. J. Phys. Anthropol. 102, 283-294.

Smith, T.M., Olejniczak, A.J., Reid, D.J., Ferrell, R., Hublin, J-J., 2006a. Modern human molar enamel thickness and enamel dentine junction shape. Arch. Oral Biol. 51, 974-995.

Smith, T.M., Olejniczak, A.J., Tafforeau, P., Reid, D.J., Grine, F.E., Hublin, J-J., 2006b. Molar crown thickness, volume, and development in South African Middle Stone Age humans. S. Afr. J. Sci. 102, 513-517.

Sperber, G., 1974. Morphology of the cheek teeth of early South African hominids. Ph.D. Dissertation, University of Witwatersrand.

Stone, A.C., Griffiths, R.C., Zegura, S.L., Hammer, M.F., 2002. High levels of Y-chromosome nucleotide diversity in the genus Pan. Proc. Nat. Acad. Sci., U.S.A. 99, 43-48.

Suwa, G., 1996. Serial allocations of isolated mandibular molars of unknown taxonomic affinities from the Shungura and Unso Formations, Ethiopia, a combined method approach. Human Evolution 11, 269-282.

Suwa, G. Kono, R.T., 2005. A micro-CT based study of linear enamel thickness in the mesial cusp section of human molars: reevaluation of methodology and assessment of within-tooth, serial, and individual variation. Anthropol. Sci. 113, 273-289.

Suwa, G., Kono, R.T., Katoh, S., Asfaw, B., Beyene, Y., 2007. A new species of great ape from the late Miocene epoch in Ethiopia. Nature 448, 921-924.

Suwa, G., White, T.D., Howell, F.C., 1996. Mandibular postcanine dentition from the Shungura Formation, Ethiopia: crown morphology, taxonomic allocations, and Plio-Pleistocene hominid evolution. Am. J. Phys. Anthropol. 101, 247-282.

Suwa, G., Wood, B.A., White, T.D., 1994. Further analysis of mandibular molar crown and cusp areas in Pliocene and Early Pleistocene hominids. American Journal of Physical Anthropology 93, 407-426.

Swails, N.J., 1993. The evolutionary implications of primate tooth-germ development: using ontogenetic data to make phylogenetic inferences. Ph.D. Dissertation, University of Washington.

Tafforeau, P., 2004. Phylogenetic and functional aspects of tooth enamel microstructure and three-dimensional structure of modern and fossil primate molars. Ph.D. Dissertation, Université de Montpellier II.

Ten Cate, A.R. (2007). Oral Histology: Development, Structure and Function, 7th Edition. C.V. Mosby Company, St. Louis.

Thomas, B.L., Tucker, A.S., Qiu, M., Ferguson, C., Hardcastle, Z., Rubenstein, J.L.R., Sharpe, P.T., 1997. Role of Dlx-1 and Dlx-2 genes in patterning of the murine dentition. Development 124, 4811-4818.

Tobias, P.V., Copley, K., Brain, C., 1977. South Africa. In: Catalogue of Fossil Hominids. Part 1: Africa (2nd Edition), Oakley, K.P., Campbell, B.G., Molleson, T. I., (Eds.). British Museum of Natural History, London.

Tucker, A.S., Headon, D.J., Courtney, J.-M., Overbeek, P., Sharpe, P.T., 2004. The activation level of the TNF family receptor, Edar, determines cusp number and tooth number during tooth development. Dev. Biol. 268, 185-194.

Tucker, A.S., Matthews, K.L., Sharpe, P.T., 1998. Transformation of tooth type induced by inhibition of BMP signaling. Science 282, 1136-1138.

Turner II, C.G., Nichol, C.R., Scott, G.R., 1991. Scoring procedures for key morphological traits of the permanent dentition: the Arizona State University Dental Anthropology System. In: Kelley, M.A., Larsen, C.S. (Eds.), Advances in Dental Anthropology. Wiley-Liss, New York, pp. 13-31.

Uchida, A., 1992. Intra-species variation among the great apes: implications for taxonomy of fossil hominoids. Ph.D. Dissertation, Harvard University.

Uchida, A., 1996. Craniodental Variation Among the Great Apes. Peabody Museum of Archaeology and Ethnology, Harvard University, Cambridge.

Uchida, A., 1998a. Variation in tooth morphology of *Gorilla gorilla*. J. Hum. Evol. 34, 55-70.

Uchida, A., 1998b. Variation in tooth morphology of *Pongo pygmaeus*. J. Hum. Evol. 34, 71-79.

van Genderen, C., Okamura, R.M., Farinas, I., 1994. Development of several organs that require inductive epithelial-mesenchymal interactions is impaired in LEF-1 deficient mice. Gen. Dev. 8, 2691-2703.

Van Reenen, J., Reid, C., 1995. The Carabelli trait in early South African hominids: a morphological study. In: Moggi-Cecchi, J. (Ed.), Aspects of Dental Biology: Paleontology, Anthropology and Evolution. International Institute for the Study of Man, Florence, pp. 291-298.

von Koenigswald, G.H.R., 1952. *Gigantopithecus blacki*, a giant fossil hominid from the Pleistocene of southern China. Anthropol. Pap. Am. Mus. Nat. Hist. 43, 295-325.

Weaver, T.D., Roseman, C.C., Stringer, C.B., 2007. Were Neandertal and modern human cranial differences produced by natural selection or genetic drift. J. Hum. Evol. 53, 135-145.

Weidenreich, F., 1937. The dentition of *Sinanthropus pekinensis*: a comparative odontography of the hominids. Palaeontologica Sinica, Series D, I, 1-180.

Weidenreich, F., 1945. Giant early man rom Java and South China. Anthropol. Pap. Am. Mus. Nat. Hist. 40, 1-134.

Weiss, K.M., Stock, D.W., Zhao, Z., 1998. Dynamic interactions and the evolutionary genetics of dental patterning. Crit. Rev. Oral Biol. Med. 9, 369-398.

Won, Y-J., Hey, J., 2005. Divergence population genetics of chimpanzees. Mol. Biol. Evol. 22, 297-307.

Wood, B.A., 1991. Hominid Cranial Remains. In: Koobi Fora Research Project, vol. 4. Clarendon Press, Oxford.

Wood, B.A., Abbott, S.A., 1983. Analysis of the dental morphology of Plio-Pleistocene hominids. I. Mandibular molars: crown area measurements and morphological traits. J. Anat. 136, 197-219.

Wood, B.A., Abbott, S.A., Graham, S.H., 1983. Analysis of the dental morphology of Plio-Plesitocene hominids. II. Mandibular molars - study of cusp areas, fissure patterns and cross sectional shape of the crown. J. Anat. 137, 287-314.

Wood, B.A., Constantino, P., 2007. *Paranthropus boisei*: fifty years of evidence and analysis. Yearb. Phys. Anthropol. 50, 106-132.

Wood, B.A., Richmond, B.R., 2000. Human evolution: taxonomy and paleobiology. J. Anat. 196, 19-60.

Wu, L., Turner, C.G., 1993. Variation in the frequency and form of the lower permanent molar middle trigonid crest. Am. J. Phys. Anthropol. 91, 245-248.

Zilberman, U., Skinner, M., Smith, P., 1992. Tooth components of mandibular deciduous molars of *Homo sapiens sapiens* and *Homo sapiens neanderthalensis*: a radiographic study. Am. J. Phys. Anthropol. 87, 255-262.

Appendix A. Molar sample used in this thesis including locality/site information and inclusion in particular analyses.

Genus	Species	Subspecies	Source[1]	Locality or Site	Accession[2]	Tooth	Side	Chap_2	Chap_3	Chap_4	Chap_5
Gorilla	*gorilla*	*beringei*	NMNH	Rwanda	545037	LM2	R	Y		Y	
Gorilla	*gorilla*	*beringei*	NMNH	Rwanda	543034	LM3	R	Y		Y	
Homo	*sapiens*	*sapiens*	NMNH	Unknown	SI_34*	LM1/2	L			Y	
Homo	*sapiens*	*sapiens*	NMNH	Unknown	SI_37*	LM1/2	L			Y	
Homo	*sapiens*	*sapiens*	MPI-EVA	Inverness, Scotland	SKB_30*	LM2	L			Y	
Homo	*sapiens*	*sapiens*	MPI-EVA	Garrowby Wold 101	SKB_71*	LM2	R			Y	
Pan	*paniscus*	*paniscus*	MRAC	DR Congo, Ibembo	5374	LM1	L	Y			
Pan	*paniscus*	*paniscus*	MRAC	DR Congo, Ponthierville	27009	LM1	L	Y			
Pan	*paniscus*	*paniscus*	MRAC	DR Congo, Djolu	29010	LM1	R	Y			
Pan	*paniscus*	*paniscus*	MRAC	DR Congo, Djolu	29016	LM1	R	Y			
Pan	*paniscus*	*paniscus*	MRAC	DR Congo, Djolu	29024	LM1	L	Y			
Pan	*paniscus*	*paniscus*	MRAC	DR Congo, Djolu	29026	LM1	R	Y			
Pan	*paniscus*	*paniscus*	MRAC	DR Congo, Djolu	29030	LM1	R	Y			
Pan	*paniscus*	*paniscus*	MRAC	DR Congo, Dongo	29048	LM1	R	Y			
Pan	sp	ssp	MRAC	Unknown	84036M11	LM1	L	Y			
Pan	*paniscus*	*paniscus*	MRAC	DR Congo, Coquilhatville	22908	LM2	L	Y			
Pan	*paniscus*	*paniscus*	MRAC	DR Congo, Djolu	29030	LM2	L	Y			
Pan	*paniscus*	*paniscus*	MRAC	DR Congo, Djolu	29033	LM2	L	Y			
Pan	*paniscus*	*paniscus*	MRAC	DR Congo, Bokungu	29041	LM2	L	Y			
Pan	*paniscus*	*paniscus*	MRAC	DR Congo, Batiakayandja	29055	LM2	L	Y			
Pan	*paniscus*	*paniscus*	MRAC	DR Congo, Bore	29056	LM2	R	Y			
Pan	*paniscus*	*paniscus*	MRAC	DR Congo, Lubutu	29066	LM2	L	Y			
Pan	*paniscus*	*paniscus*	MRAC	DR Congo, Ponthierville	84036M03	LM2	R	Y			
Pan	*paniscus*	*paniscus*	MRAC	DR Congo, Yahuma	84036M04	LM2	L	Y			
Pan	sp	ssp	MRAC	Unknown	84036M10	LM2	L	Y			
Pan	sp	ssp	MRAC	Unknown	84036M11	LM2	L	Y			
Pongo	*pygmaeus*	*abelli*	ZMB	Sumatra, Indonesia	38606	LM1	L			Y	
Pongo	*pygmaeus*	*pygmaeus*	ZMB	Borneo, Indonesia	30946	LM1	R			Y	

Pongo	*pygmaeus*	ssp	ZMB	Captive	6987	LM1	L		Y
Pan	sp	ssp	ZMB	Unknown	20811	LM1	R	Y	
Pan	sp	ssp	ZMB	Captive	47506	LM1	L	Y	
Pan	sp	ssp	ZMB	Captive	72844	LM1	R	Y	
Pan	sp	ssp	ZMB	Unknown	0.A809	LM1	R	Y	
Pan	*troglodytes*	*troglodytes*	ZMB	Cameroon, Ebolowa	15849	LM1	L	Y	
Pan	*troglodytes*	*troglodytes*	ZMB	Cameroon, Akonolinga	30847	LM1	R	Y	
Pan	sp	ssp	ZMB	Unknown	32052	LM1	R	Y	
Pan	sp	ssp	ZMB	Unknown	32356	LM1	R	Y	
Pan	*troglodytes*	*troglodytes*	ZMB	Cameroon, Yaounde	35526	LM1	R	Y	
Pan	*troglodytes*	*troglodytes*	ZMB	Cameroon, Bipindi	83604	LM1	L	Y	
Pan	*troglodytes*	*troglodytes*	ZMB	Cameroon, Yakuduma	83623	LM1	L	Y	
Pan	*troglodytes*	*troglodytes*	ZMB	Cameroon, Ukalla Nsama	83673	LM1	L	Y	
Pan	*troglodytes*	*troglodytes*	ZMB	Cameroon, Basho	A162.07	LM1	L	Y	
Pan	*troglodytes*	*verus*	MPI-EVA	Cote D'Ivoire, Tai Forest	11791	LM1	L	Y	
Pan	*troglodytes*	*verus*	MPI-EVA	Cote D'Ivoire, Tai Forest	11792	LM1	R	Y	
Pan	*troglodytes*	*verus*	MPI-EVA	Cote D'Ivoire, Tai Forest	11798	LM1	L	Y	Y
Pan	*troglodytes*	*verus*	MPI-EVA	Cote D'Ivoire, Tai Forest	11800	LM1	R	Y	
Pan	*troglodytes*	*verus*	MPI-EVA	Cote D'Ivoire, Tai Forest	11903	LM1	R		Y
Pan	*troglodytes*	*verus*	MPI-EVA	Cote D'Ivoire, Tai Forest	12176	LM1	R		Y
Pan	*troglodytes*	*verus*	MPI-EVA	Cote D'Ivoire, Tai Forest	13433	LM1	L	Y	Y
Pan	*troglodytes*	*verus*	MPI-EVA	Cote D'Ivoire, Tai Forest	14992	LM1	L	Y	Y
Pan	*troglodytes*	*verus*	MPI-EVA	Cote D'Ivoire, Tai Forest	14995	LM1	L	Y	Y
Pan	*troglodytes*	*verus*	MPI-EVA	Cote D'Ivoire, Tai Forest	15011	LM1	R	Y	
Pan	sp	ssp	ZMB	West Africa	6983	LM1	R	Y	
Pan	sp	ssp	ZMB	Bugoie Wald, Rwanda	24838	LM2	L	Y	
Pan	sp	ssp	ZMB	Egypt	33489	LM2	L	Y	
Pan	sp	ssp	ZMB	Captive	72844	LM2	R	Y	
Pan	*troglodytes*	*troglodytes*	ZMB	Cameroon, Akonolinga	30846	LM2	R	Y	
Pan	*troglodytes*	*troglodytes*	ZMB	Cameroon, Akonolinga	30847	LM2	L	Y	

Pan	*troglodytes*	*troglodytes*	ZMB	Mburu Ogowe (Gabon?)	31279	LM2	R	Y				
Pan	*troglodytes*	*troglodytes*	ZMB	Cameroon, Buea	46095	LM2	L	Y				
Pan	*troglodytes*	*troglodytes*	ZMB	Cameroon, Lomie	83635	LM2	L	Y				
Pan	*troglodytes*	*troglodytes*	ZMB	Cameroon, Akonolinga	83639	LM2	R	Y				
Pan	*troglodytes*	*troglodytes*	ZMB	Gabon, Mayumba	83685	LM2	R	Y				
Pan	*troglodytes*	*verus*	MPI-EVA	Côte d'Ivoire, Tai Forest	11778	LM2	R			Y		
Pan	*troglodytes*	*verus*	MPI-EVA	Côte d'Ivoire, Tai Forest	11779	LM2	R			Y		
Pan	*troglodytes*	*verus*	MPI-EVA	Côte d'Ivoire, Tai Forest	11784	LM2	R			Y		
Pan	*troglodytes*	*verus*	MPI-EVA	Côte d'Ivoire, Tai Forest	11790	LM2	R	Y		Y		
Pan	*troglodytes*	*verus*	MPI-EVA	Côte d'Ivoire, Tai Forest	11791	LM2	R	Y				
Pan	*troglodytes*	*verus*	MPI-EVA	Côte d'Ivoire, Tai Forest	11792	LM2	L	Y				
Pan	*troglodytes*	*verus*	MPI-EVA	Côte d'Ivoire, Tai Forest	11800	LM2	R	Y		Y		
Pan	*troglodytes*	*verus*	MPI-EVA	Côte d'Ivoire, Tai Forest	12176	LM2	R	Y		Y		
Pan	*troglodytes*	*verus*	MPI-EVA	Côte d'Ivoire, Tai Forest	13433	LM2	R	Y		Y		
Pan	*troglodytes*	*verus*	MPI-EVA	Côte d'Ivoire, Tai Forest	13437	LM2	R	Y		Y		
Pan	*troglodytes*	*verus*	MPI-EVA	Côte d'Ivoire, Tai Forest	13438	LM2	R			Y		
Pan	*troglodytes*	*verus*	MPI-EVA	Côte d'Ivoire, Tai Forest	13439	LM2	R			Y		
Pan	*troglodytes*	*verus*	MPI-EVA	Côte d'Ivoire, Tai Forest	14992	LM2	L	Y		Y		
Pan	*troglodytes*	*verus*	MPI-EVA	Côte d'Ivoire, Tai Forest	15008	LM2	R	Y				
Pan	*troglodytes*	*verus*	MPI-EVA	Côte d'Ivoire, Tai Forest	15012	LM2	R	Y		Y		
Pan	*troglodytes*	*verus*	MPI-EVA	Côte d'Ivoire, Tai Forest	15014	LM2	R			Y		
Pan	*troglodytes*	*verus*	MPI-EVA	Côte d'Ivoire, Tai Forest	11790	LM3	L			Y		
Gigantopithecus	*blacki*	*blacki*	SFN	Unknown	CA_736	LM2/3	L	Y		Y		
Homo	*neanderthalensis*	*neanderthalensis*	MNCN	El Sidron, Spain	SD_331c	LM1	L			Y		
Homo	*neanderthalensis*	*neanderthalensis*	MNCN	El Sidron, Spain	SD_540	LM1	L			Y		
Homo	*neanderthalensis*	*neanderthalensis*	MNCN	El Sidron, Spain	SD_756	LM1	R			Y		
Homo	*neanderthalensis*	*neanderthalensis*	MNCN	El Sidron, Spain	SD_780	LM1	L			Y		
Australopithecus	*africanus*	*africanus*	UW	Sterkfontein, South Africa	STW_145	LM1	R		Y			Y
Australopithecus	*africanus*	*africanus*	UW	Sterkfontein, South Africa	STW_291	LM1	R					Y
Australopithecus	*africanus*	*africanus*	UW	Sterkfontein, South Africa	STW_364	LM1	R					Y

Australopithecus	*africanus*	*africanus*	TM	Sterkfontein, South Africa	STS_9	LM1	R	Y		Y
Australopithecus	*africanus*	*africanus*	UW	Sterkfontein, South Africa	STW_309A	LM1	R	Y		Y
Australopithecus	*africanus*	*africanus*	UW	Sterkfontein, South Africa	STW_421A	LM1	R	Y		Y
Australopithecus	*africanus*	*africanus*	UW	Sterkfontein, South Africa	STW_421B	LM1	L		Y	Y
Australopithecus	*africanus*	*africanus*	UW	Sterkfontein, South Africa	STW_3	LM2	L	Y		Y
Australopithecus	*africanus*	*africanus*	UW	Sterkfontein, South Africa	STW_296	LM2	R	Y		Y
Australopithecus	*africanus*	*africanus*	UW	Sterkfontein, South Africa	STW_424	LM2	L	Y	Y	Y
Australopithecus	*africanus*	*africanus*	UW	Sterkfontein, South Africa	STW_213	LM2	L	Y		Y
Australopithecus	*africanus*	*africanus*	UW	Sterkfontein, South Africa	STW_213	LM2	R			Y
Australopithecus	*africanus*	*africanus*	UW	Sterkfontein, South Africa	STW_412A	LM2	R			Y
Australopithecus	*africanus*	*africanus*	UW	Sterkfontein, South Africa	STW_412B	LM2	L	Y		Y
Australopithecus	*africanus*	*africanus*	UW	Sterkfontein, South Africa	STW_537	LM2	R	Y		Y
Australopithecus	*africanus*	*africanus*	UW	Sterkfontein, South Africa	STW_537	LM2	L	Y		Y
Australopithecus	*africanus*	*africanus*	UW	Sterkfontein, South Africa	STW_560D	LM2	L			Y
Australopithecus	*africanus*	*africanus*	UW	Sterkfontein, South Africa	STW_560E	LM2	R	Y	Y	Y
Australopithecus	*africanus*	*africanus*	TM	Sterkfontein, South Africa	TM_1520	LM3	L			Y
Australopithecus	*africanus*	*africanus*	UW	Sterkfontein, South Africa	STW_520	LM3	R	Y		Y
Australopithecus	*africanus*	*africanus*	UW	Sterkfontein, South Africa	STS_55B	LM3	L			Y
Australopithecus	*africanus*	*africanus*	UW	Sterkfontein, South Africa	STW_280	LM3	R	Y		Y
Australopithecus	*africanus*	*africanus*	UW	Sterkfontein, South Africa	STW_491	LM3	L	Y		Y
Australopithecus	*africanus*	*africanus*	UW	Sterkfontein, South Africa	STW_529	LM3	L	Y		Y
Australopithecus	*africanus*	*africanus*	UW	Sterkfontein, South Africa	STW_537	LM3	L			Y
Australopithecus	*africanus*	*africanus*	UW	Sterkfontein, South Africa	STW_537	LM3	R	Y		Y
Australopithecus	*africanus*	*africanus*	UW	Sterkfontein, South Africa	STW_560A	LM3	R		Y	Y
Australopithecus	*africanus*	*africanus*	UW	Sterkfontein, South Africa	STW_560B	LM3	L	Y		Y
Paranthropus	*cf. robustus*	*robustus*	UW	Gondolin, South Africa	GDA_2	LM2	L	Y		
Paranthropus	*robustus*	*robustus*	TM	Swartkrans, South Africa	SK_104	LM1	R	Y		Y
Paranthropus	*robustus*	*robustus*	TM	Swartkrans, South Africa	SK_3974	LM1	R	Y	Y	Y
Paranthropus	*robustus*	*robustus*	TM	Swartkrans, South Africa	SK_828	LM1	L	Y	Y	Y
Paranthropus	*robustus*	*robustus*	TM	Swartkrans, South Africa	SK_846A	LM1	R	Y		

Paranthropus	*robustus*	*robustus*	UW	Drimolen, South Africa	DNH_60b	LM1	R	Y		Y
Paranthropus	*robustus*	*robustus*	UW	Drimolen, South Africa	DNH_67	LM1	R	Y	Y	Y
Paranthropus	*robustus*	*robustus*	TM	Swartkrans, South Africa	SK_843	LM1	L	Y		Y
Paranthropus	*robustus*	*robustus*	TM	Swartkrans, South Africa	SK_1	LM2	L	Y		Y
Paranthropus	*robustus*	*robustus*	TM	Swartkrans, South Africa	SK_1587B	LM2	R	Y		Y
Paranthropus	*robustus*	*robustus*	UW	Drimolen, South Africa	DNH_60c	LM2	R	Y	Y	Y
Paranthropus	*robustus*	*robustus*	TM	Swartkrans, South Africa	SK_6	LM2	R	Y		Y
Paranthropus	*robustus*	*robustus*	TM	Swartkrans, South Africa	SK_843	LM2	L	Y		Y
Paranthropus	*robustus*	*robustus*	TM	Kromdraai, South Africa	TM_1600	LM2	L	Y		
Paranthropus	*robustus*	*robustus*	TM	Swartkrans, South Africa	SK_22	LM3	R	Y		Y
Paranthropus	*robustus*	*robustus*	TM	Swartkrans, South Africa	SK_75	LM3	R	Y		Y
Paranthropus	*robustus*	*robustus*	TM	Swartkrans, South Africa	SK_851	LM3	R	Y		Y
Paranthropus	*robustus*	*robustus*	TM	Swartkrans, South Africa	SK_6	LM3	R	Y		Y
Paranthropus	*robustus*	*robustus*	TM	Swartkrans, South Africa	SK_841b	LM3	L	Y		Y
Paranthropus	*robustus*	*robustus*	TM	Swartkrans, South Africa	SKX_10642	LM3	L	Y		Y
Paranthropus	*robustus*	*robustus*	TM	Swartkrans, South Africa	SKX_10643	LM3	R			Y
Paranthropus	*robustus*	*robustus*	TM	Swartkrans, South Africa	SKX_5002	LM3	L	Y		Y
Paranthropus	*robustus*	*robustus*	TM	Swartkrans, South Africa	SKX_5014	LM3	R	Y		Y

1. Source codes: MPI-EVA, Max Planck Institute for Evolutionary Anthropology, Leipzig, Germany; NMNH, National Museum of Natural History, Washington, DC, USA; ZMB, Museum für Naturkunde, Humboldt Universität, Berlin, Germany; SFN, Senckenberg Forschungsinstitut und Naturmuseum, Frankfurt, Germany; MNCN, Museo Nacional de Ciencias Naturales, Madrid, Spain, TM, Transvaal Museum, Pretoria, South Africa; UW, University of Witwatersrand, Johannesburg, South Africa.
2. (*) - Indicates that the specimen has no museum accession number and that the listed accession number is an internal number of the MPI-EVA.

Appendix B.

This appendix is composed of an example of the Mathematica code used to perform a Procrustes superimposition on the landmark data to create a sample of a homologous landmark set for each specimen. In this case the code pertains to the analysis of the combined first and second molar sample of *Pan* (Chapter 2).

Step 1. Identify appropriate data files

```
surface = Import["P:\\PROJECTS_CURRENT\Pan_Taxonomy\PAN_MASTER_SURFACE.ply"]
```

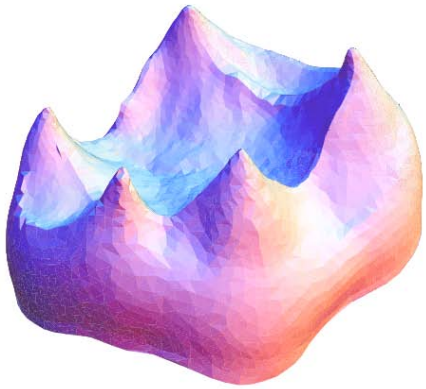

►Reads in reference surface model representing a generic EDJ surface.

```
pathM1 = DirectoryName[
   "P:\PROJECTS_CURRENT\Pan_Taxonomy\LOWER_FIRST_MOLARS\Ppan_5374_LLM1_MAIN.landmarkAscii"];
filenamesM1 = FileNames["*MAIN.landmarkAscii", pathM1];
CEJM1 = FileNames["*CEJ.landmarkAscii", pathM1];
EDJM1 = FileNames["*EDJ_RIDGE_SIMPLE.landmarkAscii", pathM1];
namesM1 = StringDrop[#, StringLength[pathM1]] & /@ (StringDrop[#, -19] & /@ filenamesM1);

pathM2 = DirectoryName[
   "P:\PROJECTS_CURRENT\Pan_Taxonomy\LOWER_SECOND_MOLARS\Ppan_22908_LLM2_MAIN.landmarkAscii
     "];
filenamesM2 = FileNames["*MAIN.landmarkAscii", pathM2];
CEJM2 = FileNames["*CEJ.landmarkAscii", pathM2];
EDJM2 = FileNames["*EDJ_RIDGE_SIMPLE.landmarkAscii", pathM2];
namesM2 = StringDrop[#, StringLength[pathM2]] & /@ (StringDrop[#, -19] & /@ filenamesM2);

names = Flatten[{namesM1, namesM2}];
lmsfiles = Flatten[{filenamesM1, filenamesM2}];

curvefiles = Flatten[{{EDJM1, EDJM2}}];
curvefiles2 = Flatten[{CEJM1, CEJM2}];
```

►Identifies the MAIN, RIDGE and CERVIX landmark text files. In this case for both first and second molars of the *Pan* sample.

►Gets names of specimens from landmark files

Step 2. Import of landmark data

```
ref = Position[names, "TAI_11791_LLM1"][[1, 1]]
```

```
10
```

```
lms = Table[Drop[Import[lmsfiles[[i]], "Table", "IgnoreEmptyLines" → True], 10],
   {i, 1, Length[lmsfiles]}];
curves = Table[Drop[Import[curvefiles[[i]], "Table", "IgnoreEmptyLines" → True], 10],
   {i, 1, Length[curvefiles]}];
curves2 = Table[Drop[Import[curvefiles2[[i]], "Table", "IgnoreEmptyLines" → True], 10],
   {i, 1, Length[curvefiles]}];

Dimensions /@ {lms, curves, curves2}
```

```
{{62, 8, 3}, {62}, {62}}
```

►Designates the reference specimen

►Imports the landmark data.

Step 3. Create and sample EDJ RIDGE curve

```
selectcurves = curves;
n = Length[curves];
splines = Table[SplineFit[selectcurves[[i]], Cubic], {i, 1, n}];
diskret = Table[Table[{splines[[i]][x], x, IntegerPart[(x - 0.0001) / 0.08 + 1]},
    {x, 0.0001, splines[[i, 2, 2]], 0.08}], {i, 1, n}];

dentin1 = Table[Flatten[{
     aequi[1, project[diskret[[i]], lms[[i, 6]]][[3]], 7, diskret[[i]]]
    }, 1], {i, 1, n}];
dentin2 = Table[Flatten[{
     aequi[project[diskret[[i]], lms[[i, 6]]][[3]],
      project[diskret[[i]], lms[[i, 2]]][[3]], 7, diskret[[i]]]
    }, 1], {i, 1, n}];
dentin3 = Table[Flatten[{
     aequi[project[diskret[[i]], lms[[i, 2]]][[3]],
      project[diskret[[i]], lms[[i, 3]]][[3]], 10, diskret[[i]]]
    }, 1], {i, 1, n}];
dentin4 = Table[Flatten[{
     aequi[project[diskret[[i]], lms[[i, 3]]][[3]],
      project[diskret[[i]], lms[[i, 5]]][[3]], 10, diskret[[i]]]
    }, 1], {i, 1, n}];
dentin5 = Table[Flatten[{
     aequi[project[diskret[[i]], lms[[i, 5]]][[3]],
      project[diskret[[i]], lms[[i, 7]]][[3]], 4, diskret[[i]]]
    }, 1], {i, 1, n}];
dentin6 = Table[Flatten[{
     aequi[project[diskret[[i]], lms[[i, 7]]][[3]],
      project[diskret[[i]], lms[[i, 4]]][[3]], 4, diskret[[i]]]
    }, 1], {i, 1, n}];
dentin7 = Table[Flatten[{
     aequi[project[diskret[[i]], lms[[i, 4]]][[3]],
      project[diskret[[i]], lms[[i, 8]]][[3]], 5, diskret[[i]]]
    }, 1], {i, 1, n}];
dentin8 = Table[Flatten[{
     aequi[project[diskret[[i]], lms[[i, 8]]][[3]], diskret[[i, -1]][[3]], 5, diskret[[i]]]
    }, 1], {i, 1, n}];
```

►Fits a cubic spline function to the MAIN and RIDGE landmarks of each specimen.

►Divides this spline curve into 8 sections based on MAIN landmarks.

►Calculates a number of equally spaced landmarks on the spline curve between adjacent landmarks. For example for "dentin1" it calculates 7 equally spaced landmarks between MAIN landmarks #1 and #6 (see Fig. 2.1)

Step 4. Create and sample CERVIX curve

```
selectcurves = curves2;
n = Length[curves2];
splines = Table[SplineFit[selectcurves[[i]], Cubic], {i, 1, n}];
diskret = Table[Table[{splines[[i]][x], x, IntegerPart[(x - 0.0001) / 0.08 + 1]},
    {x, 0.0001, splines[[i, 2, 2]], 0.08}], {i, 1, n}];

diskret // Dimensions

{62}

base = Table[Flatten[{
     aequi[1, diskret[[i, -1]][[3]], 70, diskret[[i]]]
    }, 1], {i, 1, n}];
```

►Fits a cubic spline function to the CERVIX landmarks of each specimen.
►Calculates 70 equally spaced landmarks along the cubic spline.

Step 5. Procrustes superimposition of specimens

```
fulldata =
  Table[Flatten[{lms[[a]], dentin1[[a, All, 1]], dentin2[[a, All, 1]], dentin3[[a, All, 1]],
     dentin4[[a, All, 1]], dentin5[[a, All, 1]], dentin6[[a, All, 1]], dentin7[[a, All, 1]],
     dentin8[[a, All, 1]], base[[a, All, 1]]}, 1], {a, 1, n}];


ListPointPlot3D[fulldata // Procrustes, BoxRatios → Automatic,
 Boxed → False, Axes → False, PlotStyle → PointSize[Tiny]]
```

►All specimens after Procrustes superimposition.

Step 6. Create matrix of Procrustes coordinates

```
fulldata // Dimensions
```

```
{62, 130, 3}
```

```
procrdata = Procrustes[fulldata];
cs = CentroidSize[fulldata];
```

```
sdata = Table[Flatten[{procrdata[[i]], Log[cs[[i]]]}], {i, 1, Length[procrdata]}];
```

```
sdata = Table[Flatten[{procrdata[[i]]}], {i, 1, Length[procrdata]}];
```

Step 7. Check for outliers

```
sev = Eigenvectors[Transpose[ZeroMean[sdata]].ZeroMean[sdata]];
seval = Eigenvalues[Transpose[ZeroMean[sdata]].ZeroMean[sdata]];
scores = ZeroMean[sdata].Transpose[sev[[{1, 2, 3}]]];
```

```
Sum[seval[[i]], {i, 1, 3}] / Sum[seval[[i]], {i, 1, Length[seval]}] * 100
```

```
58.3447
```

```
Show[TextListPlot[scores[[All, {1, 2}]], names], AspectRatio → Automatic,
 TextStyle → {FontFamily → "Arial", FontSize → 9}, Frame → True, Axes → False, PlotRange → All]
```

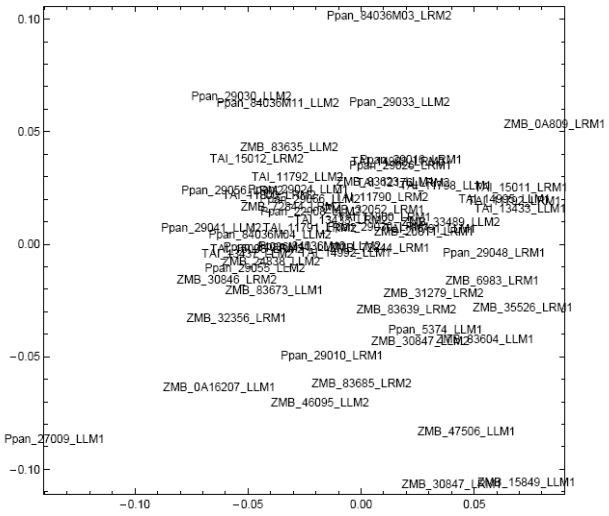

►PCA of Procrustes coordinates to check for outliers due to methodological errors (e.g., mistakes during landmark collection on original EDJ surface).

```
thecurve = Last[FindShortestTour[fulldata[[ref]]]]
```

```
{1, 9, 10, 11, 12, 13, 14, 15, 6, 16, 17, 18, 19, 20, 21, 22, 2, 23, 24, 25, 26, 27, 28, 29, 30,
 31, 32, 3, 33, 34, 35, 36, 37, 38, 39, 40, 41, 42, 5, 43, 44, 45, 46, 7, 47, 48, 49, 50,
 4, 51, 52, 53, 54, 55, 8, 56, 130, 129, 128, 127, 126, 125, 124, 123, 122, 121, 120, 119,
 118, 117, 116, 115, 114, 113, 112, 111, 110, 109, 108, 107, 106, 105, 104, 103, 102, 101,
 100, 99, 98, 97, 96, 95, 94, 93, 92, 91, 90, 89, 88, 87, 86, 85, 84, 83, 82, 81, 80, 79,
 78, 77, 76, 75, 74, 73, 72, 71, 70, 69, 68, 67, 66, 65, 64, 63, 62, 61, 57, 58, 59, 60}
```

►Identifies the order of points along each curve

```
RIDGE = {1, 9, 10, 11, 12, 13, 14, 15, 6, 16, 17, 18, 19, 20, 21, 22, 2, 23, 24,
   25, 26, 27, 28, 29, 30, 31, 32, 3, 33, 34, 35, 36, 37, 38, 39, 40, 41, 42, 5, 43,
   44, 45, 46, 7, 47, 48, 49, 50, 4, 51, 52, 53, 54, 55, 8, 56, 57, 58, 59, 60, 1};
CERVIX = {61, 62, 63, 64, 65, 66, 67, 68, 69, 70, 71, 72, 73, 74, 75, 76, 77, 78, 79,
   80, 81, 82, 83, 84, 85, 86, 87, 88, 89, 90, 91, 92, 93, 94, 95, 96, 97, 98, 99,
   100, 101, 102, 103, 104, 105, 106, 107, 108, 109, 110, 111, 112, 113, 114, 115,
   116, 117, 118, 119, 120, 121, 122, 123, 124, 125, 126, 127, 128, 129, 130, 61};
```

```
thecurve = Flatten[{RIDGE, CERVIX}];
```

```
ref = 5; Show[Graphics3D[Line[fulldata[[ref, thecurve]]]],
 TextListPlot3D[fulldata[[ref]], Range[2000]], surface, Boxed → False]
```

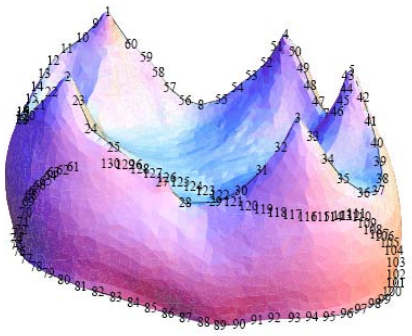

►Illustration of specimen number 5 with landmark locations.

Step 8. Slide landmarks on RIDGE and CERVIX curves

```
curvesemilm = Complement[Range[Length[fulldata[[1]]]], {1, 2, 3, 4, 5, 61}];
slidinglandmarks = curvesemilm;

mycurve = (Flatten[Position[{RIDGE, CERVIX}, #]] & /@ curvesemilm)[[All, 1]];

chordtangents = Table[ChordTangenten[fulldata[[i]], curvesemilm, thecurve], {i, 1, n}];
vecs = Table[Flatten[{Transpose[{chordtangents[[i]], chordtangents[[i]]}]}, 1], {i, 1, n}];
```

►Calculates vectors between adjacent landmarks that are tangent to the curve and along with landmarks will be allowed to slide.

```
a = ref;
Show[ListVectorFieldPlot3D[Transpose[{fulldata[[a, curvesemilm]], 0.2 vecs[[a, All, 1]]}]],
 ListVectorFieldPlot3D[Transpose[{fulldata[[a, curvesemilm]], -0.2 vecs[[a, All, 1]]}]]]
```

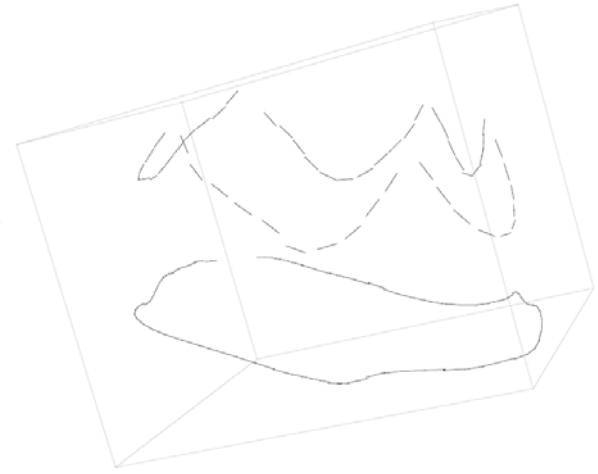

►Illustration of the vectors calculated for specimen 5. Note vectors are not calculated adjacent to MAIN landmarks because these landmarks are not allowed to slide.

```
cons = Consensus[Procrustes[fulldata]];

sliddata = Table[MissingDataSliding3DRidge[cons, fulldata[[i]], vecs[[i]], {61}], {i, 1, n}];

slidcoord = sliddata[[All, 1]];
```

►Writes new matrix of coordinates after sliding.

```
a = 2; ListVectorFieldPlot3D[
 Transpose[{fulldata[[a]], slidcoord[[a]] - fulldata[[a]]}], VectorHeads → True]
```

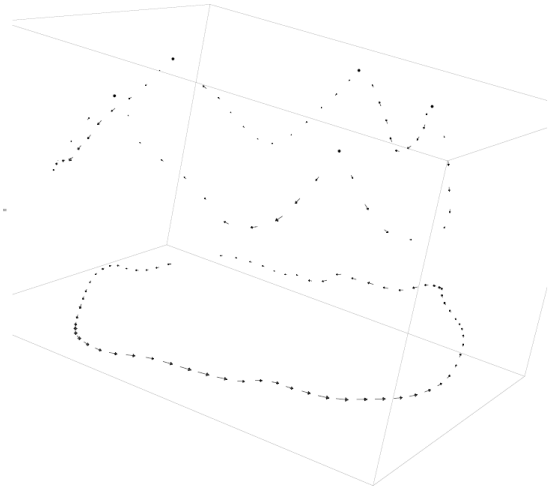

►Shows displacement of landmarks for specimen #2.

```
procrdata = Procrustes[slidcoord];
cs = CentroidSize[slidcoord];

sdata = Table[Flatten[{procrdata[[i]], Log[cs[[i]]]}], {i, 1, Length[procrdata]}];

sdata = Table[Flatten[{procrdata[[i]]}], {i, 1, Length[procrdata]}];

sev = Eigenvectors[Transpose[ZeroMean[sdata]].ZeroMean[sdata]];
seval = Eigenvalues[Transpose[ZeroMean[sdata]].ZeroMean[sdata]];
scores = ZeroMean[sdata].Transpose[sev[[{1, 2, 3}]]];
fullscores = ZeroMean[sdata].Transpose[sev];

Sum[seval[[i]], {i, 1, 3}] / Sum[seval[[i]], {i, 1, Length[seval]}] * 100
```

```
53.9347
```

►Calculates Procrustes superimposition on all specimens after first sliding.

```
Show[TextListPlot[scores[[All, {1, 2}]], names], AspectRatio → Automatic,
 TextStyle → {FontFamily → "Arial", FontSize → 9}, Frame → True, Axes → False, PlotRange → All]
```

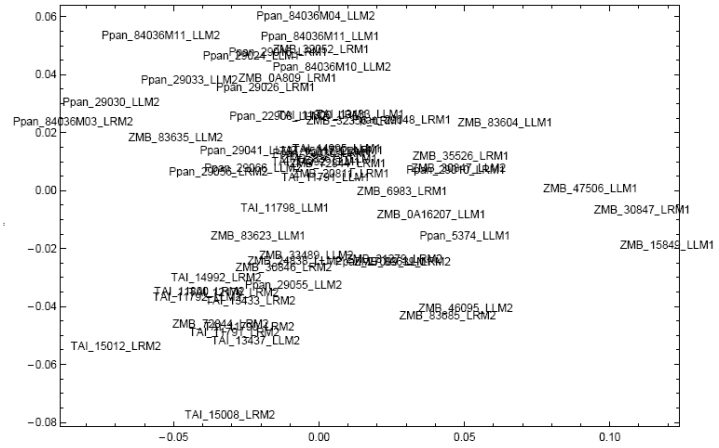

►PCA after first sliding.

Step 9. Slide landmarks a second time

```
curves = {RIDGE, CERVIX};

curvecoords =
  Table[Table[fulldata[[i, curves[[j]]]], {i, 1, Length[fulldata]}], {j, 1, Length[curves]}];

splines = Table[Table[SplineFit[curvecoords[[j, i]], Cubic], {i, 1, Length[fulldata]}],
   {j, 1, Length[curves]}];

diskret = Table[Table[splines[[j, i]][x], {i, 1, Length[fulldata]},
    {x, 0.0001, splines[[j, i, 2, 2]], 0.05}], {j, 1, Length[curves]}];
```

►Reimpliments the sliding routine

```
a = 2; Show[ListPointPlot3D[diskret[[All, a]], BoxRatios → Automatic],
 ListPointPlot3D[slidcoord[[a]], BoxRatios → Automatic]]
```

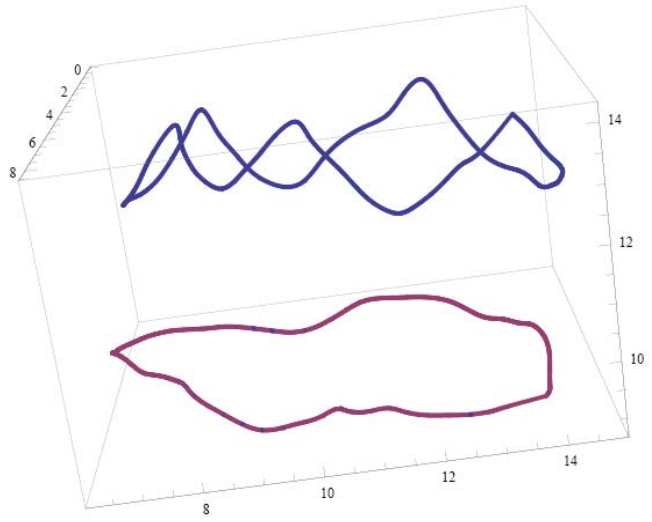

►Curves upon which slide landmarks are projected back onto after sliding along their associated vectors.

```
curveprojection = Table[
   Flatten /@ Table[Nearest[diskret[[mycurve[[i]], a]], slidcoord[[a]][[curvesemilm[[i]]]]],
     {i, 1, Length[curvesemilm]}], {a, 1, Length[fulldata]}];
```

```
a = 2; Show[ListVectorFieldPlot3D[
   Transpose[{curveprojection[[a]], slidcoord[[a, curvesemilm]] - curveprojection[[a]]}],
   VectorHeads → True]]
```

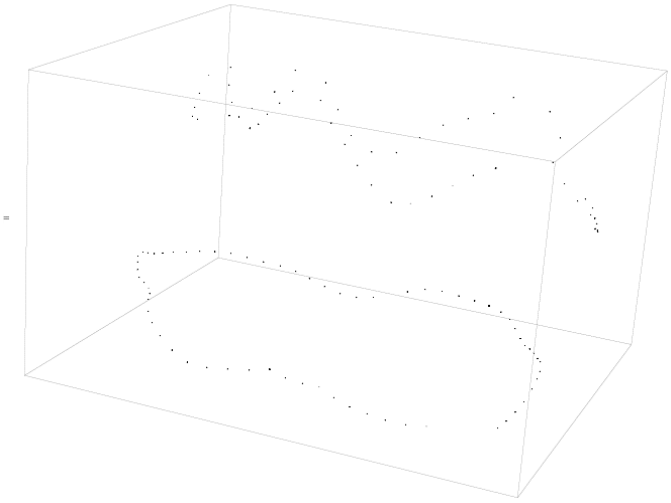

► Shows displacement of landmarks for specimen #2 after second sliding. Note the marked reduction in the degree of landmark displacement compared to first sliding.

```
slidcoord2 = slidcoord;
slidcoord2[[All, curvesemilm]] = curveprojection;
```

```
cons = Consensus[Procrustes[slidcoord2]];

chordtangents = Table[ChordTangenten[slidcoord2[[i]], curvesemilm, thecurve], {i, 1, n}];
vecs = Table[Flatten[{Transpose[{chordtangents[[i]], chordtangents[[i]]}]}, 1], {i, 1, n}];

sliddata2 =
  Table[MissingDataSliding3DRidge[cons, slidcoord2[[i]], vecs[[i]], {61}], {i, 1, n}];

slidcoord3 = sliddata2[[All, 1]];
```

Step 10. Final Procrustes superimposition

```
procrdata = Procrustes[slidcoord3];
cs = CentroidSize[slidcoord3];

sdata = Table[Flatten[{procrdata[[i]], Log[cs[[i]]]}], {i, 1, Length[procrdata]}];

sdata = Table[Flatten[{procrdata[[i]]}], {i, 1, Length[procrdata]}];

sev = Eigenvectors[Transpose[ZeroMean[sdata]].ZeroMean[sdata]];
seval = Eigenvalues[Transpose[ZeroMean[sdata]].ZeroMean[sdata]];
scores = ZeroMean[sdata].Transpose[sev[[{1, 2, 3}]]];
fullscores = ZeroMean[sdata].Transpose[sev];

Sum[seval[[i]], {i, 1, 3}] / Sum[seval[[i]], {i, 1, Length[seval]}] * 100
```

```
54.5476
```

```
Show[TextListPlot[scores[[All, {1, 2}]], names], AspectRatio → Automatic,
 TextStyle → {FontFamily → "Arial", FontSize → 9}, Frame → True, Axes → False, PlotRange → All]
```

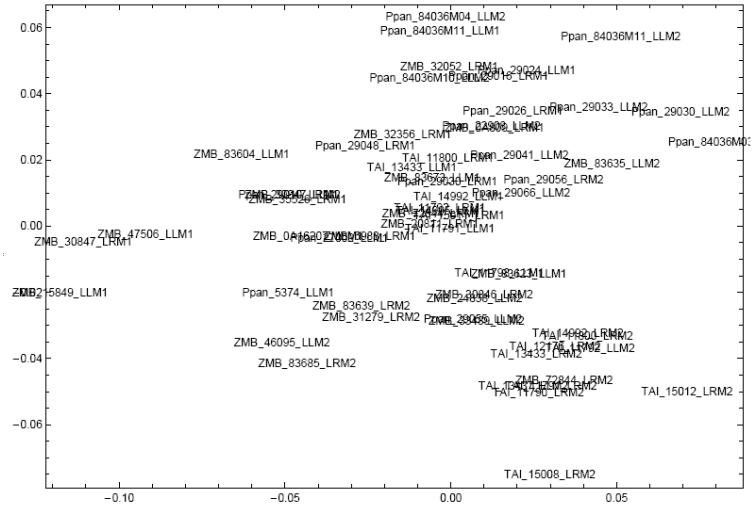


```
sdata = Table[Flatten[{procrdata[[i]], Log[cs[[i]]]}], {i, 1, Length[procrdata]}];

sdata = Flatten /@ procrdata;

sdata // Dimensions
```

```
{62, 390}
```

Step 11. Export of homologous landmark datasets

```
Export[Experimental`FileBrowse[True], sdata, "Table"]
```

```
P:\PROJECTS_CURRENT\Pan_Taxonomy\621_M1M2_CS.txt
```

►Exports the homologous landmark sets for each specimen.

```
Log[cs]
```

```
{3.95417, 3.8018, 3.9134, 3.82458, 3.8534, 3.92041, 3.89691, 3.85723,
 3.95339, 3.9477, 4.05376, 4.00387, 4.00574, 3.99412, 3.97227, 4.02158, 4.0439,
 3.92843, 3.97513, 3.90712, 4.02477, 3.91251, 3.90145, 3.97575, 4.05851, 3.95523,
 3.96971, 3.98924, 4.01417, 3.95757, 3.99376, 3.86225, 3.95295, 3.93155, 3.9719,
 3.96039, 3.92119, 3.92665, 3.93042, 3.92195, 3.87882, 3.97995, 4.0182, 3.91554,
 4.07715, 4.03171, 4.01576, 3.97943, 4.01154, 3.98217, 4.07324, 4.12538, 4.04876,
 4.09756, 3.95054, 3.90754, 4.02159, 3.97843, 4.00377, 4.05168, 3.96716, 3.9126}
```

►Lists centroid sizes for each specimen.

```
slidcoord3 // Dimensions
```

```
{62, 130, 3}
```

```
Write["P:\\PROJECTS_CURRENT\Pan_Taxonomy\621_130p_slidcoordsPan.mathdata", slidcoord3]
```